NAG3 - 2745

FLUID STRUCTURE INTERACTION IN A TURBINE BLADE

Professor Rama S.R. Gorla

CLEVELAND STATE UNIVERSITY

August, 2004

FLUID STRUCTURE INTERACTION IN A TURBINE BLADE

ABSTRACT

An unsteady, three dimensional Navier-Stokes solution in rotating frame formulation for turbomachinery applications is presented. Casting the governing equations in a rotating frame enabled the freezing of grid motion and resulted in substantial savings in computer time.

The turbine blade was computationally simulated and probabilistically evaluated in view of several uncertainties in the aerodynamic, structural, material and thermal variables that govern the turbine blade. The interconnection between the computational fluid dynamics code and finite element structural analysis code was necessary to couple the thermal profiles with the structural design. The stresses and their variations were evaluated at critical points on the Turbine blade. Cumulative distribution functions and sensitivity factors were computed for stress responses due to aerodynamic, geometric, mechanical and thermal random variables.

TABLE OF CONTENTS

Pages

LIST OF TABLES.....viii

LIST OF FIGURES.....x

CHAPTER

I INTRODUCTION.....01

II LITERATURE REVIEW.....05

2.1 Rotor Stator Interaction in a turbine and its CFD analysis.....05

2.2 Probabilistic analysis.....15

III GOVERNING EQUATIONS.....19

IV VANE AND BLADE CONFIGURATION.....27

4.1 Aerodynamic design.....27

4.2 Airfoil Definition.....28

4.3 Airfoil Durability.....34

4.4 Vane Materials.....34

4.5 Blade Materials.....35

V RESULTS AND DISCUSSION OF THE AERODYNAMIC DATA.....37

5.1 Stator suction surface graphs for hot case.....39

5.2 Stator pressure surface graphs for hot case.....41

5.3 Rotor suction surface graphs for hot case.....43

5.4 Rotor pressure surface graphs for hot case.....45

5.5 Amplitude of unsteady pressure coefficient and phase angle

distribution for stator suction surface.....48

5.6 Amplitude of unsteady pressure coefficient and phase angle distribution for stator pressure surface.....49

5.7 Amplitude of unsteady pressure coefficient and phase angle distribution for rotor suction surface.....50

5.8 Amplitude of unsteady pressure coefficient and phase angle distribution for rotor pressure surface.....51

VI FINITE ELEMENT ANALYSIS.....52

VII RESULTS AND DISCUSSION FOR FINITE ELEMENT ANALYSIS.....56

VIII PROBABILISTIC ANALYSIS.....64

IX RESULTS AND DISCUSSION OF PROBABILISTIC ANALYSIS.....70

X CONCLUDING REMARKS.....124

BIBLIOGRAPHY.....125

APPENDICES.....131

LIST OF TABLES

Table Page

4.1 Summary of Vane Materials.....35

4.2 Summary of Blade Materials.....36

7.1 Finite element analysis results for the stator at 1900th iteration.....58

7.2 Finite element analysis results for the stator at 1960th iteration.....59

7.3 Finite element analysis results for the stator at 2000th iteration.....60

7.4 Finite element analysis results for the rotor at 1900th iteration.....61

7.5 Finite element analysis results for the rotor at 1960th iteration.....62

7.6 Finite element analysis results for the rotor at 2000th iteration.....63

A.1 Stator mean coordinates.....131

A.2 Stator tip coordinates.....132

A.3 Stator root coordinates.....133

A.4 Rotor mean coordinates.....135

A.5 Rotor tip coordinates.....136

A.6 Rotor root coordinates.....138

B.1 Stator suction side static pressure.....139

B.2 Stator pressure side static pressure.....140

B.3 Stator suction side static temperature.....141

B.4 Stator pressure side static temperature.....142

B.5 Rotor suction side static pressure.....143

B.6 Rotor pressure side static pressure.....144

B.7 Rotor suction side static temperature.....145

B.8 Rotor pressure side static temperature.....146

C.1 Sensitivity and Probability levels for stator at 1900th iteration.....147

C.2 Sensitivity and Probability levels for stator at 1960th iteration.....147

C.3 Sensitivity and Probability levels for stator at 2000th iteration.....147

C.4 Random variables and sensitivity factors values for

Stator at 1900th iteration.....149

C.5 Random variables and sensitivity factors values for

Stator at 1960th iteration.....151

C.6 Random variables and sensitivity factors values for

Stator at 2000th iteration.....154

C.7 Sensitivity and Probability levels for Rotor at 1900th iteration.....155

C.8 Sensitivity and Probability levels for Rotor at 1960th iteration.....155

C.9 Sensitivity and Probability levels for Rotor at 2000th iteration.....155

C.10 Random variables and sensitivity factors values for

Rotor at 1900th iteration.....157

C.11 Random variables and sensitivity factors values for

Rotor at 1960th iteration.....160

C.12 Random variables and sensitivity factors values for

Rotor at 2000th iteration.....163

LIST OF FIGURES

Figure Page

1.1 Stator and Rotor stacking.....03

3.1 Coordinate Transformation for speed in vector invariant form.....20

4.1 Flow path for Stator and Rotor.....27

4.2 Mean section for Stator.....29

4.3 Root section for Stator.....29

4.4 Tip section for Stator.....30

4.5 Stator stacking.....30

4.6 Blade inlet angle.....31

4.7 Mean section for Rotor.....32

4.8 Root section for Rotor.....32

4.9 Tip section for Rotor.....33

4.10 Rotor Stacking.....33

Cold Case Graphs (5.1- 5.18)

5.1 Stator suction surface static pressure vs. % chord length.....39

5.2 Stator suction surface static temperature vs. % chord length.....39

5.3 Stator suction surface total pressure vs. % chord length.....40

5.4 Stator suction surface total temperature vs. % chord length.....40

5.5 Stator pressure surface static pressure vs. % chord length.....41

5.6 Stator pressure surface static temperature vs. % chord length.....41

5.7 Stator pressure surface total pressure vs. % chord length.....42

5.8 Stator pressure surface total temperature vs. % chord length.....42

5.9 Rotor suction surface static pressure vs. % chord length.....43

5.10 Rotor suction surface static temperature vs. % chord length.....43

5.11 Rotor suction surface total pressure vs. % chord length.....44

5.12 Rotor suction surface total temperature vs. % chord length.....44

5.13 Rotor pressure surface static pressure vs. % chord length.....45

5.14 Rotor pressure surface static temperature vs. % chord length.....45

5.15 Rotor pressure surface total pressure vs. % chord Length.....46

5.16 Rotor Pressure Surface Total Temperature vs. % chord Length.....46

5.17 Stator C_p vs. % chord length.....47

5.18 Rotor C_p vs. % chord length.....47

5.19 Stator suction surface pressure amplitude vs. % chord length.....48

5.20 Stator suction surface phase angle vs. % chord length 48

5.21 Stator pressure surface pressure amplitude vs. % chord length.....49

5.22 Stator pressure surface phase angle vs. % chord length.....49

5.23 Rotor suction surface pressure amplitude vs. % chord length.....50

5.24 Rotor pressure surface pressure amplitude vs. % chord length.....50

5.25 Rotor suction surface phase angle vs. % chord length.....51

5.26 Rotor pressure surface phase angle vs. % chord length.....51

6.1 Coupling between CFD and Structural and Probabilistic analysis.....55

7.1 Default value of stress for the stator at 1900th iteration.....58

7.2 Default value of stress for the stator at 1960th iteration.....59

7.3 Default value of stress for the stator at 2000th iteration.....60

7.4 Default value of stress for the stator at 1900th iteration.....61

7.5 Default value of stress for the stator at 1960th iteration.....62

7.6 Default value of stress for the stator at 2000th iteration.....63

9.1 Cumulative probability of thermal stress for stator at 1900th iteration.....71

Sensitivity factors vs. Random variables for stress at 1900th iteration for stator:

9.2 Probability: 0.001.....72

9.3 Probability: 0.01.....72

9.4 Probability: 0.1.....73

9.5 Probability: 0.2.....73

9.6 Probability: 0.4.....74

9.7 Probability: 0.5.....74

9.8 Probability: 0.6.....75

9.9 Probability: 0.8.....75

9.10 Probability: 0.9.....76

9.11 Probability: 0.95.....76

9.12 Probability: 0.99.....77

9.13 Probability: 0.999.....77

9.14 Cumulative probability of thermal stress for stator at 1960th iteration.....78

Sensitivity factors vs. Random variables for stress at 1960th iteration for stator:

9.15 Probability: 0.001....78

9.16 Probability: 0.01....79

9.17 Probability: 0.1....79

9.18 Probability: 0.2....80

9.19 Probability: 0.4....80

9.20 Probability: 0.5....81

9.21 Probability: 0.6....81

9.22 Probability: 0.8....82

9.23 Probability: 0.9....82

9.24 Probability: 0.95....83

9.25 Probability: 0.99....83

9.26 Probability: 0.999....84

9.27 Cumulative probability of thermal stress for stator at 2000th iteration....84

Sensitivity factors vs. Random variables for stress at 2000th iteration for stator:

9.28 Probability: 0.001....85

9.29 Probability: 0.01....85

9.30 Probability: 0.1....86

9.31 Probability: 0.2....86

9.32 Probability: 0.4....87

9.33 Probability: 0.5.....87

9.34 Probability: 0.6.....88

9.35 Probability: 0.8.....88

9.36 Probability: 0.9.....89

9.37 Probability: 0.95.....89

9.38 Probability: 0.99.....90

9.39 Probability: 0.999.....90

9.40 Cumulative probability of thermal stress

for Rotor at 1900th iteration.....91

Sensitivity factors vs. Random variables for stress at 1900th iteration for

Rotor:

9.41 Probability: 0.001.....92

9.42 Probability: 0.01.....92

9.43 Probability: 0.1.....93

9.44 Probability: 0.2.....93

9.45 Probability: 0.4.....94

9.46 Probability: 0.5.....94

9.47 Probability: 0.6.....95

9.48 Probability: 0.8.....95

9.49 Probability: 0.9.....96

9.50 Probability: 0.95.....96

9.51 Probability: 0.99.....97

9.52 Cumulative probability of thermal stress for Rotor at 1960th iteration.....97

Sensitivity factors vs. Random variables for stress at 1960th iteration for Rotor:

9.53 Probability: 0.001.....98

9.54 Probability: 0.01.....98

9.55 Probability: 0.1.....99

9.56 Probability: 0.2.....99

9.57 Probability: 0.4.....100

9.58 Probability: 0.5.....100

9.59 Probability: 0.6.....101

9.60 Probability: 0.8.....101

9.61 Probability: 0.9.....102

9.62 Probability: 0.95.....102

9.63 Probability: 0.99.....103

9.64 Cumulative probability of thermal stress for Rotor at 2000th iteration.....103

Sensitivity factors vs. Random variables for stress at 2000th iteration for Rotor:

9.65 Probability:0.001.....104

9.66 Probability: 0.01.....104

9.67 Probability: .1.....105

9.68 Probability: 0.2.....105

9.69 Probability: 0.4.....106

9.70 Probability: 0.5.....106

9.71 Probability: 0.6.....107

9.72 Probability: 0.8.....107

9.73 Probability: 0.9.....108

9.74 Probability: 0.95.....108

9.75 Probability: 0.99.....109

Graphs comparing all the three iterations namely 1900th, 1960th and 2000th for Sensitivity factors vs. random variables for Stator.

9.76 Probability: 0.001.....110

9.77 Probability: 0.01.....111

9.78 Probability: 0.1.....111

9.79 Probability: 0.2.....112

9.80 Probability: 0.4.....112

9.81 Probability: 0.5.....113

9.82 Probability: 0.6.....113

9.83 Probability: 0.8.....114

9.84 Probability: 0.9.....114

9.85 Probability: 0.95.....115

9.86 Probability: 0.99.....115

9.87 Probability: 0.999.....116

Graphs comparing all the three iterations namely 1900th, 1960th and 2000th for Sensitivity factors vs. random variables for Rotor.

9.88 Probability: 0.001.....117

9.89 Probability: 0.01.....118

9.90 Probability: 0.1.....118

9.91 Probability: 0.2.....119

9.92 Probability: 0.4.....119

9.93 Probability: 0.5.....120

9.94 Probability: 0.6.....120

9.95 Probability: 0.8.....121

9.96 Probability: 0.9.....121

9.97 Probability: 0.95.....122

9.98 Probability: 0.99.....122

9.99 Probability: 0.999.....123

CHAPTER I

INTRODUCTION

Unsteady flow phenomena have become an active area for turbomachinery research. It is well recognized that flows within single and multi stage turbomachinery are inherently unsteady as a result of relative motion between blade rows. This unsteady flow field is a source of aerodynamic noise, as well as mechanical excitations that can cause serious vibration problems. It is plausible that unsteady flow phenomena can have either a favorable or unfavorable impact on the performance of blade row and their thermal environment. Because these important issues have a direct impact on the turbine development, considerable time and effort continues to be devoted to modeling and quantifying unsteady flow phenomena in turbomachinery.

Predictive technologies based on probabilistic method of problem solving are gaining a steady foothold as a method of finding answers to engineering problems. These can be used for the design, sensitivity analysis, mathematical modeling of complex

processes, uncertainty analysis, competitive analysis and process optimization. With the increase in the gas turbine structural complexity and performance over the past 50 years, structural engineers have created an array of safety nets to ensure against component failures in turbine engines. In order to reduce what is now considered to be excessive conservatism and yet maintain the same adequate margins of safety, there is a pressing need to explore methods of incorporating probabilistic design procedures into engine development.

Probabilistic methods combine and prioritize the statistical distributions of each design variable, generate an interactive distribution and offer the designer a quantified relationship between robustness, endurance and performance. The designer can therefore iterate between weight reduction, life increase engine size reduction and speed increase etc.

Chapter II deals with the previous research work accomplished in the past few years and describes the various methods that were used to study the unsteady flow in turbomachinery.

Chapter III deals with the governing equations, the three dimensional, unsteady, compressible Navier-Stokes equations coupled with the $k-\varepsilon$ turbulence model in a rotating system of coordinates.

Chapter IV deals with the aerodynamic model of the turbine blade and the

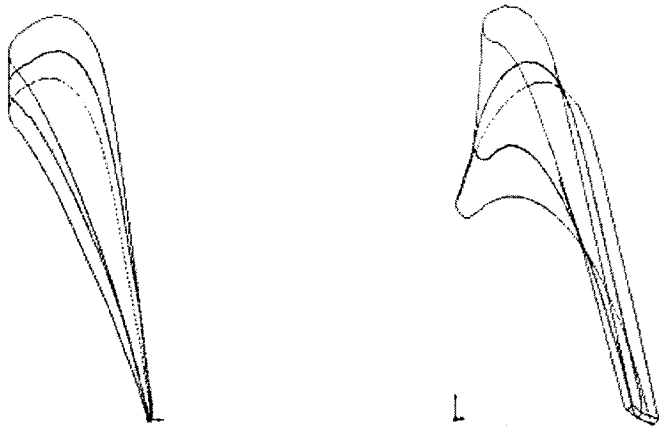

Figure 1.1: Stator and Rotor stacking

description of the Stator-Rotor and also the design and material details of each. The design detail is explained elaborately here.

Chapter V deals with the results of the aerodynamic analysis. In the present report, the hot case is considered where the working temperatures are very high. Hot case corresponds to air temperature of 1100° C.

Chapter VI deals with the Finite element analysis. The general finite element equations of motion may be written as

$$[M]\{\ddot{u}\}+[C]\{\dot{u}\}+[K]\{u\}=F(t),$$

where $[M],[C],[K]$ denote the mass, damping and stiffness matrices respectively. Further $\{\ddot{u}\}$, $\{\dot{u}\}$ and $\{u\}$ are the acceleration, velocity and displacement vectors at each node, respectively.

Chapter VII deals with the FEM results and also the perturbations of the random variables with $+10\%$ and -10% each. The results for the mean line case are presented.

Chapter VIII explains briefly about the theory behind the probabilistic methods and also about the FPI (Fast Probability techniques).

Using the techniques mentioned in chapter IX, the results are computed using a software program NESTEM, which incorporates the FPI techniques and the results are shown here for the mean line as well as the perturbation cases.

CHAPTER II

LITERATURE REVIEW

Research in the field of unsteady aerodynamics of Turbo machinery has been extensively investigated for a long while. The use of Probabilistic Methods for finding the uncertainties is getting more attention recently. The investigations are summarized below:

2.1 Rotor Stator Interaction in a turbine and its CFD analysis:

Janus and Whitfield.[1] presented a Advanced 3-D viscous SSME turbine Rotor stator CFD algorithms. Some of these 3-D viscous phenomena included wakes; the boundary layers in the hub, the shroud and the blades; junction flows; and tip clearance flows. The objective was to present, and evaluate a parallel computational procedure that simulated the incompressible flow through the SSME Turbine.

Janus and Whitfield [2] presented a simple time accurate algorithm in turbomachinery which calculated the numerical solutions of an un even blade count configuration. Jung, Mayer and Stetter,[3] presented the Simulation of the Unsteady Flow in a Turbine Stage with Outlet Guide Vane using a Time-Inclination Method. Flow solver ITSM3D was used which provided the solution for the three dimensional Navier Stokes Equations which incorporated the cell-vortex finite-volume discretization, structured meshes, multiblock topology and modified Baldwin-Lomax turbulence model.

Caloni, [4], presented the numerical investigation of the unsteady flow field in one and a half stage high pressure transonic turbine. The code was validated against the existing time resolved measurements of the static pressure around the rotor blade. They observed that the static pressure variation was due to the passage of the rotor across the stator first trailing edge shockwave. The interaction of the rotor with the stator wake follows a different timing and is investigated and finally the unsteady computations were performed for four clocking positions.

Unsteady Euler/ Navier-Stokes flow solver for turbomachinery rotor-stator flows have been under development since mid 1980s. Rai, [5] developed the Navier stokes Simulations for the Rotor/stator Interactions using the patched, and Over set Grid methods. In the patch algorithm for each cell node on the "to" side, a local polynomial fit relates the physical coordinates x, y, z to the patch surface coordinates xie, yie, zie on the "to" side. The "to" cell centers xc, yc, zc are then backed out by setting xie, yie, zie to 0.5, 0.5. Similarly, on the "from" side, a polynomial fit relates the physical coordinates of each cell node to the local coordinates on that side. A

search was then done on the from side to find the xie, yie, zie coordinates xiec, yiec, ziec corresponding to xc, yc, zc. If requested, corrections to xiec yiec, ziec were done to insure that the xie=0 and/or yiec=0, ziec =0 boundaries on either side of the patch interface were coincident

Fernandez, Diaz and Morros [6], presented the unsteady flow analysis of the stator–rotor interaction in an axial flow fan. URANS numerical modeling of the unsteady flow characteristics of one state sub axial flow fan with a reaction degree greater than 1. The focus was placed on the stator rotor interaction performance. Both 2D and 3D models were developed and an unsteady simulation was achieved to carry out the main characteristics of the flow inside the turbo machine. Lewis and Delaney and Hall [7] presented the Numerical prediction of the turbine Vane-Blade interaction. During this period, a turbomachinery flow simulation code (TURBO) has been developed at Mississippi State University to provide an analytical tool for unsteady fluid dynamics within turbomachinery.

Chen and Whitfield, [8] presented the Navier-Stokes calculations for the unsteady Flow Field of Turbomachinery which led to various research codes, each having its own functionality. These codes have recently been written for single processor computers. This serial version of the production TURBO code is capable of both aerodynamic and aero elastic analysis for compressor and turbine designs. The large computational cost of direct computation in all blade passages of a multiple blade-row simulation leads to long run times even with today's best serial computers. This limits the routine use of the serial TURBO code in an industrial environment,

since industrial design practice requires rapid turnaround time, usually within 24 hours, if simulations are to have timely impact on the development of a new design.

Erdos, Alzner and McNally, [9] presented a numerical solution of Periodic Transonic Flow through a fan stage. They used the phase lag boundary conditions which are the most effective way to reduce the computing resources for unsteady simulations of blade row interaction which allow modeling of a rotor-stator interaction using only a single blade passage in each blade row. This technique can greatly reduce the computing resources even required for simulations of stages with irreducible blade counts.

Chen and Barter [10] presented a comparison of time accurate calculations fore the unsteady interaction in turbomachinery stage. They reported that the Phase-lag boundary conditions were useful for unsteady analyses dominated by unsteadiness at the adjacent blade passing frequency. The single-stage phase-lag capability had been successfully implemented in TURBO using a more general approach suitable for simulating multiple stage interaction.

Numerical simulation of unsteady viscous flows within single and multiple stages of turbomachinery is becoming increasingly helpful in understanding these complex flows. However, these simulations can require computing resources far exceeding the practical limits of most single-processor supercomputers. Such large-scale simulations are enabled by scalable parallel computing. With the large memory and computing power available on the modern distributed-memory systems, large-scale computations are becoming more commonplace in current sophisticated design environments.

Henley and Janus [11] presented the parallelization and convergence of a three dimensional, implicit, and unsteady turbomachinery flow code. They used the modified TURBO code i.e. the Parallelized code for Parallel computation. Luke [12] presented the use of the parallel TURBO code in his thesis "Development of a scalable parallel 3-D CFD algorithm for the Turbomachinery". Many CFD codes have been converted for parallel computation in recent years, including early research version of the TURBO and other turbomachinery flow solvers given.

Zhu and Shih [13] presented the CMOTT turbulence module for NPARC. The governing equations were the unsteady Reynolds averaged N-S equations and a NASA/ CMOTT k - ε turbulence model. These governing equations were formulated in a rotating frame attached to the blades, and with velocity retained in the absolute vector basis. Two levels of sub-iteration at each time step are available in the implicit solver. The outer layer is an approximate Newton iteration to solve the nonlinear system obtained from discretizing the governing equations.

WhitField, Janus and Simpson [14] presented the implicit finite volume high resolution wave split scheme for solving the unsteady 3-D Euler and Navier-Stokes equations on stationery or dynamic grids. Details of the above algorithm are also presented here.

Pankajakshan [15] presented the parallel solution for the unsteady incompressible viscous flows using multiblock structured grids. The basic MPI parallel communication framework from this existing code (UNCLE) was used for message passing in the present code (TURBO) and was extended to handle data communication between blade rows associated with the sliding interface and phase-

lag boundary conditions. The code also retained many essential elements of the single processor version of the TURBO code.

McBean, Liu and Thompson [16] presented the there dimensional Navier-Stokes code for the aero elasticity in Turbomachinery. A multi block method was used. The method employed a fully coupled approach and the structural model involves modal reduction. Transfinite interpolation was used to adapt the fluid grid to the moving structure.

Dunn et al. [17], investigated the unsteady interaction between a transonic turbine stage and down stream components. Results from a numerical simulation of the unsteady flow through one quarter of the circumference of a transonic high pressure turbine stage, transition duct, and low-pressure turbine first vane were presented and compared with experimental data. Analysis of the unsteady pressure field resulting from the simulation showed the effects of not only the rotor/stator interaction of the high-pressure turbine stage but also new details of the interaction between the blade and the downstream transition duct and low-pressure turbine vane. Blade trailing edge shocks propagate downstream, strike, and reflect off of the transition duct hub and/or downstream vane leading to high unsteady pressure on these downstream components.

Barter, Vitt, and Chen [18] studied the interaction effects in a transonic turbine. They presented a 3-D viscous, time accurate code and used this to predict the time dependent flow field in a transonic turbine stage. Two analytical techniques were used to understand the unsteady physics. One technique takes into account the interaction effects associated with the reflected waves bouncing between blade rows

while the other neglects them. Both techniques model the exact blade counts using the phase lag boundary conditions.

There have been several studies, both analytical and experimental, which have focused on unsteady loading and interaction loss in single-stage high-pressure turbines. Dunn, et al. [19] investigated the unsteady flow through a transonic turbine stage and experimental versus numerical data comparison for time averaged and phase resolved pressure data. They also made time-resolved pressure measurements on the vane blade surface of the VBI turbine at several vane-blade spacing.

Rao, Delaney, and Dunn [20] studied the vane blade interaction in a transonic turbine. They used a two dimensional Navier-Stokes based code to predict the unsteadiness in the VBI turbine at mid span with a fair agreement between the analytical and measured unsteady results. Rao and Delaney [21] compared the results from two-dimensional and three-dimensional Euler based codes and found that at mid span the result from the 2D and 3D analyses were similar. Venable, et al. [22] more recently compared the predictive accuracy of four two-dimensional and three-dimensional Navier-Stokes codes for the VBI turbine at the three different values of vane/blade spacing. While qualitatively similar, there were notable differences between the predicted unsteady pressure envelopes from the different codes. They also found that, as might be expected, the amount of unsteadiness decreased significantly as the vane/blade spacing increased while the stage loss coefficient was only a week function of spacing. Results from these studies also showed a strong similarity between the results from 2D and 3D codes at mid span.

Jennions and Adamczyk [23] showed that time-dependent analyses could be used to predict the interaction loss associated with blade row interaction in transonic turbine stages. They examined the cause of interaction loss and attributed it to the unsteady flow processes in the gap between the blade and vane.

Matsunuma, Hiroyuki and Tasukata [24] studied the unsteady flow at the mid span in a turbine rotor due to rotor-stator interaction. In this study the unsteady field at the mid span in an axial flow turbine rotor at low Reynolds number $\left(3.6\times10^{4}\right)$ was investigated experimentally using Laser Doppler velocimetry (LDV) system. The time averaged and time dependent distributions of velocity flow angle, vorticity, turbulence intensity, and Reynolds stresses were analyzed in terms of both absolute and relative reference frames.

Ji and Liu [25] presented the flutter computation of turbomachinery cascades using a parallel unsteady Navier-Stokes code. A quasi-three-dimensional multigrid Navier–Stokes solver on single- and multiple-passage domains was presented for solving unsteady flows around oscillating turbine and compressor blades. The conventional direct store method was used for applying the phase-shifted periodic boundary condition over a single blade passage. A parallel version of the solver using the message passing interface standard was developed for multiple-passage computations.

Yao, Jameson, Alonso and Liu [26] developed and validated a massively parallel flow solver for turbomachinery. The unsteady Reynolds-averaged Navier–Stokes equations were solved using a cell centered discretization on arbitrary multiblock meshes. The solution procedure was based on efficient explicit Runge–

Kutta methods with several convergence acceleration techniques such as multigrid, implicit residual smoothing, and local time stepping. The solver was parallelized using domain decomposition, a single program multiple data strategy, and the message passing interface standard.

Adamczyk [27] exploited a sequence of three different averaging procedures (in time, space and periodic boundaries) and special "gate functions". The final result was a system of "averaged passage equations" which could be applied to each single blade row. In these equations some additional terms are included as a consequence of the averaging procedure and represent the effect of unsteadiness on the average flow field.

Whitehead, Crawley and Hall [28] worked on the quasi unsteady modeling. Most of these approaches were derived from the small perturbation theory applied in aero elasticity problems. The effects of mutual rotor stator interaction were accounted as a perturbation of a steady solution. The linearization of the Euler equations was applied and a linear system was obtained in which the unknown variables were represented by the parameters of the selected spinning mode.

Giles and Rai [29] introduced the concept of unsteady modeling. The first application of CFD solvers for the unsteady simulation of turbomachinery stages were documented at the end of 80's with their work. The management of space and time periodicity was pursued using a "time inclined computational grid" and the "phase lag" condition. The main advantage of the phase-lagged approach was the possibility to compute a single passage for each row. The unsteady solution was

stored over the entire period on the boundaries of the stator and rotor vanes to ensure the actual periodicity between the two rows.

Erdos and Rusanov [30] suggested different definitions of the 'phase-lag', while recently other CFD approaches have been developed to cope with time dependent flow processes. A straightforward alternative procedure to the Giles method consists in the modification of the actual blade count ratio. Accordingly, a simple arithmetic ratio (like 1:2, 2:3...) was used to lessen the number of periodic blade passages. The predicted amplitude and frequency in the stator/rotor interaction were somewhat changed by the bias enforced in the physical problem.

Ruprecht et al [31] studied the parallel computation of stator and rotor interaction in an axial turbine. Parallelization was obtained by domain decomposition with overlapping meshes. The interaction of rotor and stator was handled by a sliding interface where downstream the node values are interpolated and upstream the flux integrals are exchanged.

Lampart and Gardzilewicz [32] studied the energy conversion in turbomachinery flows. Extremely complex three dimensional geometries were considered. The approach presented enables the injection of the medium at arbitrary velocities and angles, determination of the effect of mixing of injected medium with the main flow which is the main source of entropy creation due to tip leakage and windage flows, secondary flows or separations.

2.2 Probabilistic Analysis:

Engineers always face uncertainties in design, whether it is in the prediction of future loads, variability of material properties or uncertainties in predicting system response under load. For aging structures, probabilistic mechanics provides the means to quantify the safety of the structure. For new design, probabilistic mechanics provides the means to explicitly treat uncertainties to achieve truly optimal design. Probabilistic methods provide the engineer with a way to quantify uncertainties and treat all problem uncertainties consistently. The traditional approach of using arbitrary design safety factors does not provide a means to quantify the design reliability and can sometimes lead to unbalanced designs wherein some components are over designed and some may be under designed.

Different kinds of analyses accounting for uncertainties can be carried out. Second moment analysis aims at characterizing the second-order statistical moments, i.e. means and variances of response quantities (displacements, strain and stress components, etc.) from those of the input variables.

Liu, Belytschko and Mani [33] studied the perturbation method and related the and related the probabilistic methods to the Finite element methods for non-linear structural dynamics. The existing Probabilistic Finite element methods (PFEM) have been applied to solve two kinds of problems:

1. Determination of the response uncertainty in terms of the mean, variance and correlation coefficients.

2. Determination of the probability of failure associated with the prescribed limit states.

The perturbation method has been extensively used in developing PFEM because of its simplicity and versatility. The PFEM was based on the second order perturbation method and has been developed to estimate the statistic moments of the response for linear static problems

Takada [34], and Deodatis and Shinozuka [35] presented the weighted integral method. Stochastic part of element conductivity was represented as a linear combination of number of weighted integrals (NWI) random variables $X_i^{(e)}$ called weighted integrals,

$$\Delta C^{(e)} = \sum_{i=0}^{NWI-1} X_i^{(e)} \Delta C_i^{(e)}.$$

The number of weighted integrals depend on the choice of the finite element. The weighted integrals are generally defined as

$$X_i^{(e)} = \int_{(e)} x^i r(x) dx$$

the element matrices $\Delta C_i^{(e)}$, $i = 1,.....,NWI$ are all deterministic.

Ditlevsen and Madsen [36] described the first order reliability method (FORM) and second order reliability method (SORM) approximations and various simulation methods commonly used in reliability analysis. Because of the typically high level of reliability of civil structures, the failure probability is usually small (in the order of $10^{-2} - 10^{-6}$).

To account for the spatial variability of uncertain quantities (for instance, that of a material property), a characterization in terms of a random field was usually

employed. Through a process of discretization, it was possible to represent the random field by a vector of random variables. One of the methods mentioned above was then used to carry out second-moment or reliability analysis.

Ghanem and Spanos [37] proposed the spectral stochastic finite element method (SSFEM), an approach well suited to analysis involving random fields. It was based on two discretizations of the system of (stochastic) partial differential equations governing the problem under consideration, one in the spatial domain and one in the probabilistic domain. The response (e.g. the random vector of nodal displacements) was cast as series expansion in standard normal random variables. This can be interpreted as an 'intrinsic' representation of the random response, from which quantities such as statistical moments can be computed by post-processing, either analytically or by simulation.

In the past, SSFEM has been applied to various kinds of problems including two-dimensional elasticity [38], soil mechanics [39], and soil dynamics [40]. Waubke first attempted to include material non-linearity such as plasticity. In these applications, the authors computed the coefficients of the series expansion of the response and in most cases post-process the polynomial expression to compute the mean and standard deviation of various response quantities.

A probabilistic design system was developed by Fox [42] at Pratt and Whitney for the purpose of integrating deterministic design methods with probabilistic design techniques. Here, two different approaches were used for estimating uncertainty. A Monte Carlo approach was used on design codes that were judged to run relatively quickly. For more computationally intensive design codes, a second order response

surface model in conjunction with Box-Behnken design experiments was used and then a Monte Carlo simulation was executed. Several researchers at NASA Glenn Research Center have applied the probabilistic design approaches to turbine engines and related systems.

Chamis [43] developed a Probabilistic Structural Analysis Method (PSAM) using different distributions such as the Weibull, normal, log-normal etc. to describe the uncertainties in the structural and load parameters or primitive variables.

Nagpal, Rubinstein and Chamis [44] presented a probabilistic study of turbo pump blades of the Space Shuttle Main Engine (SSME). They found that random variations or uncertainties in geometry have statistically significant influence on the response variable and random variations in material properties have statistically insignificant effects.

Gorla [45] computationally simulated and probabilistically evaluated a combustor liner in view of several uncertainties in the aerodynamic, structural, material and thermal variables that govern the combustor liner.

CHAPTER III

GOVERNING EQUATIONS

The formulation of compressible equations in relative frame coordinate system is presented in this chapter. The equations are developed with an objective to implement these into existing absolute frame code. The current formulation uses the absolute velocity, i.e. velocity with respect to inertial frame to achieve this objective.

The vector invariant form of the Navier Stokes Equations in a rotating frame with rotational speed vector of Ω is

$$\frac{\partial \rho \underset{\sim}{v}}{\partial t} + div\left(\rho \underset{\sim}{v}\,\underset{\sim}{v}\right) + \rho \underset{\sim}{A} = div\left(\tilde{T}\right) + \rho \underset{\sim}{f} \tag{3.1}$$

$$\underset{\sim}{A} = 2\underset{\sim}{\Omega} \times \underset{\sim}{v} + \underset{\sim}{\Omega} \times \left(\underset{\sim}{\Omega} \times \underset{\sim}{r}\right) + \underset{\sim}{\Omega} \times \underset{\sim}{r}$$

where $\underset{\sim}{v}$ and $\underset{\sim}{r}$ are the velocity and position vectors relating to the rotating frame. $\tilde{T}$ is the viscous stress tensor and $\underset{\sim}{f}$ is the body force vector. Expanding equation. (3.1) together with the continuity and energy equations in a rotating Cartesian coordinates as shown below.

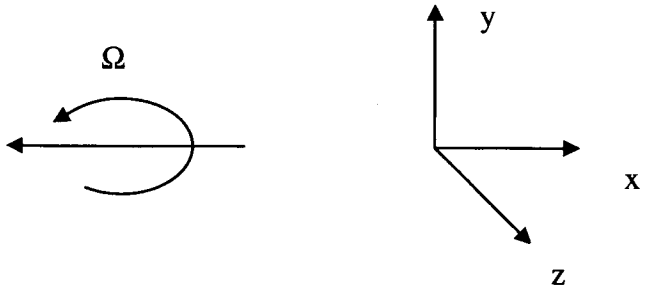

Figure 3.1

where y and z axes rotate about the x axis at a constant speed Ω results in

$$\frac{\partial q}{\partial t}+\frac{\partial f}{\partial x}+\frac{\partial g}{\partial y}+\frac{\partial h}{\partial z}=\frac{\partial f_v}{\partial x}+\frac{\partial g_v}{\partial y}+\frac{\partial h_v}{\partial z}+S \tag{3.2}$$

where

$$q=\begin{bmatrix}\rho\\ \rho u_r\\ \rho v_r\\ \rho w_r\\ \rho E\end{bmatrix},\ f=\begin{bmatrix}\rho u_r\\ \rho u_r^2+p\\ \rho u_r v_r\\ \rho u_r w_r\\ \rho u_r H\end{bmatrix},\ g=\begin{bmatrix}\rho v_r\\ \rho v_r u_r\\ \rho v_r^2+p\\ \rho v_r w_r\\ \rho v_r H\end{bmatrix},\ g=\begin{bmatrix}\rho w_r\\ \rho w_r u_r\\ \rho w_r v_r\\ \rho v_r^2+p\\ \rho w_r H\end{bmatrix}$$

$$E = \frac{p}{(\gamma-1)\rho} + \frac{1}{2}\left(u_r^2 + v_r^2 + w_r^2\right) - \frac{1}{2}\left(v_\Omega^2 + w_\Omega^2\right)$$

$$H = E + \frac{p}{\rho}, v_\Omega = \Omega z, w_\Omega = -\Omega y$$

and

$$f_v = \begin{bmatrix} 0 \\ \tau_{xx} \\ \tau_{xy} \\ \tau_{xz} \\ Q_x \end{bmatrix}, g_v = \begin{bmatrix} 0 \\ \tau_{yx} \\ \tau_{yy} \\ \tau_{yz} \\ Q_y \end{bmatrix}, h_v = \begin{bmatrix} 0 \\ \tau_{zx} \\ \tau_{zy} \\ \tau_{zz} \\ Q_z \end{bmatrix}$$

with

$$Q_x = u_r\tau_{xx} + v_r\tau_{xy} + w_r\tau_{xz} - q_x$$
$$Q_y = u_r\tau_{yx} + v_r\tau_{yy} + w_r\tau_{yz} - q_y$$
$$Q_z = u_r\tau_{zx} + v_r\tau_{zy} + w_r\tau_{zz} - q_z$$

and

$$S = \begin{bmatrix} 0 \\ 0 \\ \rho\Omega^2 y - 2\rho\Omega w_r \\ \rho\Omega^2 z + 2\rho\Omega v_r \\ 0 \end{bmatrix}$$

Equation (3.2) is the vector form of the governing equations with the velocity components relative to a rotating frame. We now consider the following velocity transformation. This objective can be achieved by considering a velocity

transformation. At every point $\underset{\sim}{r}$ ($\underset{\sim}{r}$ being the position vector to the rotating frame), define the velocity vector as $\underset{\sim}{V}$

$$\underset{\sim}{V} = \underset{\sim}{V}_r + \underset{\sim}{\Omega} \times \underset{\sim}{r}$$

i.e.

$$\begin{aligned} u &= u_r & & & u_r &= u \\ v &= v_r + \Omega z & & \Rightarrow & v_r &= v - \Omega z \\ w &= w_r - \Omega y & & & w_r &= w + \Omega z \end{aligned}$$

Notice that the components of this velocity vector (u, v, w) are the quantities with respect to the rotating frame. At some instant in time, the rotating frame matches the fixed frame. It is at this instant that one can choose the same Cartesian coordinates to specify the unit vectors of both the frames. Therefore the velocity vector (u, v, w) is exactly the same as one would see with respect to the fixed frame. It is for this reason that (u, v, w) can be thought as the absolute velocity even though it is viewed from the rotating frame.

After the velocity transformation, Equation. (3.2) becomes

$$\frac{\partial q}{\partial t} + \frac{\partial f}{\partial x} + \frac{\partial}{\partial y}(g - \Omega z q) + \frac{\partial}{\partial z}(h + \Omega y q) = \frac{\partial f_v}{\partial x} + \frac{\partial g_v}{\partial y} + \frac{\partial h_v}{\partial z} + S \qquad (3.3)$$

where

$$q = \begin{bmatrix} \rho \\ \rho u \\ \rho v \\ \rho w \\ \rho E \end{bmatrix}, \; f = \begin{bmatrix} \rho u \\ \rho u^2 + p \\ \rho uv \\ \rho uw \\ u(e+p) \end{bmatrix}, \; g = \begin{bmatrix} \rho v \\ \rho vu \\ \rho v^2 + p \\ \rho vw \\ v(e+p) \end{bmatrix}, \; h = \begin{bmatrix} \rho w \\ \rho wu \\ \rho wv \\ \rho w^2 + p \\ w(e+p) \end{bmatrix}$$

and

$$f_v = \begin{bmatrix} 0 \\ \tau_{xx} \\ \tau_{xy} \\ \tau_{xz} \\ Q_x \end{bmatrix}, g_v = \begin{bmatrix} 0 \\ \tau_{yx} \\ \tau_{yy} \\ \tau_{yz} \\ Q_y \end{bmatrix}, h_v = \begin{bmatrix} 0 \\ \tau_{zx} \\ \tau_{zy} \\ \tau_{zz} \\ Q_z \end{bmatrix}$$

with

$$\begin{aligned} Q_x &= u\tau_{xx} + v\tau_{xy} + w\tau_{xz} - q_x \\ Q_y &= u\tau_{yx} + v\tau_{yy} + w\tau_{yz} - q_y \\ Q_z &= u\tau_{zx} + v\tau_{zy} + w\tau_{zz} - q_z \end{aligned}$$

and

$$S = \begin{bmatrix} 0 \\ 0 \\ -\rho w\Omega \\ \rho v\Omega \\ 0 \end{bmatrix}$$

$e = \dfrac{p}{(\gamma-1)\rho} + \dfrac{1}{2}\left(u_r^2 + v_r^2 + w_r^2\right) - \dfrac{1}{2}\left(v_\Omega^2 + w_\Omega^2\right)$ is the total energy per unit

volume.

The viscous flux terms do not change their forms as a result of the transformation. Comparing equation no. (3.3) with the original fixed frame formulation, one can see that the differences are the additional source term on the right hand side and the extra flux terms associated with the rotational motion on the left hand side. Equation (3.3) is the formulation of the Navier Stokes Equation written in a rotating frame while using the components of the absolute velocity. Another point worth noting is that even though emphasis has been placed on achieving a steady state solution with this formulation, there is nothing in the formulation per se that prevents it from being used to compute unsteady flows relative to a rotating frame.

A curvilinear coordinate transformation is used to facilitate the numerical computation of the governing equations on a body- conforming grid. This transformation can be performed on either static or dynamic grid. To simplify the problem, a static grid is used here.

$$t = \tau$$

$$x = x(\xi, \eta, \zeta)$$

$$y = y(\xi, \eta, \zeta)$$

$$z = z(\xi, \eta, \zeta)$$

where ξ is the streamwise, η is the spanwise, and ζ the pitchwise directions. As no solid interface is encountered in the stream wise direction, viscous terms in the ξ direction are neglected. The resulting curvilinear formulation is

$$\frac{\partial Q}{\partial \tau}+\frac{\partial F}{\partial \xi}+\frac{\partial G}{\partial \eta}+\frac{\partial H}{\partial \zeta}=\frac{\partial G_v}{\partial \eta}+\frac{\partial H_v}{\partial \zeta}+S \tag{3.4}$$

$$Q=J\begin{bmatrix}\rho\\ \rho u\\ \rho v\\ \rho w\\ \rho e\end{bmatrix},\ \overline{K}=J\begin{bmatrix}\rho K^{'}\\ \rho u K^{'}+k_x p\\ \rho v K^{'}+k_y p\\ \rho w K^{'}+k_z p\\ e K^{'}+pK\end{bmatrix},\ S=\begin{bmatrix}0\\ 0\\ -\rho w\Omega\\ \rho v\Omega\\ 0\end{bmatrix}$$

where

$$K^{'}=k_x u+k_y(v-\Omega z)+k_z(w+\Omega y)=k_x u+k_y v+k_z w+k_t$$

$$k_t=-k_y\Omega z+k_z\Omega y, K=k_x u+k_y v+k_z w$$

$\overline{K}=F,G,H$ For $k=\xi$, η and ζ respectively.

Here, k_t may be interpreted as the grid speed.

Numerical Method:

The algorithm presented is an implicit finite volume solver designed for general unsteady multiple blade row turbomachinery computations. It solves the thin layer Navier stokes equation in Cartesian coordinate system with all the flow variables with respect to the fixed frame. The k-ε turbulence model was used. The inviscid flux Jacobians were evaluated by flux-vector splitting method. Viscous flux Jacobians were computed numerically. Newton sub-iteration was used to find an

approximate solution to the nonlinear finite volume equation at each time step. Symmetric Gauss-Seidel relaxation is used for matrix inversion.

With the above governing equation formulation in a rotating frame, it becomes very easy to modify the original fixed frame code to a rotating frame code. There are three changes which have to be implemented to solve the above equations. They are

1. To freeze the grid motion
2. to evaluate the grid speed analytically
3. To add the source term explicitly in the flux balance.

No other changes are needed because like in the fixed frame, formulation, absolute velocity is used to each piece of information in the numerical scheme.

CHAPTER IV

VANE AND BLADE CONFIGURATION

4.1 Aerodynamic design:

The flow path for the low pressure turbine component is presented in the figure shown below, showing the turbine elevation and the axial length.

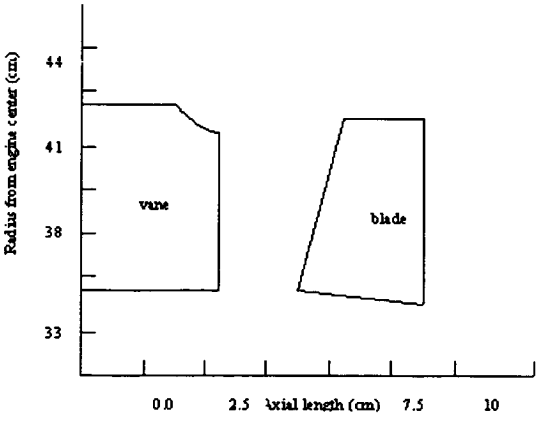

Figure 4.1: Flow path for Stator and Rotor.

The vanes are characterized by aerodynamic sections having blunt leading edge and a long chord with the maximum airfoil thickness near the leading edge. The inner vane end wall is cylindrical, while the outer is contoured in an "S" shape. The large aerodynamic section thickness reduces the losses associated with the introduction of cooling flow and the "S" wall design reduces end wall pressure losses. In addition, the number of vanes minimizes blockage as well as optimizes the positioning of the vanes with the combustor fuel injector nozzles.

The blades are highly tapered with a conical inner wall. Blade axial chord taper was selected to accommodate stress requirements. Also, the stage is defined with a high reaction level to enhance the efficiency. On the basis of design analysis, it was shown that higher reaction levels produced higher efficiencies.

4.2 Airfoil Definition:

Several analytical techniques were used to establish the turbine airfoil definitions. Streamline computer design simulation generated the radial aerodynamic environment. This information serves as input to the interactive airfoil design system for a definition of the exterior contour of the airfoil.

Analysis is then performed to ascertain pressure distribution and boundary layer characteristics. On the basis of these results, iterations of the airfoil shape are made to optimize pressure distribution, boundary layer and low loss characteristics. Using these methods, vane sections were analytically defined. The sections were designed so that the flow accelerated past the throat area with low, smooth backend diffusion. The uncovered turning and exit wedge angle were optimized to minimize

the pressure distribution criteria as the vane. Uncovered turning and exit angle were optimized to reduce blade profile, trailing edge and shock losses.

Figures (4.2 to 4.5) present the airfoil contours of the vane mean, root and tip sections, respectively along with a summary of the section aerodynamics and corresponding static pressure distribution.

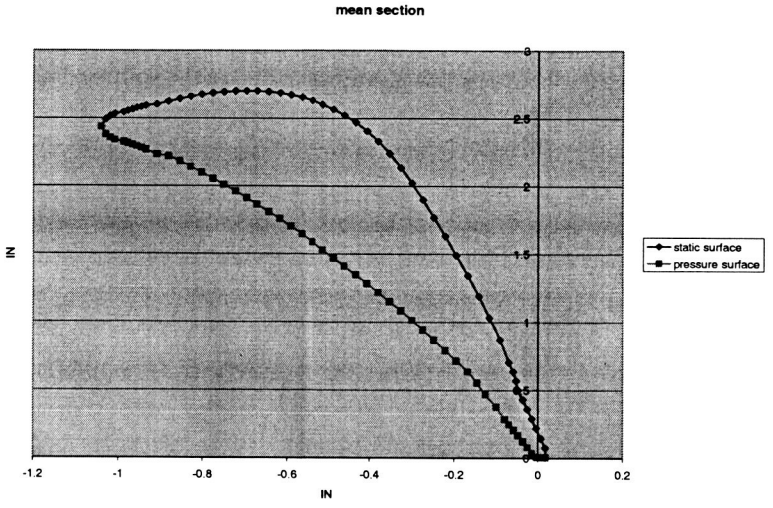

Figure 4.2: Mean section for Stator.

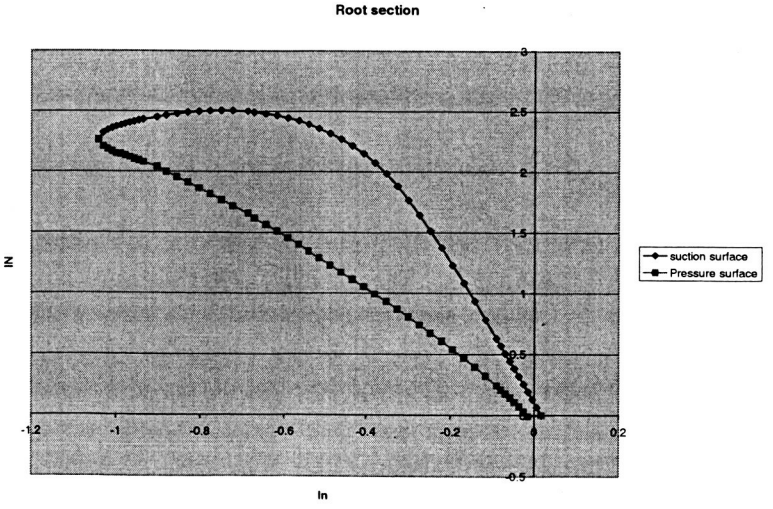

Figure 4.3: Root section for Stator.

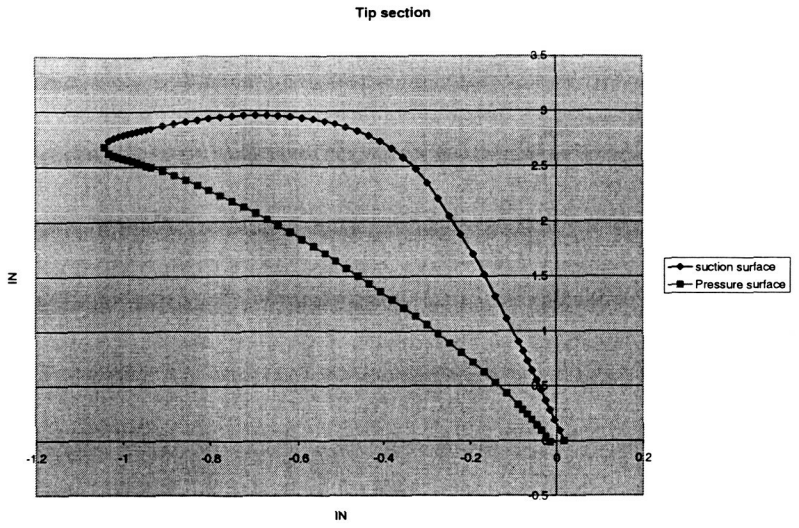

Figure 4.4: Tip section for Stator.

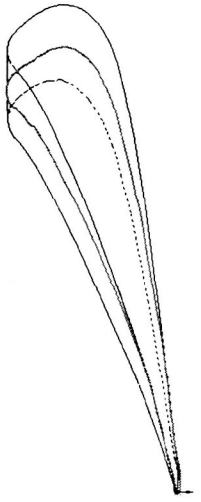

Figure 4.5: Stator stacking for Stator.

The below figure shows blade inlet angle has been adjusted to account for

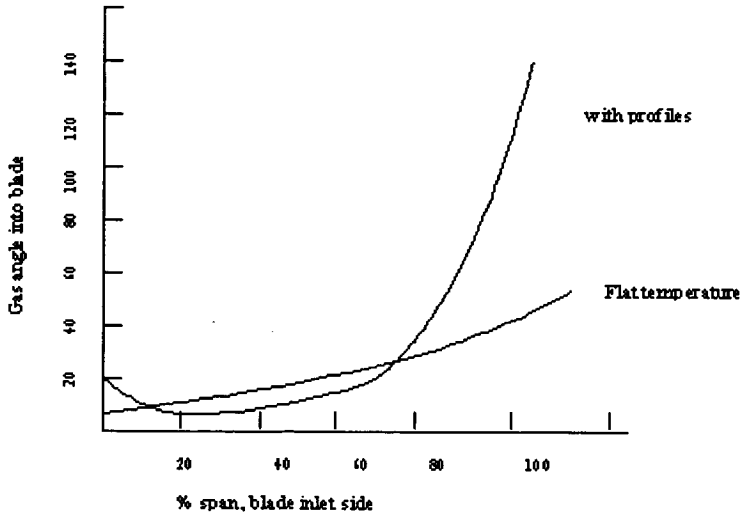

Figure 4.6: Blade inlet angle.

difference between a rig and engine environment. The result is a blade design with the root and tip sections that are under cambered 5 and 10 degrees, respectively, and the mean section is over cambered 8 degrees in comparison to the rig contours.

Similar design information is presented for the blade in the figures (4.7 to 4.10) which represent the mean, root and the tip sections for the rotor. The cross section of the rotor is different from that of the stator as shown in the figures below.

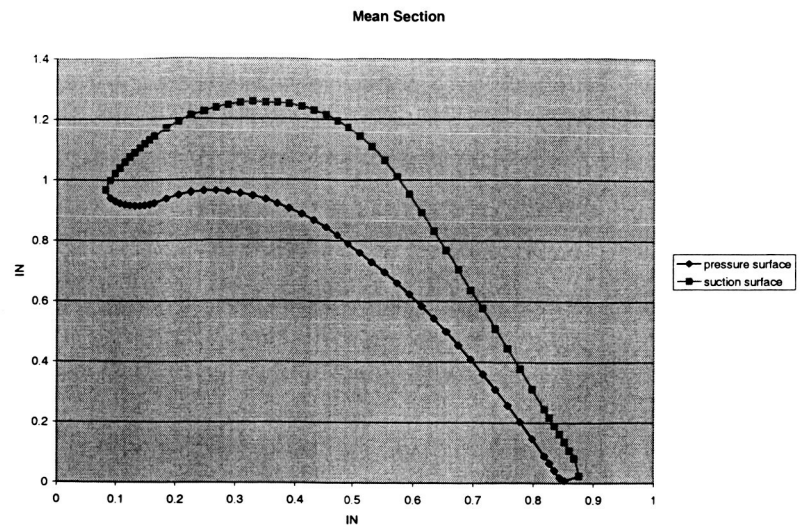

Figure 4.7: Mean section for Rotor.

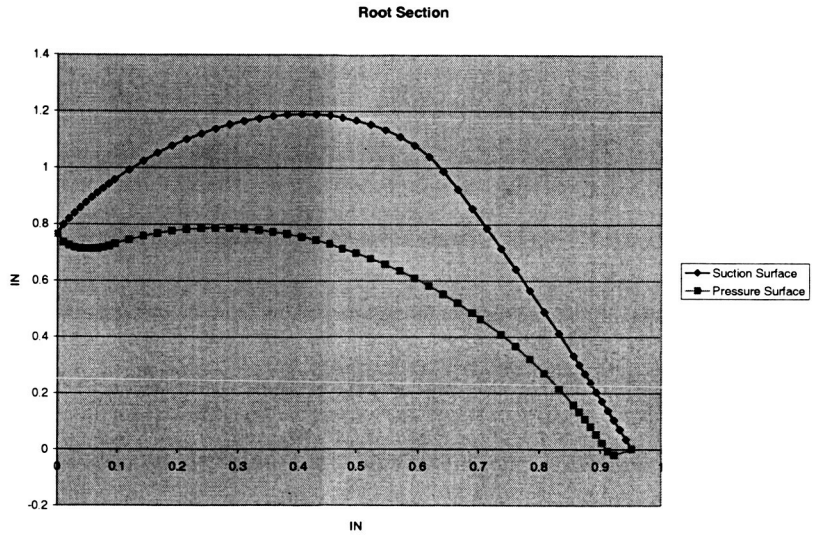

Figure 4.8: Root section for Rotor.

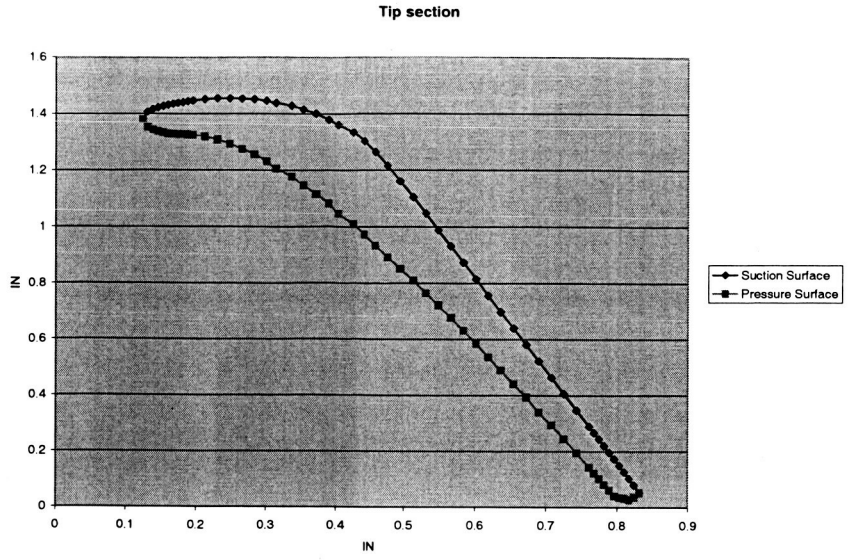

Figure 4.9: Tip Section for Rotor.

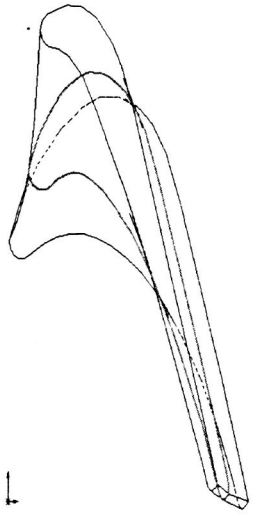

Figure 4.10: Rotor Stacking for Rotor.

4.3 Airfoil Durability:

The Low pressure turbine design emphasizes operation at a moderately high combustor exit temperature with a minimum of cooling to maximize fuel efficiency. This must be achieved, however with no compromise in the component durability.

Vanes in the Low pressure turbine, as aerodynamically defined, are physically larger than turbine vanes in current gas turbine engines because of the selection of a low number of airfoils. This increases vane surface area and causes inherently longer surfaces that must be cooled. In turn longer surfaces necessitate a greater number of film cooling rows to maintain acceptable metal surface temperature levels.

4.4 Vane Materials:

A summary of the vane coating and materials is given in the table below. The base alloy is SC 2000 nickel base single crystal material, which affords both high strength and high temperature capability. For the integrated core, vanes will be fabricated from PWA 1480 single crystal material. This material provides an approximate 10°C metal temperature advantage over directionally solidified material used for the turbine airfoils. The external temperature of the airfoil is coated with an oxidation-erosion resistant coating (NICoCr Alloy). A thermal barrier coating (PWA 264) is also applied to the hot gas surface of the platform.

Table 4.1: Summary of Vane Materials

	Flight propulsion system	Integrated core/Low
Base alloy	SC 2000 (Advanced single crystal)	PWA 1480 (Single crystal)
External coating	PWA 286 (Advanced NiCoCrA1Y Overlay)	PWA 270 (NiCoCrA1Y)
Internal coating	PWA 275 (Aluminide)	None
Platform coating	TBC 100	PWA 264

4.5 Blade Materials:

A summary of the blade materials and coatings selected for the turbine blade is presented in the table below. For both applications, the base materials and coatings are the same as for the turbine vane. The base material is an advanced nickel base single crystal alloy and the blade is coated with an advanced oxidation resistant coating. The major difference is that a thermal barrier coating on the platform is not required.

Table: 4.2: Summary of Blade Materials

	Flight propulsion system	Integrated core/Low
Base alloy	SC 2000 (Advanced single crystal)	PWA 1480 (Single crystal)
External coating	PWA 286 (Advanced NiCoCrA1Y)	PWA 270 (NiCoCrA1Y)
Internal coating	PWA 275 (Aluminide)	None

In the present study, an efficient, portable, scalable parallel methodology is developed for the production version of TURBO. The basic parallel implementation is well described in the literature survey. The two scalable treatments are developed for data communication associated with the sliding interface between blade rows, one for full-simulation case and other for phase-lag approximation.

CHAPTER V

RESULTS AND DISCUSSION OF THE AERODYNAMIC DATA:

The results for the aerodynamic analysis are presented below; the parallel version of the MSU-TURBO was used to compute the aerodynamic results.

In the present situation, the hot case is considered where the working temperatures are very high. Hot case corresponds to air temperature of approximately 1100° C at the inlet of the stator.

The graphs shown below are for the mean line case, at the mid span of the vane and blade cross section. The variation of the Temperatures and Pressures for different iterations and at different chord length is shown.

Figures 5.1-5.4 show the distribution of temperature and pressure over the suction surface. The maximum static pressure on the suction surface was 177175.0 N/m^2 and maximum static temperature on the suction surface was $1101.48\,^0C$.

Figures 5.5-5.8 shows the graphs for the pressure and temperature distribution across the % chord length over the pressure surfaces for the stator. The maximum value of static pressure for the pressure surface was $177167.90\,N/m^2$ and

the maximum static temperature was $1101.34\,^{0}C$. The values of temperature and pressures obtained from the aerodynamic results were used to find the thermal stresses and also the structural analysis.

Figures 5.9-5.12 shows the pressure and temperature distribution on the suction surface of the rotor. In case of the rotor the maximum value of static pressure on the suction side was found to be $175620.32\,N/m^2$ and the maximum static temperature was $1077.75\ ^{0}C$

Figures 5.13-5.16 shows the distribution of the pressure and temperature for the rotor pressure surface across the % chord length for different iterations i.e. from 1900 to 2000. The maximum value of static pressure on the pressure surface of the rotor was found to be $175514.68\ N/m^2$ and maximum value of static temperature on the pressure side was $1073.49\,^{0}C$.

Figures 5.19-5.26 shows the distribution of the unsteady pressure coefficient and distribution of phase angles across the percentage chord length for the stator and rotor on the suction and pressure surface. MATLAB was used to plot the amplitudes of the unsteady pressure coefficient and phase angles. All the pressure values were taken and then FFT method was used to calculate the real and imaginary parts. The maximum values in all the cases and for all the iterations were taken and then they were plotted separately. The real values plotted across the % chord length represent the amplitude of the unsteady pressure coefficient and the imaginary values plotted across the % chord length represent the phase angles.

5.1 Stator suction surface graphs for the hot Case:

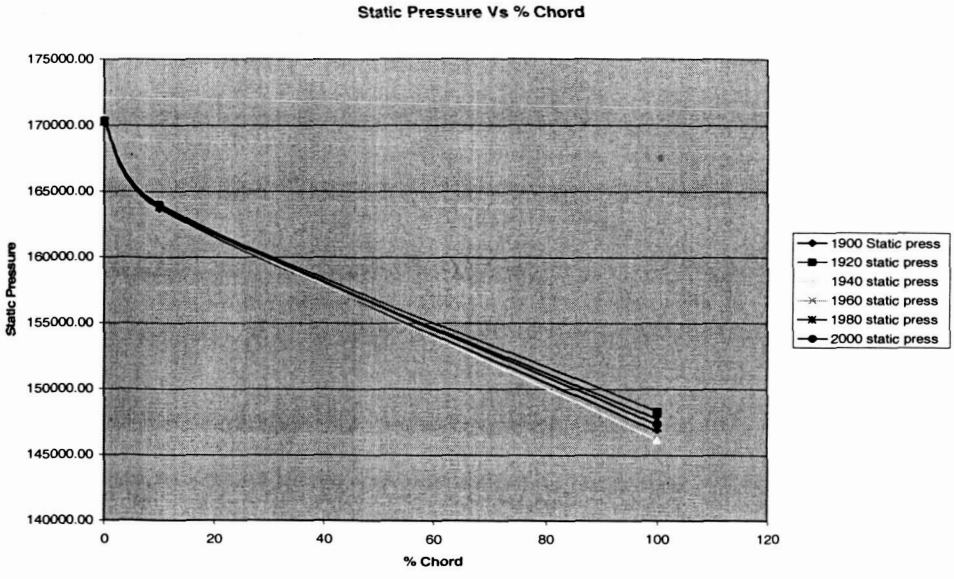

Figure 5.1: Stator suction surface static pressure vs. % chord length.

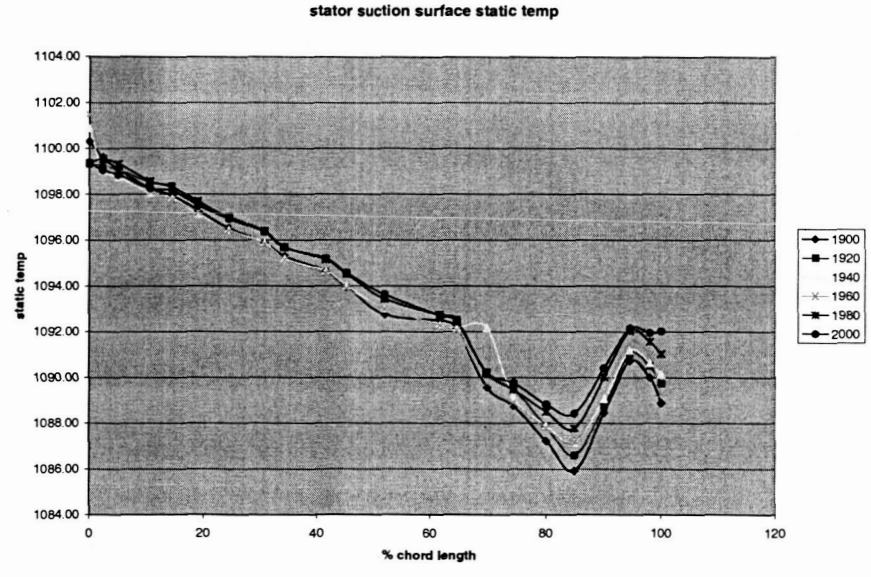

Figure 5.2: Stator suction surface static temperature vs. % chord length

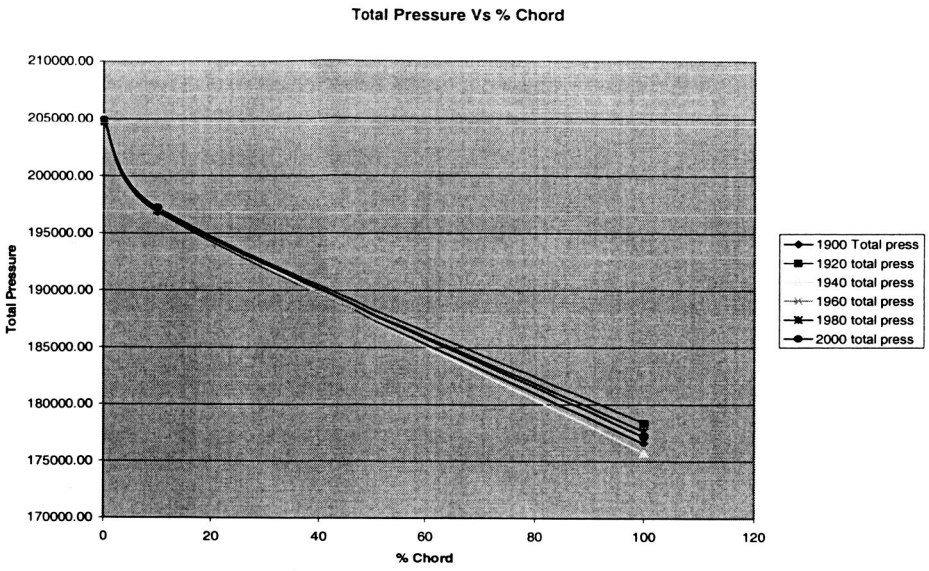

Figure 5.3: Stator suction surface total pressure vs. % chord length.

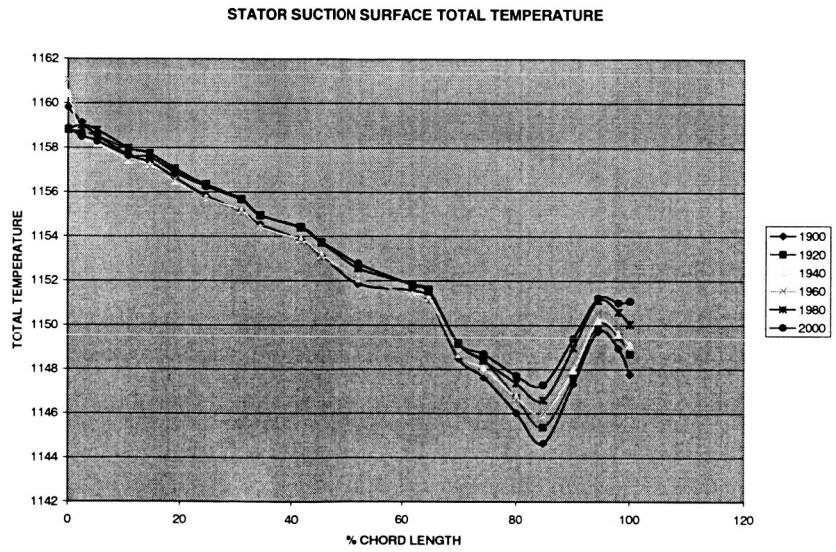

Figure 5.4: Stator suction surface total temperature vs. % chord length

5.2 Stator pressure surface graphs for hot case:

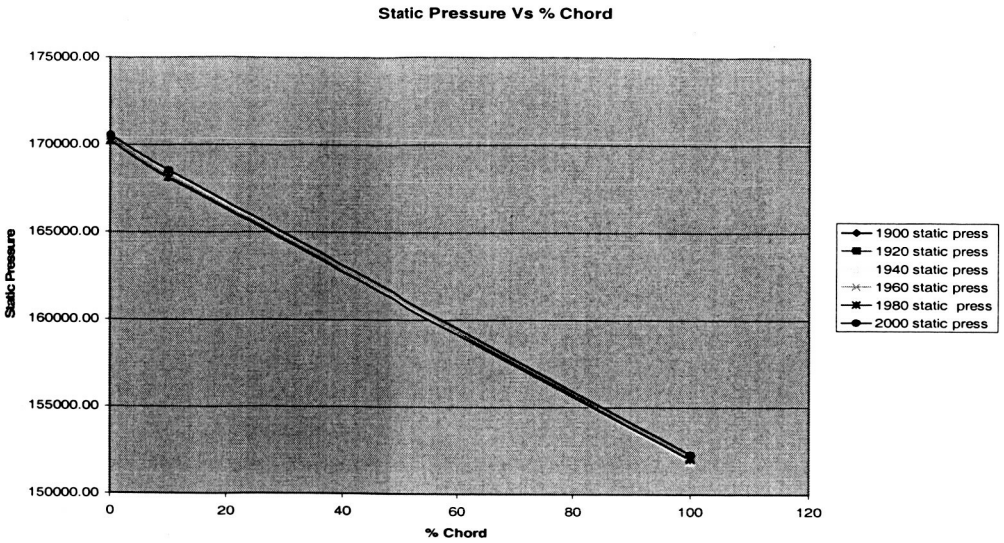

Figure 5.5: Stator pressure surface static pressure vs. % chord length.

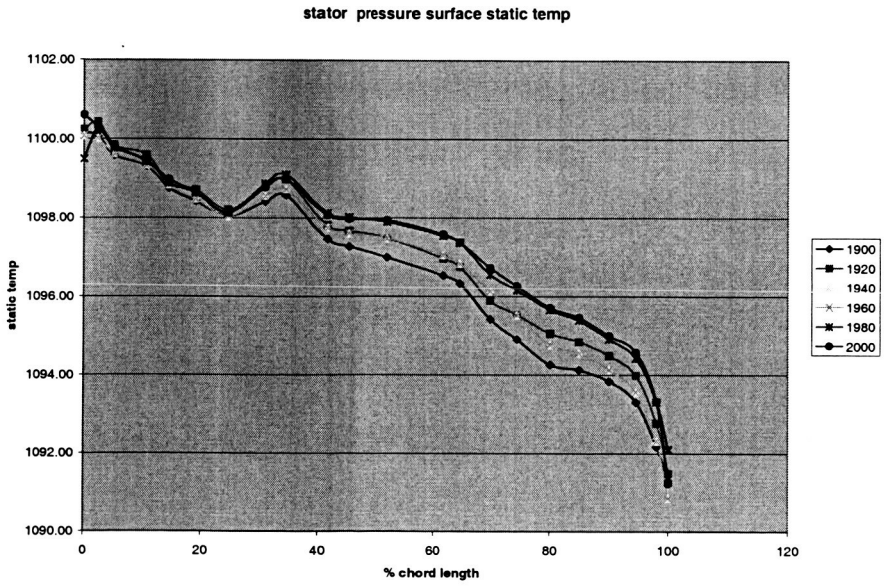

Figure 5.6: Stator pressure surface static temperature vs. % chord length

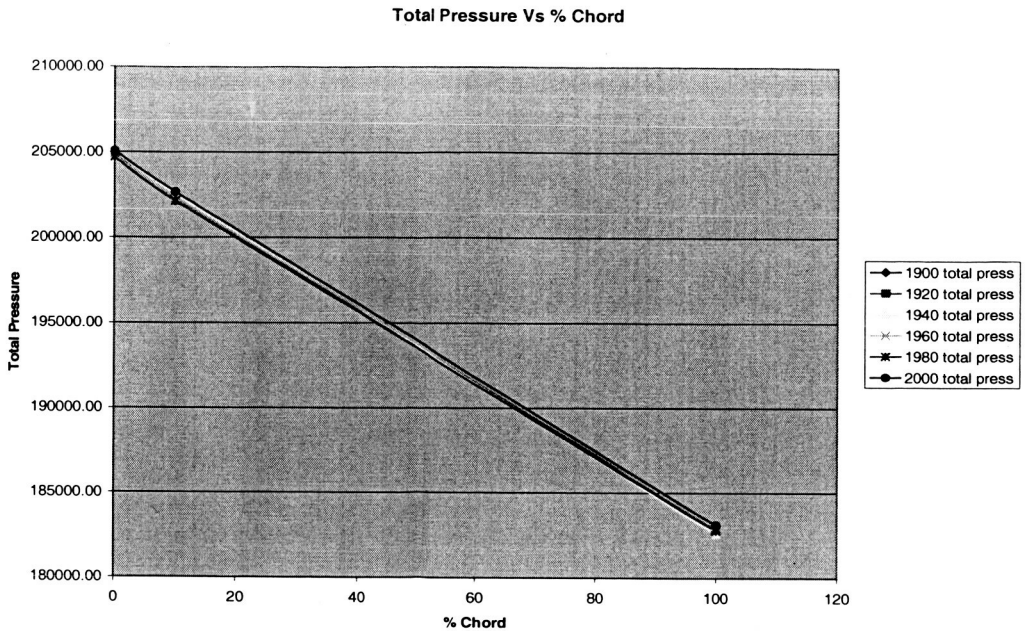

Figure 5.7: Stator pressure surface total pressure vs. % chord length.

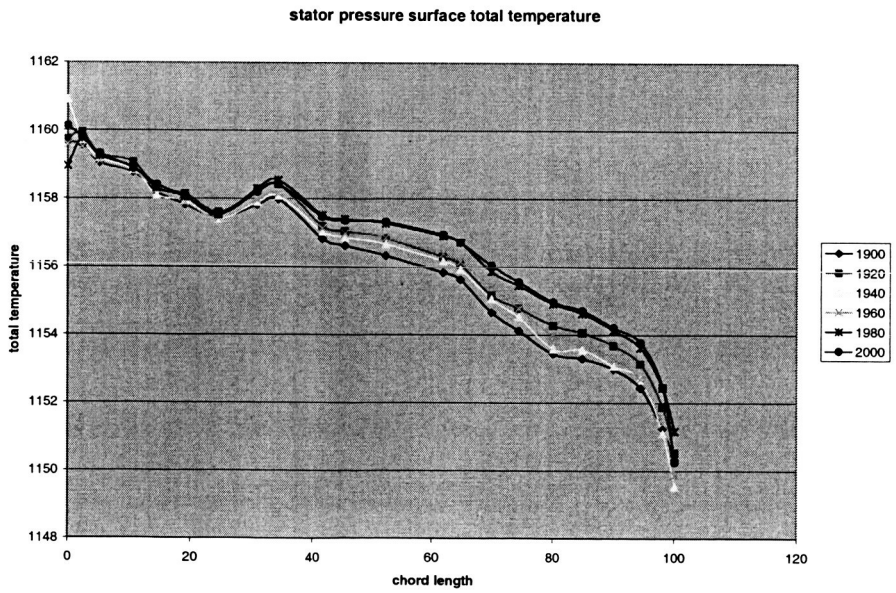

Figure 5.8: Stator pressure surface total temperature vs. % chord length

5.3 Rotor suction surface graphs for the hot case:

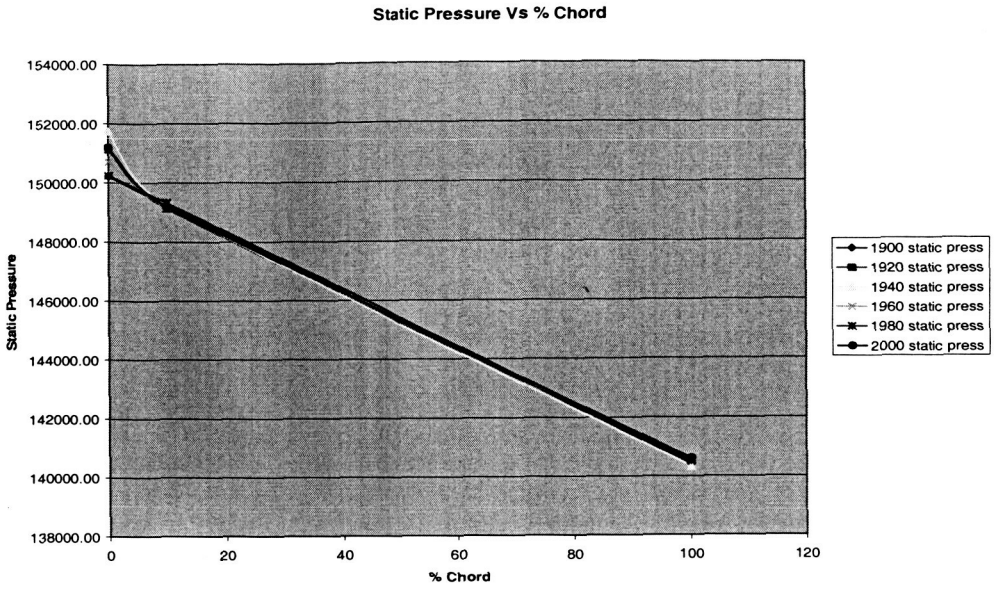

Figure 5.9: Rotor suction surface static pressure vs. % chord length.

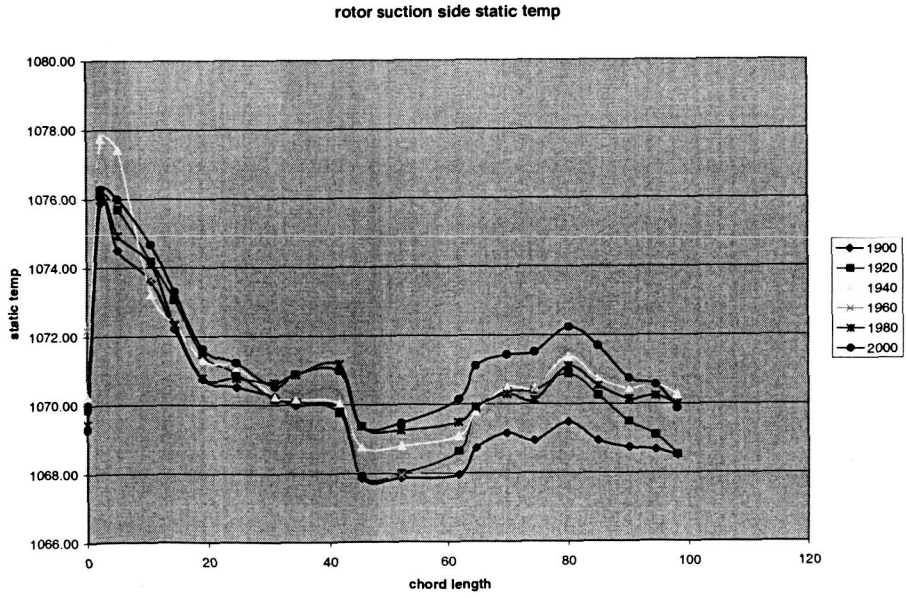

Figure 5.10: Rotor suction surface static temperature vs. % chord length

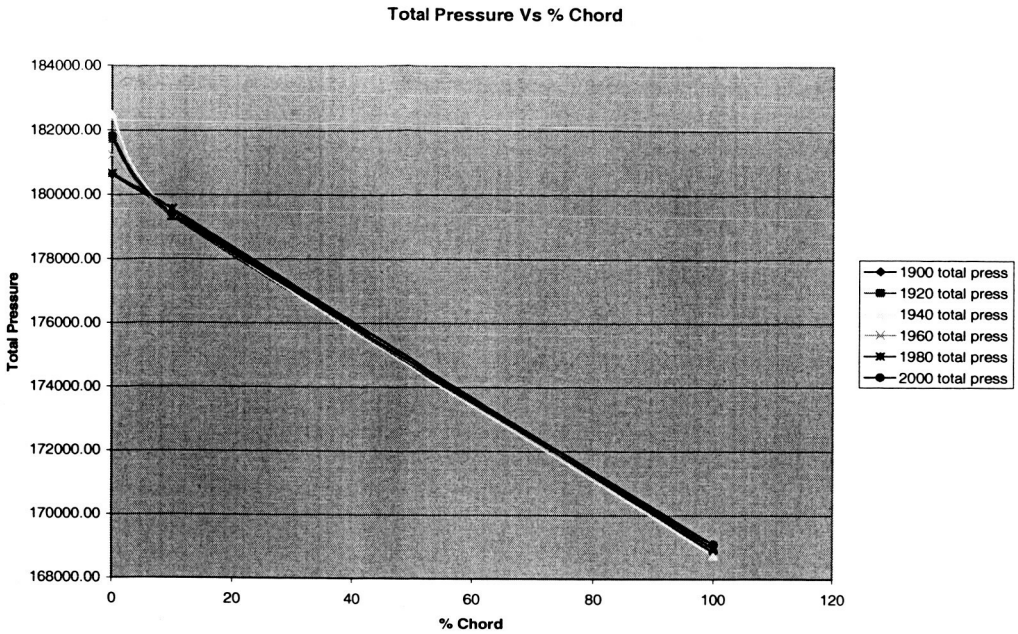

Figure 5.11: Rotor suction surface total pressure vs. % chord length.

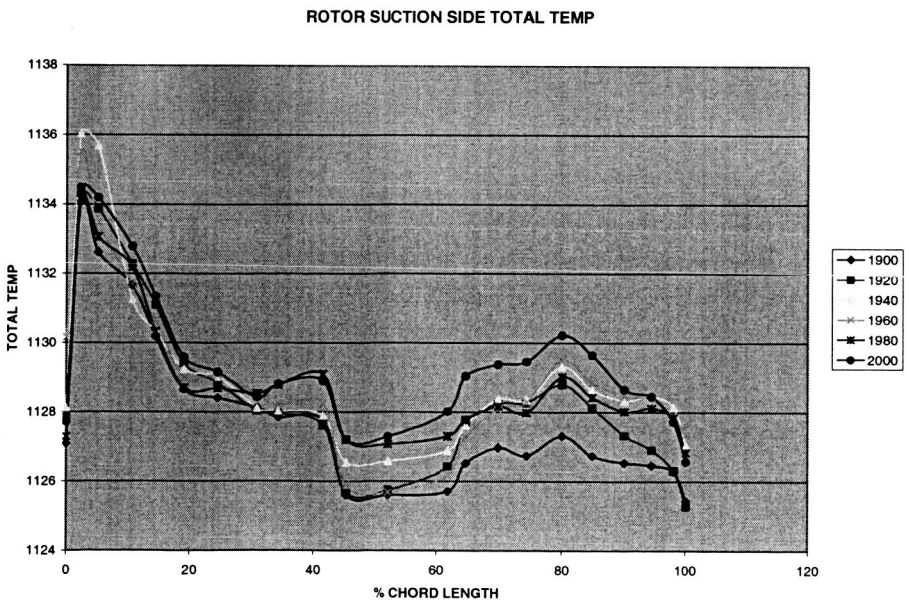

Figure 5.12: Rotor suction surface total temperature vs. % chord length

5.4 Rotor pressure surface graphs for the hot case:

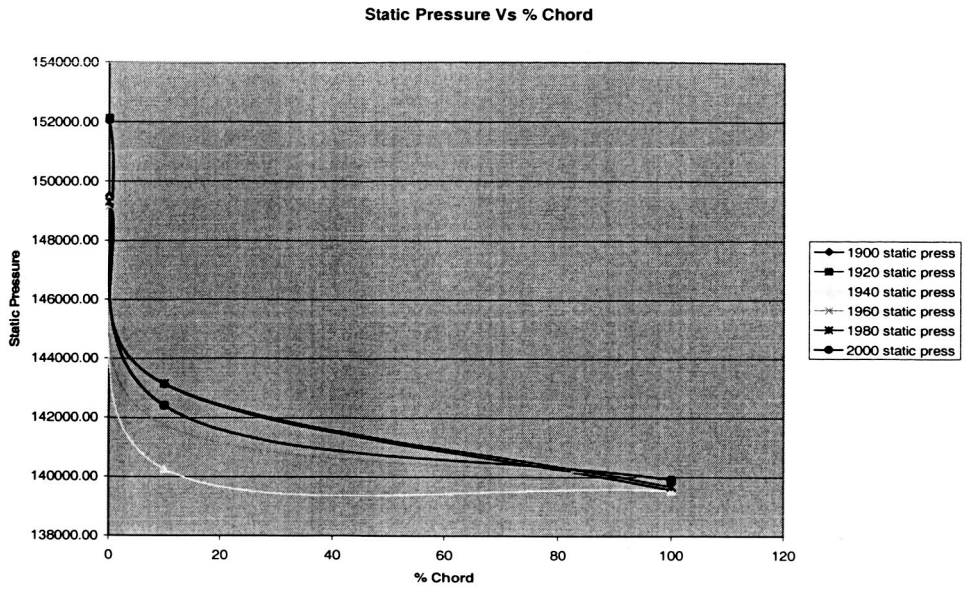

Figure 5.13: Rotor pressure surface static pressure vs. % chord length.

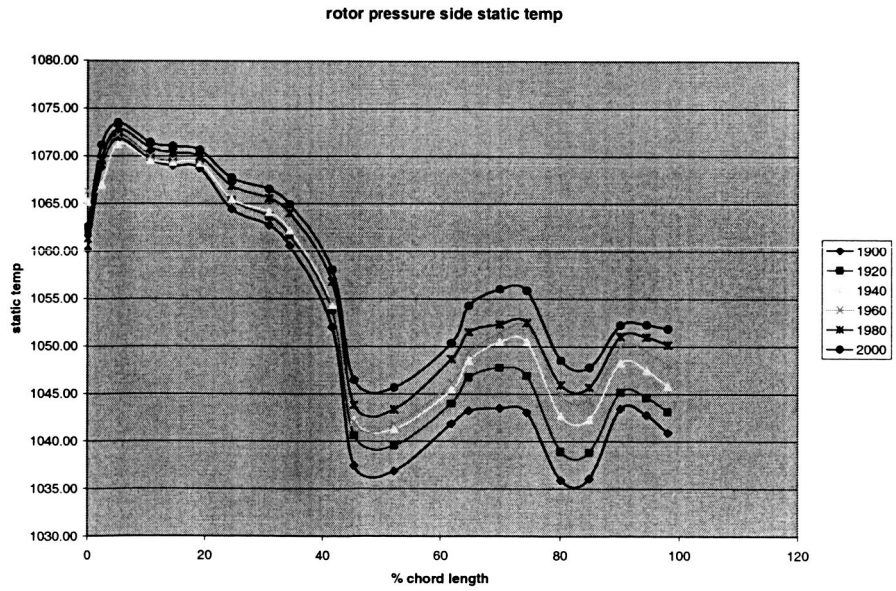

Figure 5.14: Rotor pressure surface static temperature vs. % chord length

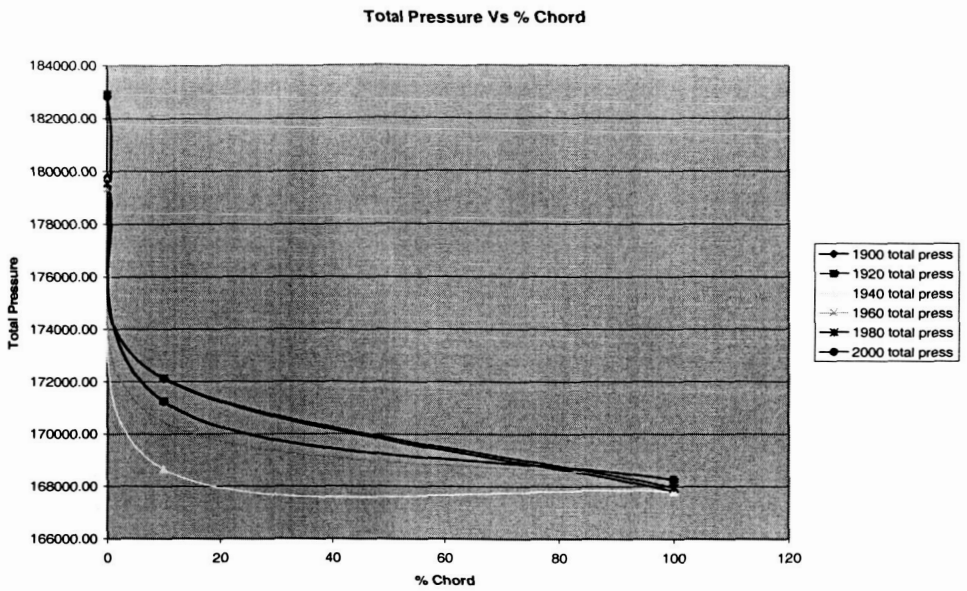

Figure 5.15: Rotor pressure surface total pressure vs. % chord length.

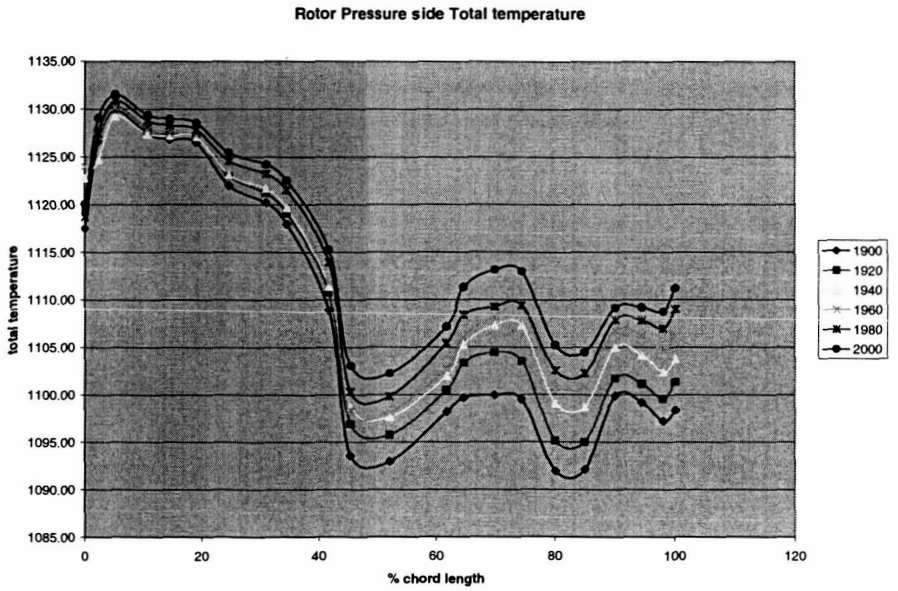

Figure 5.16: Rotor pressure surface total temperature vs. % chord length

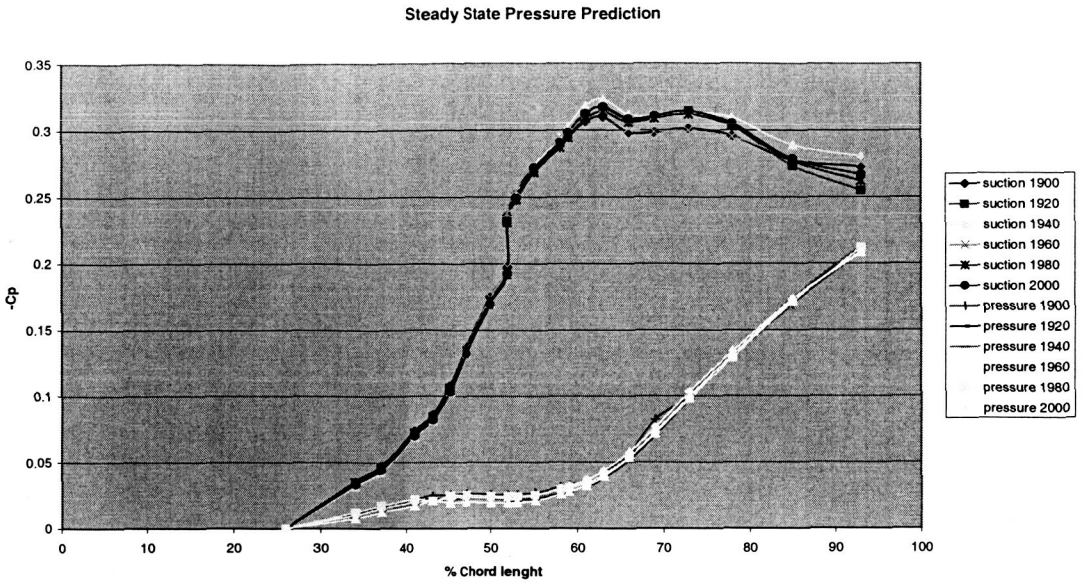

Figure 5.17: Stator $C_P(vs)\%chord$

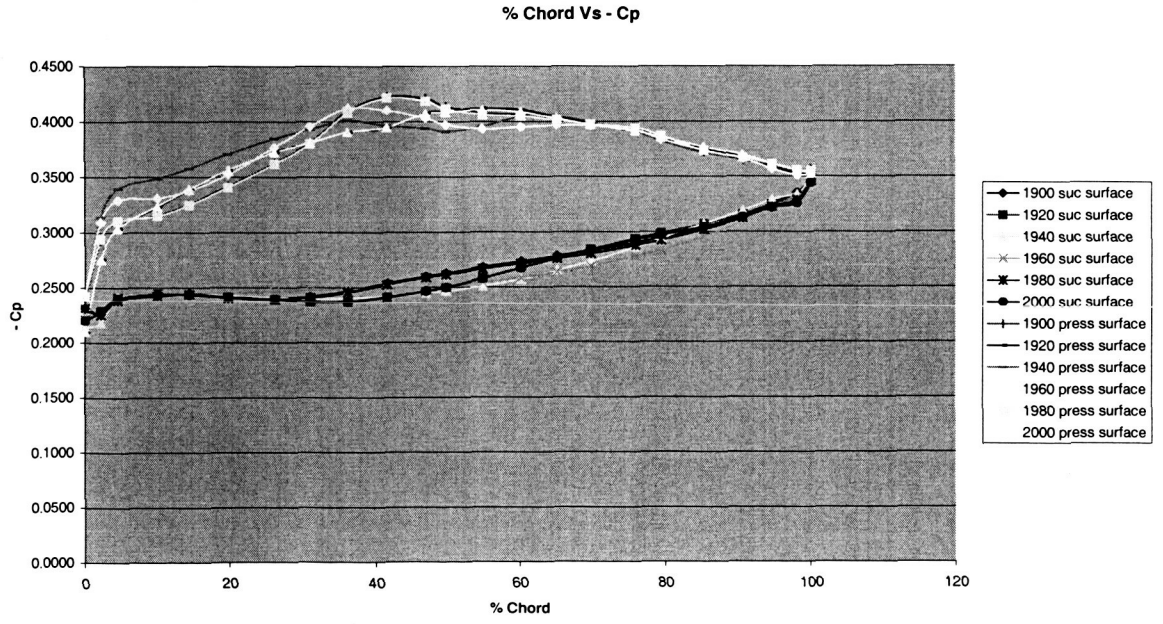

Figure 5.18: Rotor $C_P(vs)\%chord$

5.5 Amplitude of unsteady pressure coefficient and phase angle distribution for stator suction surface:

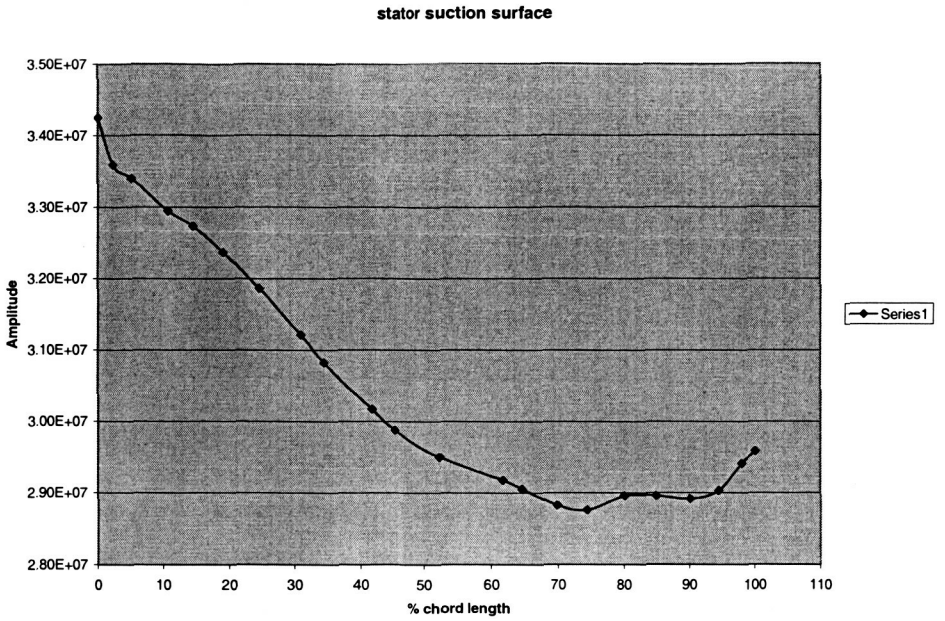

Figure 19: Stator suction surface pressure amplitude vs. % chord length

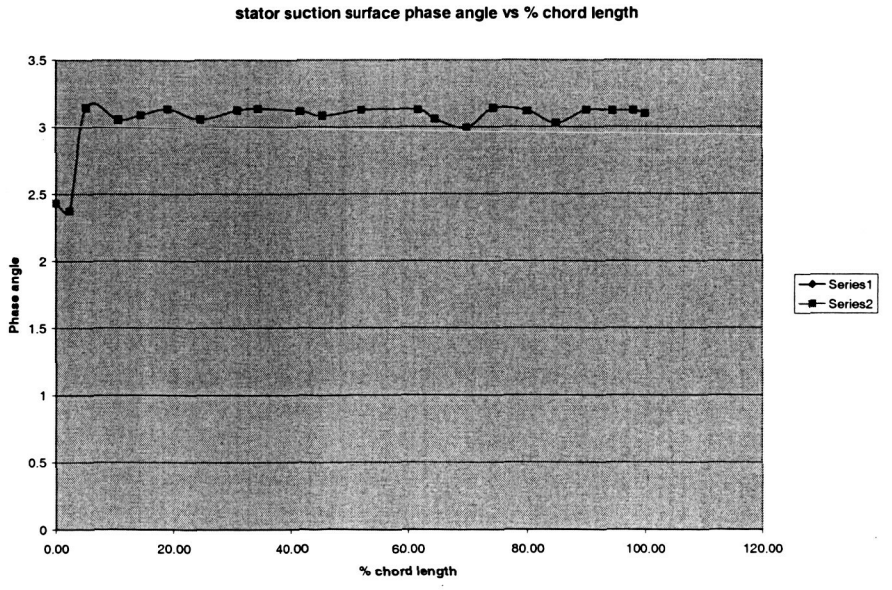

Figure 5.20 Stator suction surface phase angle vs. % chord length

5.6 Amplitude of unsteady pressure coefficient and phase angle distribution for stator pressure surface:

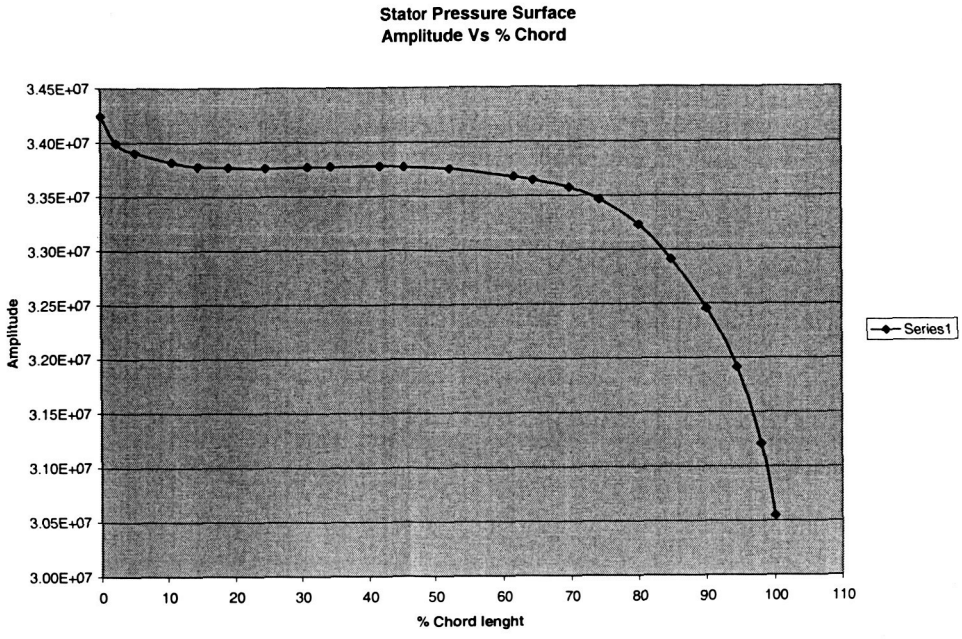

Figure 21: Stator pressure surface pressure amplitude vs. % chord length

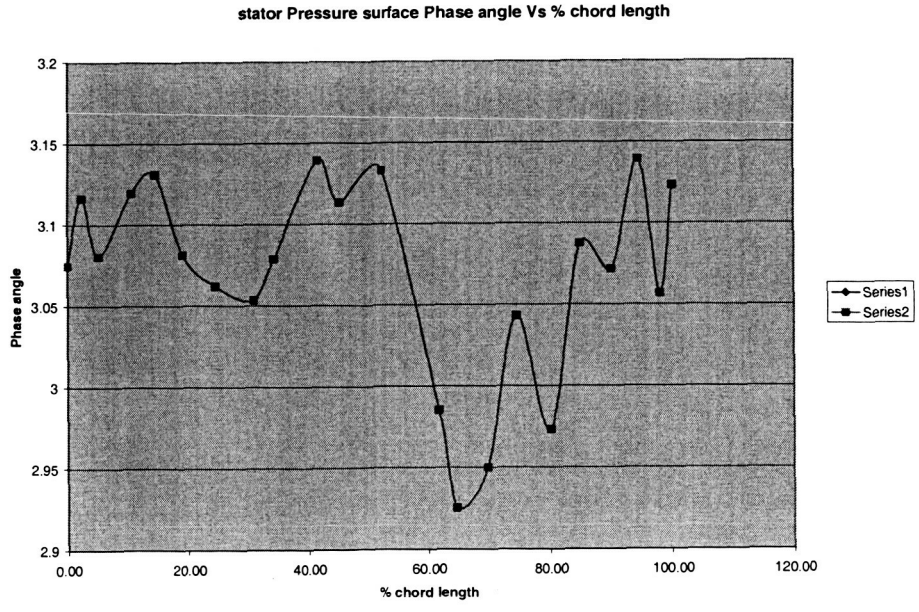

Figure 5.22: Stator pressure surface phase angle vs. % chord length

5.7 Amplitude of unsteady pressure coefficient and phase angle distribution for rotor suction surface:

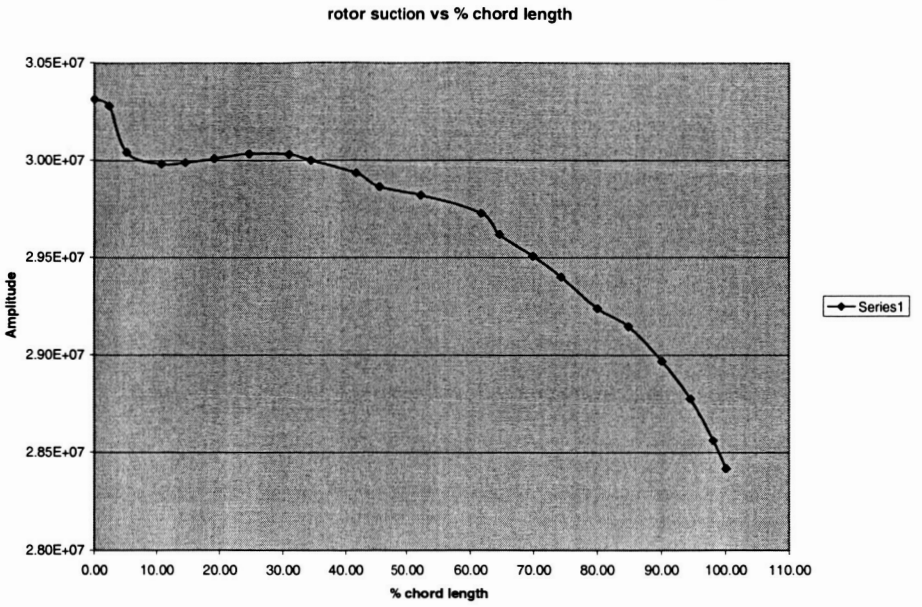

Figure 23: Rotor suction surface pressure amplitude vs. % chord length

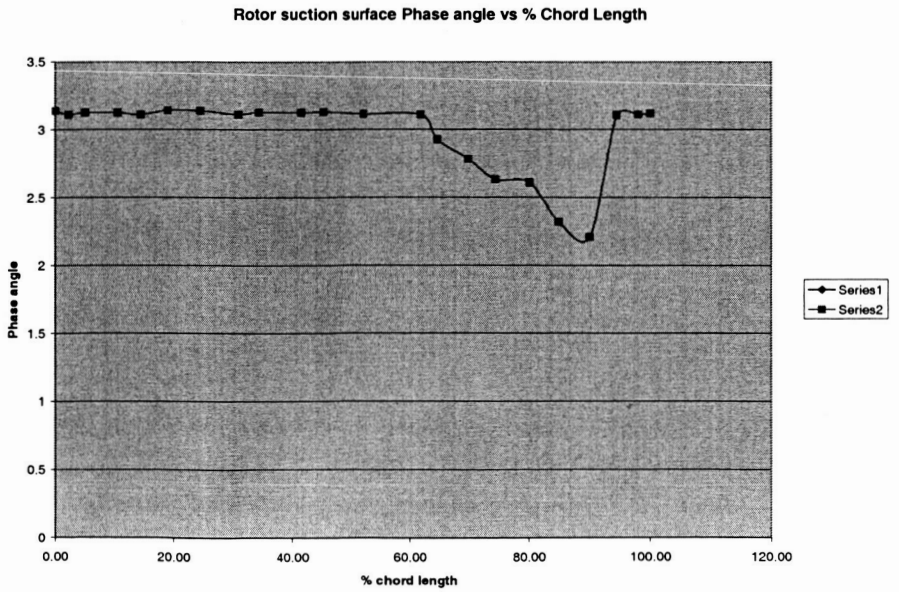

Figure 5.24: Rotor suction surface phase angle vs. % chord length

5.8 Amplitude of unsteady pressure coefficient and phase angle distribution for rotor pressure surface:

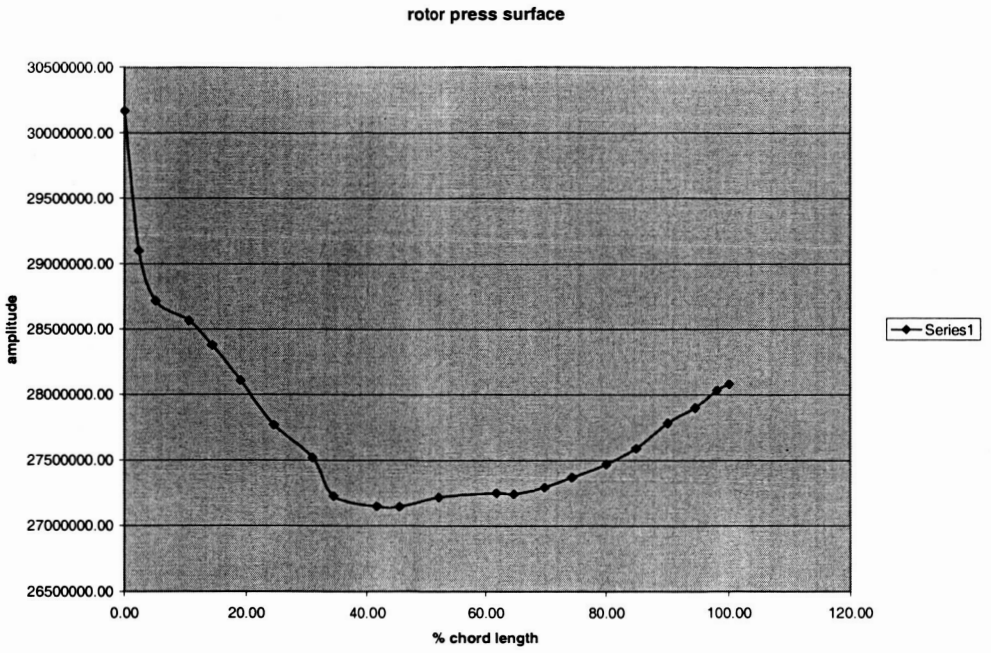

Figure 25: Rotor pressure surface pressure amplitude vs. % chord length

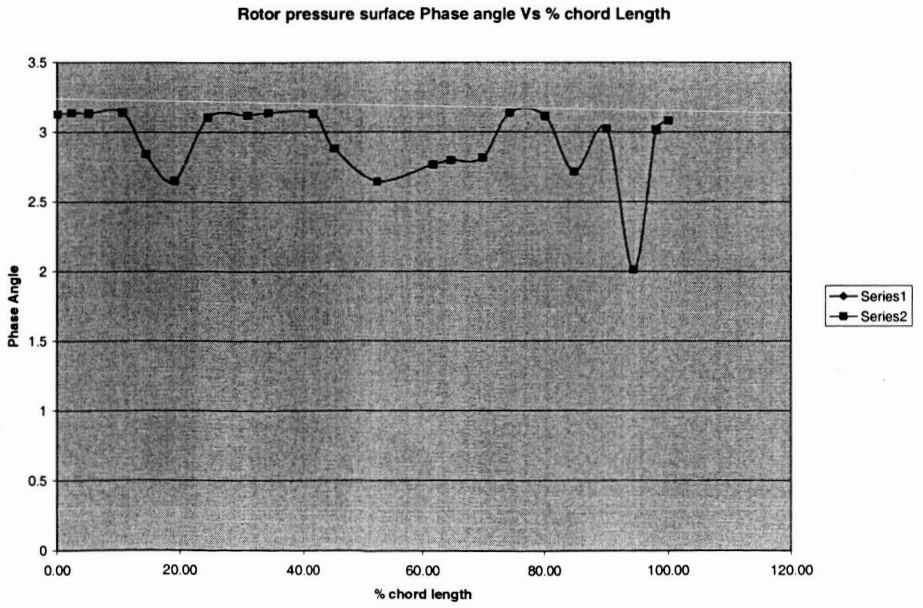

Figure 5.26: Rotor pressure surface phase angle vs. % chord length

CHAPTER VI

FINITE ELEMENT ANALYSIS

Let us consider a two-dimensional partial differential equation of the form

$$\frac{\partial}{\partial x}\left[K_x(x,y)\frac{\partial T}{\partial x}\right]+\frac{\partial}{\partial y}\left[K_y(x,y)\frac{\partial T}{\partial y}\right]+P(x,y)T+Q(x,y)=0. \tag{6.1}$$

The above equation is valid over an area A. We assume that on a portion of the boundary

$$\mathrm{L}_1, \mathrm{T}=\mathrm{T}_0(x,y) \tag{6.2}$$

On the remainder of the boundary, labeled L_2, the general derivative boundary condition is specified in the form

$$K_x(x,y)\frac{\partial T}{\partial X}n_x + K_y(x,y)\frac{\partial T}{\partial y}n_y+ \alpha(x,y)T+\beta(x,y)=0. \tag{6.3}$$

Here, n_x and n_y are direction cosines of the outward normal to L_2. The form of the functional may be written as

$$I(T) = \iint_A \left[\frac{1}{2} K_x \left(\frac{\partial T}{\partial x} \right)^2 + \frac{1}{2} K_y \left(\frac{\partial T}{\partial y} \right)^2 - \frac{1}{2} PT^2 - QT \right] dA + \int_{L_2} \left(\frac{\alpha T^2}{2} + \beta T \right) dL. \tag{6.4}$$

For a simplex two-dimensional element, we have extremized the above functional with respect to the unknown nodal temperatures. The resultant element matrices are then obtained from the following relation:

$$\begin{Bmatrix} \frac{\partial I}{\partial T_i} \\ \frac{\partial I}{\partial T_j} \\ \frac{\partial I}{\partial T_k} \end{Bmatrix}^{(e)} = [B]^{(e)}[T]^{(e)} - [C]^{(e)} \tag{6.5}$$

The element matrix $[B]^{(e)}$ and the element column $[C]^{(e)}$ may be written as

$$[B]^{(e)} = \begin{bmatrix} B_{ii} B_{ij} B_{ik} \\ B_{ji} B_{jj} B_{jk} \\ B_{ki} B_{kj} B_{kk} \end{bmatrix}, \quad [C]^{(e)} = \begin{Bmatrix} C_i \\ C_j \\ C_k \end{Bmatrix}^{(e)}, \tag{6.6}$$

Where

$$B_{ii} = \frac{K}{4A}(b_i^{\,2} + c_i^{\,2}) - \frac{PA}{6} + \frac{(\alpha L_{ij})_{sideij}}{3} + \frac{(\alpha L_{ki})_{sideki}}{3}, \tag{6.7}$$

$$B_{ij} = \frac{K}{4A}(b_i b_j + c_i c_j) - \frac{PA}{12} + \frac{(\alpha L_{ij})_{sideij}}{6}, \tag{6.8}$$

$$B_{ik} = \frac{K}{4A}(b_i b_k + c_i c_k) - \frac{PA}{12} + \frac{(\alpha L_{ki})_{sideki}}{3}, \tag{6.9}$$

$$B_{jj} = \frac{K}{4A}(b_j^{\,2} + c_j^{\,2}) - \frac{PA}{6} + \frac{(\alpha L_{jk})_{sidejk}}{3} + \frac{(\alpha L_{ij})_{sideij}}{3}, \tag{6.10}$$

$$B_{jk} = \frac{K}{4A}(b_j b_k + c_j c_k) - \frac{PA}{12} + \frac{(\alpha L_{jk})_{sidejk}}{6}, \tag{6.11}$$

$$B_{kk} = \frac{K}{4A}(b_k^{\,2} + c_k^{\,2}) - \frac{PA}{6} + \frac{(\alpha L_{ki})_{sideki}}{3} + \frac{(\alpha L_{jk})_{sidejk}}{3}, \tag{6.12}$$

$$C_i = \frac{QA}{3} - \frac{\beta L_{ij}}{2} - \frac{\beta L_{ki}}{2} \quad C_j = \frac{QA}{3} - \frac{\beta L_{jk}}{2} - \frac{\beta L_{ij}}{2}, \quad C_k = \frac{QA}{3} - \frac{\beta L_{ki}}{2} - \frac{\beta L_{jk}}{2} \tag{6.13}$$

The element matrices were then assembled into the global matrices and vectors. The prescribed boundary conditions were implemented at the appropriate

nodal points. The algebraic equations in the global assembled form were solved by the Gauss elimination procedure. These details may be found in reference [50].

The figure below shows the methodology to be followed to couple the unsteady aerodynamic calculations with structural and probabilistic computations.

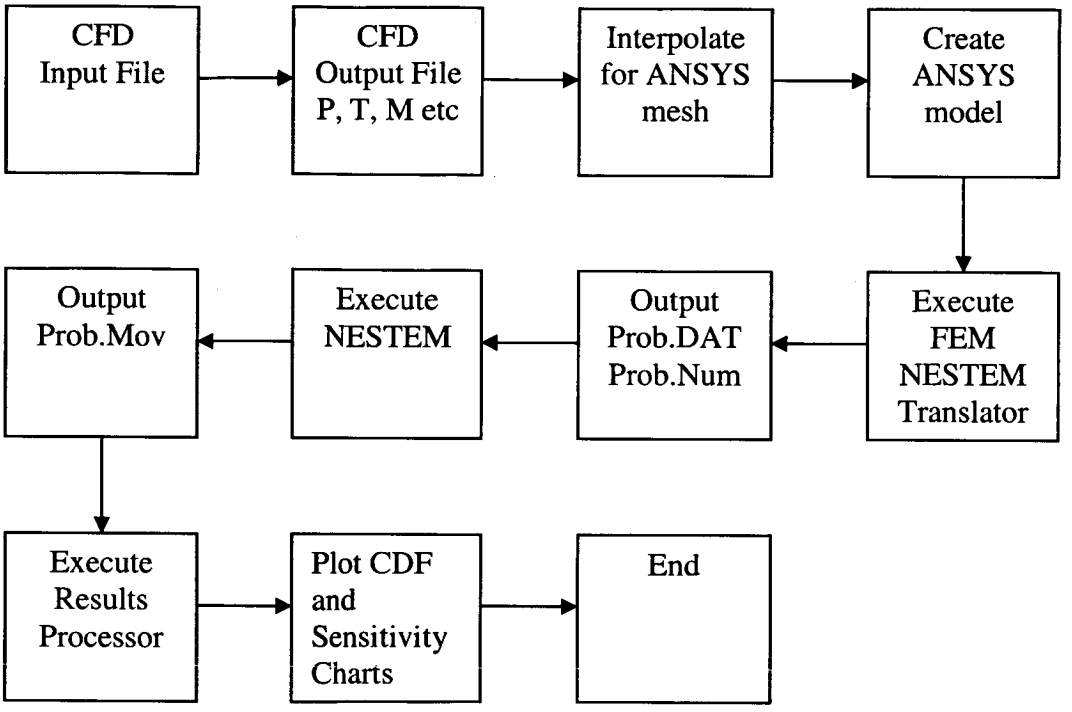

Figure 6.1: Coupling between CFD, Structural and Probabilistic analysis.

CHAPTER VII

RESULTS AND DISCUSSION FOR FINITE ELEMENT ANALYSIS

The values of stresses at different Iterations and also by varying the different Random variables by $+10\%$ and -10% are shown below.

Figure 7.1 shows the stress distribution across the stator at the 1900th iteration. The maximum value of stress was found to be 2.927237E+11 N/m^2 and this value is found to be at node number 7 whose coordinates are given by x= -0.0242291, y = 0.061337, z = -0.03429. The values of stresses obtained by perturbing the random variables with $+10\%$ and -10% are shown in the table 7.1

Similarly figure 7.2 shows the stress distribution for the 1960th iteration and maximum value is 2.926459E+11 N/m^2 and the values of stresses obtained by perturbing the random variables for the 1960th iteration is shown in table 7.2

Figure 7.3 shows the stress distribution across the stator for the 2000th iteration and the maximum value of stress is found to be 2.930746E+11 N/m^2 and the perturbed stresses are shown in table 7.3

Figure 7.4 shows the maximum value of stress for the rotor for the 1900th iteration. The maximum vale of stresses is 9.728925E+11 N/m^2 and the node number is 179 whose coordinates are given by x = 0.0230254, y = 0.000326966, z = -0.014135. The perturbed values of stresses obtained by perturbing the random variables are given in table 7.4.

Similarly Figures 7.5 and 7.6 show the stress distribution across the rotor for 1960th and 2000th iteration and the maximum value of stress in both the cases are 9.729051E+11 N/m^2 and 9.729444E+11 N/m^2 and the distribution of stresses obtained by perturbing the random variables are given in tables 7.5 and 7.6

Stator: The Results for the stator at 1900 Iteration are shown below:

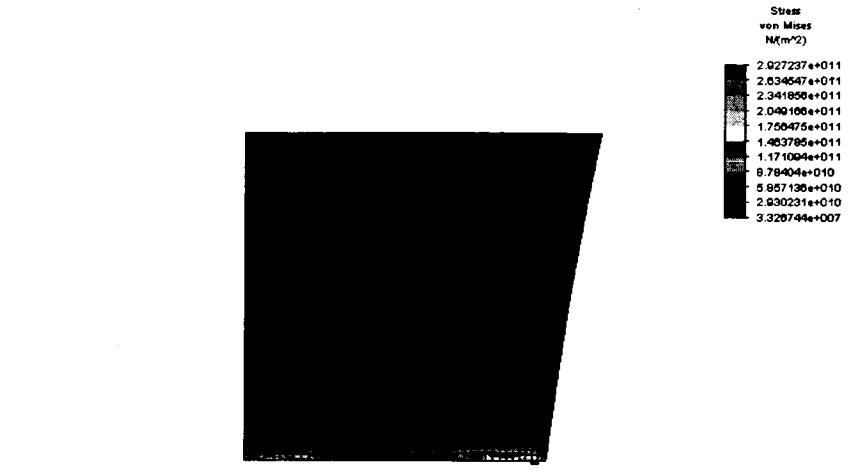

Node # 7: (X= -0.0242291, Y = 0.061337, Z = -0.03429),

Figure 7.1: Default value of stress for the stator at 1900th iteration

	Random variable	Von mises stress at mean line(N/m^2)
1	Default value	2.927237E+11
2	Thermal Conductivity raised by 10%:	2.930197E+11
3	Thermal Conductivity Decreased by 10%:	2.922539E+11
4	Modulus of Elasticity raised by 10%:	3.466889E+11
5	Modulus of Elasticity Decreased by 10%:	2.491812E+11
6	Thermal Expansion Coefficient raised by 10%	3.219803E+11
7	Thermal Expansion Coefficient Decrease by 10%	2.634671E+11
8	Poisson Ratio raised by 10%	2.898793E+11
9	Poisson Ratio Decreased by 10%	2.952894E+11
10	Heat Transfer Coefficient raised by 10%	2.927201E+11
11	Heat Transfer Coefficient decreased by 10%	2.927279E+11
12	Pressure increased by 10%	2.927395E+11
13	Pressure decreased by 10%	2.927080E+11
14	Temperature increased by 10%	2.966847E+11
15	Temperature decreased by 10%	2.893057E+11
16	chord length increased by 10 %	2.905943E+11
17	chord length decreased by 10 %	2.952864E+11

Table 7.1: Finite element analysis results for the stator at 1900th iteration

The Results for the stator at 1960 Iteration are shown below:

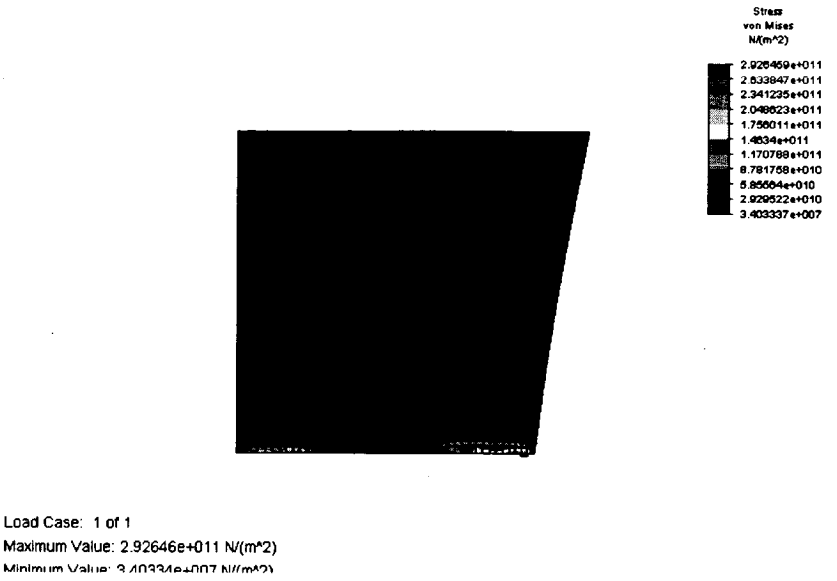

Node # 7: (X= -0.0242291, Y = 0.061337, Z = -0.03429),

Figure 7.2: Default value of stress for the stator at 1960th iteration

	Random variable	Von mises stress at mean line(N/m^2)
1	Default value	2.926459E+11
2	Thermal Conductivity raised by 10%:	2.931232E+11
3	Thermal Conductivity Decreased by 10%:	2.921270E+11
4	Modulus of Elasticity raised by 10%:	3.465961E+11
5	Modulus of Elasticity Decreased by 10%:	2.491151E+11
6	Thermal Expansion Coefficient raised by 10%	3.218947E+11
7	Thermal Expansion Coefficient Decrease by 10%	2.633970E+11
8	Poisson Ratio raised by 10%	2.898014E+11
9	Poisson Ratio Decreased by 10%	2.952108E+11
10	Heat Transfer Coefficient raised by 10%	2.926423E+11
11	Heat Transfer Coefficient decreased by 10%	2.926500E+11
12	Pressure increased by 10%	2.926616E+11
13	Pressure decreased by 10%	2.926301E+11
14	Temperature increased by 10%	2.967234E+11
15	Temperature decreased by 10%	2.892938E+11
16	Chord length increased by 10 %	2.905333E+11
17	Chord length decreased by 10 %	2.947974E+11

Table 7.2: Finite element analysis results for the stator at 1960th iteration

The Results for the stator at 2000 Iteration are shown below:

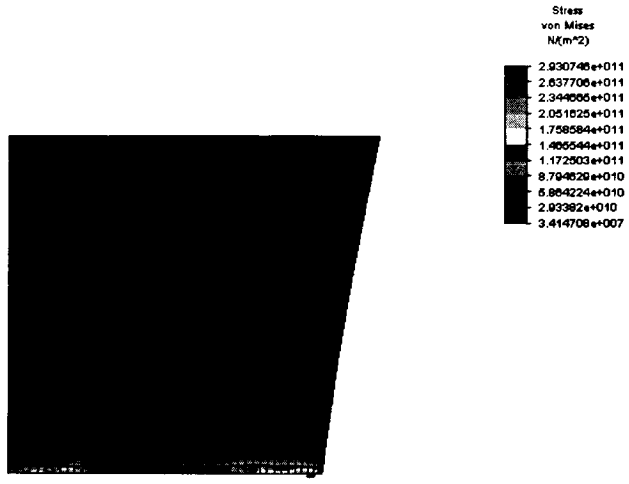

Node # 7: (X= -0.0242291, Y = 0.061337, Z = -0.03429),

Figure 7.3: Default value of stress for the stator at 2000th iteration

	Random variable	Von mises stress at mean line(N/m^2)
1	Default value	2.930746E+11
2	Thermal Conductivity raised by 10%:	2.941952E+11
3	Thermal Conductivity Decreased by 10%:	2.922476E+11
4	Modulus of Elasticity raised by 10%:	3.471041E+11
5	Modulus of Elasticity Decreased by 10%:	2.494813E+11
6	Thermal Expansion Coefficient raised by 10%	3.223663E+11
7	Thermal Expansion Coefficient Decrease by 10%	2.637829E+11
8	Poisson Ratio raised by 10%	2.902217E+11
9	Poisson Ratio Decreased by 10%	2.956430E+11
10	Heat Transfer Coefficient raised by 10%	2.930816E+11
11	Heat Transfer Coefficient decreased by 10%	2.930671E+11
12	Pressure increased by 10%	2.930904E+11
13	Pressure decreased by 10%	2.930589E+11
14	Temperature increased by 10%	2.967873E+11
15	Temperature decreased by 10%	2.894320E+11
16	Chord length increased by 10 %	2.909320E+11
17	Chord length decreased by 10 %	2.894320E+11

Table 7.3: Finite element analysis results for the stator at 2000th iteration

Rotor: The Results for the Rotor at 1900th Iteration are shown below:

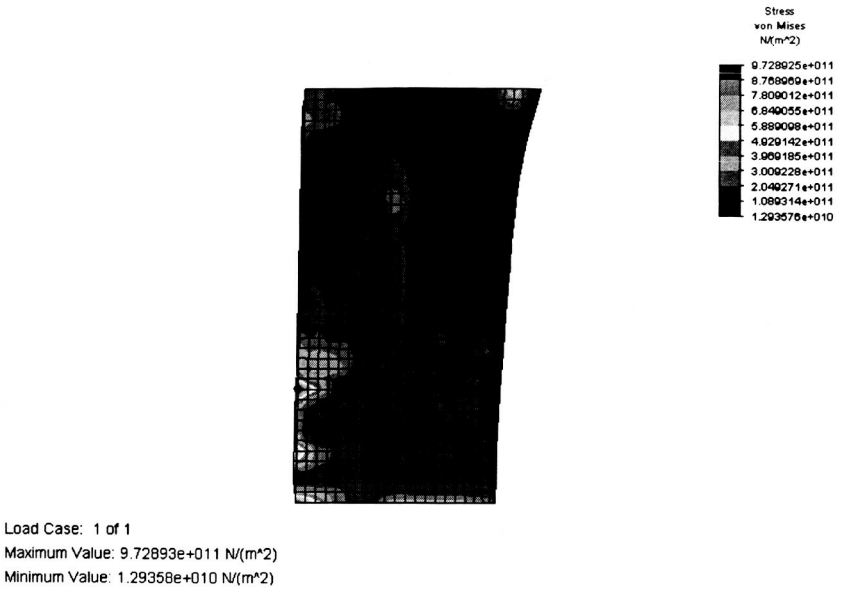

Node # 179 (X = 0.0230254, Y = 0.000326966, Z = -0.014135),

Figure 7.4: Default value of stress for the rotor at 1900th iteration

	Random variable	Von mises stress at mean line
1	Default values	9.728925E+11
2	Thermal Conductivity raised by 10%:	9.834860E+11
3	Thermal Conductivity Decreased by 10%:	9.634966E+11
4	Modulus of Elasticity raised by 10%:	9.031493E+11
5	Modulus of Elasticity Decreased by 10%:	1.122406E+12
6	Thermal Expansion Coefficient raised by 10%	9.931838E+11
7	Thermal Expansion Coefficient Decrease by 10%	9.530013E+11
8	Poisson Ratio raised by 10%	9.634860E+11
9	Poisson Ratio Decreased by 10%	9.842765E+11
10	Heat Transfer Coefficient raised by 10%	9.728879E+11
11	Heat Transfer Coefficient decreased by 10%	9.728971E+11
12	Pressure increased by 10%	9.724808E+11
13	Pressure decreased by 10%	9.733044E+11
14	Temperature increased by 10%	9.729040E+11
15	Temperature decreased by 10%	9.728704E+11
16	Speed increased by 10%	1.178293E+12
17	Speed decreased by 10%	7.870540E+11
18	Chord length increase by 10 %	9.504631E+11
19	Chord length decrease by 10 %	9.954552E+11

Table 7.4: Finite element analysis results for the rotor at 1900th iteration

The Results for the Rotor at 1960th Iteration are shown below:

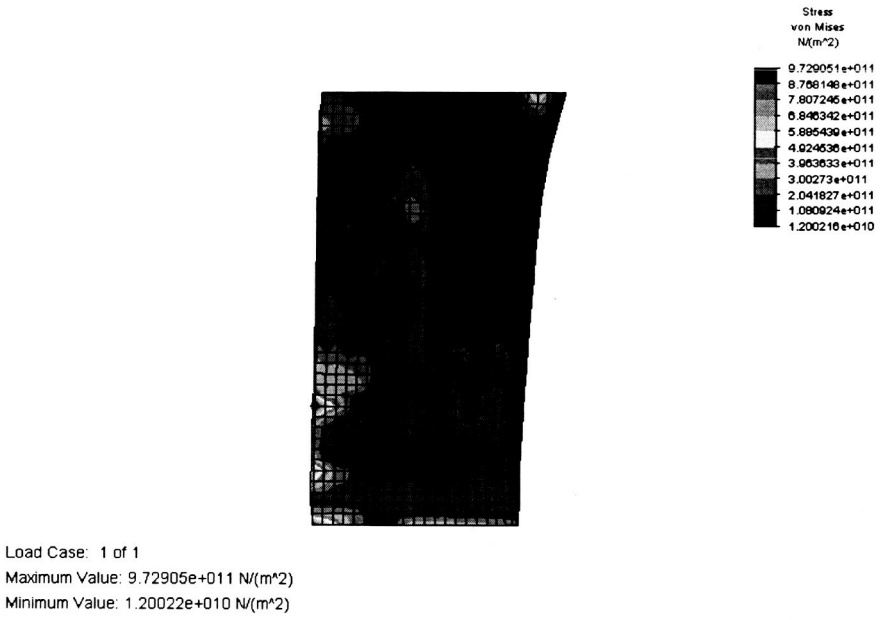

Node # 179 (X = 0.0230254, Y = 0.000326966, Z = -0.014135),

Figure 7.5: Default value of stress for the rotor at 1960th iteration

	Random variable	Von mises stress at mean line
1	Default values	9.729051E+11
2	Thermal Conductivity raised by 10%:	9.834986E+11
3	Thermal Conductivity Decreased by 10%:	9.635093E+11
4	Modulus of Elasticity raised by 10%:	9.031651E+11
5	Modulus of Elasticity Decreased by 10%:	1.122414E+12
6	Thermal Expansion Coefficient raised by 10%	9.931964E+11
7	Thermal Expansion Coefficient Decrease by 10%	9.530140E+11
8	Poisson Ratio raised by 10%	9.634987E+11
9	Poisson Ratio Decreased by 10%	9.842892E+11
10	Heat Transfer Coefficient raised by 10%	9.729011E+11
11	Heat Transfer Coefficient decreased by 10%	9.729089E+11
12	Pressure increased by 10%	9.724933E+11
13	Pressure decreased by 10%	9.733169E+11
14	Temperature increased by 10%	9.729345E+11
15	Temperature decreased by 10%	9.728936E+11
16	Speed increased by 10%	1.178306E+12
17	Speed decreased by 10%	7.870665E+11
18	Chord length increase by 10 %	9.504757E+11
19	Chord length decrease by 10 %	9.954678E+11

Table 7.5: Finite element analysis results for the rotor at 1960th iteration

The Results for the Rotor at 2000th Iteration are shown below:

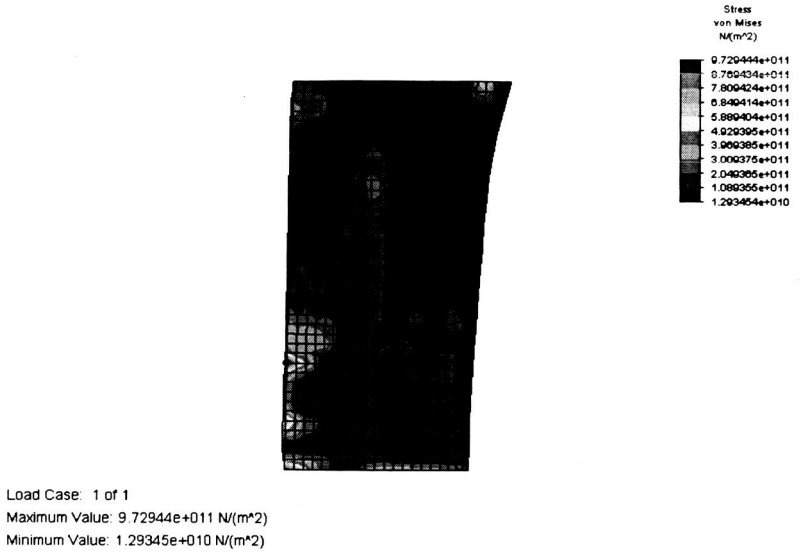

Node # 179 (X = 0.0230254, Y = 0.000326966, Z = -0.014135),

Figure 7.6: Default value of stress for the rotor at 2000th iteration

Random variable	Von mises stress at mean line
Default values	9.729444E+11
Thermal Conductivity raised by 10%:	9.835380E+11
Thermal Conductivity Decreased by 10%:	9.635486E+11
Modulus of Elasticity raised by 10%:	9.032050E+11
Modulus of Elasticity Decreased by 10%:	1.122457E+12
Thermal Expansion Coefficient raised by 10%	9.932357E+11
Thermal Expansion Coefficient Decrease by 10%	9.530533E+11
Poisson Ratio raised by 10%	9.635380E+11
Poisson Ratio Decreased by 10%	9.843285E+11
Heat Transfer Coefficient raised by 10%	9.729409E+11
Heat Transfer Coefficient decreased by 10%	9.729477E+11
Pressure increased by 10%	9.725326E+11
Pressure decreased by 10%	9.733561E+11
Temperature increased by 10%	9.729712E+11
Temperature decreased by 10%	9.729273E+11
Speed increased by 10%	1.178345E+12
Speed decreased by 10%	7.871058E+11
Chord length increase by 10 %	9.505151E+11
Chord length decrease by 10 %	9.955071E+11

Table 7.6: Finite element analysis results for the rotor at 2000th iteration

CHAPTER VIII

PROBABILISTIC ANALYSIS

Let $X_1, X_2, \ldots, X_n$ be a set of random variables defined on a (discrete) probability space Ω. The probability that the events $X_1 = x_1, X_2 = X_2, \ldots, X_n = x_n$ happen concurrently, is denoted by

$$f(x_1, x_2, \ldots, x_n) = P(X_1 = x_1, X_2 = x_2, \ldots, X_n = x_n)$$

for the set of desired solutions $A \subseteq \Omega$. If the function $f(x_1, x_2, \ldots, x_n)$ is discrete, it is called the *joint probability mass function* of $X_1, X_2, \ldots, X_n$ and has the following properties.

$$0 \leq f(x_1, x_2, \ldots, x_n) \leq 1$$

$$\sum_{(x_1, x_2, \ldots, x_n) \in \Omega} \sum f(x_1, x_2, \ldots, x_n) = 1 \tag{8.1}$$

$$P[(X_1, X_2, \ldots, X_n) \in A] = \sum_{(x_1, x_2, \ldots, x_n) \in \Omega} \sum f(x_1, x_2, \ldots, x_n) = 1, \; A \subseteq \Omega$$

If $f(x_1, x_2, \ldots, x_n)$ is continuous it is called *joint probability density function* of $X_1, X_2, \ldots, X_n$ and has the following properties

$$0 \leq f(x_1, x_2, ..., x_n)$$

$$\int_{\Omega} ... \int f(x_1, x_2, ..., x_n) dx_1 dx_2 ... dx_n = 1 \qquad (8.2)$$

$$P[(X_1, X_2, ..., X_n) \in A] = \int_A .. \int f(x_1, x_2, ..., x_n) dx_1 dx_2 ... dx_n, A \subseteq \Omega$$

If the lower bound of A, the set of desired solutions, is equal to the infimum of Ω for all X_i, i.e. if $A = [\inf_i(\Omega), a_i]$, for all $i = 1,2,3,.....n$ a function $F(a_1, a_2, a_3, ...a_n)$ can be defined, such that:

$$F(a_1, a_2, a_3, ...a_n) = P[(X_1, X_2, .., X_n) \in A] = \sum_{(x_1, x_2, ..., x_n) \in A} ... \sum f(x_1, x_2, ..., x_n), A \subseteq \Omega$$

(f is discrete) (8.3)

$$F(a_1, a_2, a_3, ...a_n) = P[(X_1, X_2, .., X_n) \in A] = \int_A .. \int f(x_1, x_2, ..., x_n) dx_1 dx_2 ... dx_n, A \subseteq \Omega$$

(f is continuous) (8.4)

F is called the joint cumulative probability distribution function. For $\Omega = R^n$ and a continuous function f:

$$F(a_1, a_2, a_3, ...a_n) = P[(X_1, X_2, .., X_n) \in A] \in ((-\infty, -\infty, ... - \infty), (a_1, a_2, ...a_n))$$

$$\int_{-\infty}^{a_n} .. \int_{-\infty}^{a_1} f(x_1, x_2, ..., x_n) dx_1 dx_2 .. dx_n \qquad (8.5)$$

The common notation $F(a_1, a_2, a_3, ...a_n) = \mathrm{P}(X_1 \leq a_1, X_2 \leq a_2, ..., X_n \leq a_n)$ will be used subsequently also.

The univariate probability function f_{xi} for each criterion X_i, obtained from the traditional probabilistic design process, can also be generated with the joint probability function $f.f_{xi}$ is called marginal probability mass or density function of X_i and is defined by:

$$fx_1 = \sum_{(x_2,...,x_n)} ... \sum_{\in R} f(x_2,...,x_n) \tag{8.6}$$

$$fx_1 = \int_R ... \int f(x_2,...,x_n) dx_2 ... dx_n \tag{8.7}$$

The joint probability function, $f_{xy}(x, y)$, creates the surface of a probability 'hump' in the x-y-*f*-space, characterized by rings of constant probabilities. The distribution curves over the x- and y-axis are the aforementioned marginal probability functions $f_x(x)$ and $f_y(y)$, respectively. The last necessary concept to mention here for the development of a joint probabilistic formulation is the concept dependence of criteria.

Two random variables X and Y are said to be independent, if $f_{xy}(x, y) = f_x(x).f_y(y)$otherwise X and Y are said to be dependent. This dependence is a mathematical notion and should not be confused with 'casual dependence'. From here on, mathematical dependence will be referred to as *correlation*. Correlation is measured by the covariance of two criteria, X and Y, defined by

$$Cov(X,Y) = E[X,Y] - E[X]E[Y] \tag{8.8}$$

It is more convenient, however, to use a covariance normalized by the standard deviations, σ_X and σ_Y, for both criteria, called *correlation coefficient.*

$$\rho = \frac{Cov(X,Y)}{\sigma_X \sigma_Y} \tag{8.9}$$

The correlation coefficient is defined over the interval [-1,1], indicating strongly positively correlated criteria at values close to1 and strongly negatively correlated criteria at values close to –1. The criteria are independent, if ρ=0. In aerospace systems design ρ can be quite difficult to calculate by equation (8.9). It is much more effective to view the correlation coefficient differently for calculation purposes. Jointly collected data from a probabilistic or any other analysis can be thought of as vectors of numbers. The correlation coefficient measures the orthogonality, i.e. independence, of both vectors. ρ is simply the cosine of the angle between the two criterion vectors, indicating their alignment. For ρ = 1, vectors are parallel and point in same direction, for ρ = -1, vectors are parallel and point in opposite direction. For ρ = 0, vectors are orthogonal and the criteria are independent. The correlation coefficient plays a significant role in the formulation of joint probability distribution models as described in the next section.

Probability Functions

Attention is now directed to the implementation of this probabilistic formulation in the design process. The necessary transition from the mathematical formulation above to a probabilistic model that yields the information relevant for multi-variate decision-making is described in this section. There are two alternatives for this task.

Joint Probability Model

The first joint probability density function introduced here is an analytical probability model for criteria whose univariate distributions and their corresponding means and standard deviations are known. All necessary information for the model can be generated by the traditional probabilistic design process, using its output of univariate criterion distributions. A particular model for two criteria with normal distributions, represented by equation (8.10), has been introduced by Garvey and Tuab. Garvey further generated models for two criteria with combinations of normal and lognormal distributions, which are summarized in reference [19].

$$f_{xy} = (x, y)\frac{1}{2\pi\,\sigma_X \sigma_Y \sqrt{1-\rho^2}} \exp\{\frac{1}{2\rho^2 - 2}[(\frac{x-\mu_x}{\sigma_X})^2 - 2\rho(\frac{x-\mu_X}{\sigma_X})(\frac{y-\mu_Y}{\sigma_Y}) + (\frac{y-\mu_Y}{\sigma_Y})^2]\} \tag{8.10}$$

Note that the only information needed for the Joint Probability Model consists of the means μ_X and μ_Y, the standard deviations σ_X and σ_Y, and the correlation coefficient ρ for the criteria x and y. The model variables, x and y, are defined over the interval of all possible criterion values. The advantage of this model is the limited information needed, which makes it very flexible for use and application. For example, if only expert knowledge and no simulation/modeling is available in the early stages of design, educated guesses for the means, standard deviations, and the correlation coefficient can be used to execute the joint probability model. It also lends itself to use in combination with increasingly important fast probability integration (FPI) techniques.

Implementation of Probabilistic Procedure Using FPI:

FPI is a probabilistic analysis tool that implements a variety of methods for probabilistic analysis. The procedure follows the steps given below:

1. Identify the independent and uncorrelated design variables with uncertainties.
2. Quantify the uncertainties of these design variables with probability distributions based on expert opinion elicitation, historical data or benchmark testing.
3. It is required that there is a response function that defines the relationship between the response and the independent variables.
4. The FPI uses the responses generated to compute the cumulative distribution functions (CDF)/probability density functions (PDF) and the corresponding sensitivities of the response.

Several methods are available in the FPI to compute a probabilistic distribution. In addition to obtaining the CDF/PDF of the response, the FPI provides additional information regarding the sensitivity of the response with respect to the primitive variables. They provide valuable information in controlling the scatter of the response variable. The random primitive variable with the highest sensitivity factor will yield the biggest payoff in controlling the scatter in that particular response variable. Such information is very useful to the test/design engineer in designing or interpreting the measured data.

CHAPTER IX

RESULTS AND DISCUSSION OF PROBABILISTIC ANALYSIS

The Probabilistic analysis is performed for all the three iterations i.e. 1900, 1960 and 2000th iteration. The maximum stress value was determined from the finite element analysis of the turbine blade. This location was used to evaluate the cumulative distribution functions (CDF) and the sensitivity factors for stress response. CDF for the stress are shown in the figures 9.1, 9.14, 9.27 for the Stator and 9.40, 9.52, 9.64 for the Rotor for three iterations 1900, 1960 and 2000.

Results and Discussion for the Stator:

The sensitivity factors for stress versus the random variables for Stator are plotted in the figures 9.2-9.13, 9.15-9.26, 9.27-9.39 for three different iterations and for different probability levels ranging form 0.001 to 0.999, and there is not much difference in all the three iterations with the change in the random variables. We observe that the thermal coefficient of expansion, and Poisson's ratio have a lot of

influence on the stress. For prescribed values of thermal coefficient of expansion, and Poisson's ratio, Reynolds number, angle of attack, gas emissivity and absorptivity, inlet temperature, inlet and exit pressures, thermal conductivity, and chord length of the material have a lot of impact on the stress.

The results for the 1900th iteration for stator are shown below:

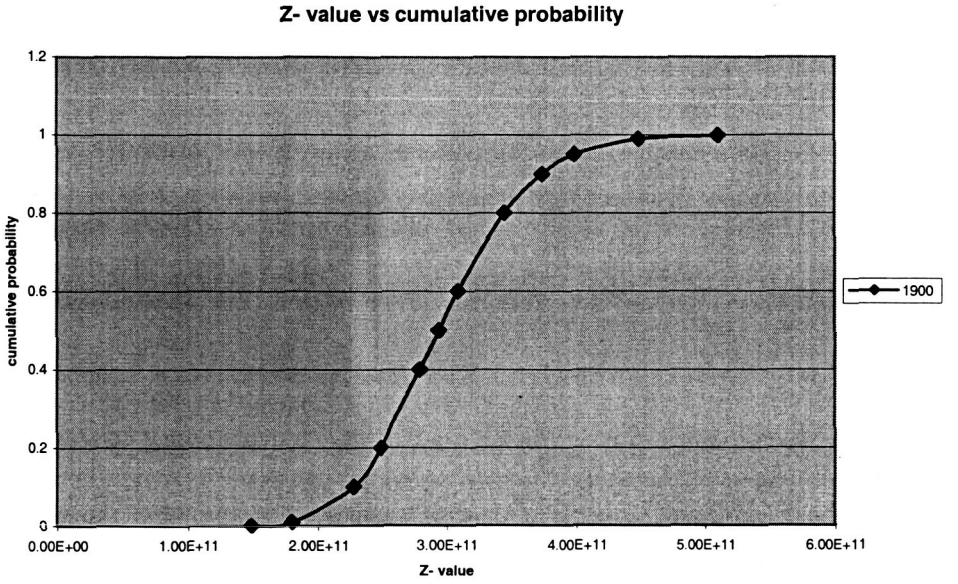

Figure 9.1: Cumulative Probability of thermal stress for stator at 1900th iteration

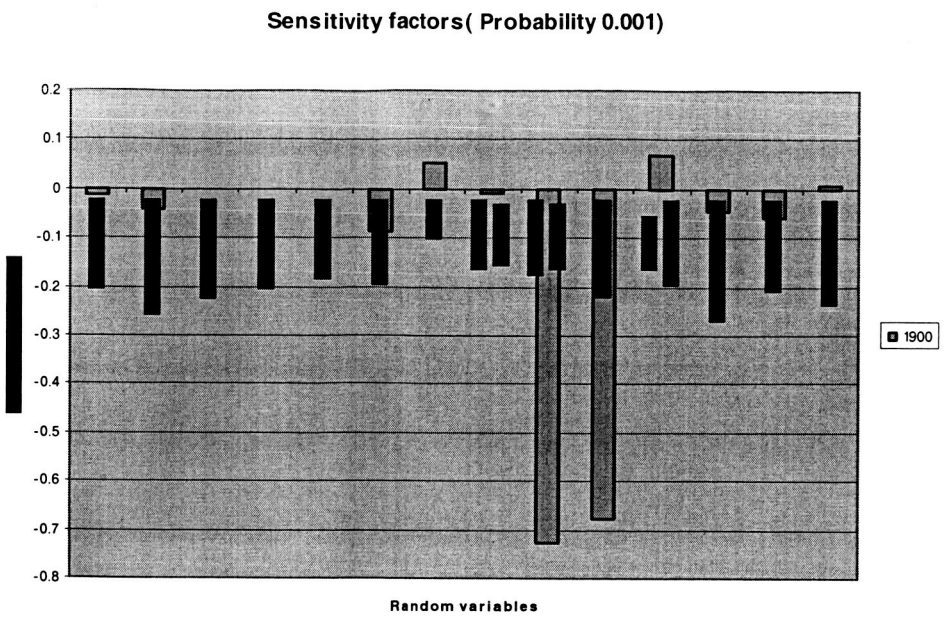

Figure 9.2: Probability 0.001

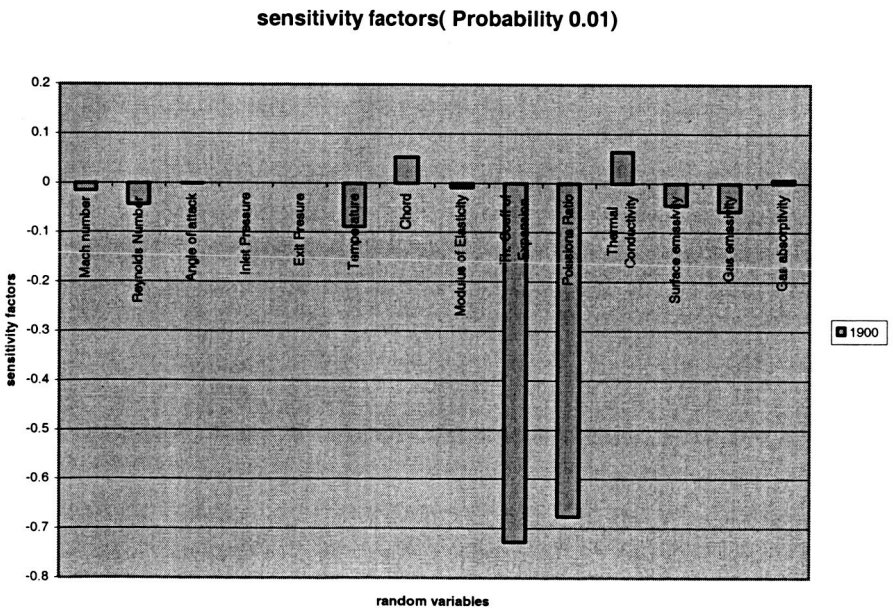

Figure 9.3: Probability 0.01

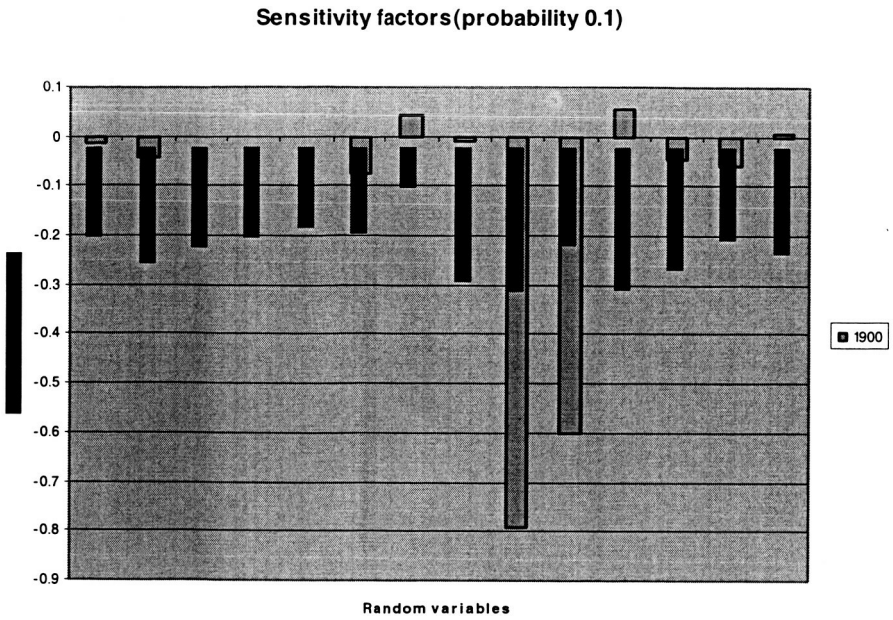

Figure 9.4: Probability 0.01

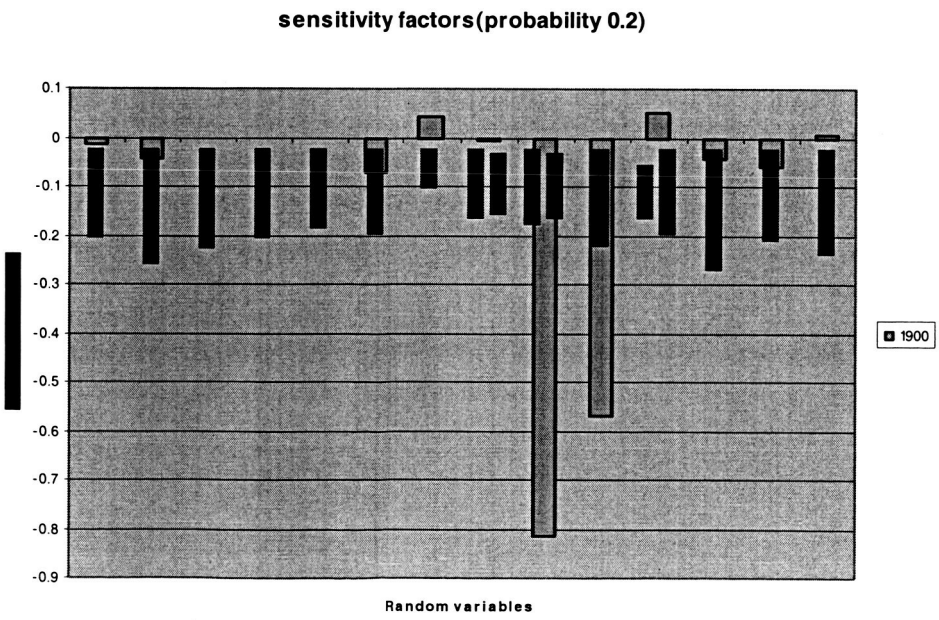

Figure 9.5: Probability 0.2

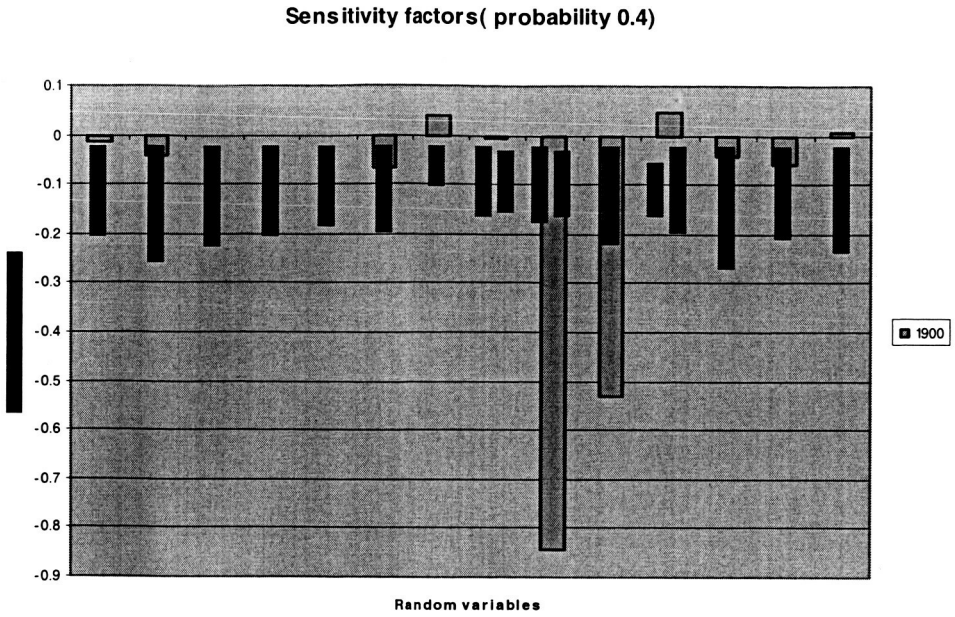

Figure 9.6: Probability 0.4

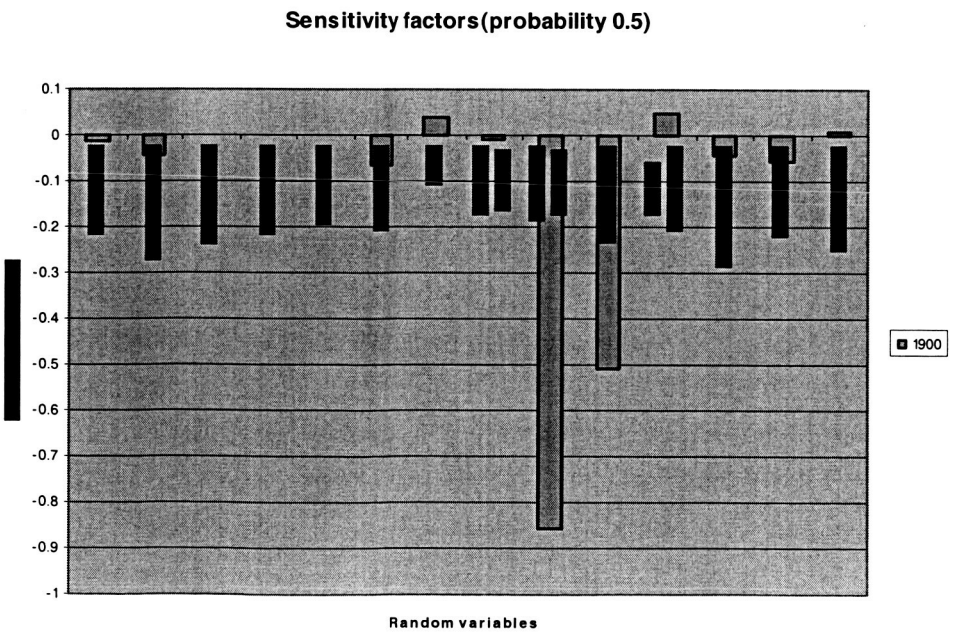

Figure 9.7: Probability 0.5

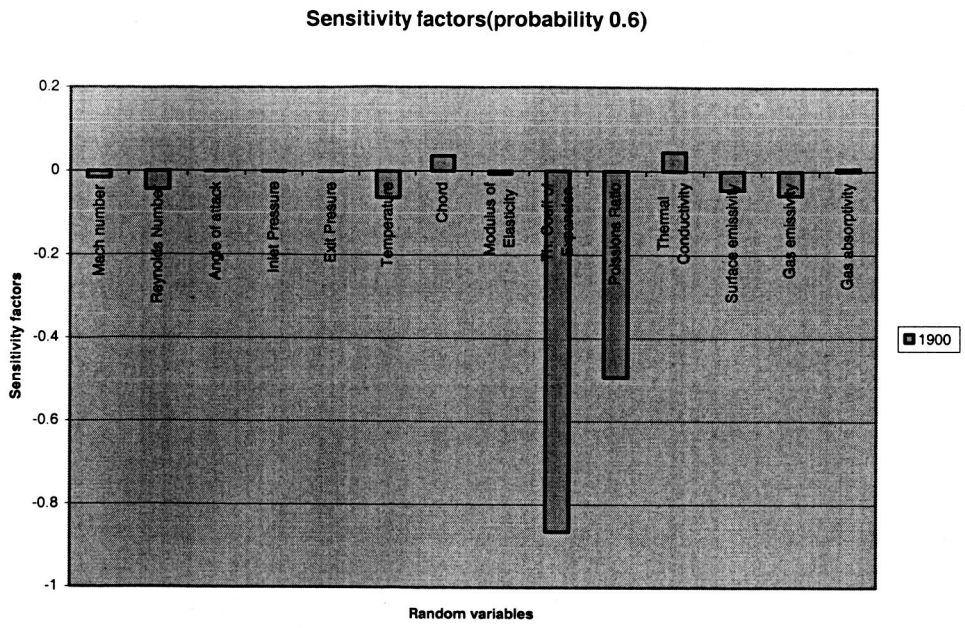

Figure 9.8: Probability 0.6

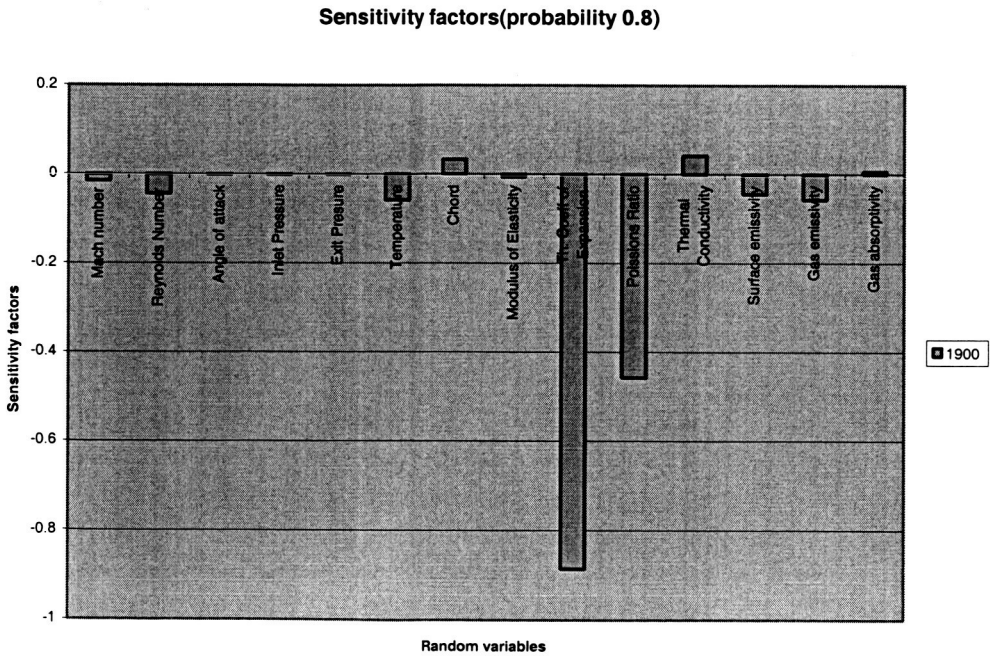

Figure 9.9: Probability 0.8

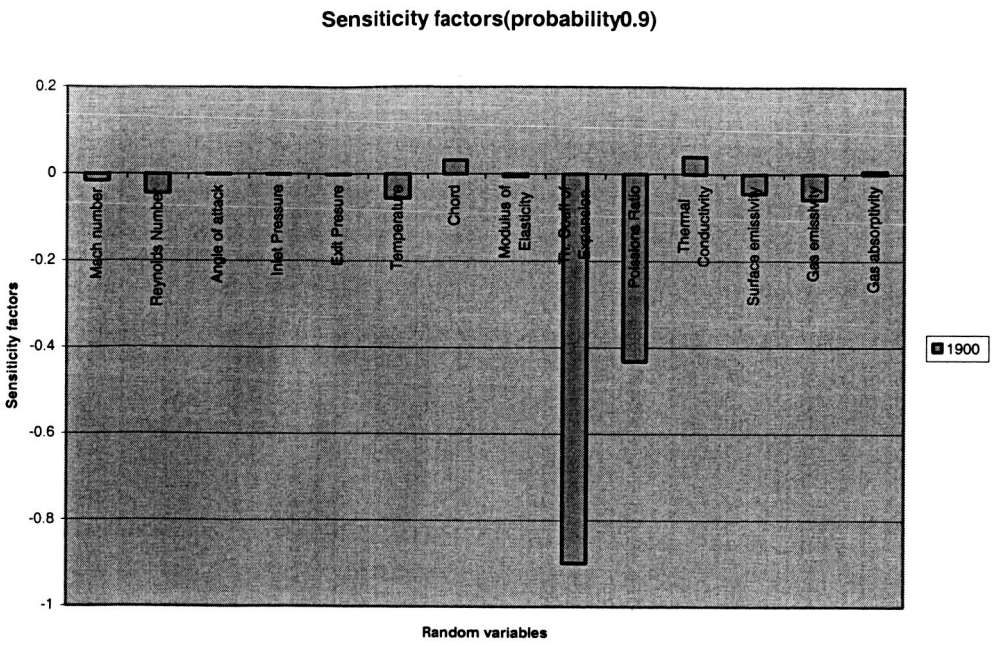

Figure 9.10: Probability 0.9

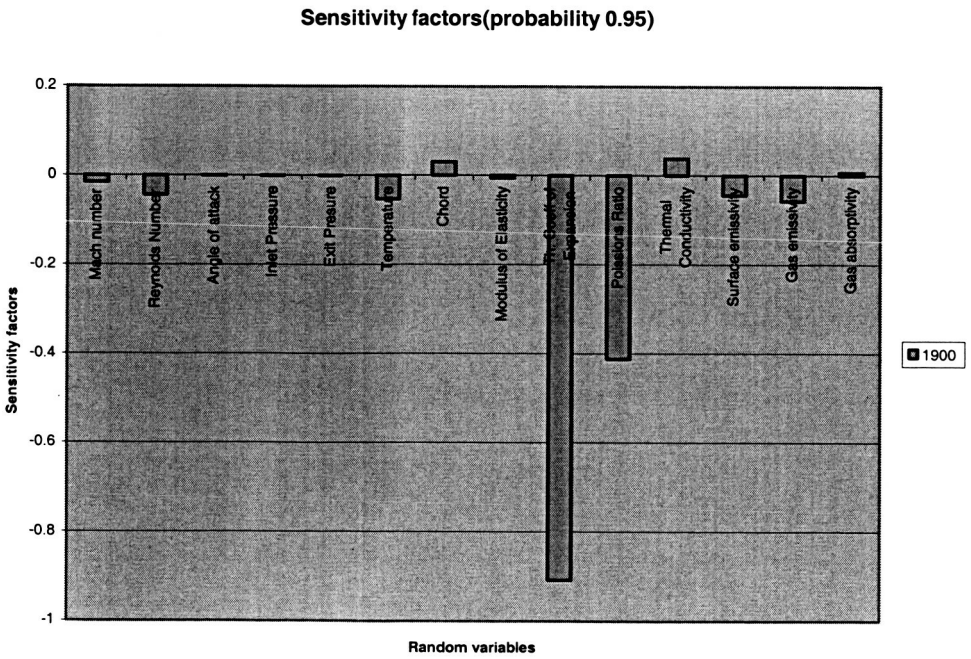

Figure 9.11: Probability 0.95

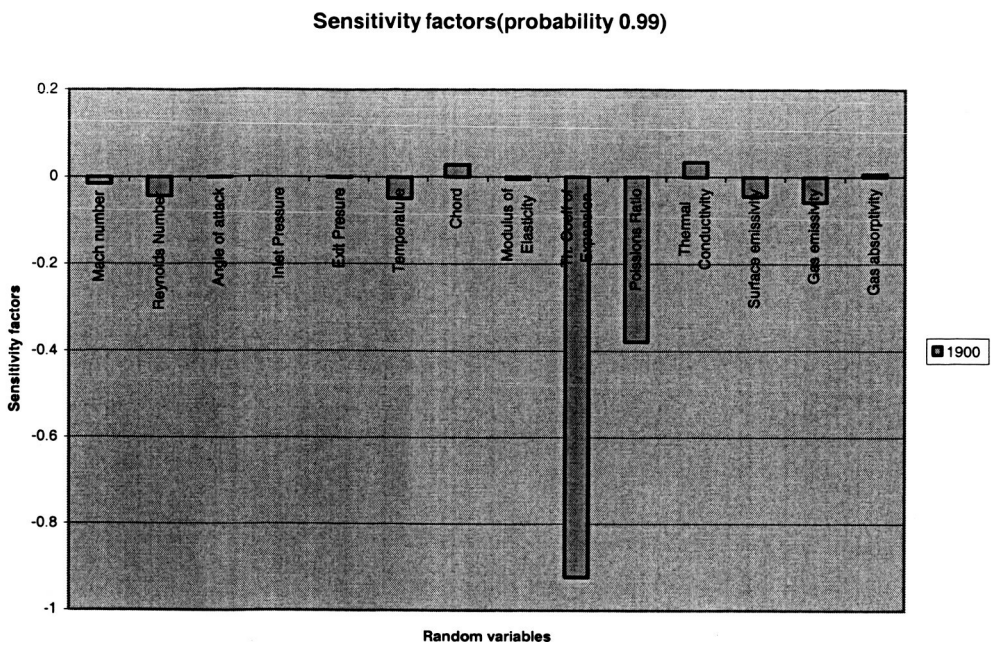

Figure 9.12: Probability 0.99

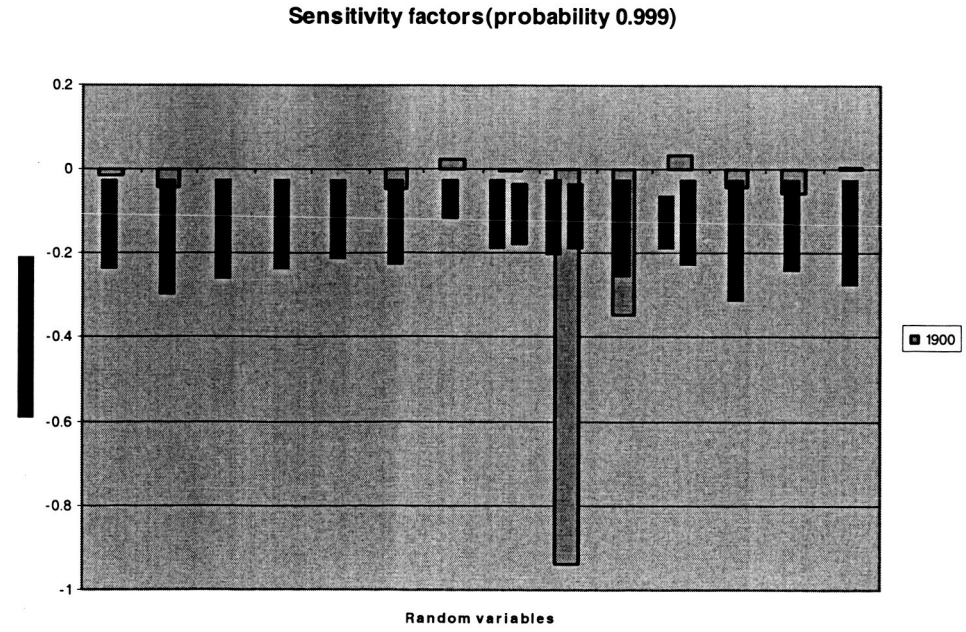

Figure 9.13: Probability 0.999

The results for the 1960th iteration are shown below:

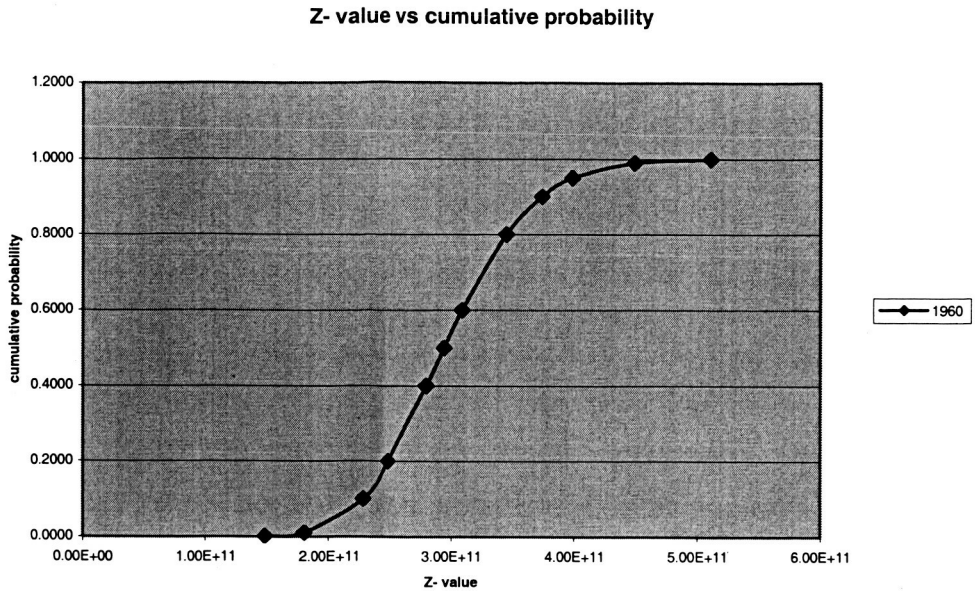

Figure 9.14: Cumulative Probability of thermal stress for stator at 1960th iteration

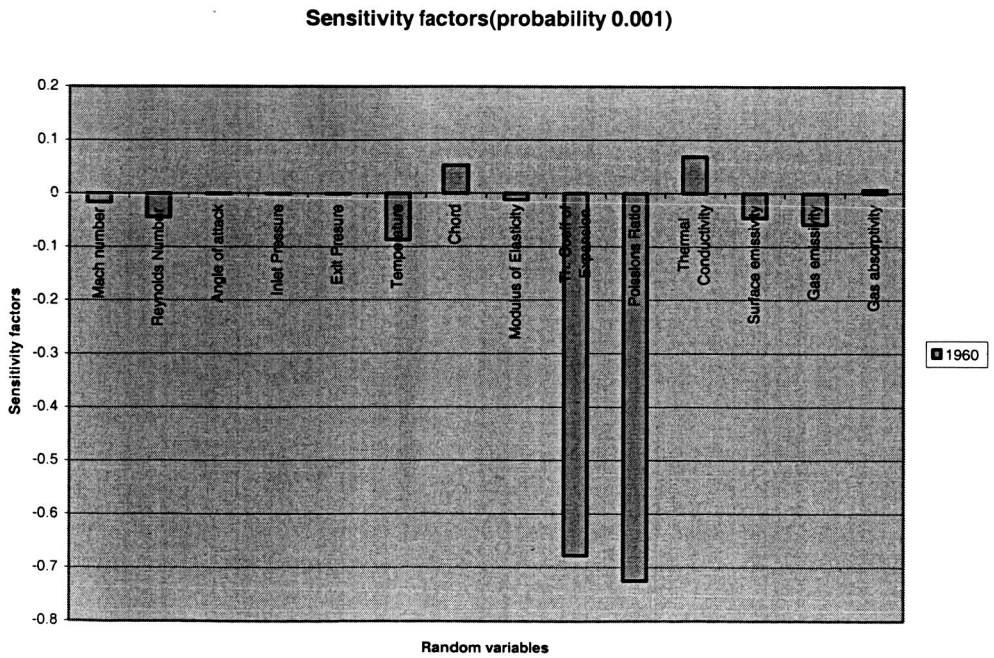

Figure 9.15: Probability 0.001

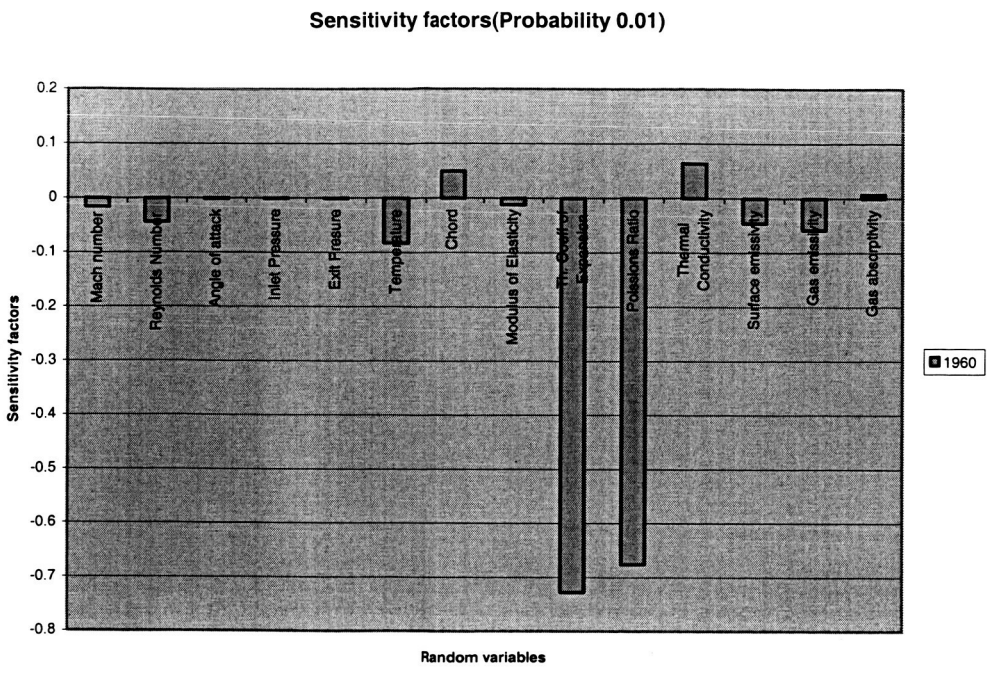

Figure 9.16: Probability 0.01

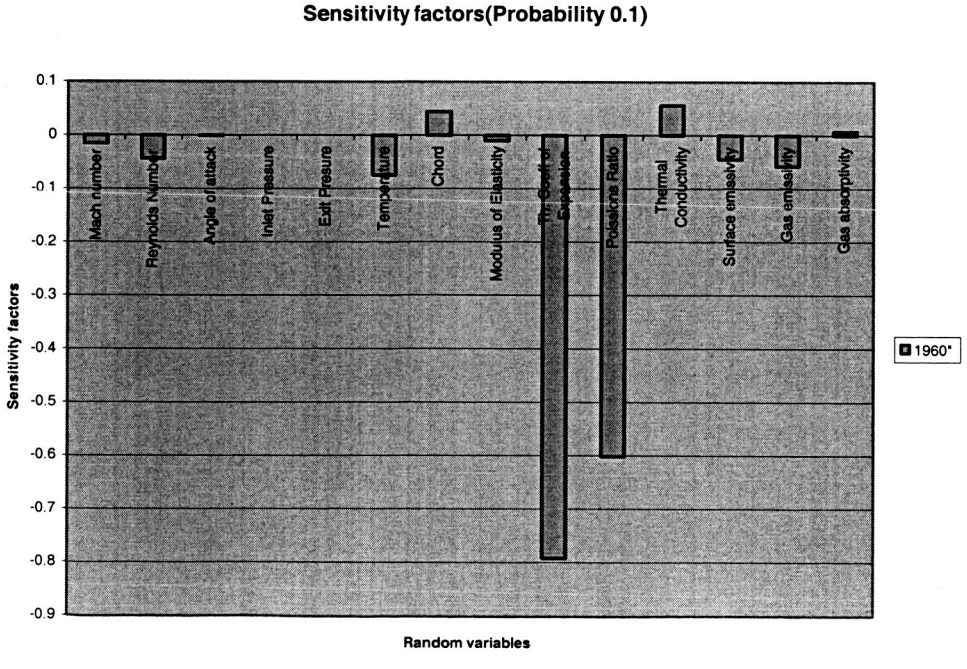

Figure 9.17: Probability 0.1

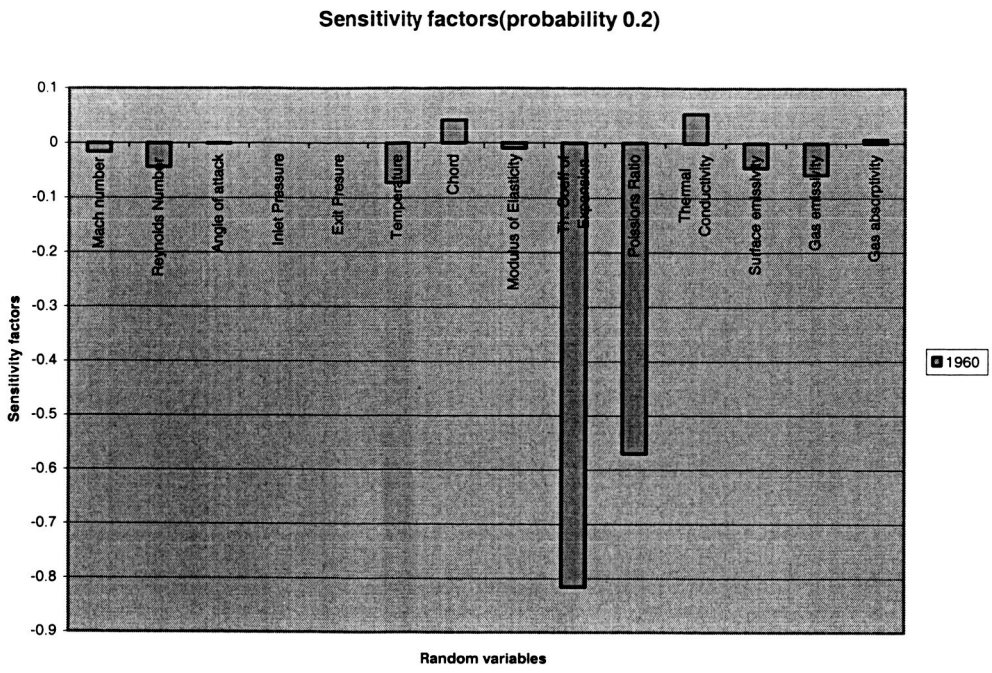

Figure 9.18: Probability 0.2

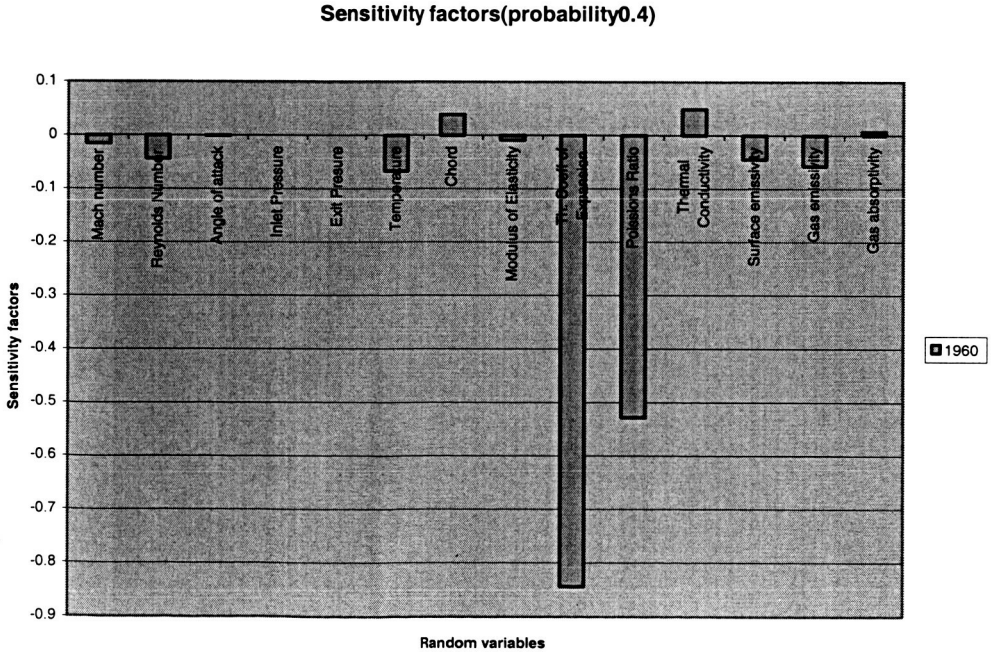

Figure 9.19: Probability 0.4

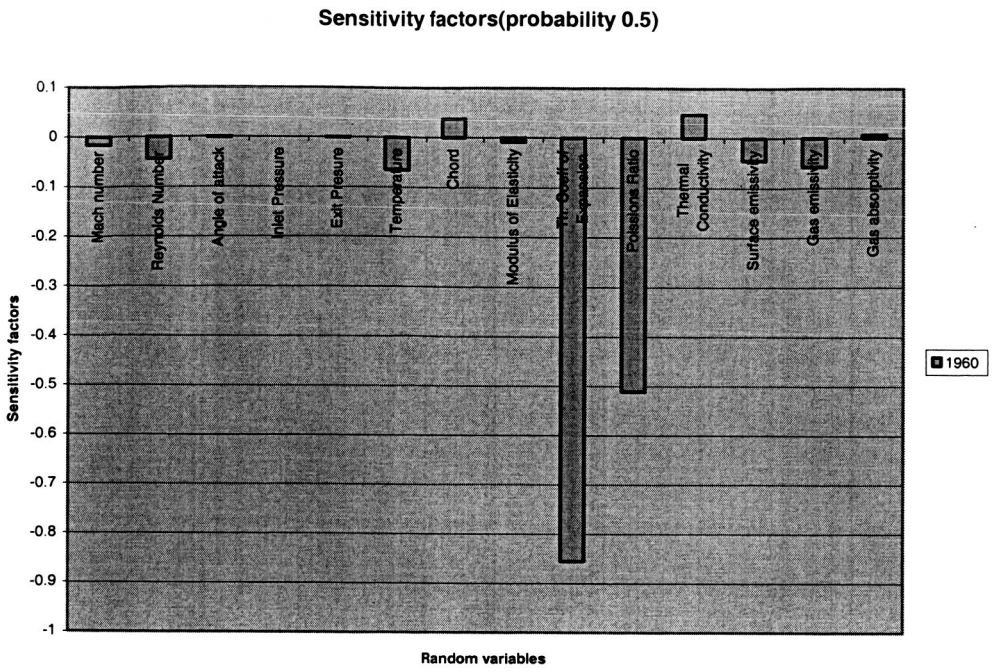

Figure 9.20: Probability 0.5

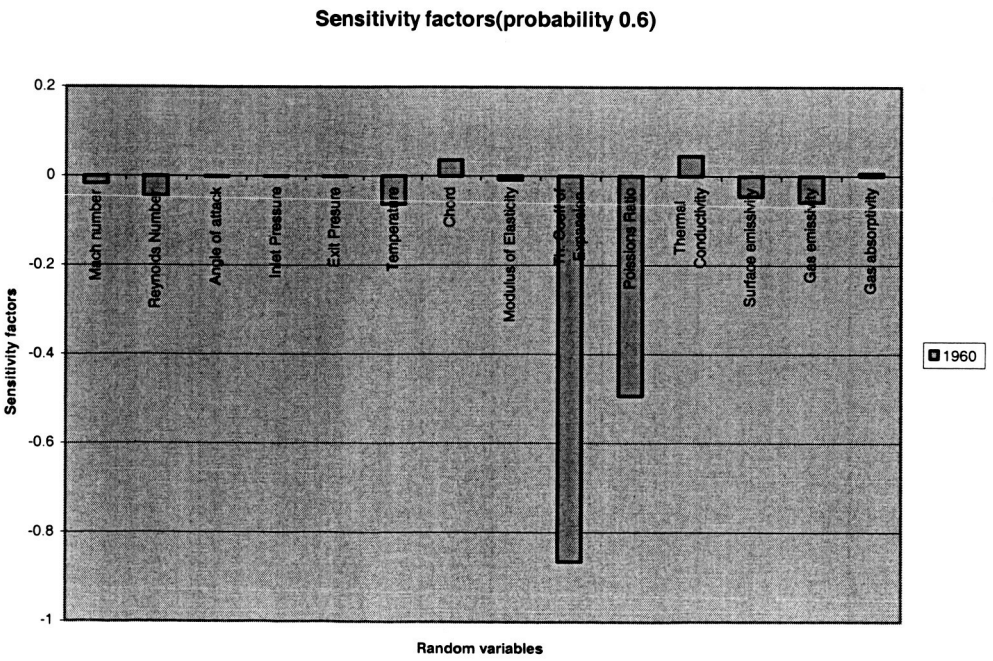

Figure 9.21: Probability 0.6

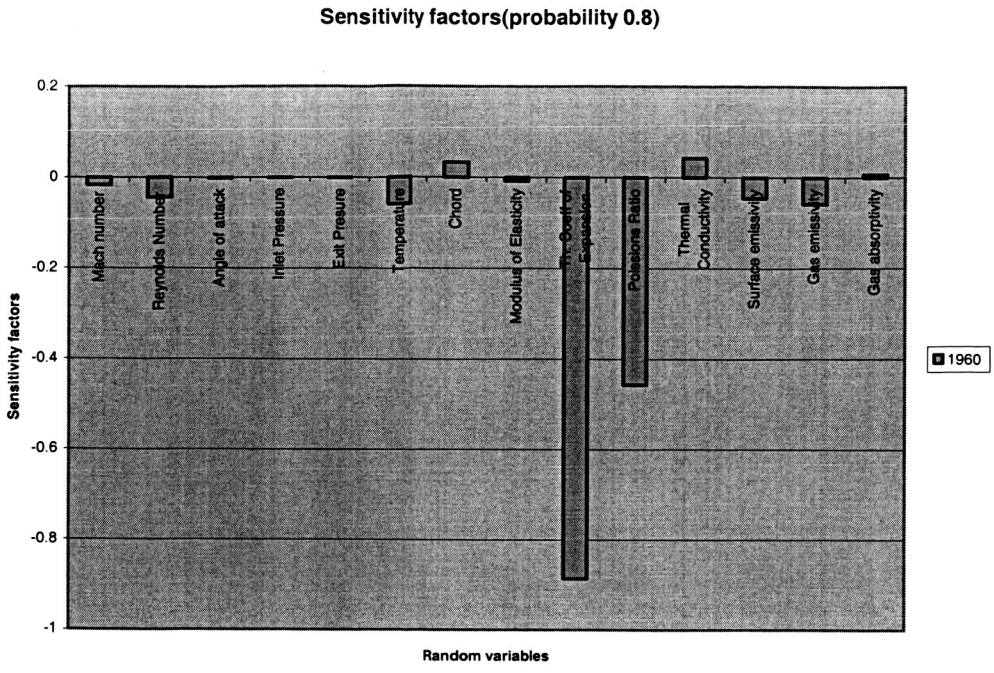

Figure9.22: Probability 0.8

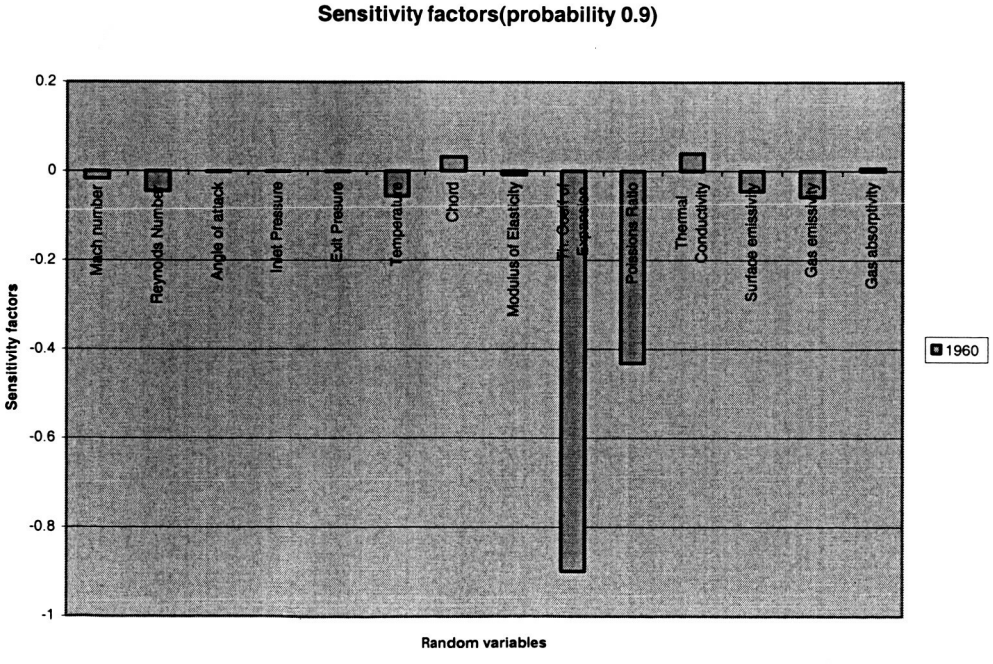

Figure 9.23: Probability 0.9

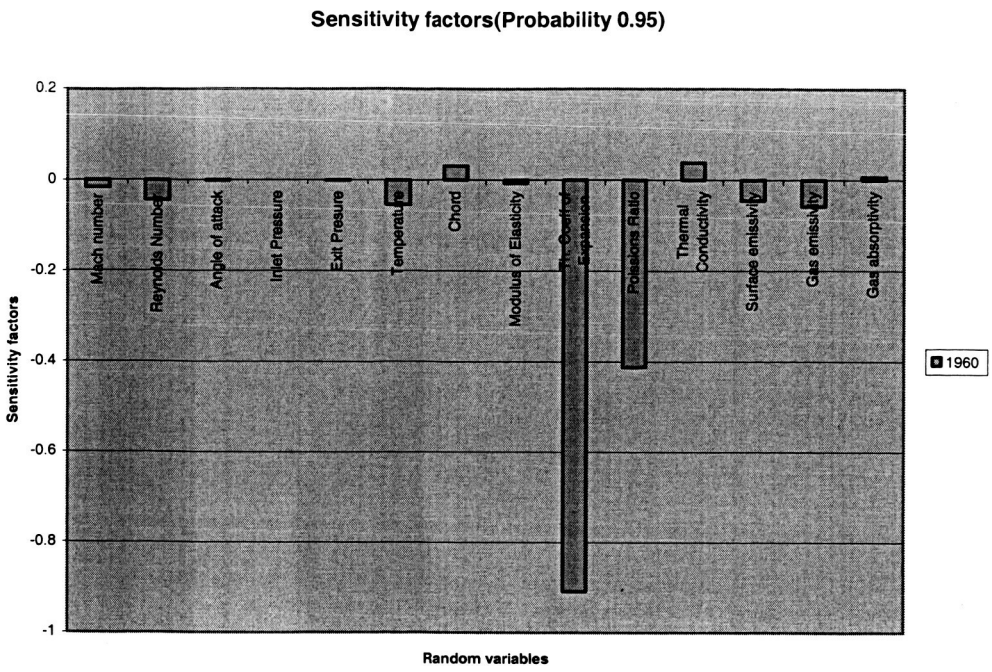

Figure 9.24: Probability 0.95

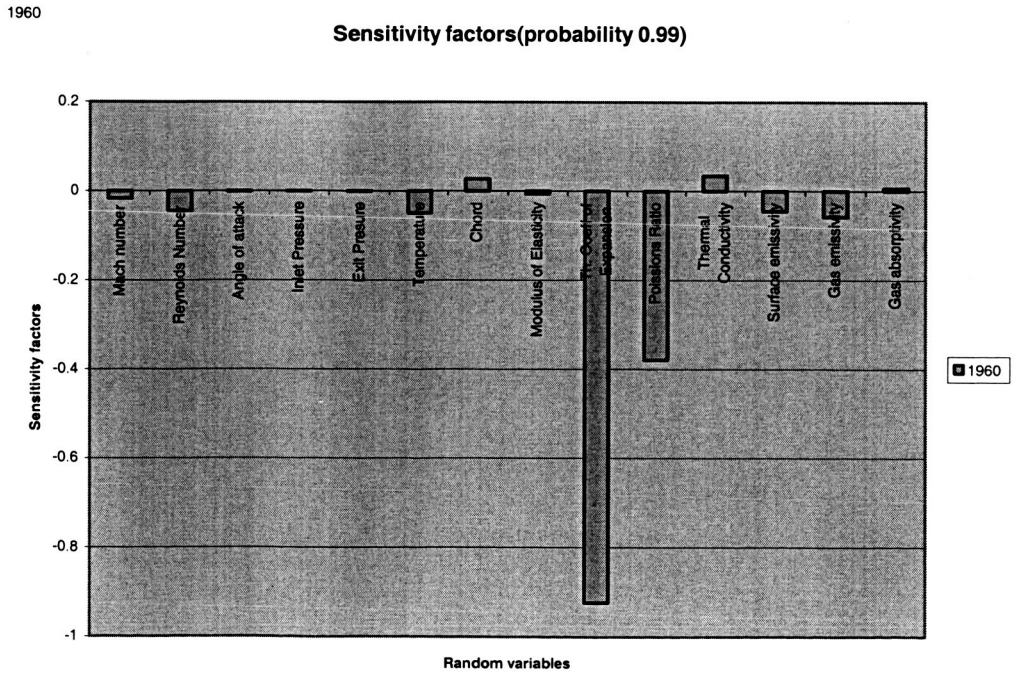

Figure9.25: Probability 0.99

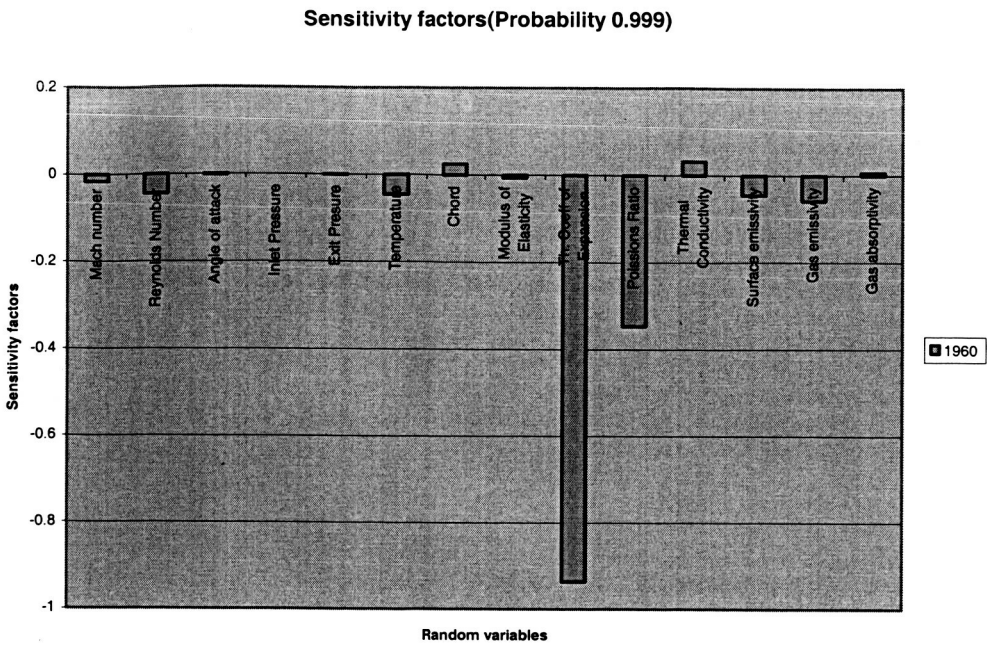

Figure 9.26: Probability 0.999

The results for the 2000th iteration are shown below:

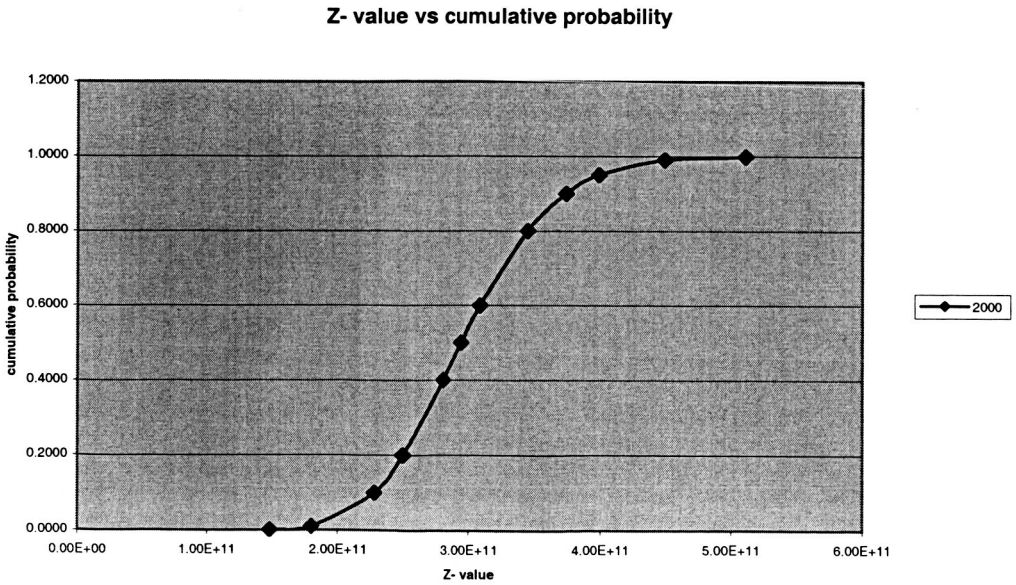

Figure 9.27: Cumulative Probability of thermal stress for stator at 2000th iteration

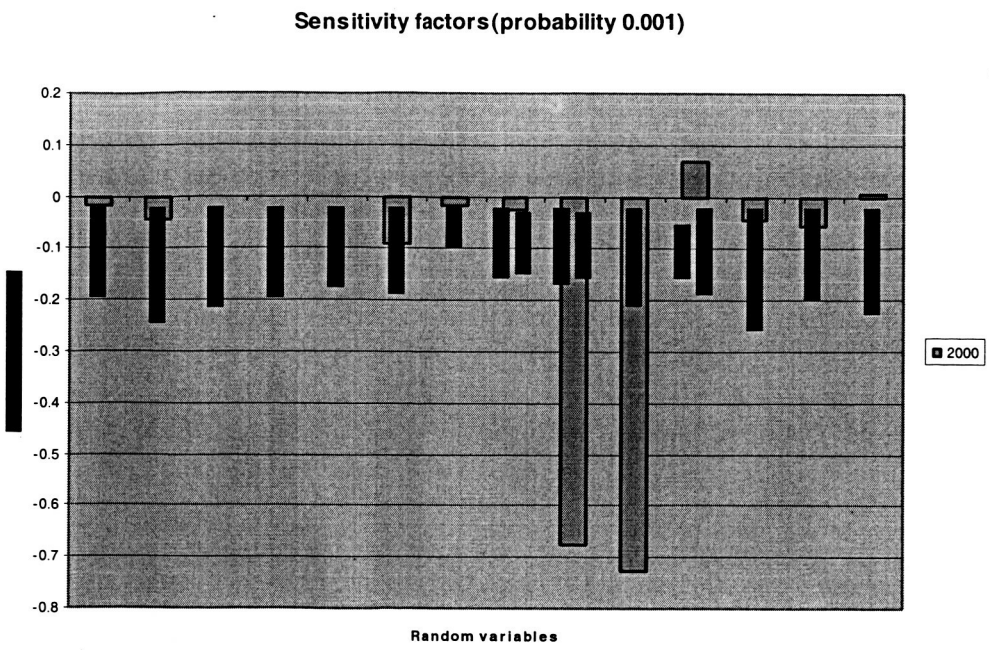

Figure9.28: Probability 0.001

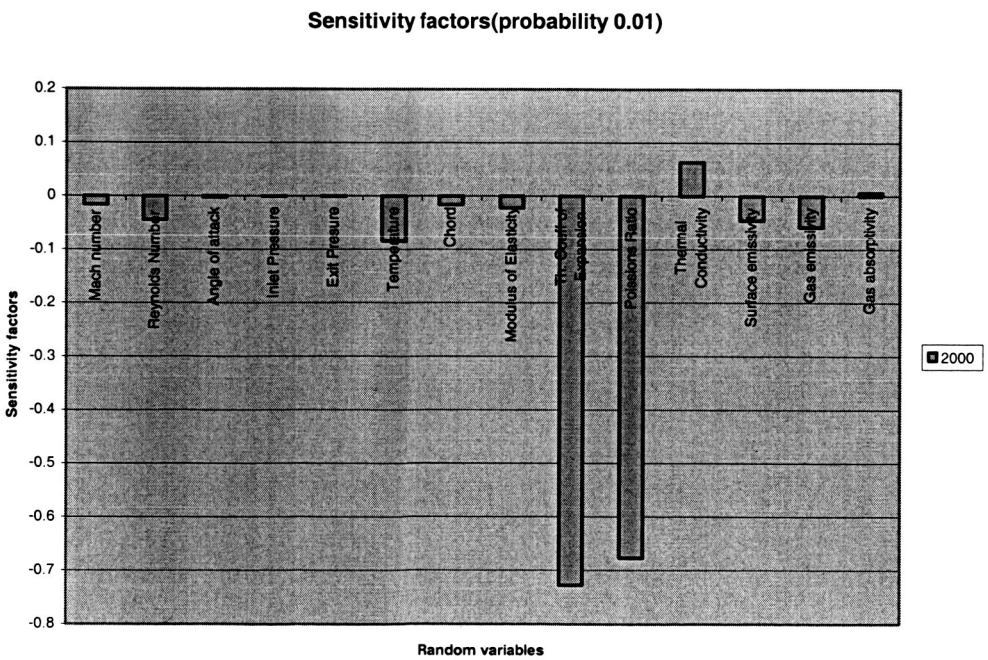

Figure 9.29: Probability 0.01

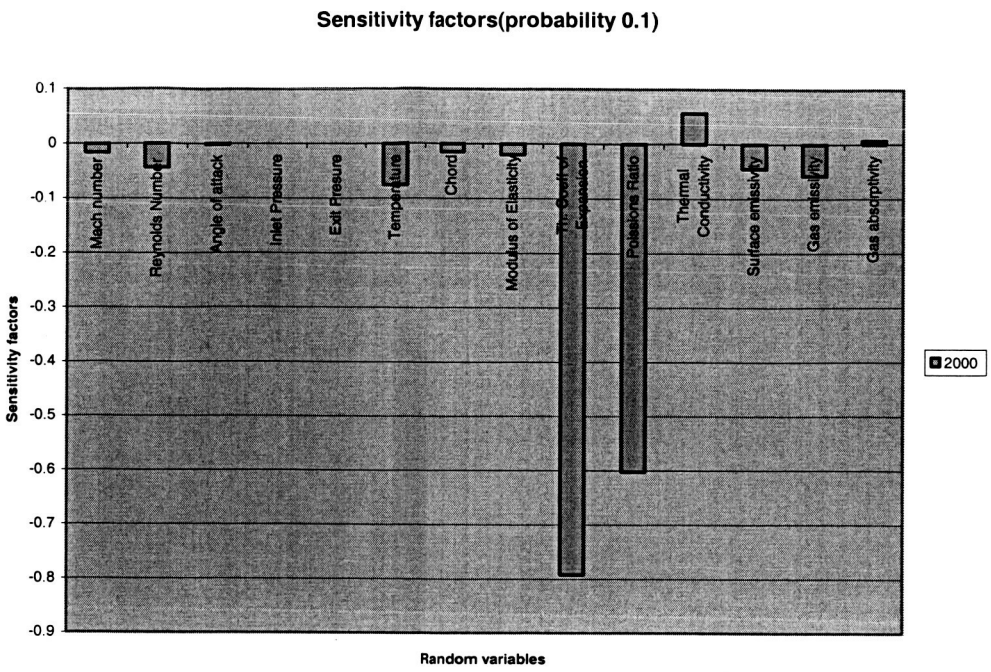

Figure 9.30: Probability 0.1

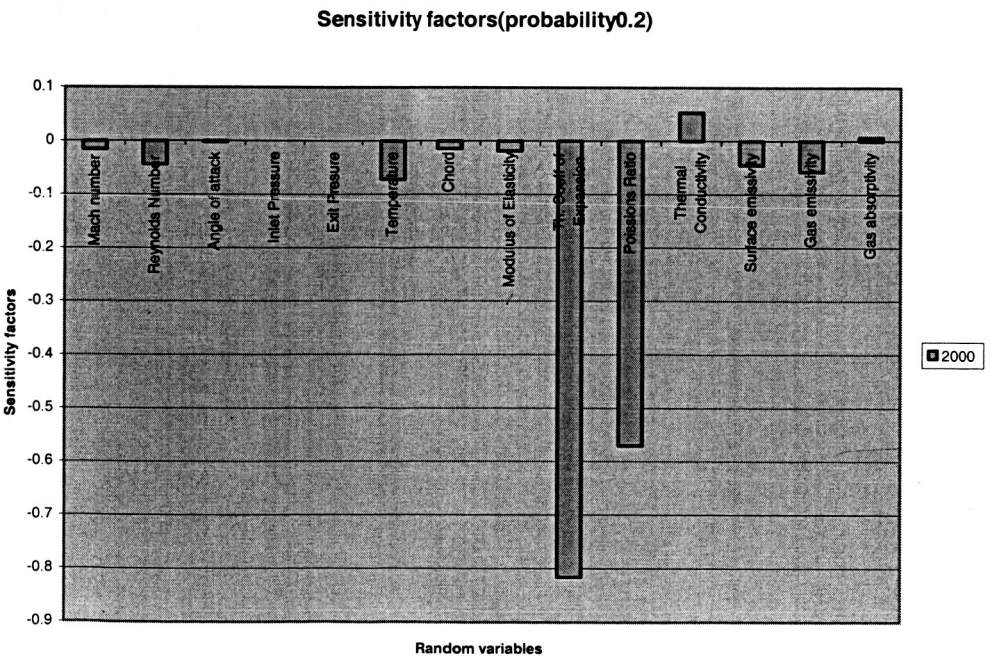

Figure 9.31: Probability 0.2

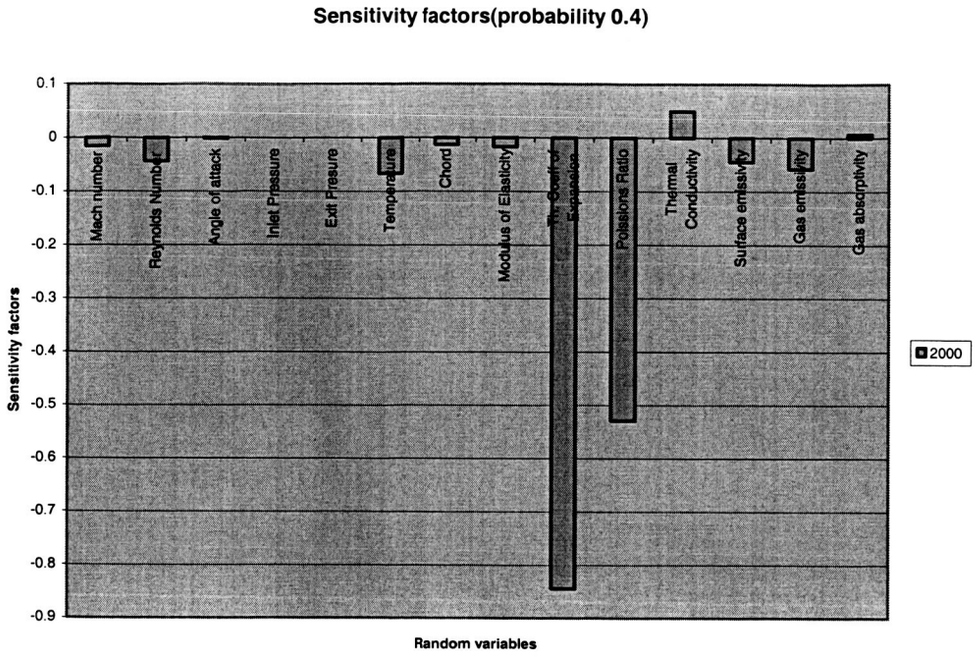

Figure9.32: Probability 0.4

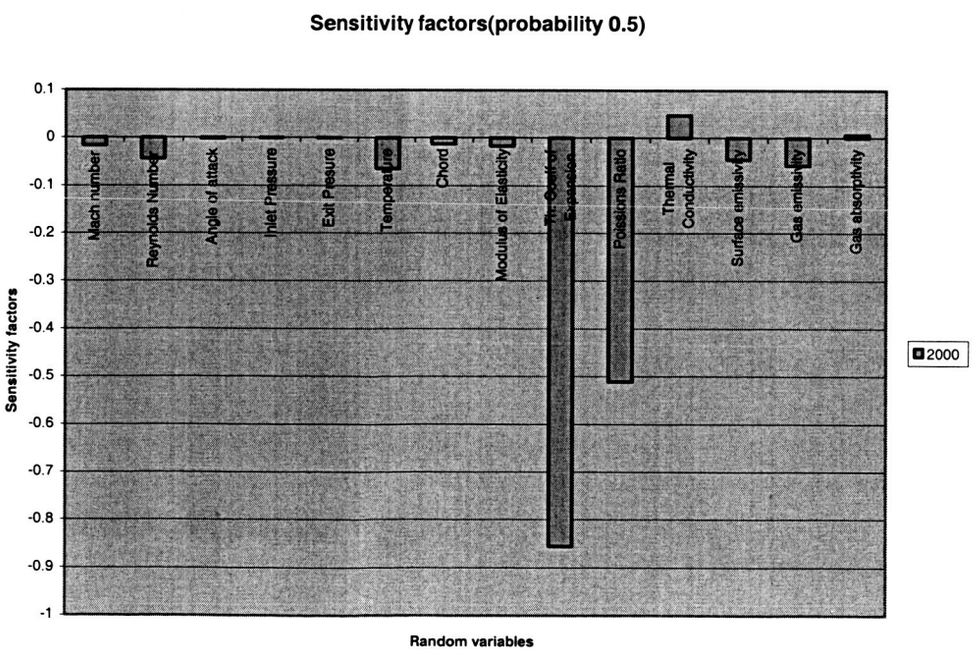

Figure 9.33: Probability 0.5

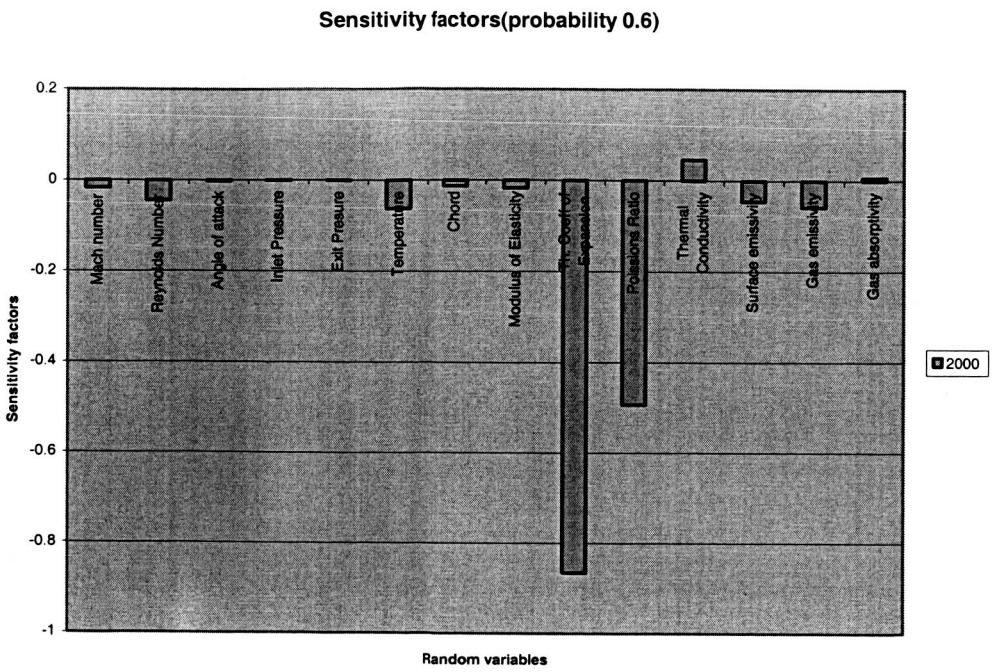

Figure 9.34: Probability 0.6

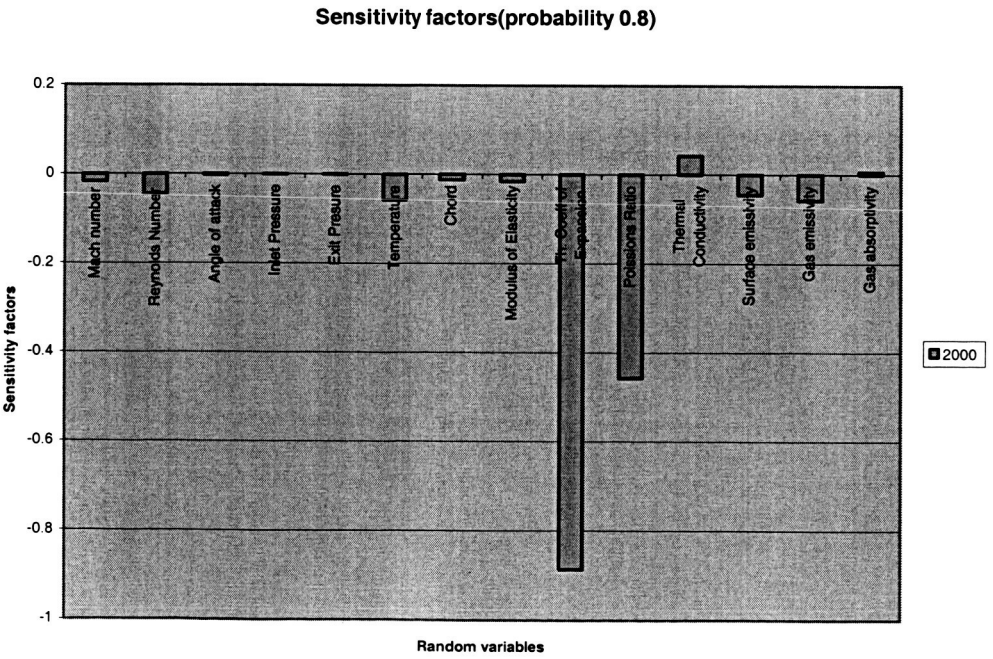

Figure 9.35: Probability 0.8

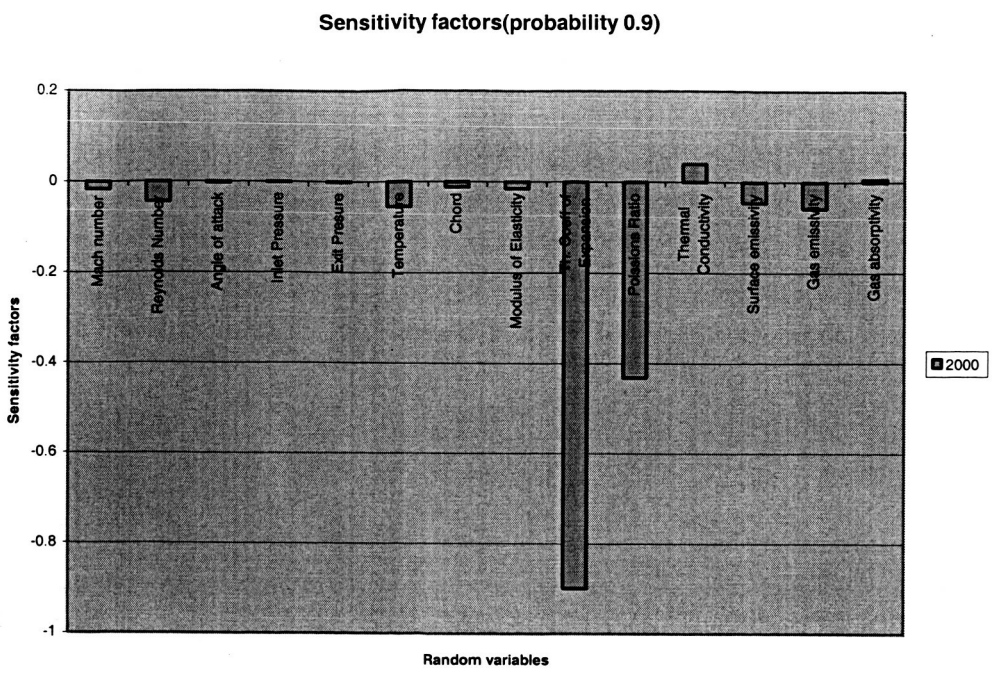

Figure 9.36: Probability 0.9

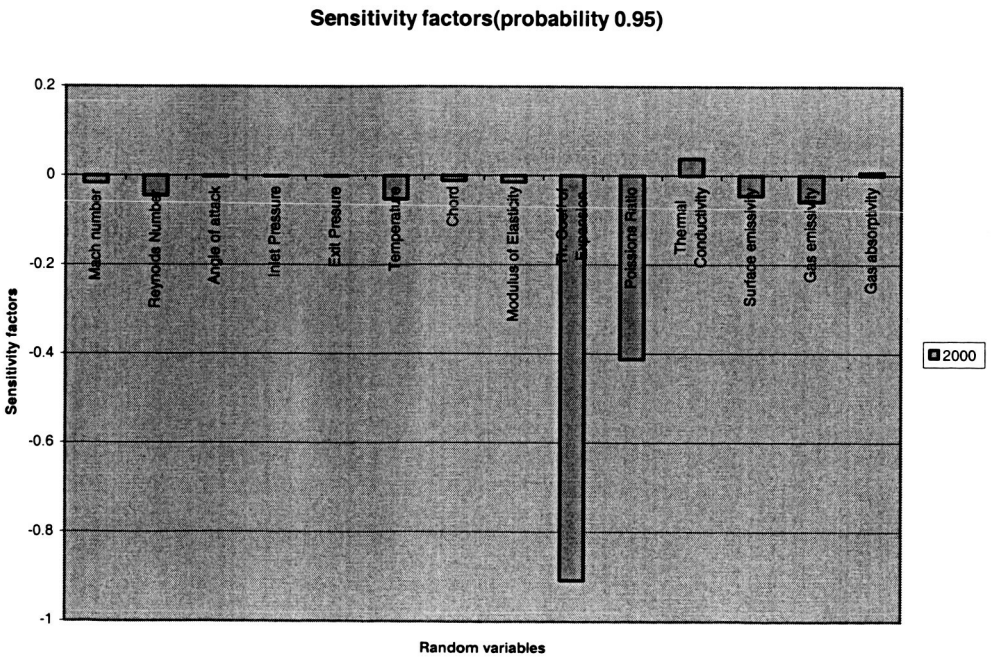

Figure 9.37: Probability 0.95

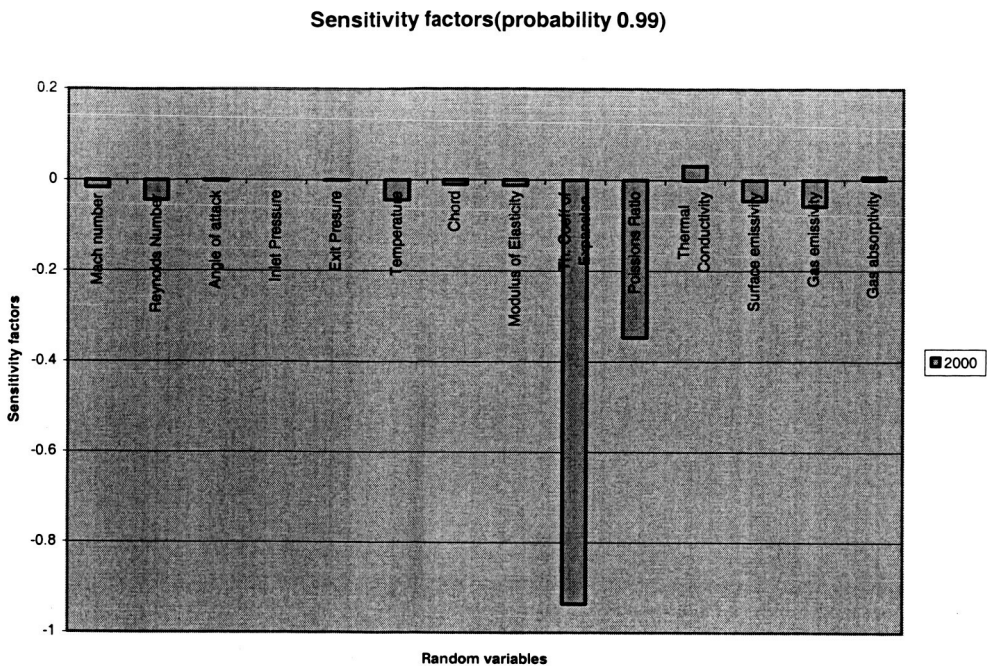

Figure 9.38: Probability 0.99

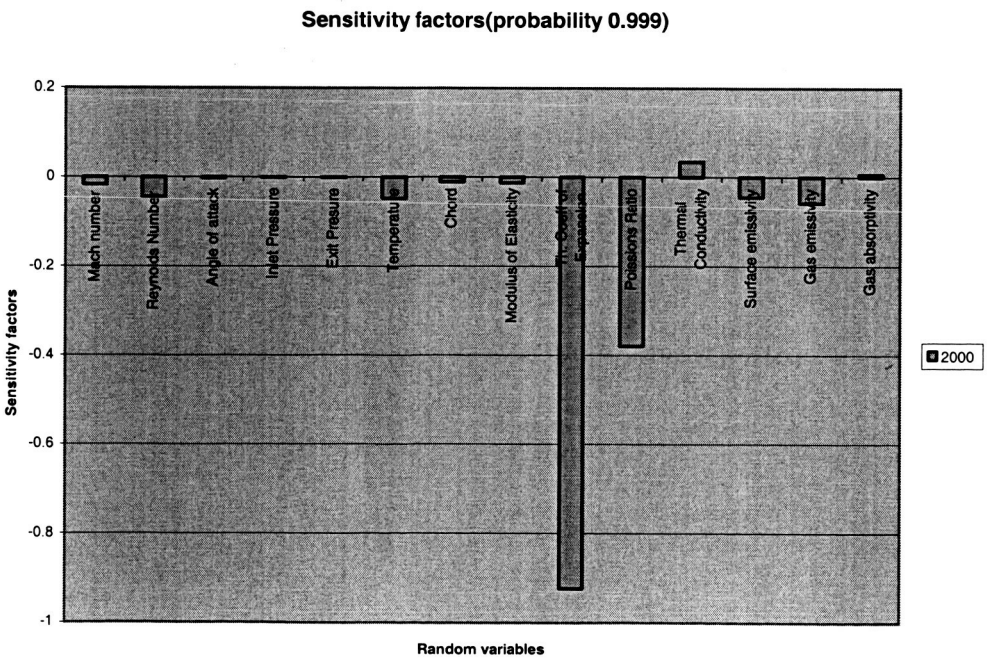

Figure 9.39: Probability 0.999

Results and Discussion for the Rotor:

The sensitivity factors for stress versus the random variables for Rotor are plotted in the figures 9.41-9.51, 9.52-9.63, 9.64-9.75 for three different iterations and for probability levels ranging from 0.001 to 0.999 and there is not much difference in all the three iterations. We observe that the thermal coefficient of expansion, Modulus of elasticity and Rotating speed have a lot of influence on the stress. For prescribed values of thermal conductivity, Poisson's ratio Reynolds number, angle of attack, gas emissivity and absorptivity, inlet temperature, inlet and exit pressures, thermal conductivity, and chord length of the material have a lot of impact on the stress. These results can be used to further optimize the design for cost effectiveness.

Results for the 1900th iteration are shown below:

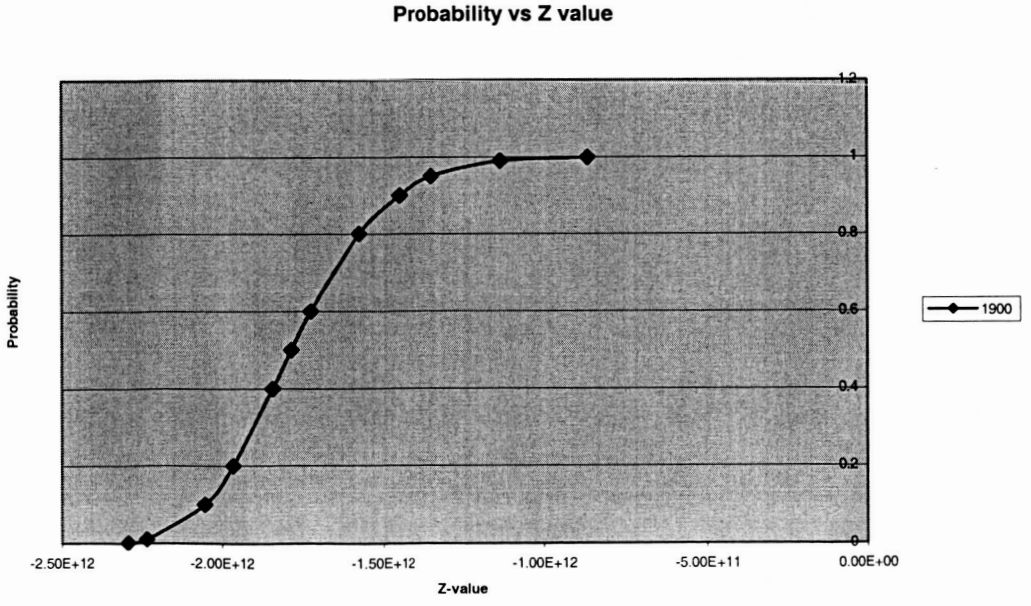

Figure 9.40: Cumulative Probability of thermal stress for rotor at 1900th iteration

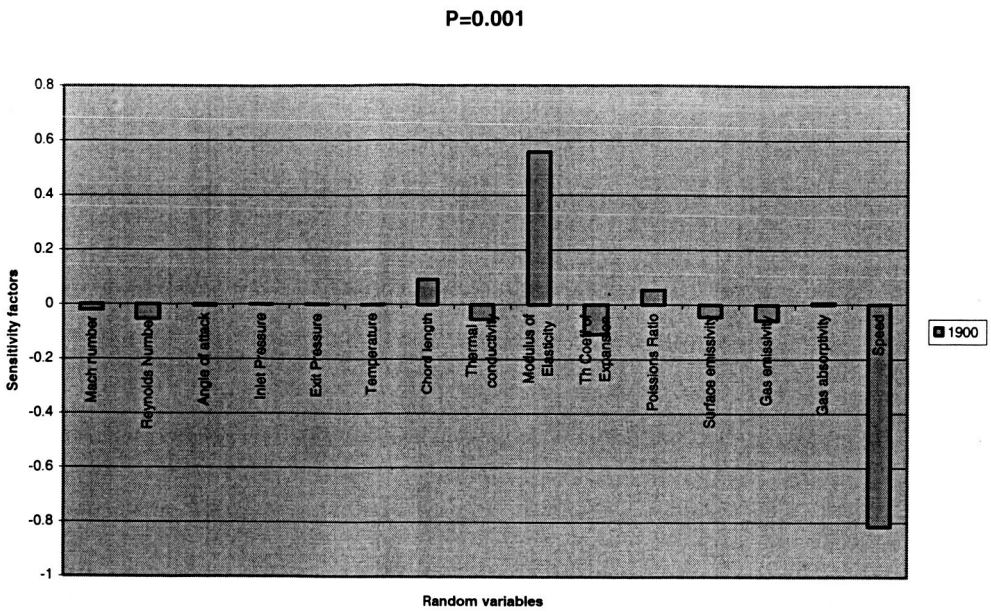

Figure 9.41: Probability 0.001

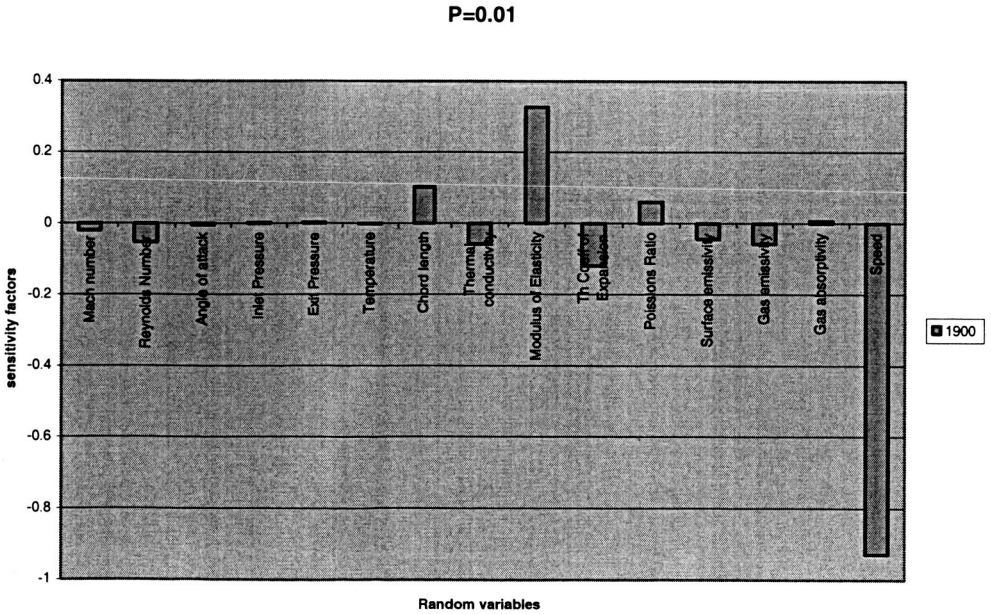

Figure 9.42: Probability 0.01

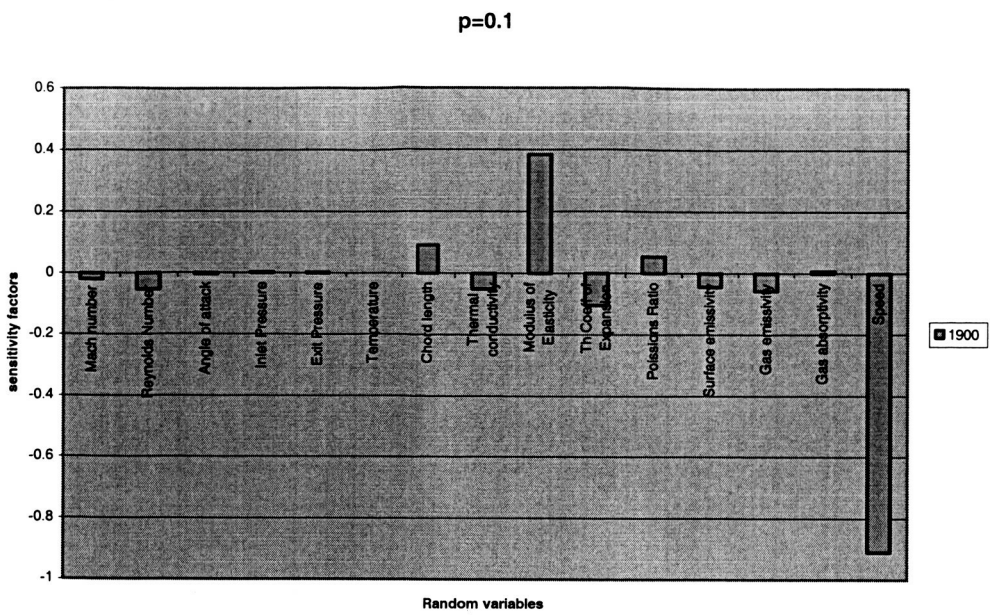

Figure 9.43: Probability 0.1

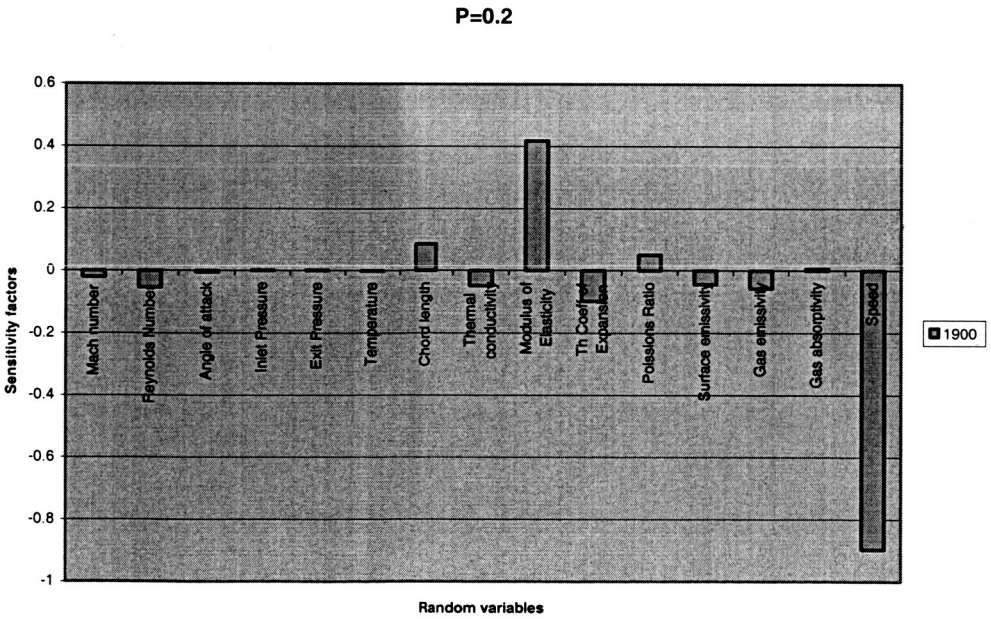

Figure 9.44: Probability 0.2

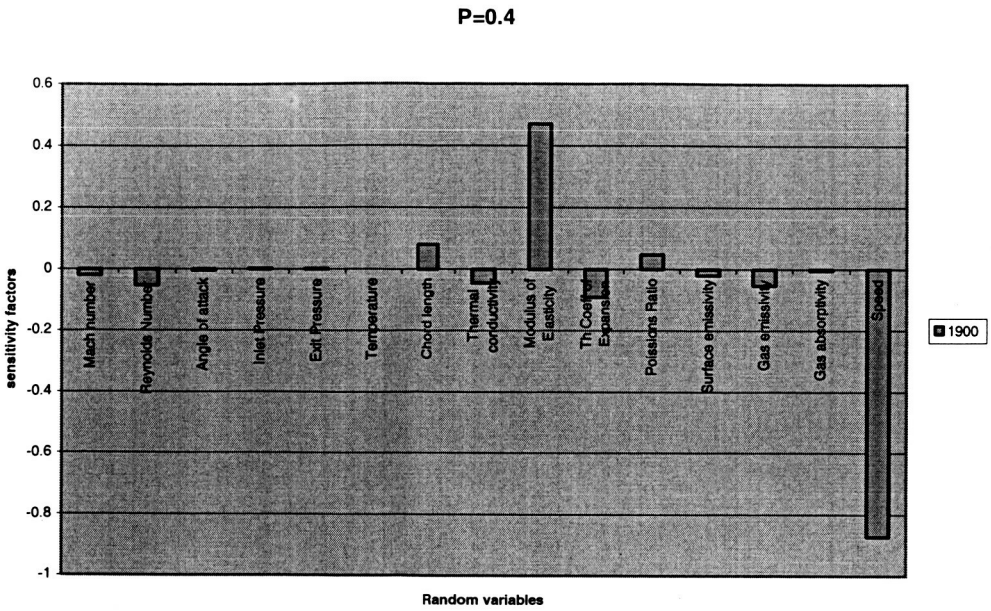

Figure 9.45: Probability 0.4

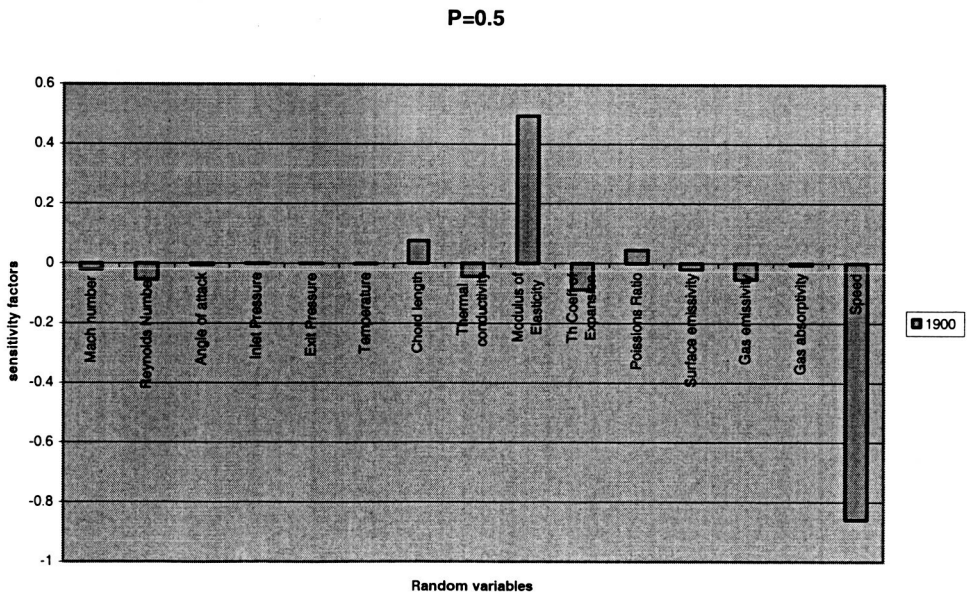

Figure 9.46: Probability 0.5

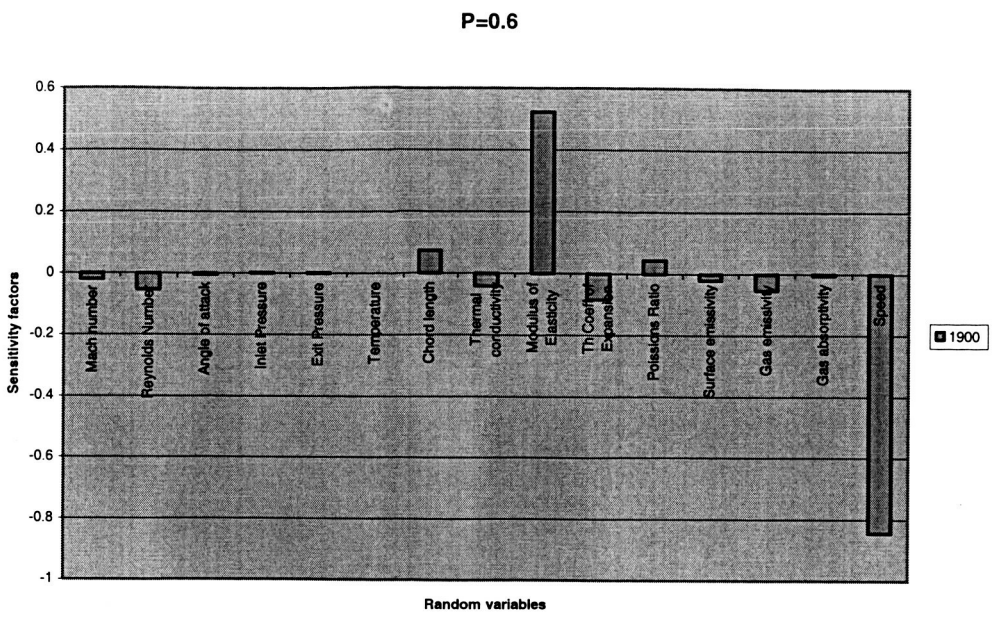

Figure 9.47: Probability 0.6

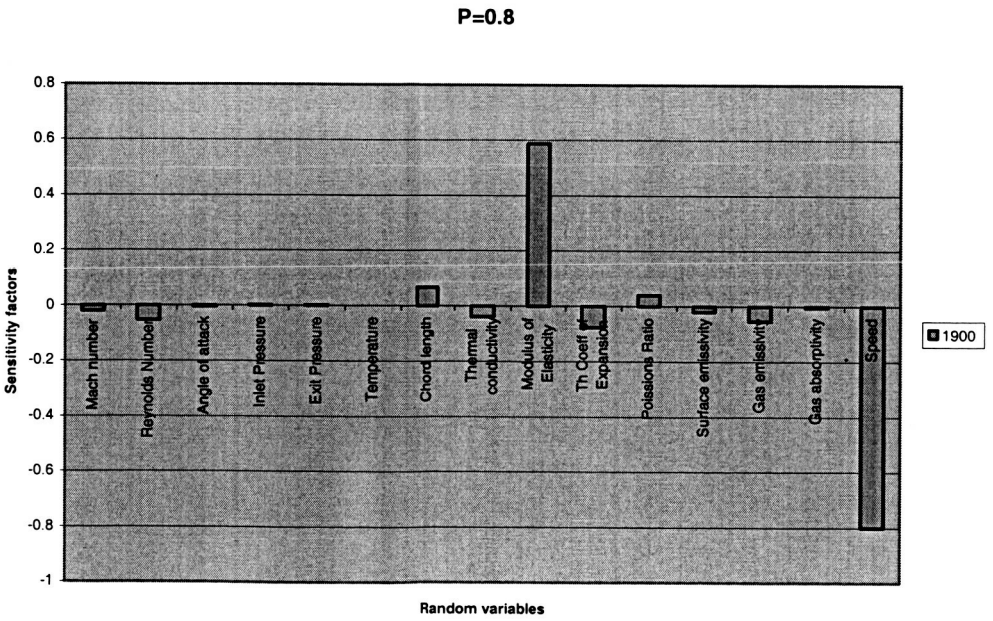

Figure 9.48: Probability 0.8

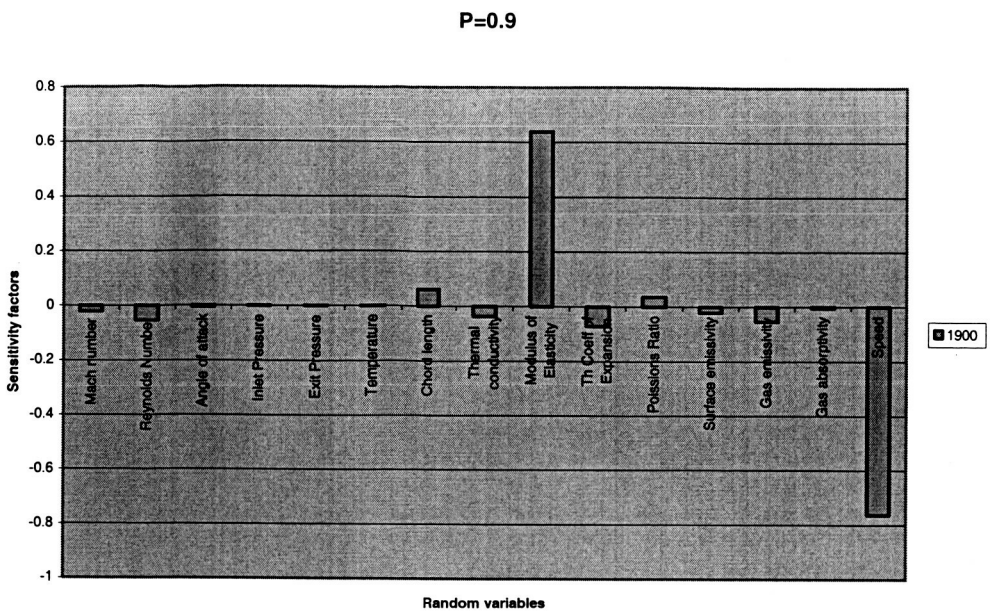

Figure 9.49: Probability 0.9

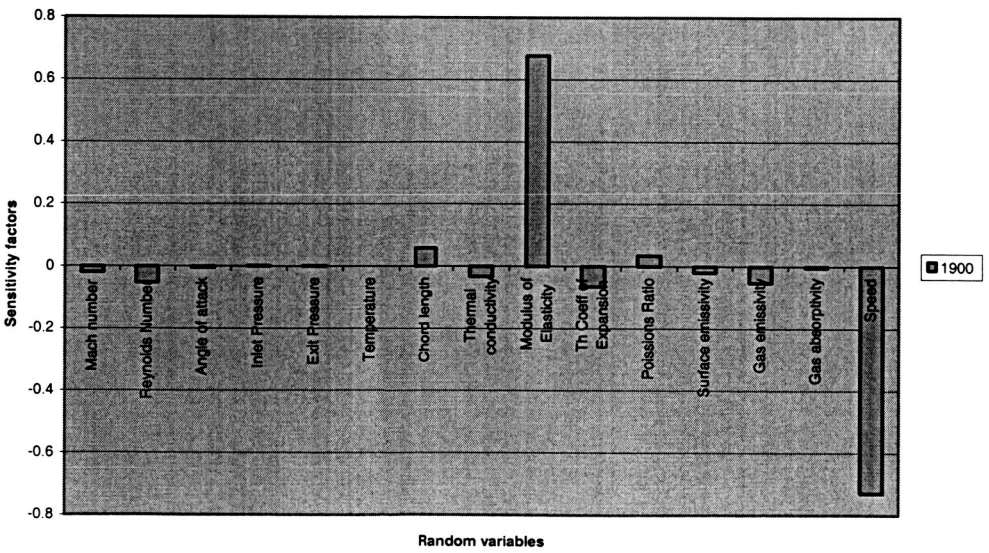

Figure 9.50: Probability 0.95

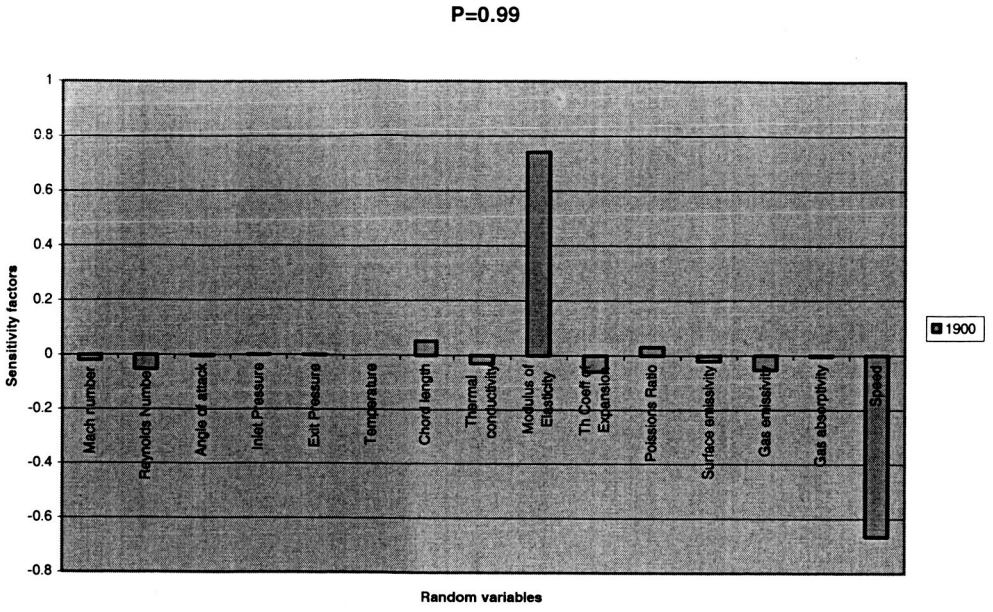

Figure 9.51: Probability 0.99

Results for the 1960th iteration:

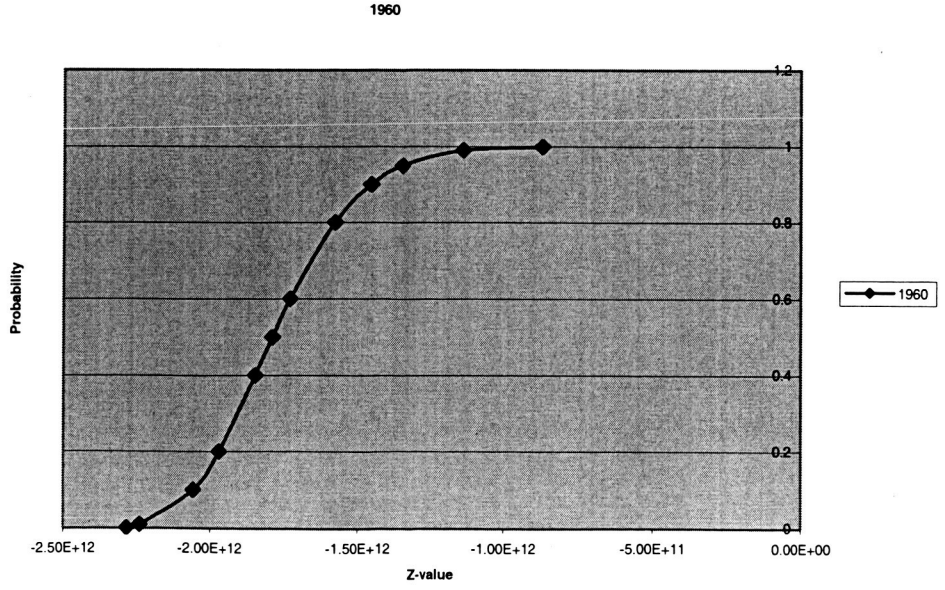

Figure 9.52: Cumulative Probability of thermal stress for rotor at 1960th iteration

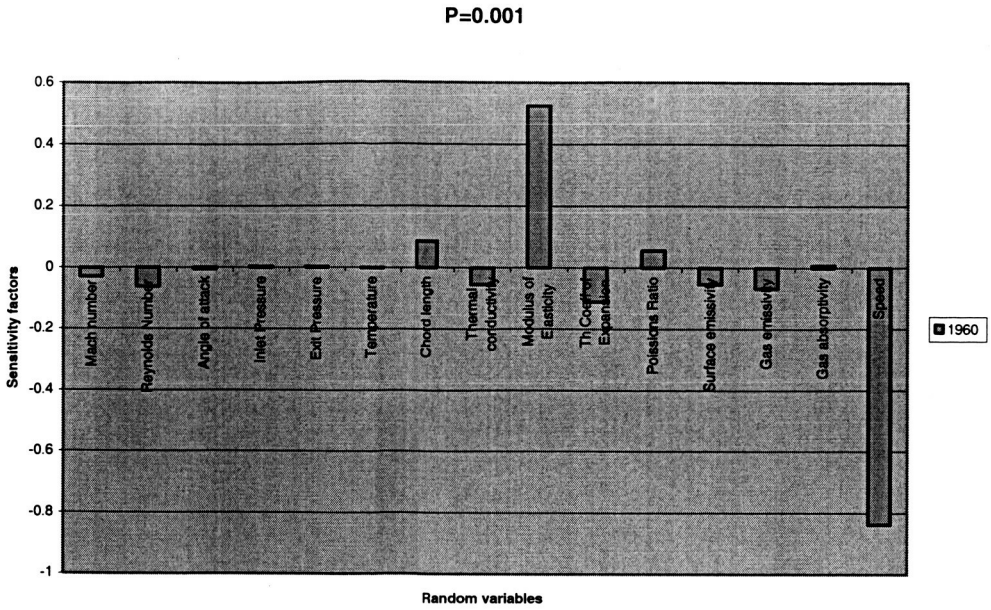

Figure 9.53: Probability 0.001

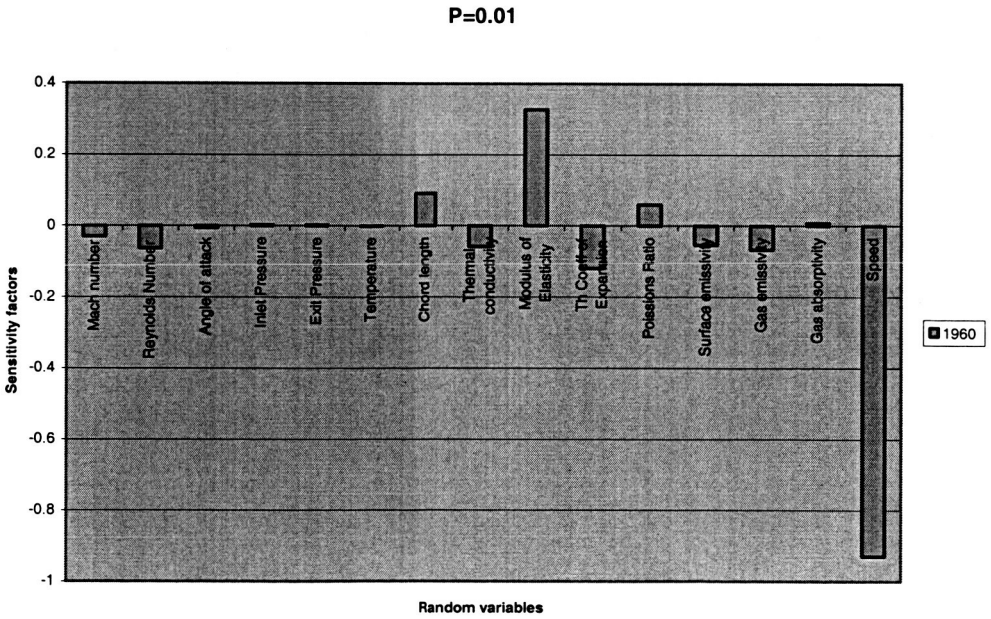

Figure 9.54: Probability 0.01

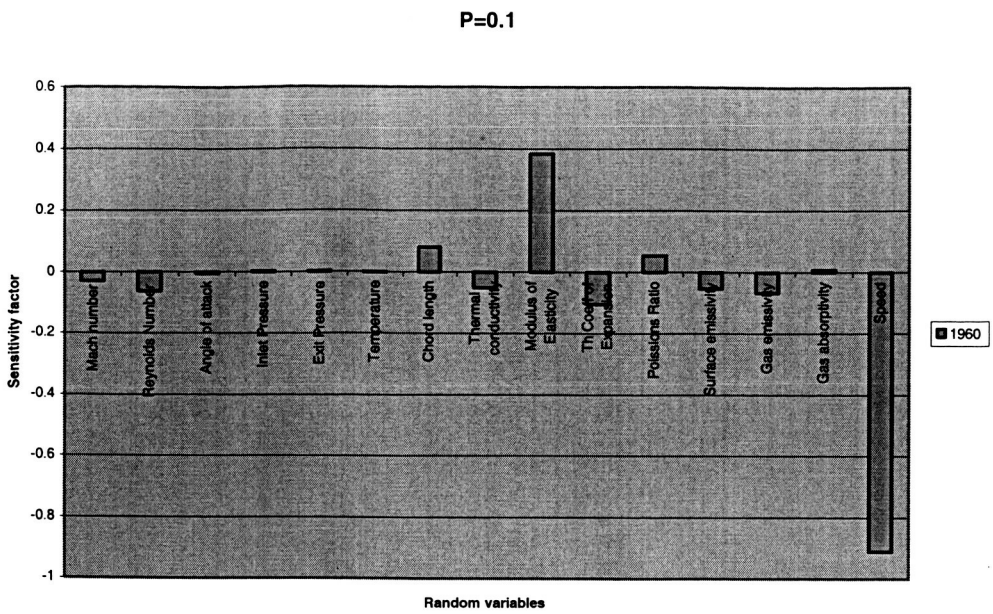

Figure 9.55: Probability 0.1

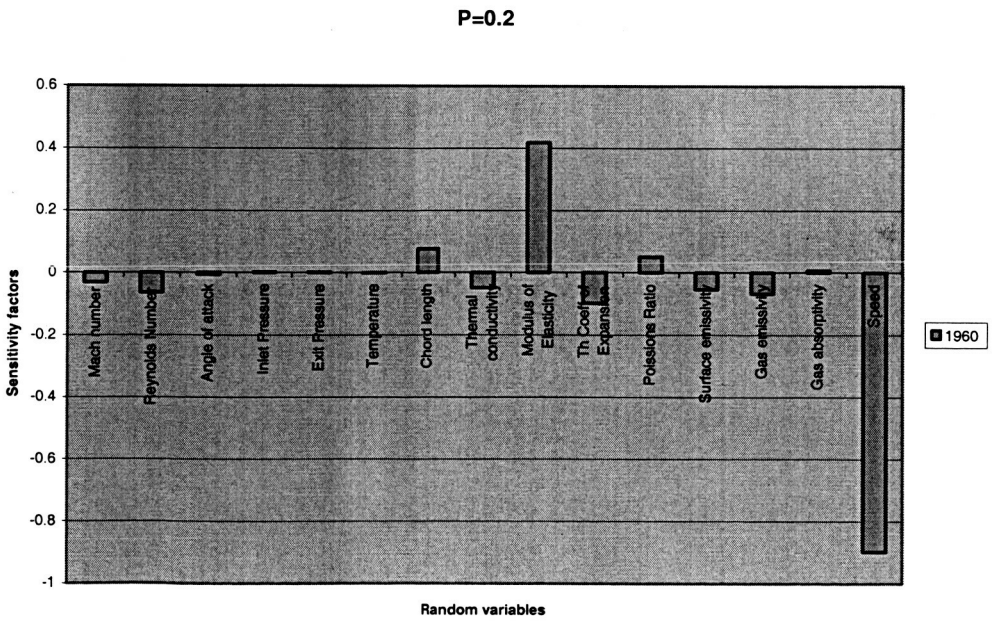

Figure 9.56: Probability 0.2

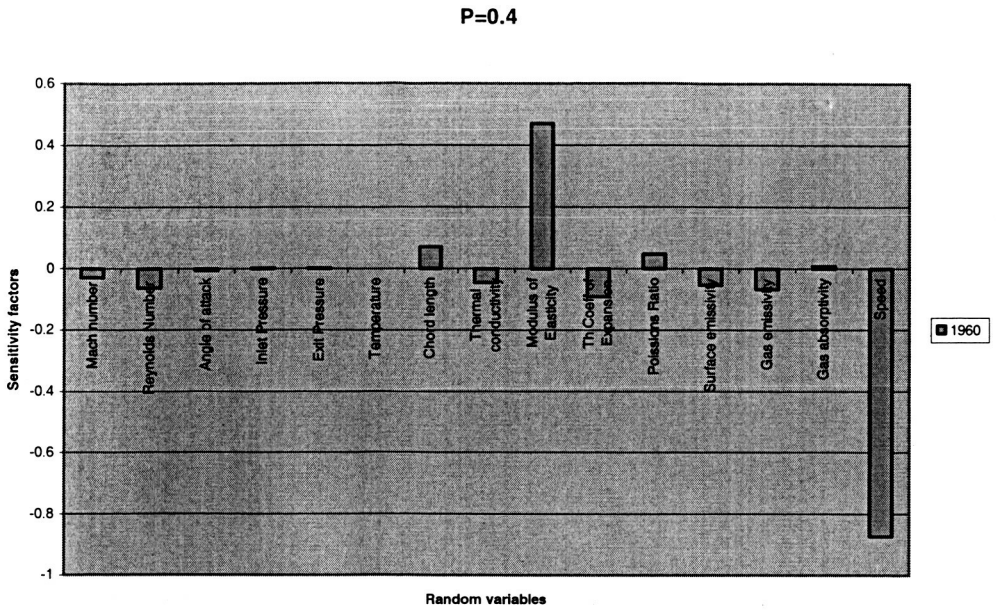

Figure 9.57: Probability 0.4

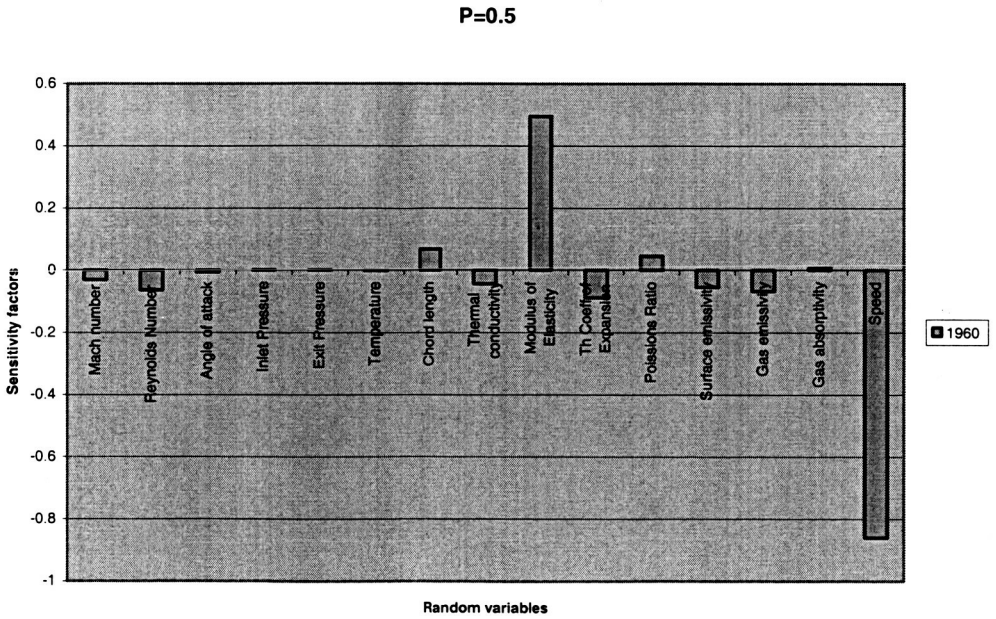

Figure 9.58: Probability 0.5

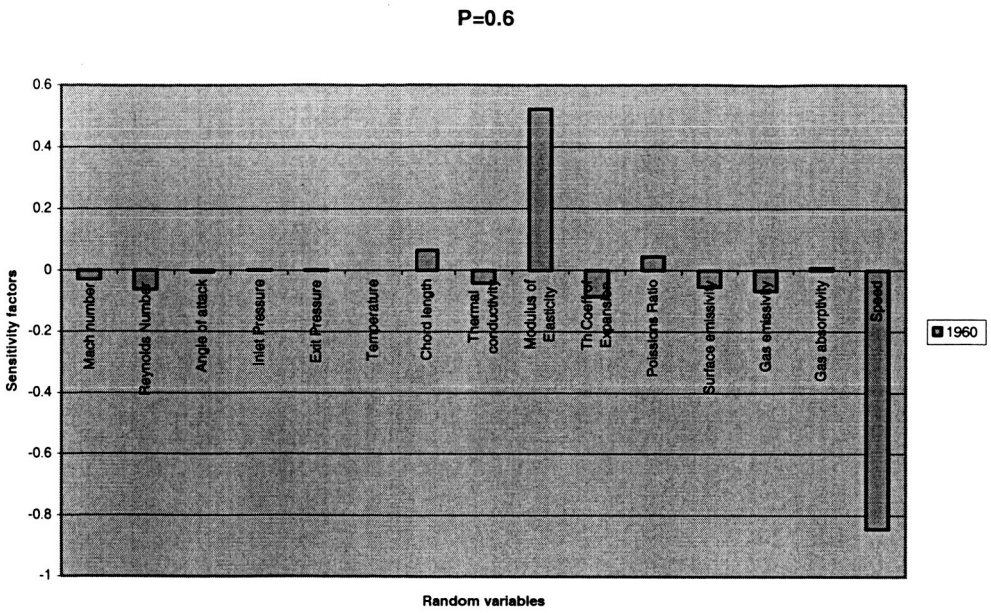

Figure 9.59: Probability 0.6

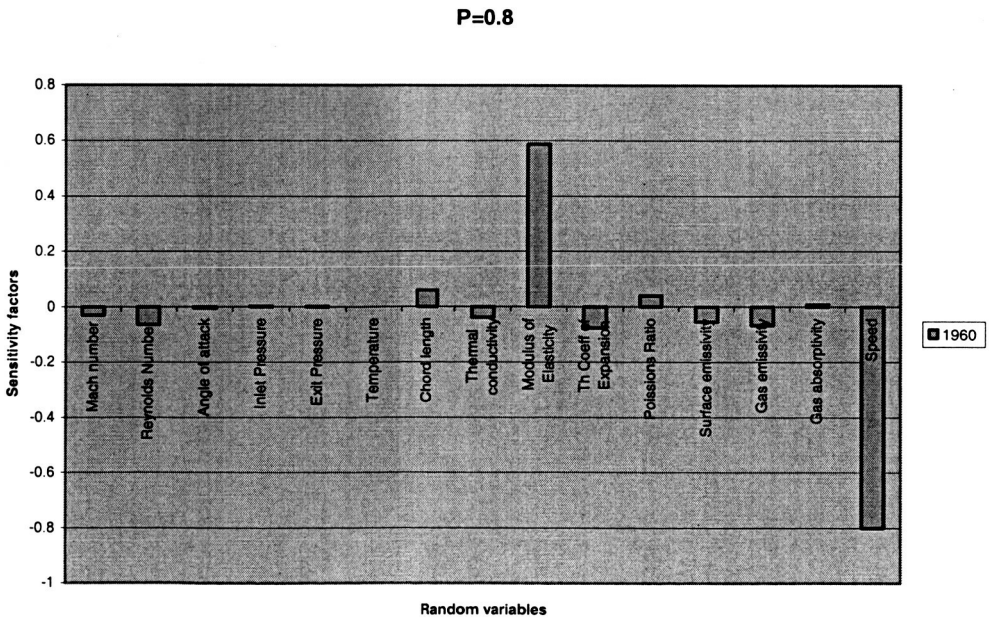

Figure 9.60: Probability 0.8

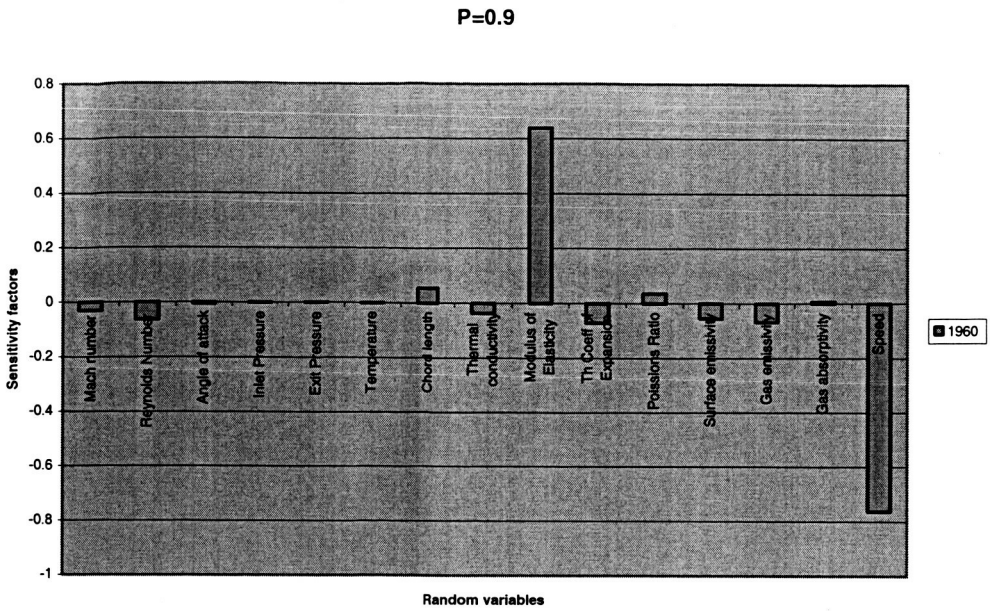

Figure 9.61: Probability 0.9

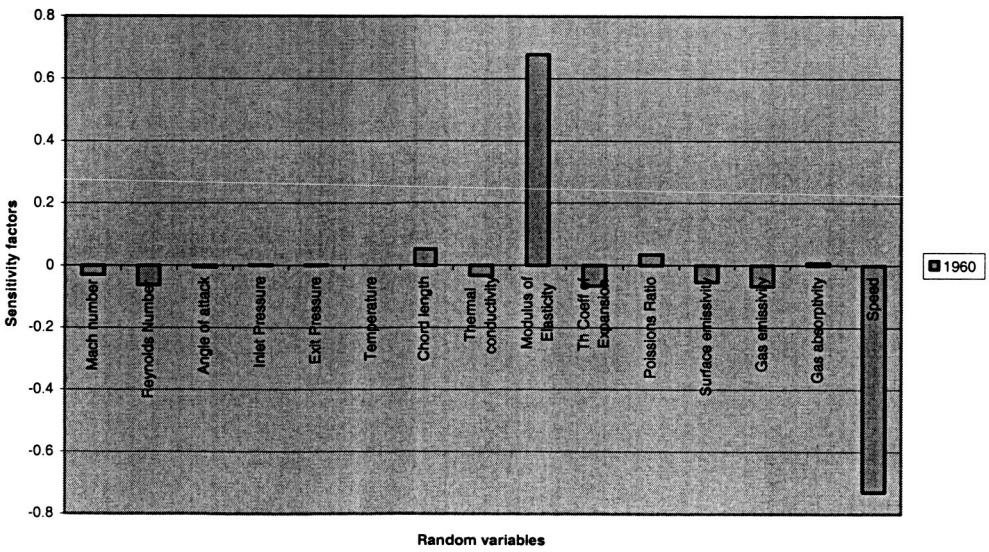

Figure 9.62: Probability 0.95

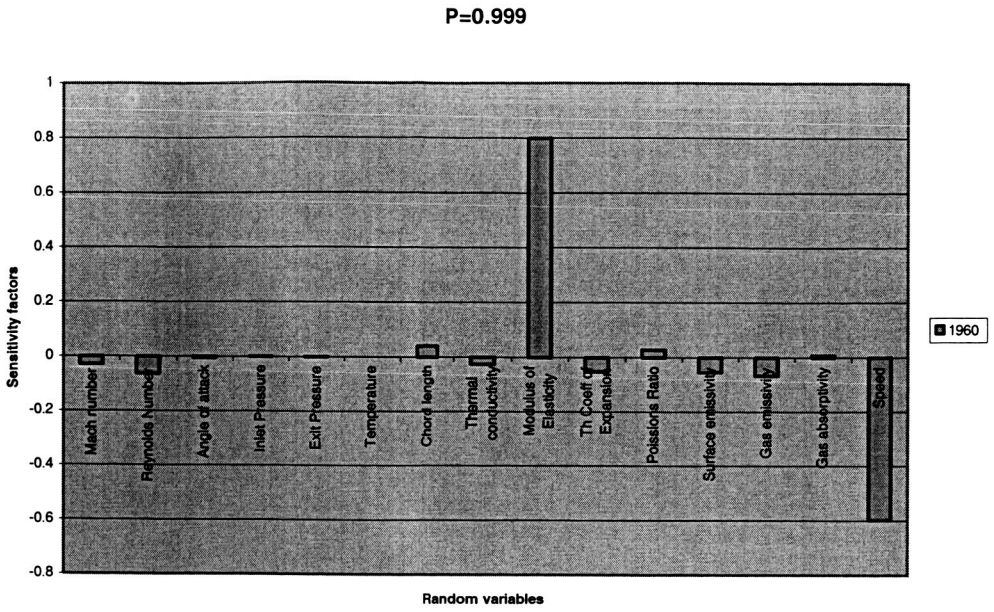

Figure 9.63: Probability 0.999

Results for the 2000th iteration:

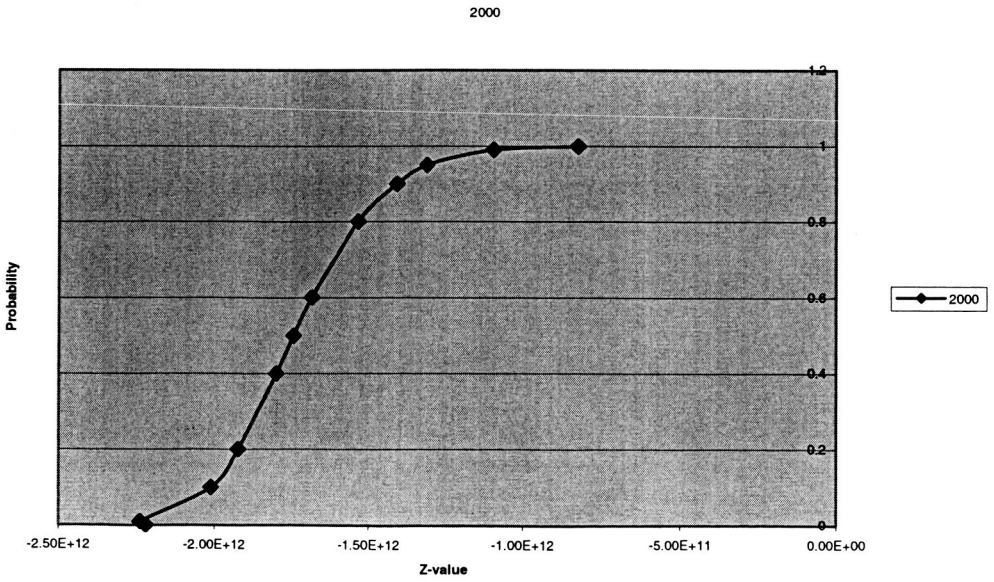

Figure 9.64: Cumulative Probability of thermal stress for rotor at 2000th iteration

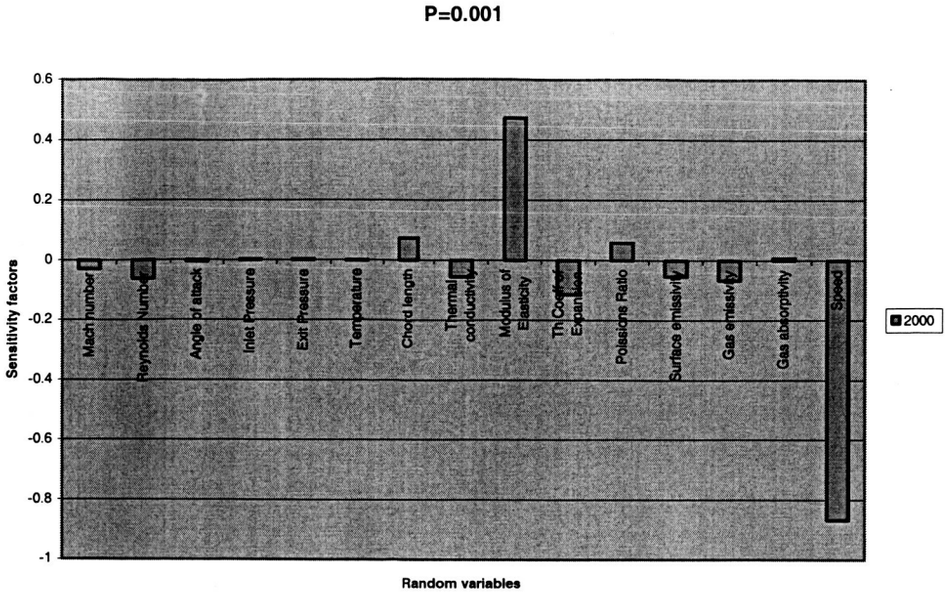

Figure 9.65: Probability 0.001

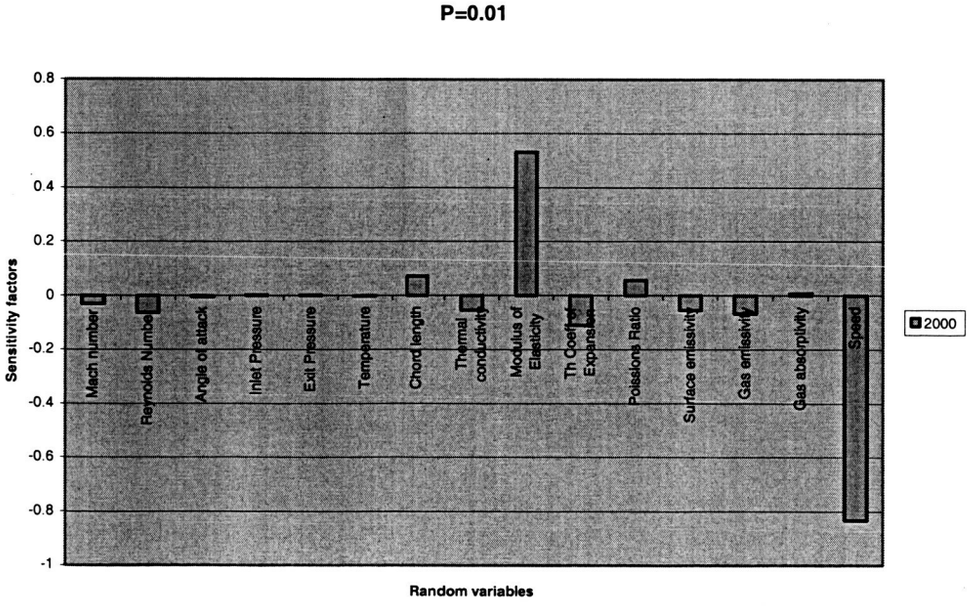

Figure 9.66: Probability 0.01

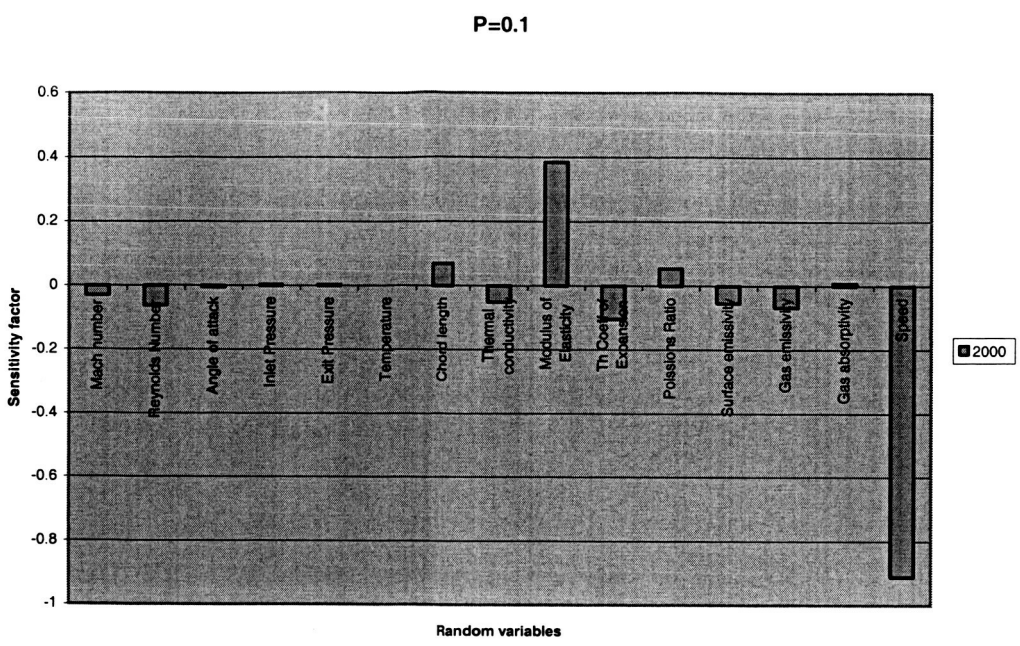

Figure 9.67: Probability 0.1

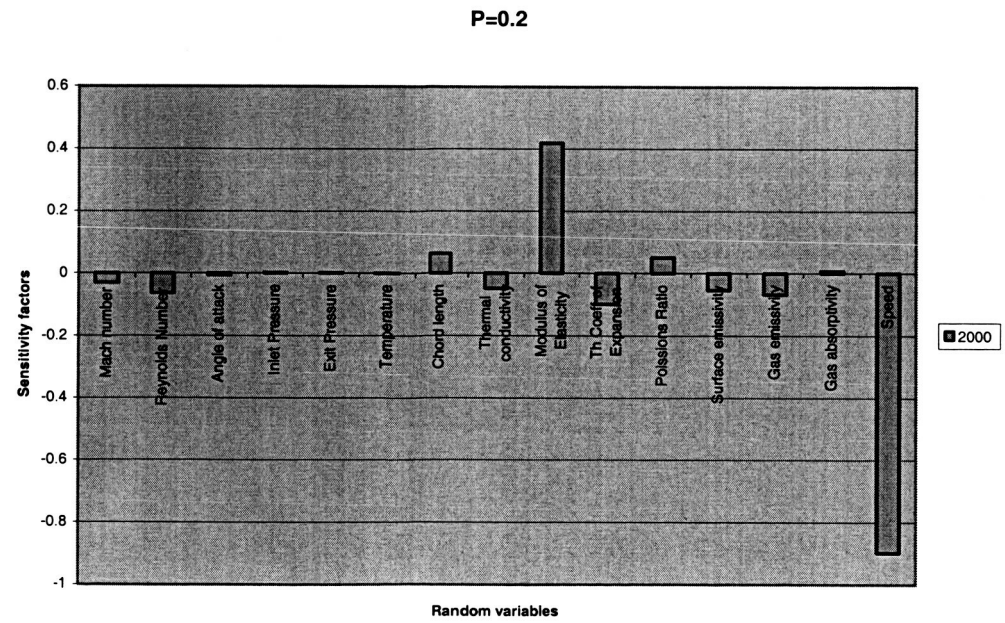

Figure 9.68: Probability 0.2

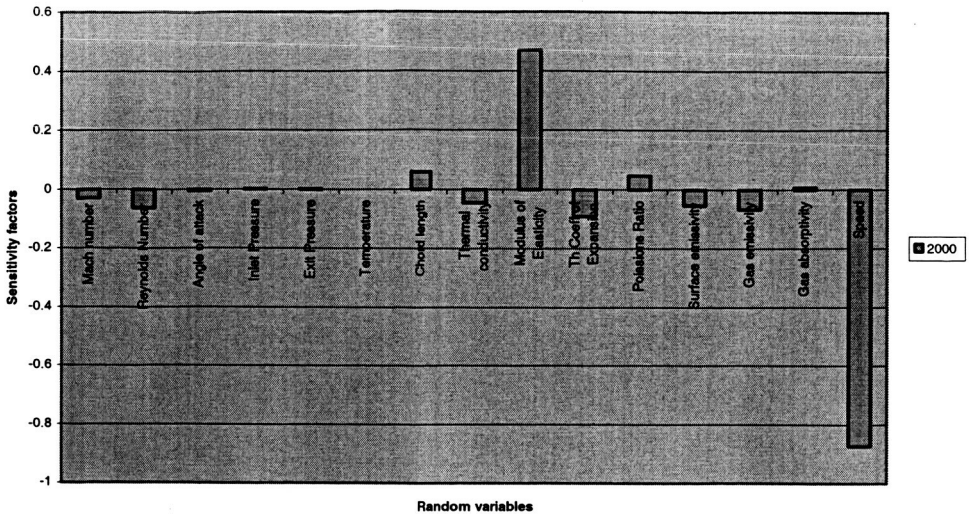

Figure 9.69: Probability 0.4

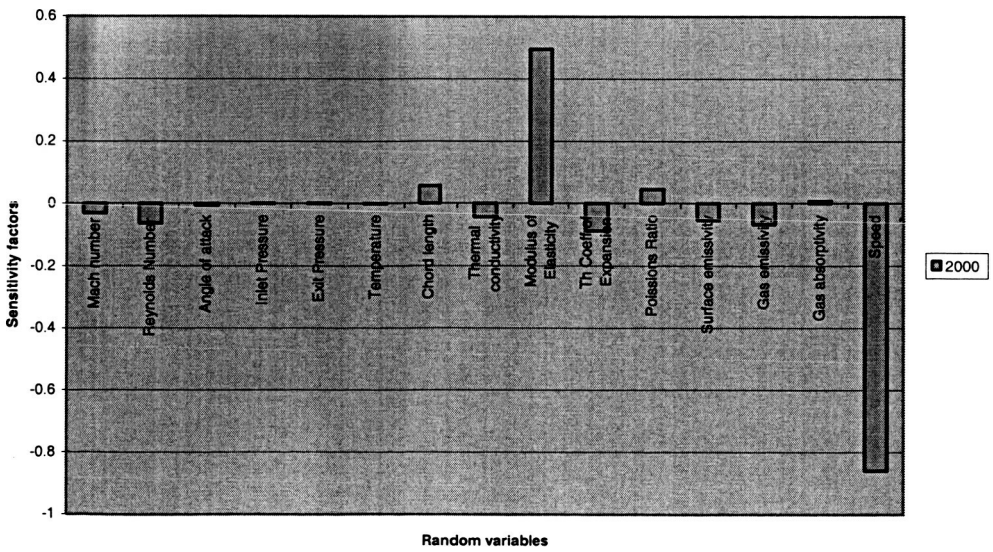

Figure 9.70: Probability 0.5

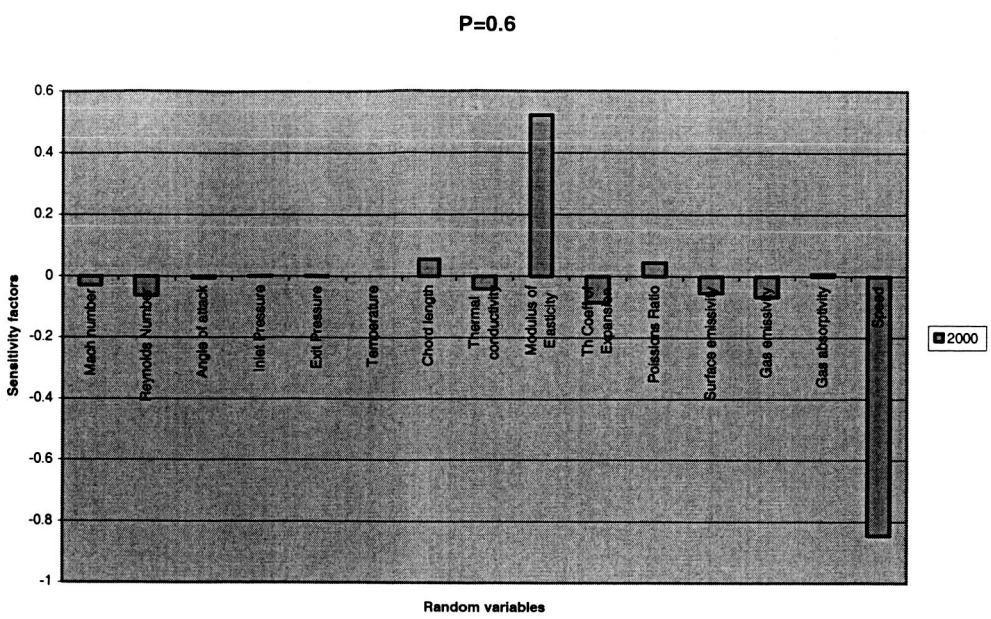

Figure 9.71: Probability 0.6

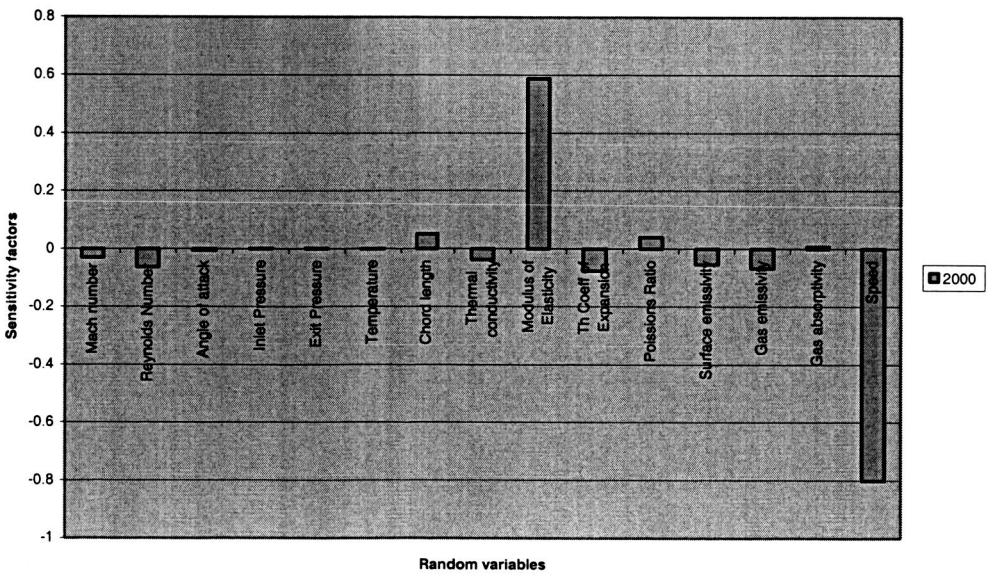

Figure 9.72: Probability 0.8

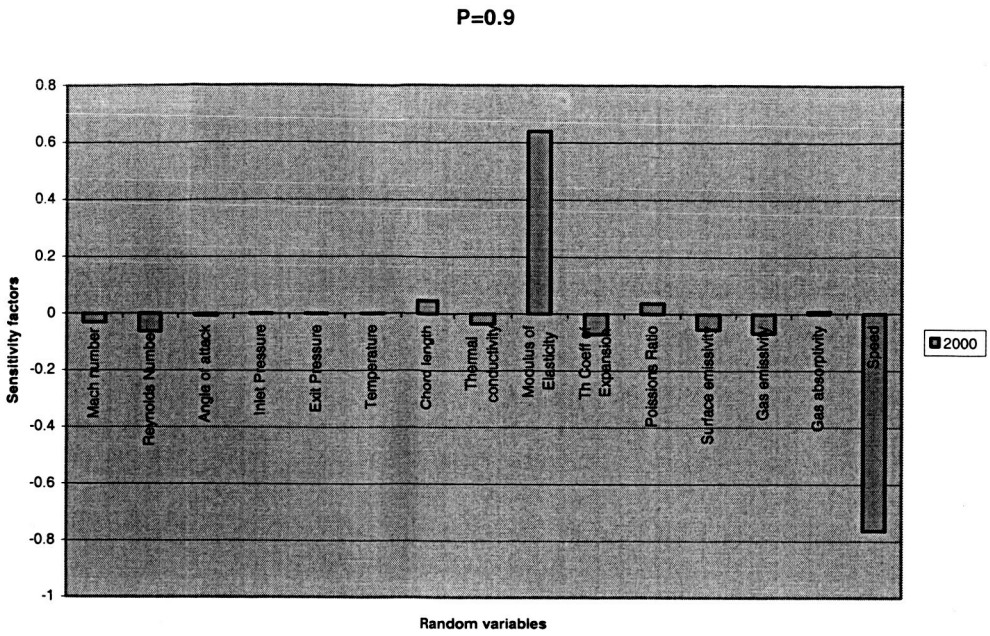

Figure 9.73: Probability 0.9

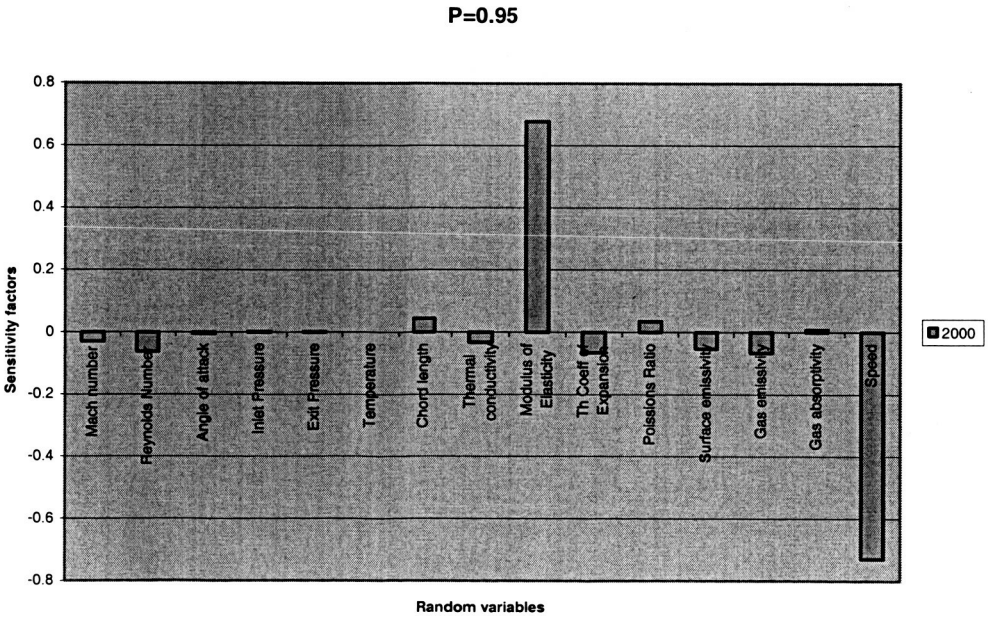

Figure 9.74: Probability 0.95

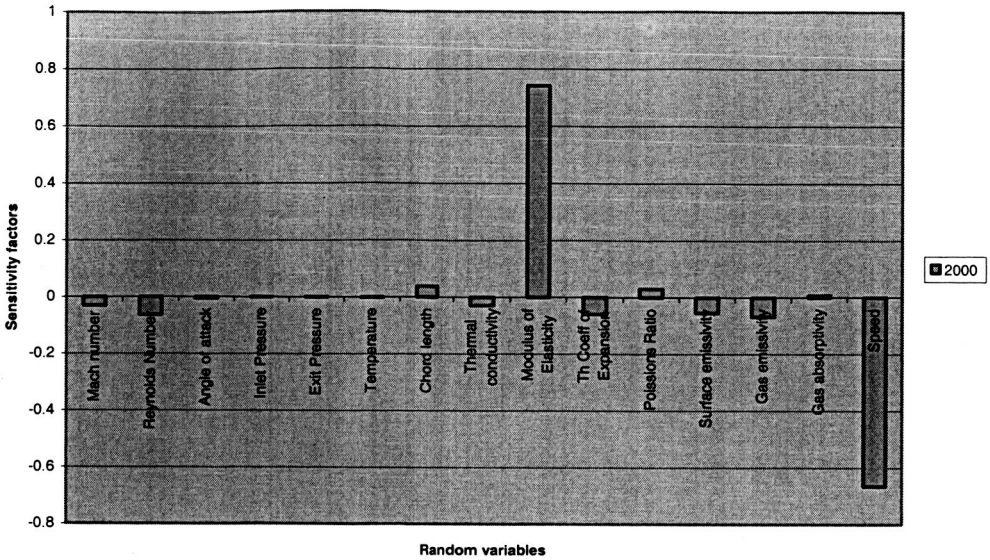

Figure 9.75: Probability 0.99

The Results for the Stator for all the three Iterations namely 1900th, 1960th, and 2000th iteration are shown below in the same graph. We can deduce from these graphs that in all the three iterations for different probability levels ranging from 0.001 to 0.999 the same random variables namely thermal coefficient of expansion and Poisson's ratio has a lot of influence on the stress. This helps us in further optimizing the design of cost effectiveness.

Graphs comparing all the three iterations 1900th, 1960th, and 2000th for sensitivity factors vs. random variables for stator.

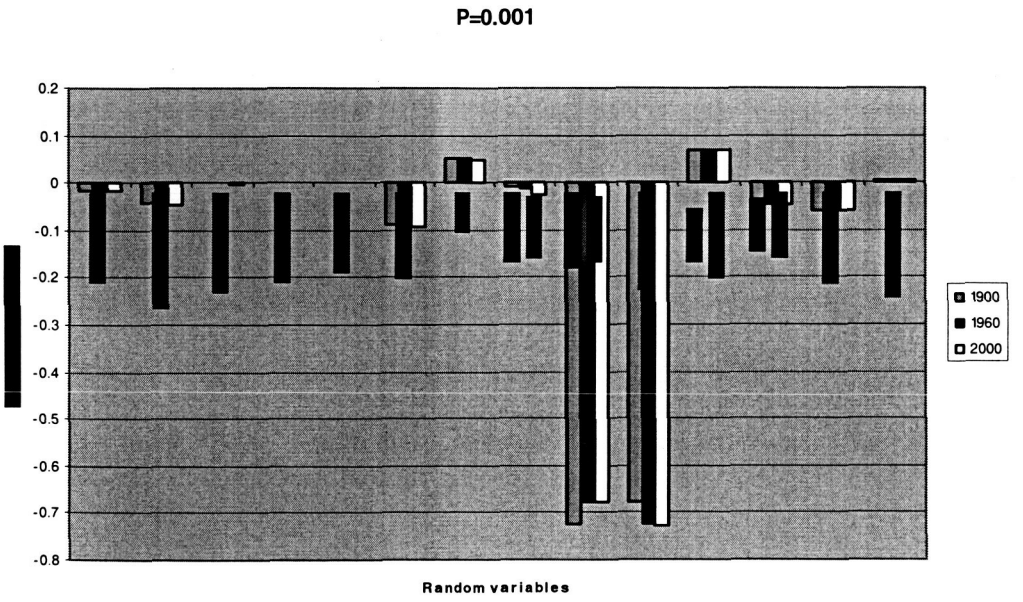

Figure 9.76: Probability 0.001

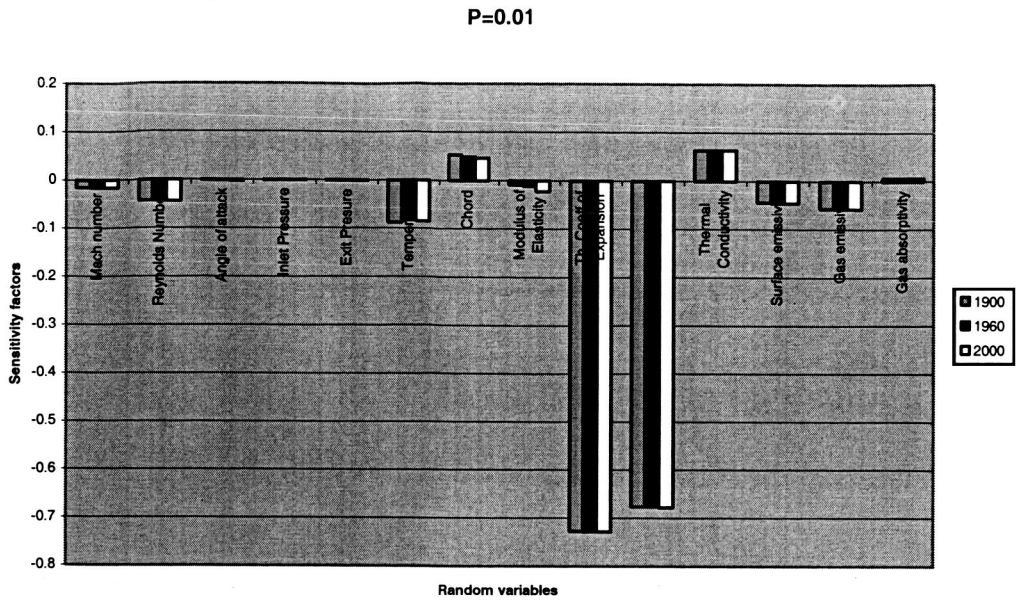

Figure 9.77: Probability 0.01

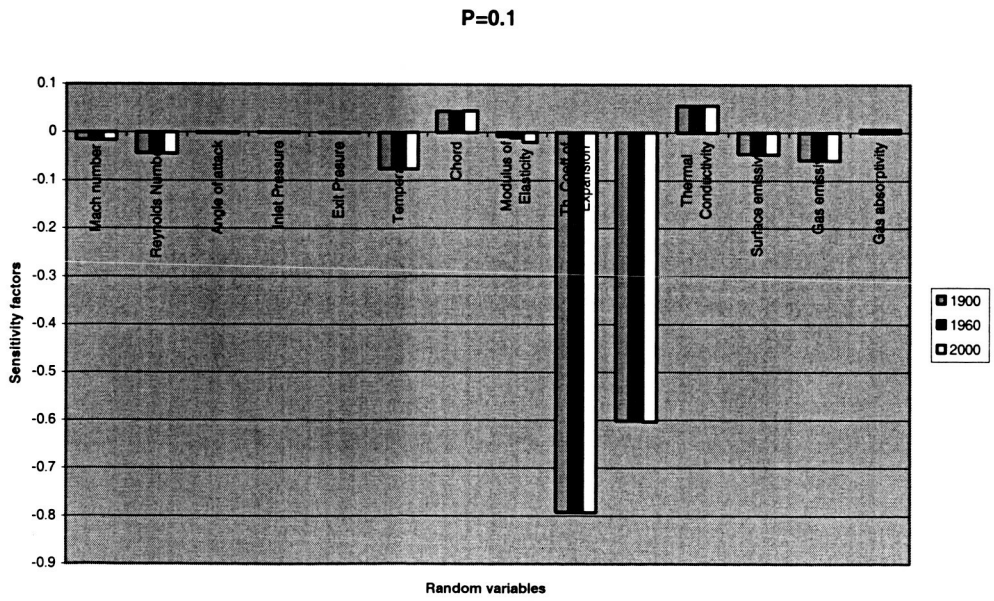

Figure: 9.78: Probability 0.1

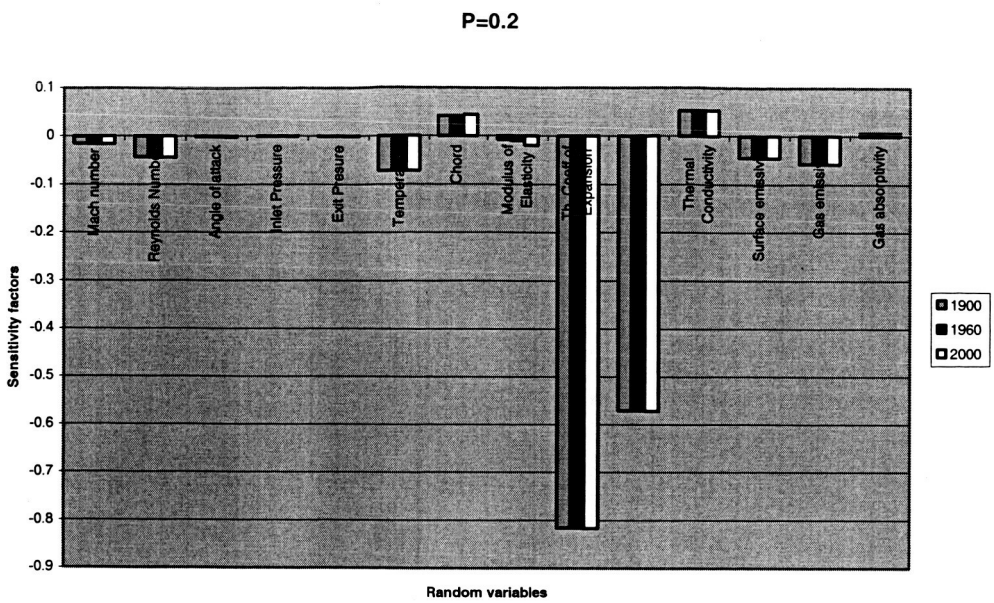

Figure: 9.79: Probability 0.2

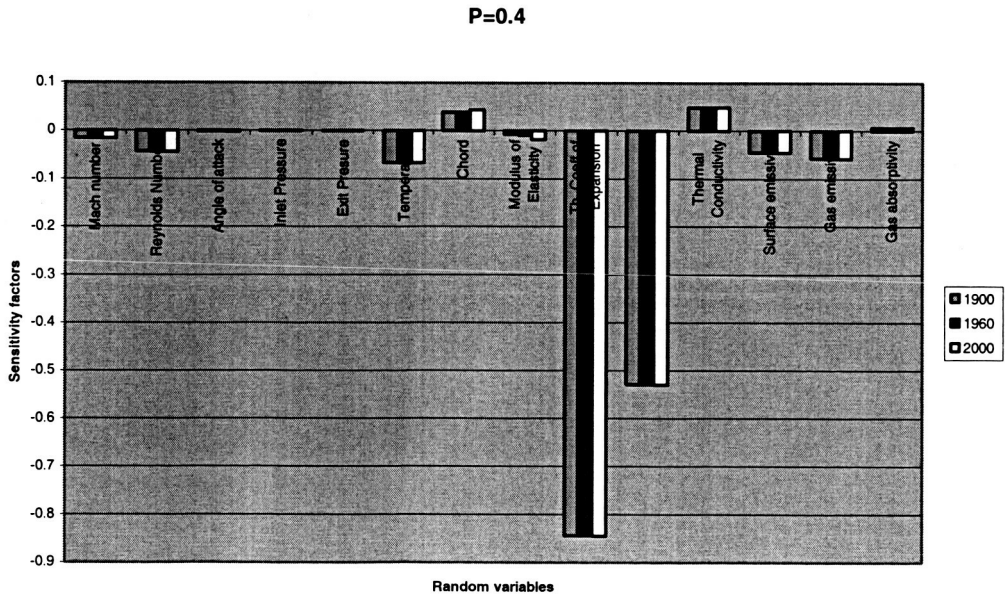

Figure: 9.80: Probability 0.4

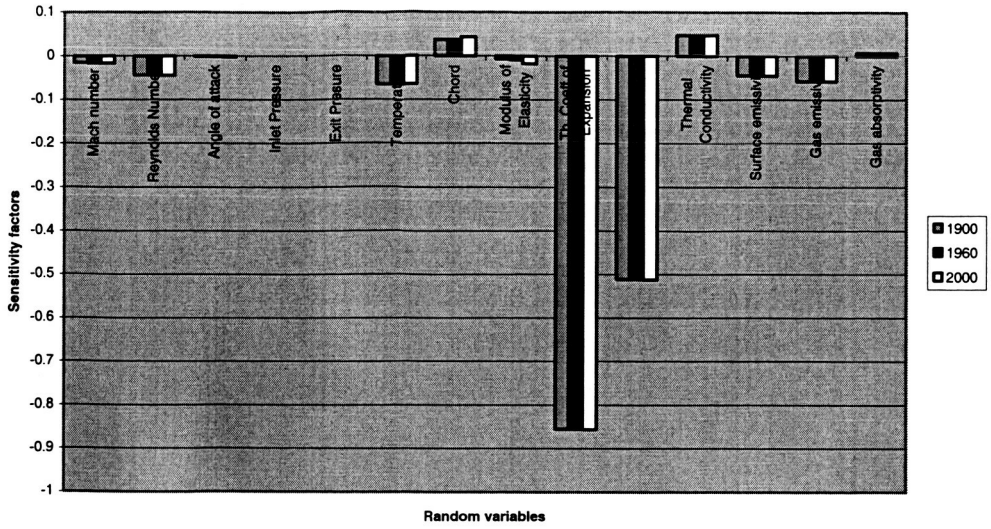

Figure: 9.81: Probability0.5

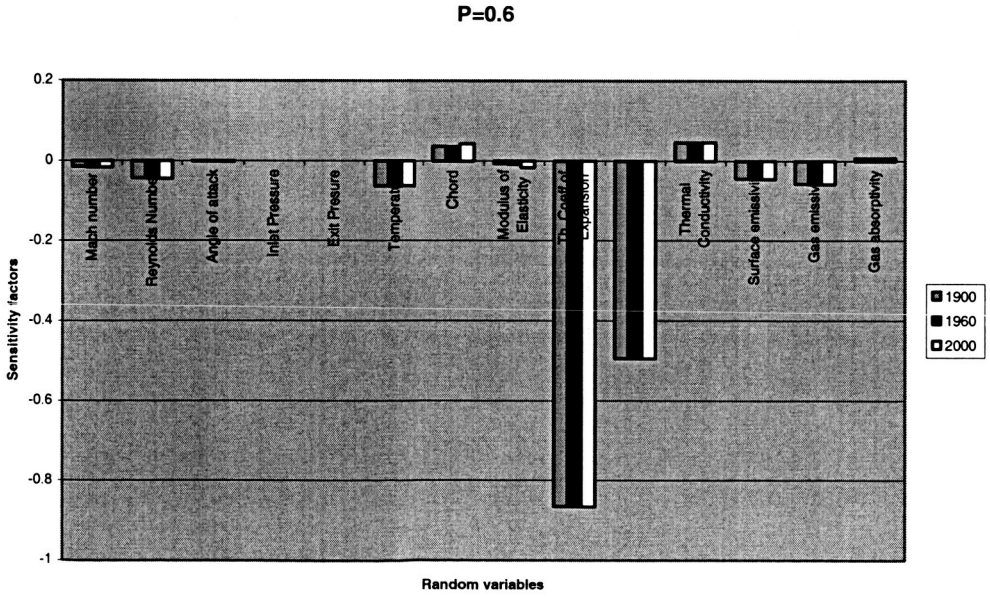

Figure: 9.82: Probability 0.6

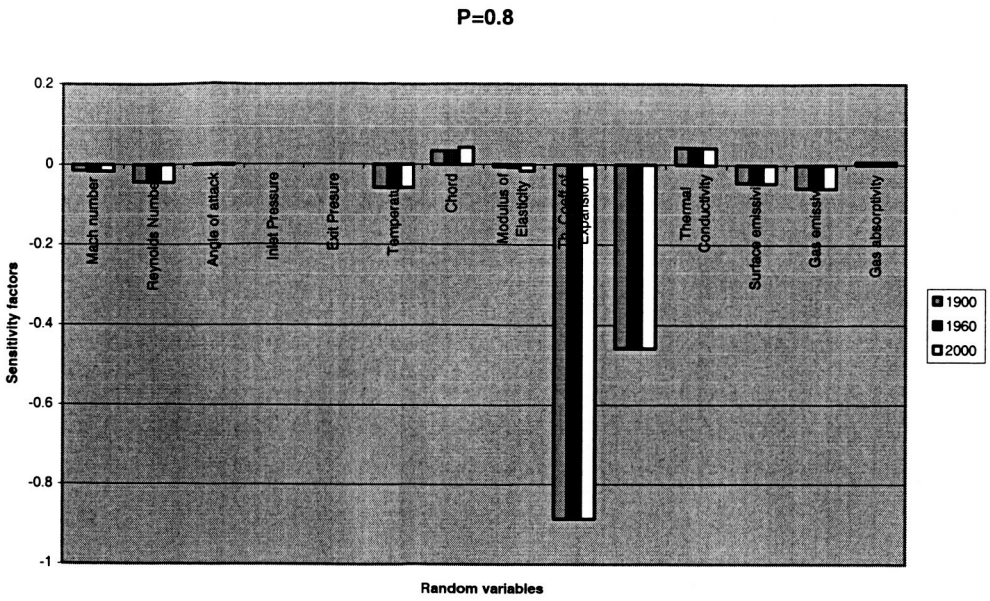

Figure: 9.83: Probability 0.8

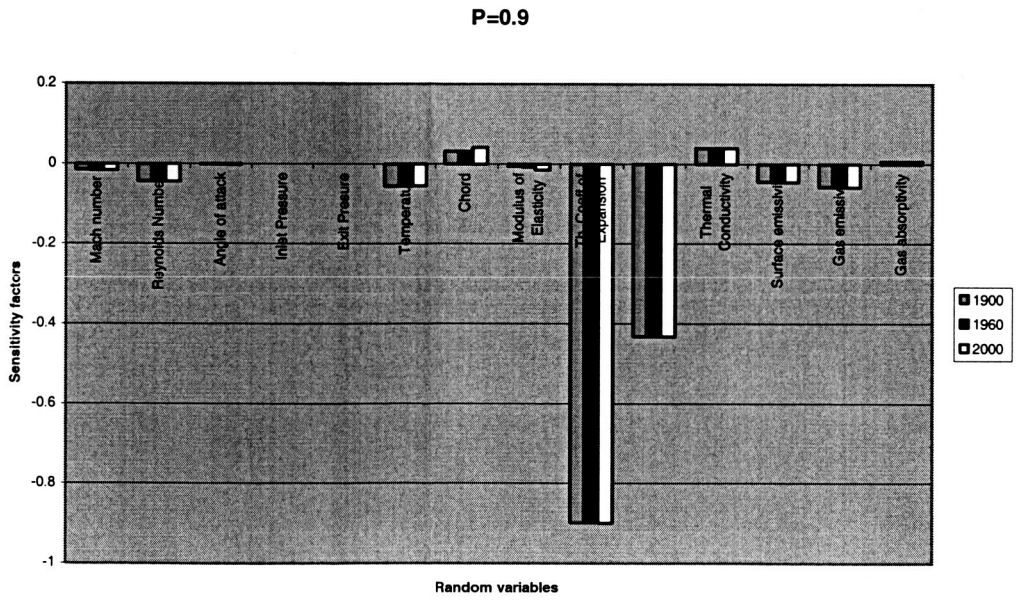

Figure: 9.84: Probability 0.9

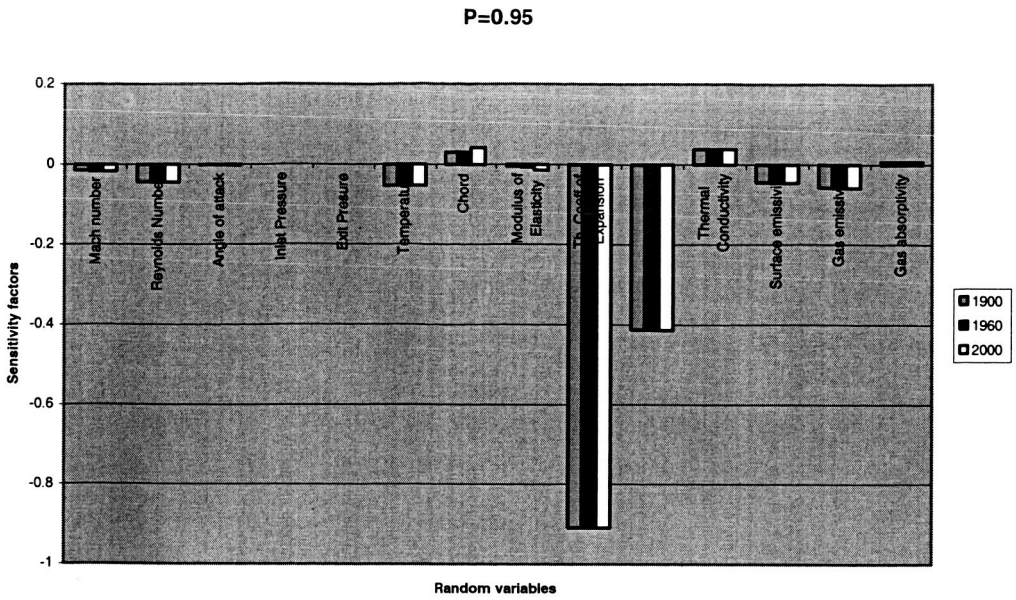

Figure: 9.85: Probability 0.95

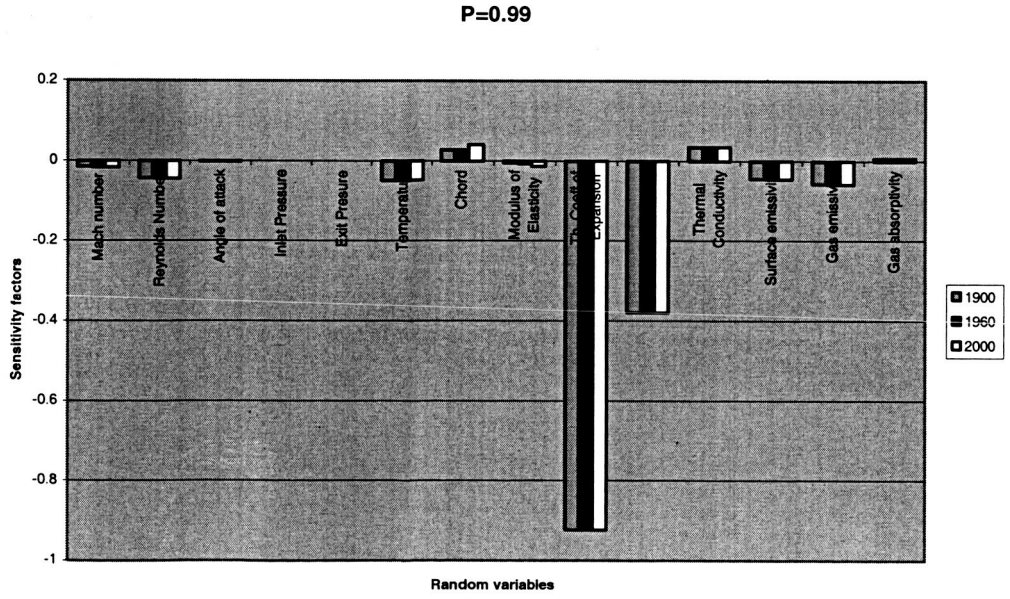

Figure: 9.86: Probability 0.99

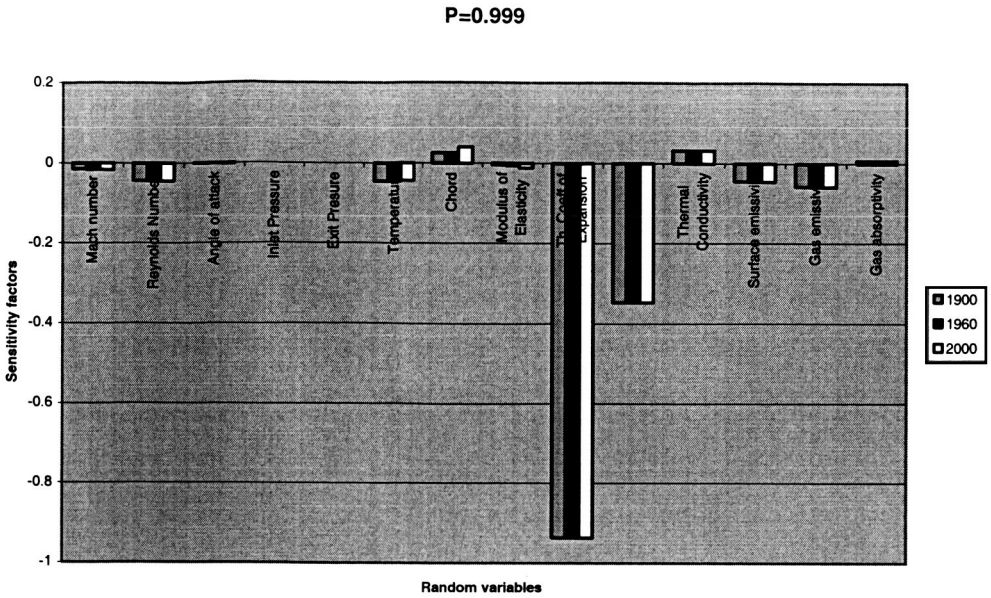

Figure: 9.87: Probability 0.999

The Results for the Rotor for all the three Iterations namely 1900th, 1960th, and 2000th iteration are shown below in the same graph. We can deduce from these graphs that in all the three iterations for different probability levels ranging from 0.001 to 0.999 the same random variables namely Modulus of elasticity, thermal coefficient of expansion and Speed has a lot of influence on the stress. This helps us in further optimizing the design of cost effectiveness.

Graphs comparing all the three iterations 1900th, 1960th, and 2000th for sensitivity factors vs. random variables for stator.

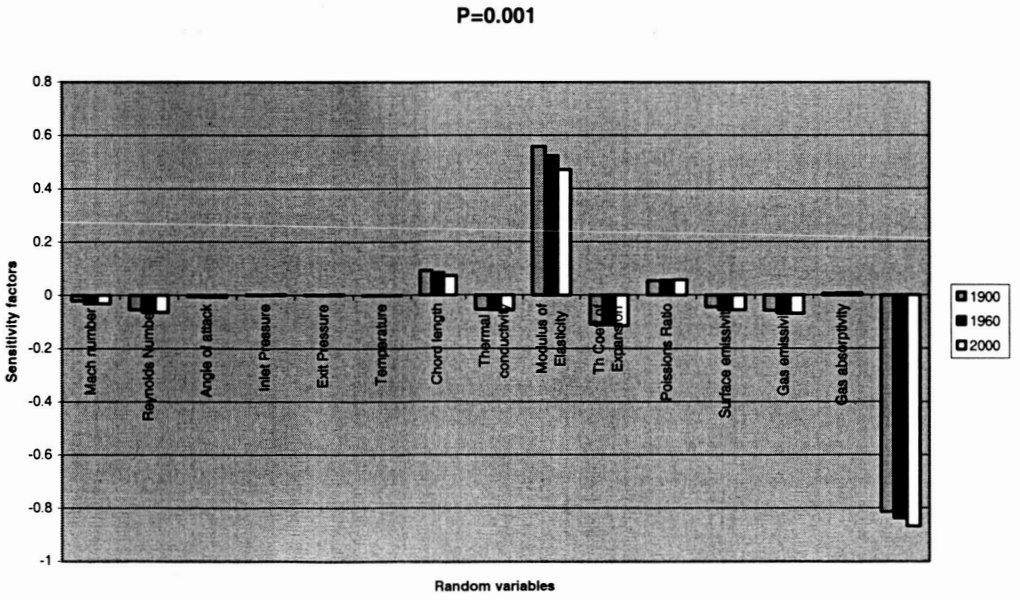

Figure 9.88: Probability 0.001

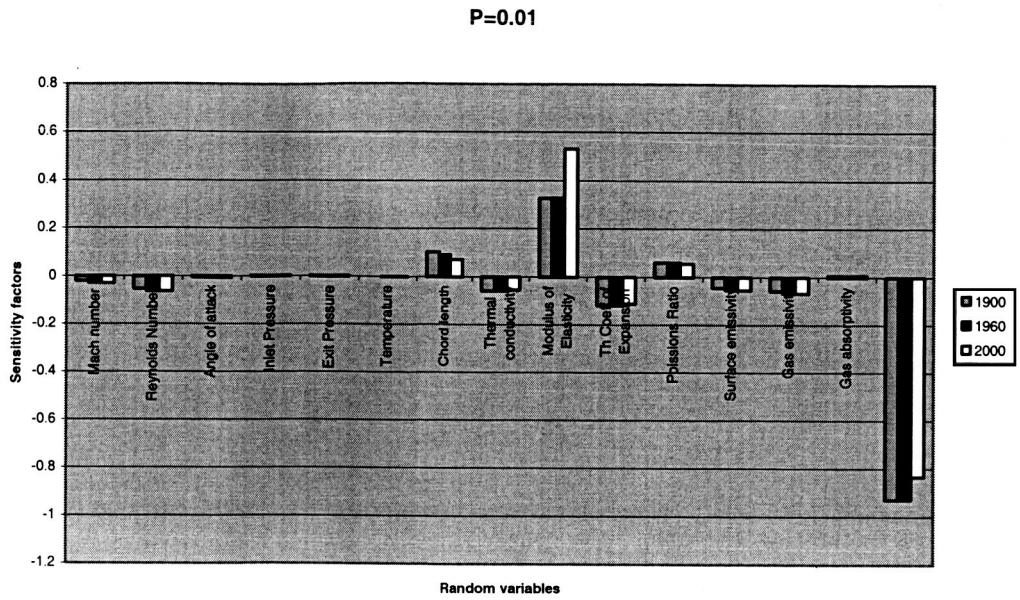

Figure 9.89: Probability 0.01

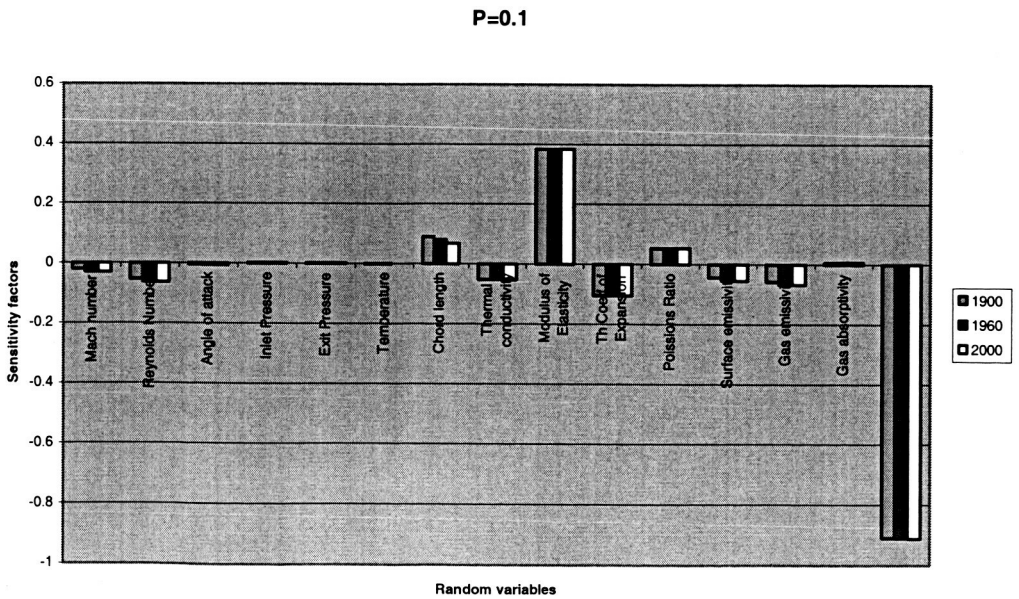

Figure 9.90: Probability 0.1

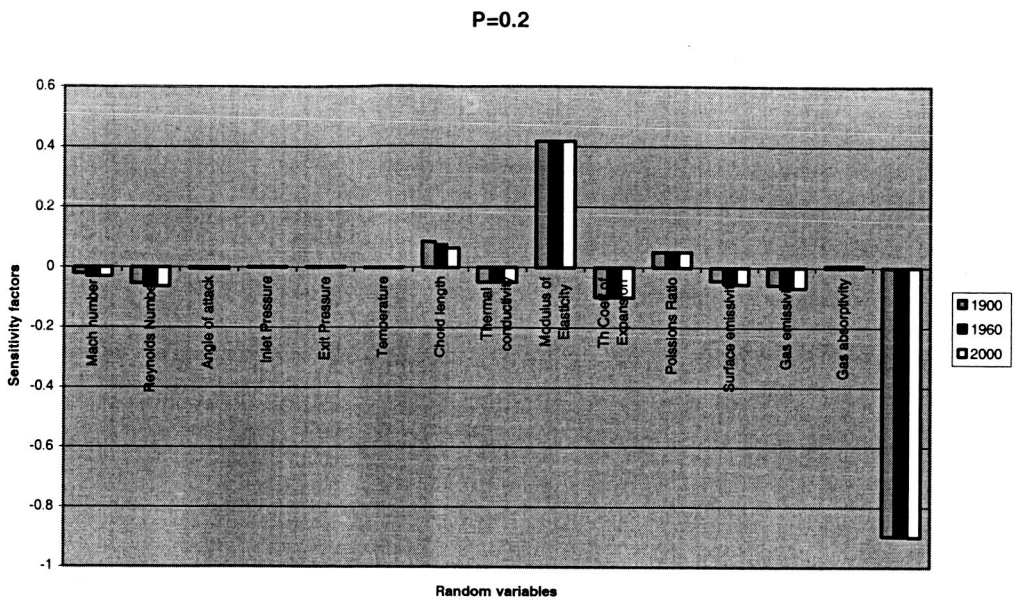

Figure 9.91: Probability 0.2

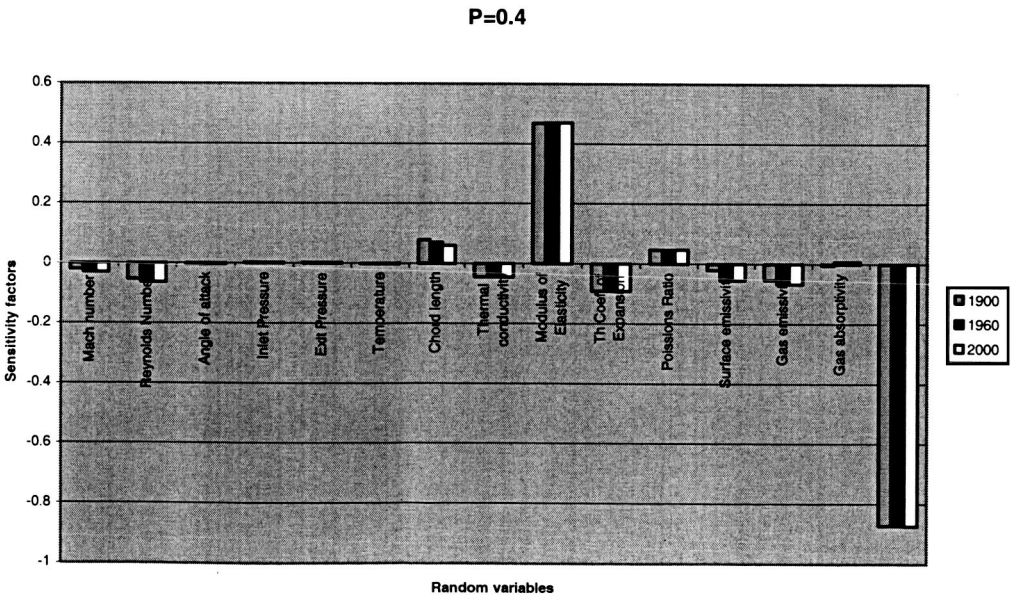

Figure 9.92: Probability 0.4

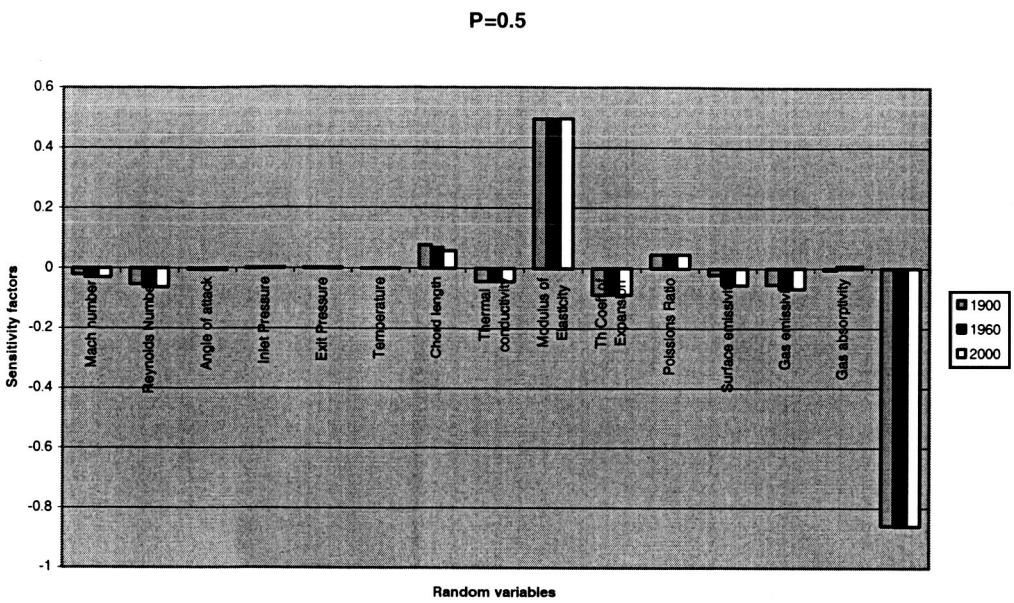

Figure 9.93: Probability 0.5

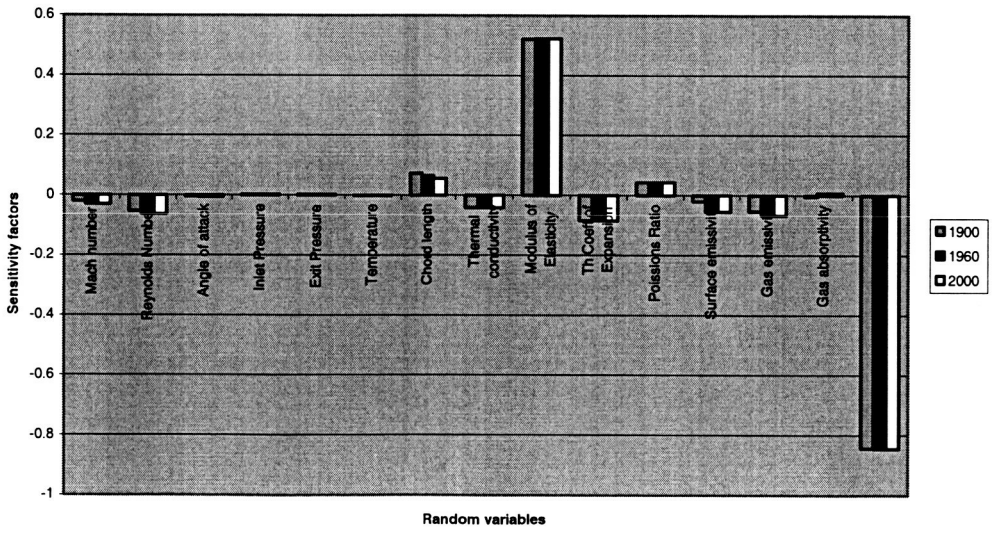

Figure 9.94: Probability 0.6

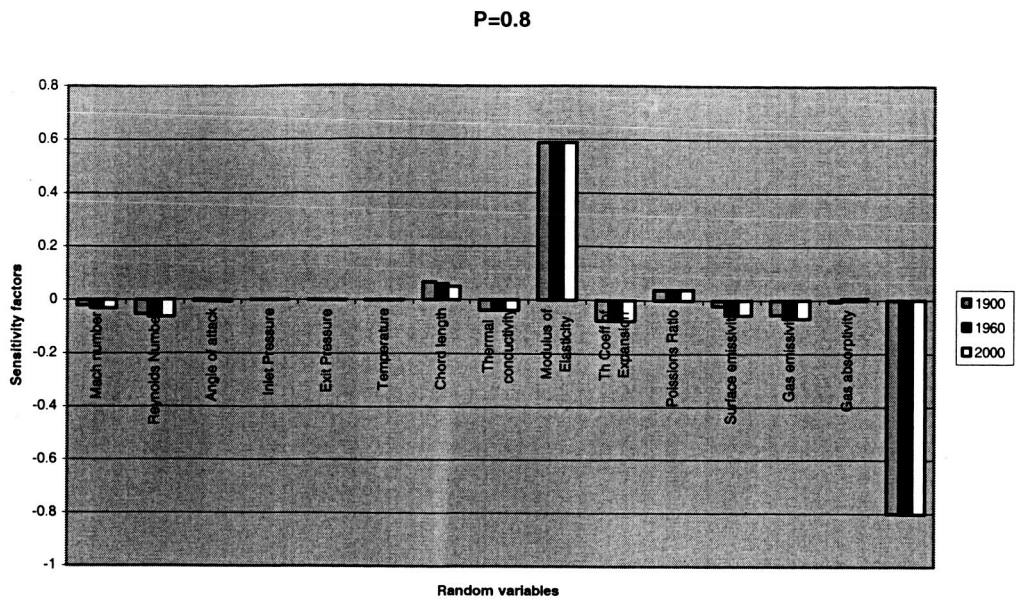

Figure 9.95: Probability 0.8

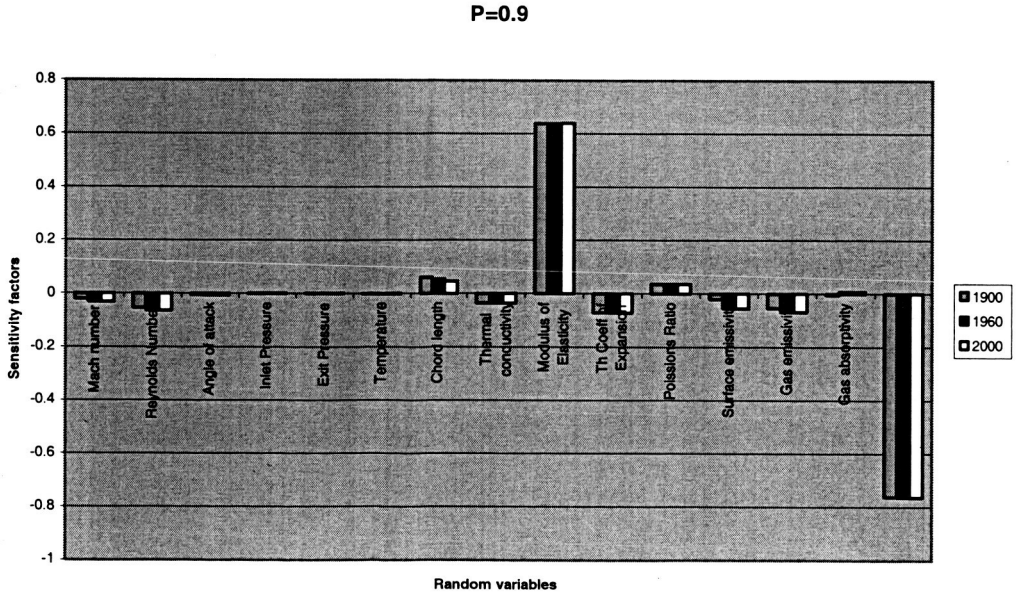

Figure 9.96: Probability 0.9

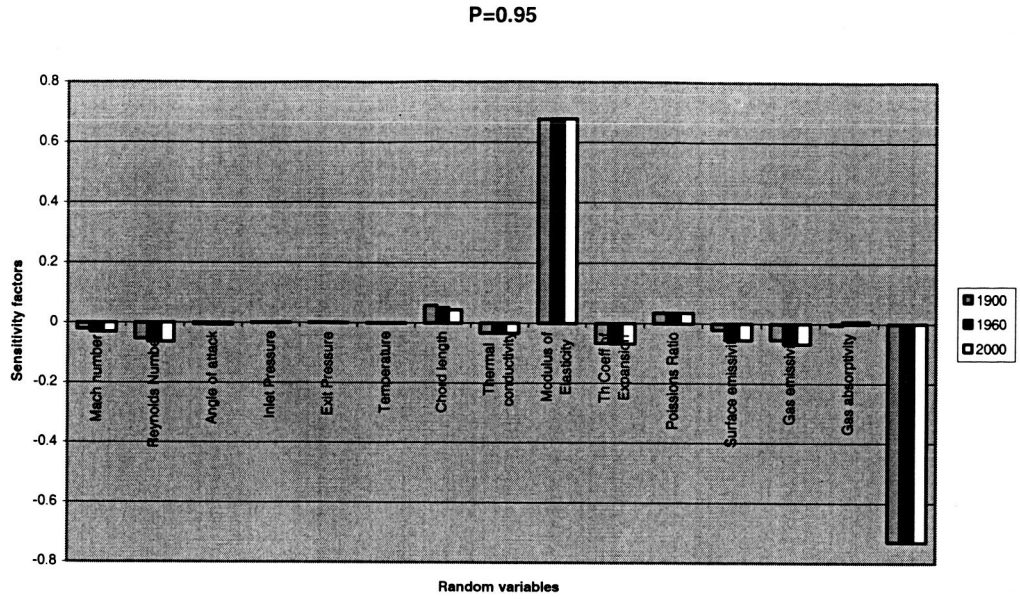

Figure 9.97: Probability 0.95

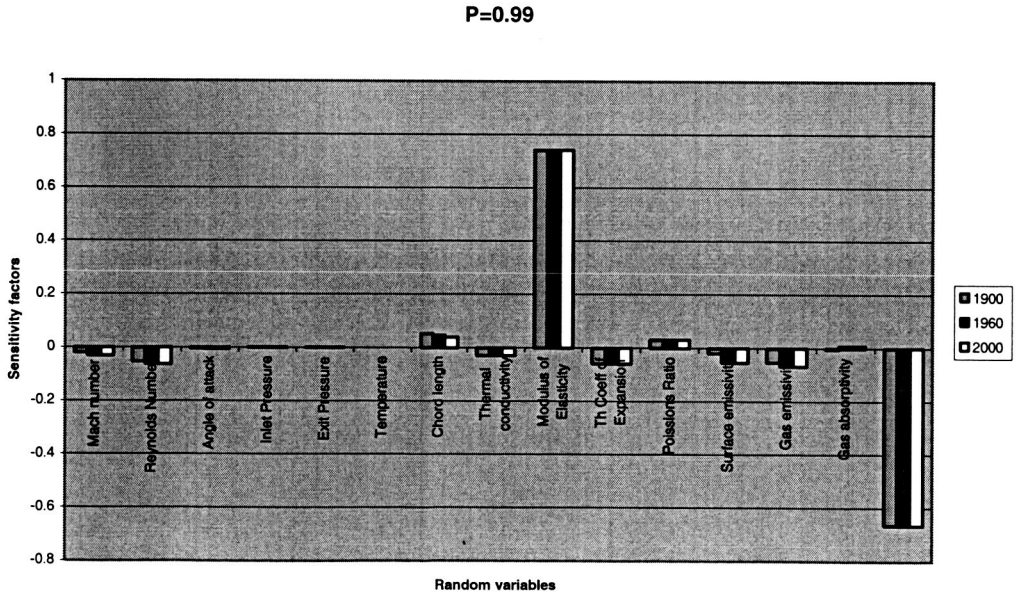

Figure 9.98: Probability 0.99

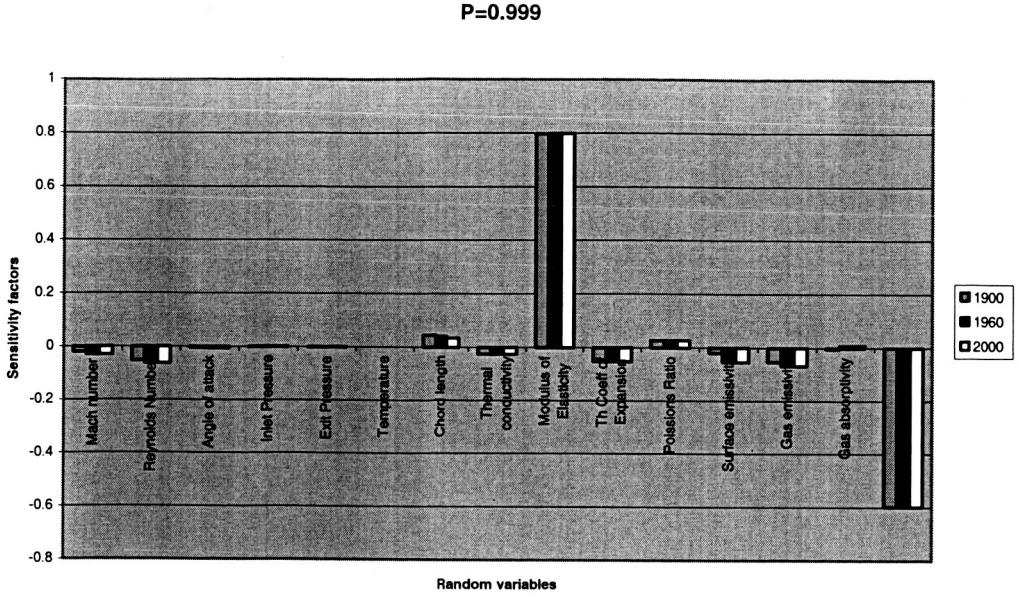

Figure 9.99: Probability 0.999

CHAPTER X

CONCLUDING REMARKS

Heat transfer to a turbine blade was computationally simulated by finite element methods and probabilistically evaluated in view of several uncertainties in performance parameters.

Cumulative distribution functions and sensitivity factors were computed for thermal stresses due to the thermal random variables. These results can be used to quickly identify the most critical design variables in order to optimize the design and make it cost effective. The analysis leads to the selection of the appropriate materials t be used and to the identification of both the most crucial measurements and parameters.

BIBLIOGRAPHY

1. Janus, J.M and Whitfield, D.L., "Advanced 3-D viscous, SSME turbine Rotor-Stator CFD algorithms," final report NAS8-36486, prepared for George C. Marshall space flight center.
2. Janus, J.M and Whitfield, D.L., "A simple Time-Accurate Turbomachinery algorithm with numerical solutions of an uneven blade count configuration," AIAA-89-0206, January, 1989.
3. A.R. Jung ,J.F. Mayer ,H. Stetter.,
4. Elisabetta Caloni., Numerical Investigation of the unsteady flow field in one and half stage HP Transonic Turbine.
5. Rai M.M., "Navier-Stokes simulations of Rotor/Stator interactions using patched and Over Set Grids," AIAA J. Propulsion and Power, 3(5), 1986, pp. 387-396.
6. Fernandez Ore, J., Argüelles Diaz, K. Santo aria Morros, C. Ballesteros Tajadura, R. [6]., "Unsteady Flow Analysis of the Stator-Rotor Interaction in an Axial Flow Fan," Proceedings of ASME FEDSM'03, 4th ASME_JSME joint fluids conference Honolulu, Hawaii, USA 6-10, 2003.
7. Giles, M.B., "Stator-Rotor Interaction in a Transonic Turbine,"AIAA-88-3093, 1988.
8. Chen J, P and Whitfield, D.L., "Navier-Stokes calculations for the unsteady Flow Field of Turbomachinery," AIAA-93-0676, January 1993.

9. Erdos, J.I, Alzner, E. and McNally. W, "Numerical Simulation of Periodic Transonic Flow through a Fan stage," AIAA.J 15(11), pp 1559-1568, 1977.

10. Chen, J.P, Barter, J.W, "Comparison of Time Accurate Calculations of the Unsteady Interaction in Turbomachinery Stage," AIAA 98-3292, July 1998.

11. Henley, G., and Janus, J.M, "Parallelization and Convergence of a 3-D, Implicit, Unsteady, Turbomachinery Flow Code," Proceedings of the fifth SIAM conference of Parallel Processing for Scientific Computing, 1991.

12. Luke, E.A, "The Development of a Scalable parallel 3-D CFD algorithm for Turbomachinery," Thesis, Mississippi State University, July 1993.

13. Zhu J, and Shih T.H, "CMOTT Turbulence Module for NPARC," NASA CR 204143, August 1997.

14. WhitField, D.L., Janus, J.M. and Simpson, L.B, "Implicit Finite Volume High Resolution wave split scheme for solving the Unsteady Three Dimensional Euler and Navier-Stokes Equations on stationery or Dynamic Grids," MSSU-ERIS-ASE-88-2, 1998.

15. Pankajakshan, R., "Parallel solution of Unsteady Incompressible Viscous Flows Using Multi block Structured Grids," PhD Dissertation, Mississippi State University, Dec 1997.

16. McBean, I.W., Liu, F. and Thompson, M.C., "Three Dimensional Navier-Stokes Code for AeroElasticity in Turbomachinery," Proceedings of the 9th International Symposium on Unsteady Aerodynamics, AeroAcoustics and AeroElasticity in Turbomachines (ISUAAAT), Lyon, France, September 4-8,

2000.

17. Roger L. Davis, Jixian Yao, Charles W. Haldeman and Michael G. Dunn, "Unsteady Interaction between a Transonic Turbine Stage and its Downstream Components," Proceedings of ASME TURBO EXPO 2002, June 7-13, Amsterdam.
18. Barter, J.W., Vitt, P.H. and Chen, J.P., "Interaction effects in a Transonic Turbine Stage", Proceedings of ASME TURBO EXPO 2000, May 8-11, Germany.
19. Dunn, M.G., Bennett, W.A., Delaney, R.A., and Rao, K. 1992, "Investigation of Unsteady flow through a Transonic Turbine Stage: Data/Prediction comparison for Time averaged and Phase-Resolved Pressure Data.", Journal of Turbomachinery, Vol. 114, pp.91-99.
20. Rao, K.V, Delaney, R. A., and Dunn, M.G., 1994, "Vane Blade Interaction in a Turbine, Part 1: Aerodynamics," AIAA journal of Propulsion of Power, Vol. 10, No. 3, pp.305-311.
21. Rao, K.V, Delaney, R. A., 1993, "3-D Euler Simulation of Vane Blade Interaction in a Transonic Turbine," AIAA paper 93-2256.
22. Venable, B.L., Delaney, R. A., Busby, J.A., Davis, R. L., 1998, "Influence of Vane-Blade spacing on a Transonic Turbine state Aerodynamics part 1: Time Averaged Data and Analysis, "ASME paper 98-GT-481.

23. Jennions, I., and Adamczyk, J.J., 1997, "Evaluation of Interaction Losses in a Transonic Turbine HP Rotor/LP Vane Configuration," Journal of Turbomachinery, Vol. 119, No 1, pp. 68-76.

24. Matsunuma Takayuki, ABE Hiroyuki and Tsutsui Yasukata, "Unsteady flow at the Midspan in a Turbine Rotor due to Rotor Stator Interaction." Bulletin of GTSG, 2003.

25. Shanhong Ji and Feng Liu, "Flutter Computation of Turbomachinery cascades using a Parallel Unsteady Navier Stokes code.", AIAA Journal Vol. 37, No. 3, March 1999.

26. Jixian Yao, Antony Jameson, and Juan Alonso, "Development and Validation of Massively parallel Flow solver for Turbomachinery Flows," Journal of Propulsion and Power, Vol. 17, No. 3, may-June 2001.

27. Adamczyk, J.J., 1985, "Model equation for simulating flows in multistage Turbomachinery," ASME paper n. 85-GT-226.

28. Hall, K.C, Whitehead, Crawley, 1997, "The influence of neighboring blade rows on the unsteady aerodynamic response of cascades," ASME journal of Turbomachinery, Vol. 119, pp. 85-93

29. Rai, M.M, and Giles, M.B., "Unsteady 3-D Navier-Stokes simulation of Turbine Rotor-Stator Interaction", AIAA 87-2058, 1987.

30. Turner, G., 1996, "Multistage Turbine simulations with Vortex blade interaction," ASME Journal of Turbomachinery, Vol. 118, pp. 643-651.

31. Ruprecht, A., Bauer, C., Gentner, C., and Lein, G. 1999, "Parallel Computation of Stator-Rotor Interaction in an Axial Turbine", ASME PVP Conference, CFD Symposium, Boston.

32. Piotr Lampart and Andrzej Gardzilewicz, " Investigations of Flow Characteristics of an HP Gas Turbine stage including the effect of tip leakage and windage flows using a 3-D Navier Stokes solver with source/sink boundary conditions." Proceedings of the 2000 International joint Power generation Conference, Miami Beach, Florida, July 23-26, 2000.

33. Liu W.K, Belytschko. T and Mani. A, "Probabilistic finite elements for non-linear structural dynamics," Computational Methods in Applied Mechanical Engineering, 1986; 56: 61-86.

34. Liu W.K, Belytschko. T and Mani. A, "Random field finite elements," International Journal for Numerical Methods in Engineering 1986; 23(10).

35. Takada T. "Weighted Integral method in Stochastic Finite Element Analysis," Probabilistic Engineering Mechanics, 1990; 5(3): 146-56.

36. Deodatis G., "The weighted integral method, I: stochastic stiffness matrix." Journal of Engineering Mechanics, 1991; 117(8): 1851-64.

37. Deodatis G, Shinozuka M., "The weighted integral method, II: response variability and reliability." Journal of Engineering Mechanics, 1991; 117(8):1865-77.

38. Ditlevsen O, Madsen .H, "Structural reliability methods." Wiley; 1996.

39. Ghanem, R.G, Spanos, P.D. "Stochastic finite elements-A spectral approach."

Berlin: ringer; 1991.

40. Ghanem, R.G, Brzkala, V. "Stochastic finite element analysis of randomly layered media." Journal of Engineering Mechanics, 1996; 122(4): 361-9.

41. Waubke, H. Dynamische Berechnungen fur den Halbraum mit streuenden Parametern mittels orthogonaler Polynome. PhD Thesis, Technische Universitat, Munchen; 1996.

42. Anders, M., Hori, M. "Stochastic finite element method for Elasto-Plastic body." Internal Journal for Numerical Methods in Engineering, 1999; 46(11): 1897-916.

43. Ghanem, R.G., Spanos, P.D., "Spectral stochastic finite-element formulation for reliability analysis." Journal of Engineering Mechanics, 1991; 117(10): 2351-72.

44. Sudret, B. and Kiureghian, A., "Comparison of Finite Element Reliability Methods," Probabilistic Engineering Mechanics, Vol.17, 2002, pp. 337-348.

45. Fox, E.P. 1994, " The Pratt & Whitney Probabilistic Design System," AIAA-94-1442-CP.

46. Chamis, C.C. 1986, "Probabilistic Structural Analysis Methods for Space Components," Space Systems Technology Conference, San Diego, California, June 9-12, 1986.

47. Nagpal, V.K., Rubinstein, R. and Chamis, C.C., 1987, "Probabilistic Structural Analysis to Quantify Uncertainties Associated with Turbo pump Blades", AIAA87-0766.

48. Chamis, C.C., 1986, "Probabilistic Structural Analysis Methods for Critical SSME Propulsion Components," Third Space Systems Technology Conference, AIAA, pp. 133-144.

49. Gorla, R.S.R., Pai, S.S. and Rusick, J.J., 2002, "Probabilistic Study of Fluid Structure Interaction," International Journal of Engineering Science, Vol. 41, 2003, pp. 271-282.

50. Allaire, P.E., "Basics of the Finite Element Method," W.C. Brown Publishers, Dubuque, IA, 1985.

Appendix A

Coordinates for the Stator and Rotor:

Stator Coordinates:

-0.026436922	0.061890535	0	-0.00146096	0.016176233	0
-0.026168184	0.063344499	0	-0.00129398	0.014462537	0
-0.025899447	0.063911518	0	-0.001177643	0.012700971	0
-0.025630709	0.064321496	0	-0.000908905	0.010940353	0
-0.025093234	0.06464632	0	-0.000640167	0.009164252	0
-0.024824654	0.064918691	0	-0.00037143	0.007376776	0
-0.024555917	0.065178423	0	-0.000102692	0.005570815	0
-0.024287179	0.065430414	0	0.000166045	0.003750161	0
-0.024018442	0.06567419	0	0.000434783	0.001913077	0
-0.023749704	0.065909592	0	0.000442366	0.000172839	0
-0.023077939	0.066136779	0	-0.026436922	0.061890535	0
-0.022406174	0.06666667	0	-0.026168184	0.060436414	0
-0.021734409	0.067140002	0	-0.025899447	0.059869553	0
-0.021062486	0.067554089	0	-0.025630709	0.059459416	0
-0.020390721	0.067905296	0	-0.025093234	0.059135224	0
-0.019718956	0.068189991	0	-0.024824654	0.05885369	0
-0.019047191	0.068403906	0	-0.024555917	0.058566784	0
-0.018375426	0.068541988	0	-0.024287179	0.058265184	0
-0.017703661	0.06859918	0	-0.024018442	0.057949524	0
-0.017031738	0.06856932	0	-0.023749704	0.057620909	0
-0.016359973	0.068445299	0	-0.023077939	0.056772287	0
-0.015688208	0.068218586	0	-0.022406174	0.056379124	0
-0.015016443	0.067880808	0	-0.021734409	0.055414607	0
-0.014344678	0.067420115	0	-0.021062486	0.054393531	0
-0.013672913	0.066824026	0	-0.020390721	0.053321108	0
-0.013001148	0.066076743	0	-0.019718956	0.052201447	0
-0.012329226	0.065159149	0	-0.019047191	0.051037865	0
-0.011657461	0.064048019	0	-0.018375426	0.049832733	0
-0.010985696	0.062710335	0	-0.017703661	0.048588419	0
-0.010313931	0.061108179	0	-0.017031738	0.047306663	0
-0.009642166	0.059185939	0	-0.016359973	0.045988727	0
-0.008970401	0.056884527	0	-0.015688208	0.044635718	0
-0.008298478	0.054254027	0	-0.015016443	0.043248267	0
-0.007626713	0.051357633	0	-0.014344678	0.041827323	0
-0.006954948	0.0482429	0	-0.013672913	0.040372885	0
-0.006283183	0.044938265	0	-0.013001148	0.03888527	0
-0.005611418	0.041465688	0	-0.012329226	0.03736432	0
-0.004939653	0.037845235	0	-0.011657461	0.035810192	0
-0.004267888	0.034089387	0	-0.010985696	0.034221781	0
-0.003595965	0.030206832	0	-0.010313931	0.03259877	0
-0.0029242	0.026208629	0	-0.009642166	0.030940686	0
-0.002252435	0.022098572	0	-0.008970401	0.029245633	0
-0.001729697	0.017885506	0	-0.008298478	0.027512662	0

-0.007626713	0.025739405	0	-0.00171496	0.006307197	0
-0.006954948	0.023923807	0	-0.00144638	0.005301129	0
-0.006283183	0.022063182	0	-0.001177643	0.004258251	0
-0.005611418	0.020153897	0	-0.000908905	0.003186302	0
-0.004939653	0.018190738	0	-0.000640167	0.002069485	0
-0.004267888	0.016168966	0	-0.00037143	0.000910327	0
-0.003697565	0.014080365	0	-0.000102692	0.000225923	0
-0.0031782	0.011915613	0	0.000166045	0.000216918	0
-0.002506435	0.009661282	0	0.000434783	0.000191165	0
-0.001983697	0.007292252	0	0.000442366	0.000172839	0

Table A.1: Stator mean coordinates.

-0.026428865	0.068122214	0.03429	-0.007624501	0.059655163	0.03429
-0.026160285	0.069575387	0.03429	-0.006952894	0.056061252	0.03429
-0.025891547	0.07014209	0.03429	-0.006281287	0.052098755	0.03429
-0.025622968	0.070551911	0.03429	-0.00560968	0.047823442	0.03429
-0.025354388	0.070877998	0.03429	-0.004938073	0.043277337	0.03429
-0.025085651	0.07115037	0.03429	-0.004266624	0.038487773	0.03429
-0.024817071	0.071410102	0.03429	-0.003595017	0.033485241	0.03429
-0.024548491	0.071661935	0.03429	-0.00292341	0.028292965	0.03429
-0.024279754	0.071905868	0.03429	-0.002251803	0.022926745	0.03429
-0.024011174	0.072141744	0.03429	-0.001983223	0.020735767	0.03429
-0.023742595	0.072369721	0.03429	-0.001714486	0.018523145	0.03429
-0.023070988	0.072903879	0.03429	-0.001445906	0.016286035	0.03429
-0.022399381	0.073386374	0.03429	-0.001177327	0.01403123	0.03429
-0.021727774	0.073815943	0.03429	-0.000908589	0.011751779	0.03429
-0.021056167	0.074191165	0.03429	-0.000640009	0.009327612	0.03429
-0.02038456	0.074509827	0.03429	-0.00037143	0.007129524	0.03429
-0.019712953	0.074769875	0.03429	-0.000102692	0.004787826	0.03429
-0.019041504	0.074969098	0.03429	0.000165887	0.002431751	0.03429
-0.018369897	0.075104177	0.03429	0.000434625	2.40142E-05	0.03429
-0.01769829	0.075171638	0.03429	-0.026428865	0.068122214	0.03429
-0.017026683	0.075167215	0.03429	-0.026160285	0.066668882	0.03429
-0.016355076	0.075086167	0.03429	-0.025891547	0.066102337	0.03429
-0.015683469	0.074922491	0.03429	-0.025622968	0.065692516	0.03429
-0.015011862	0.074669079	0.03429	-0.025354388	0.065368483	0.03429
-0.014340255	0.074317239	0.03429	-0.025085651	0.065085368	0.03429
-0.013668806	0.07385623	0.03429	-0.024817071	0.064794039	0.03429
-0.012997199	0.073272465	0.03429	-0.024548491	0.06448375	0.03429
-0.012325592	0.072548722	0.03429	-0.024279754	0.064156241	0.03429
-0.011653985	0.071660987	0.03429	-0.024011174	0.063812459	0.03429
-0.010982378	0.070575767	0.03429	-0.023742595	0.063453668	0.03429
-0.010310771	0.069248984	0.03429	-0.023070988	0.062497051	0.03429
-0.009639164	0.067600537	0.03429	-0.022399381	0.061463967	0.03429
-0.008967715	0.065501825	0.03429	-0.021727774	0.060363739	0.03429
-0.008296108	0.062834039	0.03429	-0.021056167	0.059203159	0.03429
-0.02038456	0.05798681	0.03429	-0.018369897	0.054044377	0.03429
-0.019712953	0.056719588	0.03429	-0.01769829	0.052641128	0.03429
-0.019041504	0.055404496	0.03429	-0.017026683	0.051196485	0.03429

-0.016355076	0.049711872	0.03429	-0.00560968	0.020515058	0.03429
-0.015683469	0.048188236	0.03429	-0.004938073	0.018268468	0.03429
-0.015011862	0.046626209	0.03429	-0.004266624	0.015944307	0.03429
-0.014340255	0.045026264	0.03429	-0.003595017	0.013529776	0.03429
-0.013668806	0.043389034	0.03429	-0.00292341	0.011006234	0.03429
-0.012997199	0.041714046	0.03429	-0.002251803	0.008347928	0.03429
-0.012325592	0.040000982	0.03429	-0.001983223	0.007237746	0.03429
-0.011653985	0.038249843	0.03429	-0.001714486	0.006095335	0.03429
-0.010982378	0.036459365	0.03429	-0.001445906	0.004907897	0.03429
-0.010310771	0.034628758	0.03429	-0.001177327	0.003694391	0.03429
-0.009639164	0.0327566	0.03429	-0.000908589	0.002426538	0.03429
-0.008967715	0.030840995	0.03429	-0.000640009	0.00108127	0.03429
-0.008296108	0.028876889	0.03429		-	
-0.007624501	0.026871073	0.03429	-0.00037143	0.000225923	0.03429
-0.006952894	0.02481012	0.03429	0.000434625	2.40142E-05	0.03429
-0.006281287	0.022693238	0.03429			

Table A.2: Stator tip coordinates

-0.02644261	0.057516953	-0.03429	-0.009644219	0.052665142	-0.03429
-0.026173872	0.058967757	-0.03429	-0.008972297	0.050400068	-0.03429
-0.025905134	0.059533354	-0.03429	-0.008300374	0.047804167	-0.03429
-0.025636239	0.059942227	-0.03429	-0.007628451	0.044912987	-0.03429
-0.025367501	0.06027416	-0.03429	-0.006956528	0.041765866	-0.03429
-0.025098764	0.060546689	-0.03429	-0.006284605	0.038414782	-0.03429
-0.024830026	0.060803104	-0.03429	-0.005612682	0.034904921	-0.03429
-0.02456113	0.061048933	-0.03429	-0.004940759	0.031273725	-0.03429
-0.024292393	0.061283703	-0.03429	-0.004268836	0.02754584	-0.03429
-0.024023655	0.061507572	-0.03429	-0.003596913	0.023745438	-0.03429
-0.023754918	0.061720382	-0.03429	-0.00292499	0.019887845	-0.03429
-0.022925007	0.062204299	-0.03429	-0.002253067	0.01598491	-0.03429
-0.022411072	0.062619176	-0.03429	-0.001984171	0.014412771	-0.03429
-0.021739149	0.06296359	-0.03429	-0.001715434	0.012835735	-0.03429
-0.021067068	0.063236751	-0.03429	-0.001446696	0.011254433	-0.03429
-0.020395145	0.063436922	-0.03429	-0.001177959	0.009667286	-0.03429
-0.019723222	0.063562048	-0.03429	-0.000909221	0.008076821	-0.03429
-0.019051299	0.063609919	-0.03429	-0.000640325	0.006482722	-0.03429
-0.018379376	0.063577531	-0.03429	-0.000371588	0.004884041	-0.03429
-0.017423075	0.063461726	-0.03429	-0.00010285	0.003283465	-0.03429
-0.01703553	0.063258237	-0.03429	0.000165887	0.001677833	-0.03429
-0.016363607	0.062962484	-0.03429	0.000434783	3.49153E-05	-0.03429
-0.015691684	0.062568778	-0.03429	-0.02644261	0.057516953	-0.03429
-0.015019761	0.062070325	-0.03429	-0.026173872	0.056066149	-0.03429
-0.014347838	0.061458596	-0.03429	-0.025905134	0.055500552	-0.03429
-0.013675915	0.060723794	-0.03429	-0.025636239	0.05509168	-0.03429
-0.013003992	0.059852806	-0.03429	-0.025367501	0.054599863	-0.03429
-0.012332069	0.058829834	-0.03429	-0.025098764	0.054479476	-0.03429
-0.011660146	0.05763339	-0.03429	-0.024830026	0.054180563	-0.03429
-0.010988223	0.056236303	-0.03429	-0.02456113	0.053859215	-0.03429
-0.0103163	0.054644889	-0.03429	-0.024292393	0.053519067	-0.03429

-0.024023655	0.053162488	-0.03429	-0.009644219	0.025234633	-0.03429
-0.023754918	0.052791848	-0.03429	-0.008972297	0.023666602	-0.03429
-0.022925007	0.051812323	-0.03429	-0.008300374	0.022074083	-0.03429
-0.022411072	0.050770866	-0.03429	-0.007628451	0.020456602	-0.03429
-0.021739149	0.049679011	-0.03429	-0.006956528	0.018810999	-0.03429
-0.021067068	0.048544499	-0.03429	-0.006284605	0.017135852	-0.03429
-0.020395145	0.04737286	-0.03429	-0.005612682	0.015427844	-0.03429
-0.019723222	0.046168201	-0.03429	-0.004940759	0.013682393	-0.03429
-0.019051299	0.044933841	-0.03429	-0.004268836	0.011894127	-0.03429
-0.018379376	0.043671833	-0.03429	-0.003596913	0.010055462	-0.03429
-0.017423075	0.042130389	-0.03429	-0.00292499	0.008154235	-0.03429
-0.01703553	0.041072772	-0.03429	-0.002253067	0.006174171	-0.03429
-0.016363607	0.039738406	-0.03429	-0.001984171	0.005352791	-0.03429
-0.015691684	0.038381763	-0.03429	-0.001715434	0.004510715	-0.03429
-0.015019761	0.037003949	-0.03429	-0.001446696	0.003645257	-0.03429
-0.014347838	0.035605124	-0.03429	-0.001177959	0.0027373	-0.03429
-0.013675915	0.034185601	-0.03429	-0.000909221	0.001788424	-0.03429
-0.013003992	0.032745857	-0.03429	-0.000640325	0.000774457	-0.03429
-0.012332069	0.031285574	-0.03429		-	
-0.011660146	0.02980491	-0.03429	-0.000371588	0.000225607	-0.03429
-0.010988223	0.028303076	-0.03429	0.000434783	3.49153E-05	-0.03429
-0.0103163	0.026779914	-0.03429			

Table A.3: Stator root coordinates

Rotor Coordinates:

0.002078	0.024585	0	0.009873	0.031763	0
0.002286	0.025376	0	0.010393	0.031555	0
0.002494	0.025935	0	0.010912	0.031264	0
0.002702	0.026434	0	0.011432	0.030884	0
0.00291	0.026895	0	0.011952	0.030404	0
0.003117	0.027321	0	0.012471	0.029811	0
0.003325	0.027718	0	0.012991	0.029084	0
0.003533	0.028088	0	0.013511	0.028191	0
0.003741	0.028432	0	0.01403	0.027074	0
0.003949	0.028755	0	0.01455	0.025696	0
0.004157	0.029056	0	0.01507	0.024214	0
0.004676	0.029727	0	0.01559	0.022679	0
0.005196	0.030293	0	0.016109	0.021113	0
0.005716	0.030764	0	0.016629	0.019522	0
0.006235	0.031152	0	0.017148	0.017911	0
0.006755	0.031459	0	0.017668	0.016176	0
0.007275	0.03169	0	0.018188	0.01464	0
0.007794	0.031849	0	0.018707	0.012984	0
0.008314	0.031936	0	0.019227	0.011312	0
0.008834	0.031877	0	0.019747	0.009626	0
0.009353	0.031895	0	0.020266	0.007927	0

0.020786	0.006212	0	0.009353	0.023429	0
0.020994	0.005522	0	0.009873	0.023015	0
0.021202	0.004828	0	0.010393	0.02254	0
0.02141	0.004131	0	0.010912	0.022007	0
0.021618	0.003434	0	0.011432	0.021418	0
0.021826	0.002729	0	0.011952	0.020774	0
0.022033	0.002071	0	0.012471	0.020077	0
0.022241	0.000597	0	0.012991	0.019327	0
0.002078	0.024585	0	0.013511	0.018527	0
0.002286	0.023867	0	0.01403	0.017677	0
0.002494	0.023612	0	0.01455	0.016778	0
0.002702	0.023449	0	0.01507	0.01583	0
0.00291	0.023341	0	0.01559	0.014835	0
0.003117	0.023274	0	0.016109	0.013791	0
0.003325	0.023242	0	0.016629	0.012701	0
0.003533	0.023243	0	0.017148	0.011564	0
0.003741	0.023276	0	0.017668	0.010379	0
0.003949	0.023345	0	0.018188	0.009147	0
0.004157	0.023455	0	0.018707	0.007868	0
0.004676	0.023848	0	0.019227	0.006541	0
0.005196	0.024158	0	0.019747	0.005166	0
0.005716	0.024362	0	0.020266	0.003743	0
0.006235	0.024469	0	0.020786	0.00227	0
0.006755	0.024487	0	0.020994	0.001667	0
0.007275	0.024423	0	0.021202	0.001052	0
0.007794	0.02428	0	0.02141	0.000435	0
0.008314	0.024065	0	0.021618	0.00019	0
0.008834	0.02378	0	0.022241	0.000597	0

Table A.4: Rotor mean coordinates.

Tip Coordinates:

0.003142	0.035056	0.031382	0.007634	0.036708	0.031382
0.003321	0.035728	0.031382	0.007979	0.03652	0.031382
0.003501	0.035972	0.031382	0.008533	0.036273	0.031382
0.003681	0.036134	0.031382	0.008981	0.035961	0.031382
0.00386	0.03625	0.031382	0.009431	0.035578	0.031382
0.00404	0.036351	0.031382	0.00988	0.035026	0.031382
0.00422	0.036445	0.031382	0.010233	0.034561	0.031382
0.0044	0.03653	0.031382	0.010779	0.033897	0.031382
0.004579	0.036606	0.031382	0.011228	0.033097	0.031382
0.004759	0.036676	0.031382	0.011677	0.032112	0.031382
0.004939	0.036737	0.031382	0.012127	0.030888	0.031382
0.005388	0.036856	0.031382	0.012576	0.029497	0.031382
0.005837	0.036927	0.031382	0.013025	0.028058	0.031382
0.006287	0.036948	0.031382	0.013474	0.026598	0.031382
0.006736	0.03692	0.031382	0.013924	0.025129	0.031382
0.007185	0.036841	0.031382	0.014373	0.023657	0.031382

0.014822	0.022181	0.031382	0.007634	0.031291	0.031382
0.015271	0.020702	0.031382	0.007979	0.030633	0.031382
0.015721	0.019223	0.031382	0.008533	0.029919	0.031382
0.01617	0.017742	0.031382	0.008981	0.029153	0.031382
0.016619	0.016262	0.031382	0.009431	0.028341	0.031382
0.017068	0.01478	0.031382	0.00988	0.027484	0.031382
0.017518	0.013299	0.031382	0.010233	0.026589	0.031382
0.017967	0.011816	0.031382	0.010779	0.025659	0.031382
0.018416	0.010334	0.031382	0.011228	0.024695	0.031382
0.018865	0.008851	0.031382	0.011677	0.0237	0.031382
0.019315	0.007369	0.031382	0.012127	0.022677	0.031382
0.019494	0.006776	0.031382	0.012576	0.021626	0.031382
0.019674	0.006183	0.031382	0.013025	0.020552	0.031382
0.019854	0.005588	0.031382	0.013474	0.019453	0.031382
0.020034	0.004996	0.031382	0.013924	0.018335	0.031382
0.020213	0.004403	0.031382	0.014373	0.017194	0.031382
0.020393	0.00381	0.031382	0.014822	0.016037	0.031382
0.020573	0.003216	0.031382	0.015271	0.01486	0.031382
0.020752	0.002624	0.031382	0.015721	0.013669	0.031382
0.020932	0.002029	0.031382	0.01617	0.012462	0.031382
0.021112	0.00134	0.031382	0.016619	0.011239	0.031382
0.003142	0.035056	0.031382	0.017068	0.010004	0.031382
0.003321	0.034383	0.031382	0.017518	0.00865	0.031382
0.003501	0.034139	0.031382	0.017967	0.007493	0.031382
0.003681	0.033977	0.031382	0.018416	0.006221	0.031382
0.00386	0.033863	0.031382	0.018865	0.004939	0.031382
0.00404	0.033784	0.031382	0.019315	0.003644	0.031382
0.00422	0.033734	0.031382	0.019494	0.003124	0.031382
0.0044	0.03371	0.031382	0.019674	0.002602	0.031382
0.004579	0.033705	0.031382	0.019854	0.002078	0.031382
0.004759	0.033698	0.031382	0.020034	0.001554	0.031382
0.004939	0.033664	0.031382	0.020213	0.001061	0.031382
0.005388	0.033498	0.031382	0.020393	0.000902	0.031382
0.005837	0.033227	0.031382	0.020573	0.00085	0.031382
0.006287	0.032861	0.031382	0.020752	0.000722	0.031382
0.006736	0.032411	0.031382	0.020932	0.00096	0.031382
0.007185	0.031885	0.031382	0.021112	0.00134	0.031382

Table A.5: Rotor tip coordinates

1.08E-06	0.019438	-0.0313817	0.001932	0.023546	-0.0313817
0.000242	0.020277	-0.0313817	0.002174	0.023939	-0.0313817
0.000484	0.020808	-0.0313817	0.002415	0.024317	-0.0313817
0.000725	0.021315	-0.0313817	0.003019	0.025197	-0.0313817
0.000967	0.0218	-0.0313817	0.003623	0.025993	-0.0313817
0.001208	0.022264	-0.0313817	0.004226	0.026712	-0.0313817
0.00145	0.022709	-0.0313817	0.00483	0.027357	-0.0313817
0.001691	0.023136	-0.0313817	0.005433	0.027933	-0.0313817

0.006037	0.028442	-0.0313817	0.001691	0.018143	-0.0313817
0.00664	0.028886	-0.0313817	0.001932	0.018234	-0.0313817
0.007244	0.029267	-0.0313817	0.002174	0.018383	-0.0313817
0.007848	0.029584	-0.0313817	0.002415	0.018556	-0.0313817
0.008451	0.029838	-0.0313817	0.003019	0.018939	-0.0313817
0.009055	0.030027	-0.0313817	0.003623	0.019258	-0.0313817
0.009658	0.03015	-0.0313817	0.004226	0.019516	-0.0313817
0.010262	0.030204	-0.0313817	0.00483	0.019715	-0.0313817
0.010866	0.030187	-0.0313817	0.005433	0.01986	-0.0313817
0.011469	0.030093	-0.0313817	0.006037	0.01995	-0.0313817
0.012073	0.029918	-0.0313817	0.00664	0.019989	-0.0313817
0.012676	0.029651	-0.0313817	0.007244	0.019978	-0.0313817
0.01328	0.029284	-0.0313817	0.007848	0.019917	-0.0313817
0.013883	0.028801	-0.0313817	0.008451	0.019809	-0.0313817
0.014487	0.028182	-0.0313817	0.009055	0.019652	-0.0313817
0.015091	0.027396	-0.0313817	0.009658	0.019449	-0.0313817
0.015694	0.026389	-0.0313817	0.010262	0.019199	-0.0313817
0.016298	0.025076	-0.0313817	0.010866	0.018902	-0.0313817
0.016901	0.02347	-0.0313817	0.011469	0.018558	-0.0313817
0.017505	0.021754	-0.0313817	0.012073	0.018167	-0.0313817
0.018108	0.019971	-0.0313817	0.012676	0.017729	-0.0313817
0.018712	0.018138	-0.0313817	0.01328	0.017241	-0.0313817
0.019316	0.016268	-0.0313817	0.013883	0.016704	-0.0313817
0.019919	0.014364	-0.0313817	0.014487	0.016116	-0.0313817
0.020523	0.012428	-0.0313817	0.015091	0.015476	-0.0313817
0.021127	0.01046	-0.0313817	0.015694	0.014782	-0.0313817
0.02173	0.008462	-0.0313817	0.016298	0.01403	-0.0313817
0.021971	0.007652	-0.0313817	0.016901	0.01322	-0.0313817
0.022213	0.006836	-0.0313817	0.017505	0.012348	-0.0313817
0.022454	0.006014	-0.0313817	0.017854	0.011767	-0.0313817
0.022696	0.005191	-0.0313817	0.018712	0.010398	-0.0313817
0.022937	0.004353	-0.0313817	0.019316	0.009311	-0.0313817
0.023179	0.00351	-0.0313817	0.019919	0.008141	-0.0313817
0.02342	0.00266	-0.0313817	0.020523	0.006876	-0.0313817
0.023661	0.001797	-0.0313817	0.021127	0.005509	-0.0313817
0.023903	0.000924	-0.0313817	0.02173	0.004023	-0.0313817
0.024144	3.57E-05	-0.0313817	0.021971	0.003392	-0.0313817
1.08E-06	0.019438	-0.0313817	0.022213	0.002738	-0.0313817
0.000242	0.01867	-0.0313817	0.022454	0.002054	-0.0313817
0.000484	0.018408	-0.0313817	0.022696	0.001345	-0.0313817
0.000725	0.018247	-0.0313817	0.022937	0.000605	-0.0313817
0.000967	0.01815	-0.0313817	0.023179	-0.00017	-0.0313817
0.001208	0.018104	-0.0313817	0.02342	-0.00047	-0.0313817
0.00145	0.018101	-0.0313817	0.024144	3.57E-05	-0.0313817

Table A.6: Rotor root coordinates

Appendix B

Pressure and Temperature values applied for the suction surface and Pressure values for Stator and Rotor are given in the tables below:

stator suction side static pressure

% chord length	1900	1920	1940	1960	1980	2000
0.00	176624.90	177175.70	176754.20	176274.50	176596.50	176820.00
2.37	173943.00	174742.80	174057.40	173653.80	174202.70	174315.10
5.16	173171.00	173991.00	173306.20	172942.10	173507.60	173586.90
10.70	171384.90	172281.60	171553.40	171197.10	171856.00	171903.60
14.52	170552.40	171482.60	170696.90	170353.80	171090.50	171104.10
19.11	169139.50	170125.10	169263.60	168903.50	169744.90	169745.40
24.57	167222.80	168269.80	167294.70	166896.50	167878.70	167872.10
30.91	164837.10	165945.40	164808.70	164356.20	165516.70	165503.20
34.36	163411.50	164553.70	163314.80	162822.40	164087.10	164065.50
41.60	160833.50	162006.10	160502.70	159922.40	161415.80	161337.00
45.25	160021.50	161189.20	159579.10	158962.00	160536.30	160411.20
52.30	158783.00	159896.80	158117.70	157442.00	159121.30	158932.20
61.78	157927.70	158910.20	157014.10	156302.70	157973.90	157768.90
64.63	157600.00	158570.90	156715.30	155977.10	157594.80	157425.50
69.85	156903.10	157849.60	156331.70	155511.40	156881.80	156860.70
74.37	156496.50	157330.00	156372.70	155492.90	156505.30	156683.20
80.07	156750.00	156984.50	156891.60	156197.90	156628.00	156872.60
84.91	157284.90	156828.70	157037.20	156777.70	156936.50	156924.90
90.08	158118.40	157189.80	156890.00	157265.60	157611.40	157090.80
94.54	158891.80	158101.10	157474.80	157649.70	158474.30	157901.90
98.07	159626.20	159423.60	158913.60	158240.50	159557.60	159622.90
100.08	159310.50	159929.00	160385.10	158290.40	159796.50	161133.30

Table B1: Stator suction side static pressure

Stator pressure side static pressure

% chord length	1900.00	1920.00	1940.00	1960.00	1980.00	2000.00
0.00	176557.20	176857.10	176196.90	176660.00	177167.90	176666.80
2.37	175362.60	175820.60	175315.80	175601.80	175979.50	175715.20
5.16	175030.00	175538.40	174997.30	175264.20	175673.30	175424.10
10.70	174703.50	175271.60	174669.10	174910.70	175379.00	175144.30
14.52	174542.90	175140.20	174498.60	174729.90	175236.40	175004.60
19.11	174527.40	175140.70	174456.10	174684.60	175237.20	174995.50
24.57	174492.20	175126.50	174393.90	174616.70	175210.60	174957.20
30.91	174536.50	175178.60	174391.80	174607.70	175257.70	174986.30
34.36	174556.50	175203.00	174388.00	174597.30	175276.20	174997.20
41.60	174588.60	175245.60	174367.20	174559.60	175302.60	175007.70
45.25	174588.20	175248.50	174334.90	174516.50	175295.70	174991.70
52.30	174551.50	175220.90	174234.20	174386.40	175235.30	174918.60
61.78	174318.90	175008.30	173905.40	174000.00	174951.90	174616.70
64.63	174227.50	174923.70	173777.40	173850.80	174837.00	174492.70
69.85	174007.30	174718.60	173481.00	173507.10	174560.50	174194.50
74.37	173635.70	174360.40	173032.50	173003.20	174127.30	173737.50
80.07	172835.30	173570.60	172114.50	172007.40	173236.30	172812.10
84.91	171705.60	172434.20	170854.10	170684.50	172011.70	171568.70
90.08	170106.60	170796.40	169031.30	168813.10	170244.60	169768.80
94.54	168248.40	168840.80	166886.60	166657.10	168240.70	167537.10
98.07	165680.50	166031.80	163979.10	163820.30	165730.60	164495.00
100.08	163483.40	162917.40	160806.80	160986.80	163316.90	161007.10

Table B.2: Stator pressure side static pressure

stator suction side static temperature

% chord length	1900	1920	1940	1960	1980	2000
0	1100.30	1099.33	1100.88	1101.49	1099.36	1099.40
2.37	1099.63	1099.24	1099.07	1099.50	1099.55	1099.07
5.16	1099.09	1099.07	1098.76	1098.87	1099.33	1098.85
10.7	1098.261	1098.53	1098.05	1098.12	1098.58	1098.25
14.52	1097.95	1098.36	1097.84	1097.77	1098.31	1098.17
19.11	1097.30	1097.60	1097.15	1097.22	1097.70	1097.52
24.57	1096.51	1097.03	1096.45	1096.42	1096.97	1096.93
30.91	1095.88	1096.39	1095.89	1095.81	1096.39	1096.34
34.36	1095.29	1095.68	1095.20	1095.14	1095.70	1095.69
41.6	1094.65	1095.19	1094.66	1094.55	1095.15	1095.20
45.25	1093.96	1094.55	1094.00	1093.88	1094.51	1094.56
52.3	1092.76	1093.44	1092.99	1092.99	1093.43	1093.63
61.78	1092.48	1092.75	1092.32	1092.29	1092.73	1092.71
64.63	1092.13	1092.52	1092.16	1092.06	1092.43	1092.44
69.85	1089.56	1090.19	1092.16	1089.76	1090.21	1090.23
74.37	1088.75	1089.49	1089.14	1088.90	1089.46	1089.76
80.07	1087.22	1087.87	1087.91	1087.79	1088.50	1088.82
84.91	1085.92	1086.61	1087.17	1087.19	1087.78	1088.43
90.08	1088.46	1088.75	1089.06	1089.37	1090.02	1090.41
94.54	1090.72	1091.01	1091.19	1091.52	1092.04	1092.15
98.07	1090.00	1090.50	1090.62	1090.96	1091.56	1091.95
100.08	1088.88	1089.75	1090.14	1089.29	1091.03	1092.02

Table B.3: Stator suction side static temperature

stator pressure side static temp

% chord length	1900	1920	1940	1960	1980	2000
0	1100.16	1100.24	1101.34	1100.08	1099.49	1100.61
2.37	1100.07	1100.42	1100.21	1100.02	1100.25	1100.29
5.16	1099.58	1099.83	1099.72	1099.62	1099.76	1099.84
10.7	1099.32	1099.60	1099.37	1099.34	1099.45	1099.42
14.52	1098.75	1098.85	1098.69	1098.83	1098.88	1098.97
19.11	1098.42	1098.72	1098.52	1098.47	1098.64	1098.64
24.57	1098.05	1098.21	1098.02	1098.04	1098.12	1098.14
30.91	1098.41	1098.80	1098.48	1098.55	1098.87	1098.77
34.36	1098.58	1098.98	1098.66	1098.73	1099.10	1098.97
41.6	1097.46	1097.81	1097.66	1097.75	1098.13	1098.07
45.25	1097.28	1097.68	1097.51	1097.62	1098.02	1097.98
52.3	1097.00	1097.48	1097.32	1097.49	1097.90	1097.94
61.78	1096.53	1096.96	1096.85	1097.05	1097.54	1097.58
64.63	1096.33	1096.75	1096.62	1096.83	1097.37	1097.37
69.85	1095.42	1095.89	1095.79	1096.13	1096.55	1096.72
74.37	1094.90	1095.53	1095.28	1095.52	1096.16	1096.26
80.07	1094.26	1095.05	1094.40	1094.77	1095.66	1095.71
84.91	1094.13	1094.85	1094.37	1094.56	1095.39	1095.47
90.08	1093.84	1094.49	1093.92	1094.14	1094.91	1094.99
94.54	1093.31	1093.98	1093.56	1093.56	1094.43	1094.58
98.07	1092.17	1092.77	1092.04	1092.31	1093.31	1093.32
100.08	1091.30	1091.49	1090.55	1090.86	1092.10	1091.23

Table B.4: Stator pressure side static temp

Rotor suction side static pressure

% chord length	1900	1920	1940	1960	1980	2000
0.00	176624.90	177175.70	176754.20	176274.50	176596.50	176820.00
2.37	173943.00	174742.80	174057.40	173653.80	174202.70	174315.10
5.16	173171.00	173991.00	173306.20	172942.10	173507.60	173586.90
10.70	171384.90	172281.60	171553.40	171197.10	171856.00	171903.60
14.52	170552.40	171482.60	170696.90	170353.80	171090.50	171104.10
19.11	169139.50	170125.10	169263.60	168903.50	169744.90	169745.40
24.57	167222.80	168269.80	167294.70	166896.50	167878.70	167872.10
30.91	164837.10	165945.40	164808.70	164356.20	165516.70	165503.20
34.36	163411.50	164553.70	163314.80	162822.40	164087.10	164065.50
41.60	160833.50	162006.10	160502.70	159922.40	161415.80	161337.00
45.25	160021.50	161189.20	159579.10	158962.00	160536.30	160411.20
52.30	158783.00	159896.80	158117.70	157442.00	159121.30	158932.20
61.78	157927.70	158910.20	157014.10	156302.70	157973.90	157768.90
64.63	157600.00	158570.90	156715.30	155977.10	157594.80	157425.50
69.85	156903.10	157849.60	156331.70	155511.40	156881.80	156860.70
74.37	156496.50	157330.00	156372.70	155492.90	156505.30	156683.20
80.07	156750.00	156984.50	156891.60	156197.90	156628.00	156872.60
84.91	157284.90	156828.70	157037.20	156777.70	156936.50	156924.90
90.08	158118.40	157189.80	156890.00	157265.60	157611.40	157090.80
94.54	158891.80	158101.10	157474.80	157649.70	158474.30	157901.90
98.07	159626.20	159423.60	158913.60	158240.50	159557.60	159622.90
100.08	159310.50	159929.00	160385.10	158290.40	159796.50	161133.30

Table B.5: Rotor suction side static pressure

Rotor pressure side static pressure

% chord length	1900.00	1920.00	1940.00	1960.00	1980.00	2000.00
0.00	176557.20	176857.10	176196.90	176660.00	177167.90	176666.80
2.37	175362.60	175820.60	175315.80	175601.80	175979.50	175715.20
5.16	175030.00	175538.40	174997.30	175264.20	175673.30	175424.10
10.70	174703.50	175271.60	174669.10	174910.70	175379.00	175144.30
14.52	174542.90	175140.20	174498.60	174729.90	175236.40	175004.60
19.11	174527.40	175140.70	174456.10	174684.60	175237.20	174995.50
24.57	174492.20	175126.50	174393.90	174616.70	175210.60	174957.20
30.91	174536.50	175178.60	174391.80	174607.70	175257.70	174986.30
34.36	174556.50	175203.00	174388.00	174597.30	175276.20	174997.20
41.60	174588.60	175245.60	174367.20	174559.60	175302.60	175007.70
45.25	174588.20	175248.50	174334.90	174516.50	175295.70	174991.70
52.30	174551.50	175220.90	174234.20	174386.40	175235.30	174918.60
61.78	174318.90	175008.30	173905.40	174000.00	174951.90	174616.70
64.63	174227.50	174923.70	173777.40	173850.80	174837.00	174492.70
69.85	174007.30	174718.60	173481.00	173507.10	174560.50	174194.50
74.37	173635.70	174360.40	173032.50	173003.20	174127.30	173737.50
80.07	172835.30	173570.60	172114.50	172007.40	173236.30	172812.10
84.91	171705.60	172434.20	170854.10	170684.50	172011.70	171568.70
90.08	170106.60	170796.40	169031.30	168813.10	170244.60	169768.80
94.54	168248.40	168840.80	166886.60	166657.10	168240.70	167537.10
98.07	165680.50	166031.80	163979.10	163820.30	165730.60	164495.00
100.08	163483.40	162917.40	160806.80	160986.80	163316.90	161007.10

Table B.6

ROTOR SUCTION SIDE STATIC TEMPERATURE						
% chord length	1900	1920	1940	1960	1980	2000
0	1069.27	1069.98	1070.25	1072.18	1069.46	1069.85
2.37	1075.89	1076.09	1077.75	1077.23	1075.97	1076.28
5.16	1074.51	1075.69	1077.41	1075.33	1074.93	1075.99
10.7	1073.61	1074.19	1073.21	1073.64	1074.10	1074.67
14.52	1072.20	1073.07	1072.35	1072.65	1072.34	1073.30
19.11	1070.75	1071.46	1071.29	1071.08	1070.79	1071.63
24.57	1070.51	1070.92	1071.09	1071.14	1070.78	1071.22
30.91	1070.25	1070.16	1070.24	1070.63	1070.64	1070.53
34.36	1069.99	1070.09	1070.16	1070.31	1070.88	1070.89
41.6	1069.89	1069.76	1070.03	1070.36	1071.17	1070.98
45.25	1067.86	1067.91	1068.75	1068.13	1069.37	1069.37
52.3	1067.85	1067.99	1068.78	1067.93	1069.25	1069.46
61.78	1067.95	1068.64	1069.07	1068.39	1069.47	1070.14
64.63	1068.72	1069.85	1069.77	1069.43	1069.91	1071.11
69.85	1069.15	1070.36	1070.49	1070.21	1070.29	1071.43
74.37	1068.93	1070.39	1070.46	1070.41	1070.11	1071.51
80.07	1069.47	1070.88	1071.38	1071.56	1071.09	1072.23
84.91	1068.93	1070.25	1070.73	1070.95	1070.53	1071.69
90.08	1068.74	1069.49	1070.45	1070.57	1070.14	1070.75
94.54	1068.67	1069.09	1070.55	1070.50	1070.23	1070.55
98.07	1068.50	1068.52	1070.27	1070.01	1069.98	1069.87

Table B.7: Rotor suction side static temperature

ROTOR PRESSURE SIDE STATIC TEMP						
% chord length	1900	1920	1940	1960	1980	2000
0	1060.18	1062.05	1065.18	1066.27	1061.29	1062.57
2.37	1068.83	1069.78	1066.99	1069.32	1069.58	1071.15
5.16	1071.86	1072.31	1071.25	1072.18	1072.82	1073.49
10.7	1069.60	1070.03	1069.56	1069.98	1070.87	1071.44
14.52	1069.00	1069.46	1069.35	1069.63	1070.38	1071.05
19.11	1068.71	1069.27	1069.28	1069.44	1069.96	1070.64
24.57	1064.42	1065.38	1065.47	1066.44	1066.88	1067.70
30.91	1062.74	1063.68	1064.14	1065.35	1065.58	1066.52
34.36	1060.58	1061.70	1062.20	1063.58	1064.01	1064.93
41.6	1052.03	1053.82	1054.36	1054.74	1056.78	1058.07
45.25	1037.46	1040.65	1042.33	1042.02	1043.84	1046.46
52.3	1036.88	1039.54	1041.31	1041.82	1043.37	1045.67
61.78	1041.86	1044.02	1045.43	1046.15	1048.69	1050.34
64.63	1043.25	1046.77	1048.54	1049.36	1051.52	1054.30
69.85	1043.51	1047.78	1050.49	1051.38	1052.34	1056.04
74.37	1043.08	1046.93	1050.49	1052.07	1052.50	1055.88
80.07	1035.94	1038.97	1042.69	1044.83	1045.95	1048.54
84.91	1036.10	1038.84	1042.33	1044.41	1045.70	1047.79
90.08	1043.46	1045.20	1048.30	1049.99	1051.05	1052.24
94.54	1042.78	1044.64	1047.50	1049.47	1050.98	1052.27
98.07	1040.92	1043.14	1045.81	1048.06	1050.17	1051.86

Table B.8: Rotor pressure side static temperature

Appendix C:

Level	Z-value	u(std. normal)	Probability
1	1.48E+11	-3.09025	0.001
2	1.80E+11	-2.32635	0.01
3	2.27E+11	-1.28155	0.1
4	2.49E+11	-0.84162	0.2
5	2.80E+11	-0.25335	0.4
6	2.94E+11	0	0.5
7	3.09E+11	0.25335	0.6
8	3.45E+11	0.84162	0.8
9	3.74E+11	1.28155	0.9
10	3.99E+11	1.64485	0.95
11	4.49E+11	2.32635	0.99
12	5.11E+11	3.09025	0.999

Table C.1: Sensitivity and Probability levels for stator at 1900th iteration

Level	Z-value	u(std. normal)	Probability
1	1.48E+11	-3.09025	0.0010
2	1.80E+11	-2.32635	0.0100
3	2.27E+11	-1.28155	0.1000
4	2.49E+11	-0.84162	0.2000
5	2.80E+11	-0.25335	0.4000
6	2.94E+11	0	0.5000
7	3.09E+11	0.25335	0.6000
8	3.45E+11	0.84162	0.8000
9	3.73E+11	1.28155	0.9000
10	3.98E+11	1.64485	0.9500
11	4.49E+11	2.32635	0.9900
12	5.10E+11	3.09025	0.9990

Table C.2: Sensitivity and Probability levels for stator at 1960th iteration

Level	Z-value	u(std. normal)	Probability
1	1.48E+11	-3.09025	0.0010
2	1.80E+11	-2.32635	0.0100
3	2.27E+11	-1.28155	0.1000
4	2.49E+11	-0.84162	0.2000
5	2.80E+11	-0.25335	0.4000
6	2.95E+11	0	0.5000
7	3.09E+11	0.25335	0.6000
8	3.45E+11	0.84162	0.8000
9	3.74E+11	1.28155	0.9000
10	3.99E+11	1.64485	0.9500
11	4.49E+11	2.32635	0.9900
12	5.11E+11	3.09025	0.9990

Table C.3: Sensitivity and Probability levels for stator at 2000th iteration

Name	X-value	Std. Dev. from Mean	Sensitivity factor
THERMAL	1.12E+01	-0.029152	-0.009612
MODULUS	1.64E+11	-2.055365	-0.677712
ALPHA	1.48E-05	-2.198339	-0.724854
POISSON	3.06E-01	0.207609	0.068454
PRESSURE	1.70E+05	-0.001183	-0.00039
TEMPERAT	1.06E+03	-0.266351	-0.087823
CHORD	1.52E-02	0.160546	0.052937

Name	X-value	Std. Dev. from Mean	Sensitivity factor
THERMAL	1.12E+01	-0.020328	-0.008933
MODULUS	1.73E+11	-1.655497	-0.727471
ALPHA	1.61E-05	-1.539014	-0.676285
POISSON	3.04E-01	0.14441	0.063458
PRESSURE	1.70E+05	-0.000829	-0.000364
TEMPERAT	1.07E+03	-0.188705	-0.082922
CHORD	0.1516867E-01	0.112449	0.049413

name	X-value	Std. Dev. from Mean	Sensitivity factor
THERMAL	1.12E+01	-0.009816	-0.00791
MODULUS	1.87E+11	-0.982756	-0.791953
ALPHA	1.76E-05	-0.746697	-0.601724
POISSON	3.02E-01	0.069533	0.056033
PRESSURE	1.70E+05	-0.000402	-0.000324
TEMPERAT	1.08E+03	-0.092875	-0.074843
CHORD	1.51E-02	0.054589	0.043991

. name	X-value	Std. Dev. from Mea	n Sensitivity factor
THERMAL	1.12E+01	-0.006076	-0.007483
MODULUS	1.93E+11	-0.662208	-0.815602
ALPHA	1.81E-05	-0.462949	-0.570186
POISSON	3.01E-01	0.042993	0.052952
PRESSURE	1.70E+05	-0.000249	-0.000307
TEMPERAT	1.09E+03	-0.057884	-0.071292
CHORD	1.51E-02	0.033852	0.041694

. name	X-value	Std. Dev. from Mea	n Sensitivity factor
THERMAL	1.12E+01	-0.001588	-0.00692
MODULUS	2.03E+11	-0.193656	-0.844067
ALPHA	1.88E-05	-0.12123	-0.528391
POISSON	3.00E-01	0.011222	0.048911
PRESSURE	1.70E+05	-0.000065	-0.000284
TEMPERAT	1.09E+03	-0.015254	-0.066485
CHORD	1.50E-02	0.008867	0.038647

. name	X-value	Std. Dev. from Mea	n Sensitivity factor
THERMAL	1.12E+01	0.000168	-0.006685
MODULUS	2.07E+11	0.02148	-0.855132
ALPHA	1.90E-05	0.012831	-0.510809

POISSON	3.00E-01	-0.001186	0.047223
PRESSURE	1.70E+05	0.000007	-0.000275
TEMPERAT	1.09E+03	0.001619	-0.064433
CHORD	1.50E-02	-0.000939	0.037365

. name	X-value	Std. Dev. from Mea	n	Sensitivity factor
THERMAL	1.12E+01	0.001783		-0.00646
MODULUS	2.12E+11	0.238853		-0.86524
ALPHA	1.93E-05	0.136369		-0.493994
POISSON	3.00E-01	-0.012592		0.045615
PRESSURE	1.70E+05	0.000073		-0.000266
TEMPERAT	1.10E+03	0.017241		-0.062455
CHORD	1.50E-02	-0.009976		0.036138

. name	X-value	Std. Dev. from Mea	n	Sensitivity factor
THERMAL	1.12E+01	0.005134		-0.005969
MODULUS	2.23E+11	0.761876		-0.88585
ALPHA	1.97E-05	0.393156		-0.457131
POISSON	2.99E-01	-0.036215		0.042108
PRESSURE	1.70E+05	0.000212		-0.000246
TEMPERAT	1.10E+03	0.049945		-0.058072
CHORD	1.50E-02	-0.028767		0.033448

. name	X-value	Std. Dev. from Mea	n	Sensitivity factor
THERMAL	1.12E+01	0.007305		-0.005632
MODULUS	2.31E+11	1.165812		-0.898853
ALPHA	2.01E-05	0.560011		-0.431774
POISSON	2.98E-01	-0.051504		0.03971
PRESSURE	1.70E+05	0.000301		-0.000232
TEMPERAT	1.10E+03	0.071364		-0.055022
CHORD	1.49E-02	-0.04098		0.031596

. name	X-value	Std. Dev. from Mea	n	Sensitivity factor
THERMAL	1.12E+01	0.008911		-0.005374
MODULUS	2.38E+11	1.505968		-0.908231
ALPHA	2.03E-05	0.683606		-0.412274
POISSON	2.98E-01	-0.062797		0.037872
PRESSURE	1.70E+05	0.000368		-0.000222
TEMPERAT	1.10E+03	0.087316		-0.052659
CHORD	1.49E-02	-0.050029		0.030172

. name	X-value	Std. Dev. from Mea	n	Sensitivity factor
THERMAL	1.12E+01	0.011543		-0.004933
MODULUS	2.52E+11	2.159707		-0.923066
ALPHA	2.07E-05	0.886587		-0.37893
POISSON	2.98E-01	-0.081287		0.034743
PRESSURE	1.70E+05	0.000477		-0.000204
TEMPERAT	1.11E+03	0.113674		-0.048585
CHORD	1.49E-02	-0.064894		0.027736

. name	X-value	Std. Dev. from Mea	n Sensitivity factor
THERMAL	1.12E+01	0.013978	-0.004508
MODULUS	2.67E+11	2.902577	-0.936051
ALPHA	2.10E-05	1.074835	-0.346623
POISSON	2.97E-01	-0.098372	0.031724
PRESSURE	1.70E+05	0.000579	-0.000187
TEMPERAT	1.11E+03	0.138304	-0.044602
CHORD	1.49E-02	-0.078683	0.025375

Table C.4

R.V. name	X-value	Std. Dev. from Mean	Sensitivity factor
THERMAL	1.12E+01	-0.03752	-0.012381
MODULUS	1.64E+11	-2.054328	-0.677881
ALPHA	1.48E-05	-2.196339	-0.724742
POISSON	3.06E-01	0.207458	0.068456
PRESSURE	1.70E+05	-0.001183	-0.00039
TEMPERAT	1.06E+03	-0.264524	-0.087287
CHORD	1.52E-02	0.159436	0.05261

R.V. name	X-value	Std. Dev. from Mean	Sensitivity factor
THERMAL	1.12E+01	-0.026232	-0.011539
MODULUS	1.73E+11	-1.654103	-0.727634
ALPHA	1.61E-05	-1.536986	-0.676115
POISSON	3.04E-01	0.144243	0.063452
PRESSURE	1.70E+05	-0.000828	-0.000364
TEMPERAT	1.07E+03	-0.188057	-0.082725
CHORD	1.52E-02	0.111712	0.049142

R.V. name	X-value	Std. Dev. from Mean	Sensitivity factor
THERMAL	1.12E+01	-0.012709	-0.010256
MODULUS	1.87E+11	-0.981516	-0.79203
ALPHA	1.76E-05	-0.745503	-0.601581
POISSON	3.02E-01	0.069432	0.056028
PRESSURE	1.70E+05	-0.000401	-0.000324
TEMPERAT	1.08E+03	-0.09296	-0.075014
CHORD	1.51E-02	0.054266	0.04379

R.V. name	X-value	Std. Dev. from Mean	Sensitivity factor
THERMAL	1.12E+01	-0.007889	-0.009716
MODULUS	1.93E+11	-0.662185	-0.815575
ALPHA	1.81E-05	-0.462931	-0.570165
POISSON	3.01E-01	0.042998	0.052958
PRESSURE	1.70E+05	-0.000249	-0.000307
TEMPERAT	1.09E+03	-0.058127	-0.071592
CHORD	1.51E-02	0.033715	0.041525

R.V. name	X-value	Std. Dev. from Mean	Sensitivity factor
THERMAL	1.12E+01	-0.002065	-0.009
MODULUS	2.03E+11	-0.193646	-0.844032

ALPHA	1.88E-05	-0.121224	-0.528372
POISSON	3.00E-01	0.011223	0.048916
PRESSURE	1.70E+05	-0.000065	-0.000285
TEMPERAT	1.09E+03	-0.01535	-0.066906
CHORD	1.50E-02	0.008834	0.038506

R.V. name	X-value	Std. Dev. from Mean	Sensitivity factor
THERMAL	1.12E+01	0.000219	-0.008699
MODULUS	2.07E+11	0.021483	-0.855095
ALPHA	1.90E-05	0.012833	-0.510791
POISSON	3.00E-01	-0.001187	0.047228
PRESSURE	1.70E+05	0.000007	-0.000275
TEMPERAT	1.09E+03	0.00163	-0.064895
CHORD	1.50E-02	-0.000935	0.037234

R.V. name	X-value	Std. Dev. from Mean	Sensitivity factor
THERMAL	1.12E+01	0.002322	-0.008411
MODULUS	2.12E+11	0.238847	-0.865202
ALPHA	1.93E-05	0.136367	-0.493978
POISSON	3.00E-01	-0.012594	0.04562
PRESSURE	1.70E+05	0.000073	-0.000266
TEMPERAT	1.10E+03	0.017378	-0.062951
CHORD	1.50E-02	-0.009943	0.036017

R.V. name	X-value	Std. Dev. from Mean	Sensitivity factor
THERMAL	1.12E+01	0.006692	-0.00778
MODULUS	2.23E+11	0.761846	-0.88581
ALPHA	1.97E-05	0.393148	-0.457119
POISSON	2.99E-01	-0.036219	0.042113
PRESSURE	1.70E+05	0.000212	-0.000246
TEMPERAT	1.10E+03	0.050424	-0.058629
CHORD	1.50E-02	-0.028679	0.033346

R.V. name	X-value	Std. Dev. from Mean	Sensitivity factor
THERMAL	1.12E+01	0.009529	-0.007347
MODULUS	2.31E+11	1.165763	-0.898812
ALPHA	2.01E-05	0.560001	-0.431765
POISSON	2.98E-01	-0.051509	0.039714
PRESSURE	1.70E+05	0.000302	-0.000232
TEMPERAT	1.10E+03	0.072125	-0.055609
CHORD	1.49E-02	-0.040864	0.031506

R.V. name	X-value	Std. Dev. from Mean	Sensitivity factor
THERMAL	1.12E+01	0.011631	-0.007014
MODULUS	2.38E+11	1.505984	-0.908192
ALPHA	2.03E-05	0.683623	-0.412263
POISSON	2.98E-01	-0.062806	0.037875
PRESSURE	1.70E+05	0.000368	-0.000222
TEMPERAT	1.10E+03	0.088322	-0.053263
CHORD	1.49E-02	-0.049896	0.03009

)

R.V. name	X-value	Std. Dev. from Mean	Sensitivity factor
THERMAL	1.12E+01	0.015083	-0.006444
MODULUS	2.52E+11	2.16045	-0.923044
ALPHA	2.07E-05	0.886812	-0.378887
POISSON	2.98E-01	-0.081317	0.034742
PRESSURE	1.70E+05	0.000478	-0.000204
TEMPERAT	1.11E+03	0.115161	-0.049202
CHORD	1.49E-02	-0.064751	0.027665

R.V. name	X-value	Std. Dev. from Mean	Sensitivity factor
THERMAL	1.12E+01	0.01828	-0.005893
MODULUS	2.67E+11	2.903273	-0.936028
ALPHA	2.10E-05	1.075017	-0.34659
POISSON	2.97E-01	-0.098398	0.031724
PRESSURE	1.70E+05	0.000579	-0.000187
TEMPERAT	1.11E+03	0.140274	-0.045225
CHORD	1.49E-02	-0.078521	0.025316

Table C.5:

R.V. name	X-value	Std. Dev. from Mean	Sensitivity factor
THERMAL	1.11E+01	-0.071719	-0.023609
MODULUS	1.64E+11	-2.058777	-0.677729
ALPHA	1.48E-05	-2.205076	-0.72589
POISSON	3.06E-01	0.208527	0.068645
PRESSURE	1.70E+05	-0.001186	-0.00039
TEMPERAT	1.06E+03	-0.275399	-0.090658
CHORD	1.49E-02	-0.050725	-0.016698

R.V. name	X-value	Std. Dev. from Mean	Sensitivity factor
THERMAL	1.11E+01	-0.050562	-0.022172
MODULUS	1.73E+11	-1.65917	-0.727569
ALPHA	1.61E-05	-1.544423	-0.677251
POISSON	3.04E-01	0.145093	0.063625
PRESSURE	1.70E+05	-0.00083	-0.000364
TEMPERAT	1.07E+03	-0.193194	-0.084718
CHORD	1.49E-02	-0.036658	-0.016075

R.V. name	X-value	Std. Dev. from Mean	Sensitivity factor
THERMAL	1.12E+01	-0.024753	-0.01988
MODULUS	1.86E+11	-0.986328	-0.792162
ALPHA	1.76E-05	-0.75018	-0.602501
POISSON	3.02E-01	0.06993	0.056164
PRESSURE	1.70E+05	-0.000403	-0.000324
TEMPERAT	1.08E+03	-0.094018	-0.07551
CHORD	1.50E-02	-0.018493	-0.014853

R.V. name	X-value	Std. Dev. from Mean	Sensitivity factor
THERMAL	1.12E+01	-0.01533	-0.018881

MODULUS	1.93E+11	-0.662598	-0.816054
ALPHA	1.81E-05	-0.463284	-0.57058
POISSON	3.01E-01	0.043066	0.05304
PRESSURE	1.70E+05	-0.000249	-0.000307
TEMPERAT	1.09E+03	-0.058102	-0.071559
CHORD	1.50E-02	-0.011587	-0.01427

R.V. name	X-value	Std. Dev. from Mean	Sensitivity factor
THERMAL	1.12E+01	-0.004028	-0.017555
MODULUS	2.03E+11	-0.193796	-0.844506
ALPHA	1.88E-05	-0.121324	-0.528695
POISSON	3.00E-01	0.011241	0.048983
PRESSURE	1.70E+05	-0.000065	-0.000284
TEMPERAT	1.09E+03	-0.015228	-0.06636
CHORD	1.50E-02	-0.003087	-0.013453

R.V. name	X-value	Std. Dev. from Mean	Sensitivity factor
THERMAL	1.12E+01	0.000426	-0.016993
MODULUS	2.07E+11	0.021444	-0.855561
ALPHA	1.90E-05	0.01281	-0.511079
POISSON	3.00E-01	-0.001185	0.047289
PRESSURE	1.70E+05	0.000007	-0.000275
TEMPERAT	1.09E+03	0.001608	-0.064169
CHORD	1.50E-02	0.000328	-0.013095

R.V. name	X-value	Std. Dev. from Mean	Sensitivity factor
THERMAL	1.12E+01	0.004539	-0.016453
MODULUS	2.12E+11	0.238793	-0.865651
ALPHA	1.93E-05	0.136338	-0.494242
POISSON	3.00E-01	-0.0126	0.045677
PRESSURE	1.70E+05	0.000073	-0.000266
TEMPERAT	1.10E+03	0.017123	-0.062074
CHORD	1.50E-02	0.003515	-0.012744

R.V. name	X-value	Std. Dev. from Mean	Sensitivity factor
THERMAL	1.12E+01	0.013126	-0.015263
MODULUS	2.23E+11	0.762161	-0.886236
ALPHA	1.97E-05	0.393284	-0.457308
POISSON	2.99E-01	-0.036256	0.042158
PRESSURE	1.70E+05	0.000211	-0.000246
TEMPERAT	1.10E+03	0.049424	-0.05747
CHORD	1.50E-02	0.010277	-0.01195

R.V. name	X-value	Std. Dev. from Mean	Sensitivity factor
THERMAL	1.12E+01	0.018728	-0.01444
MODULUS	2.31E+11	1.166238	-0.899213
ALPHA	2.01E-05	0.560173	-0.431914
POISSON	2.98E-01	-0.051558	0.039753
PRESSURE	1.70E+05	0.000301	-0.000232
TEMPERAT	1.10E+03	0.070426	-0.054301
CHORD	1.50E-02	0.014766	-0.011385

R.V. name	X-value	Std. Dev. from Mean	Sensitivity factor
THERMAL	1.12E+01	0.02289	-0.013804
MODULUS	2.38E+11	1.506574	-0.908571
ALPHA	2.03E-05	0.683808	-0.412385
POISSON	2.98E-01	-0.062862	0.03791
PRESSURE	1.70E+05	0.000368	-0.000222
TEMPERAT	1.10E+03	0.085995	-0.051861
CHORD	1.50E-02	0.018144	-0.010942

R.V. name	X-value	Std. Dev. from Mean	Sensitivity factor
THERMAL	1.12E+01	0.029722	-0.012716
MODULUS	2.51E+11	2.158032	-0.923319
ALPHA	2.07E-05	0.886101	-0.37912
POISSON	2.98E-01	-0.081301	0.034785
PRESSURE	1.70E+05	0.000476	-0.000204
TEMPERAT	1.11E+03	0.111488	-0.047701
CHORD	1.50E-02	0.023765	-0.010168

R.V. name	X-value	Std. Dev. from Mean	Sensitivity factor
THERMAL	1.12E+01	0.03611	-0.011653
MODULUS	2.67E+11	2.90118	-0.936279
ALPHA	2.10E-05	1.074489	-0.346763
POISSON	2.97E-01	-0.098406	0.031758
PRESSURE	1.70E+05	0.000578	-0.000186
TEMPERAT	1.11E+03	0.135253	-0.043649
CHORD	1.50E-02	0.029113	-0.009396

Table C.6:

Level	Z-value	u(std. normal)	Probability
1	-2.29E+12	-3.09025	0.001
2	-2.23E+12	-2.32635	0.01
3	-2.05E+12	-1.28155	0.1
4	-1.96E+12	-0.84162	0.2
5	-1.84E+12	-0.25335	0.4
6	-1.78E+12	0	0.5
7	-1.72E+12	0.25335	0.6
8	-1.57E+12	0.84162	0.8
9	-1.45E+12	1.28155	0.9
10	-1.34E+12	1.64485	0.95
11	-1.13E+12	2.32635	0.99
12	-8.65E+11	3.09025	0.999

Table C.7: Sensitivity and Probability levels for Rotor at 1900th iteration

Level	Z-value	u(std. normal)	Probability
1.00E+00	-2.28E+12	-3.09025	0.001
2.00E+00	-2.24E+12	-2.32635	0.01
3.00E+00	-2.06E+12	-1.28155	0.1
4.00E+00	-1.97E+12	-0.84162	0.2
5.00E+00	-1.85E+12	-0.25335	0.4
6.00E+00	-1.79E+12	0	0.5
7.00E+00	-1.73E+12	0.25335	0.6
8.00E+00	-1.58E+12	0.84162	0.8
9.00E+00	-1.45E+12	1.28155	0.9
1.00E+01	-1.35E+12	1.64485	0.95
1.10E+01	-1.14E+12	2.32635	0.99
1.20E+01	-8.70E+11	3.09025	0.999

Table C.8: Sensitivity and Probability levels for Rotor at 1960th iteration

Level	Z-value	u(std. normal)	Probability
1.00E+00	-2.22E+12	-3.09025	0.001
2.00E+00	-2.24E+12	-2.32635	0.01
3.00E+00	-2.01E+12	-1.28155	0.1
4.00E+00	-1.92E+12	-0.84162	0.2
5.00E+00	-1.80E+12	-0.25335	0.4
6.00E+00	-1.74E+12	0	0.5
7.00E+00	-1.68E+12	0.25335	0.6
8.00E+00	-1.53E+12	0.84162	0.8
9.00E+00	-1.41E+12	1.28155	0.9
1.00E+01	-1.30E+12	1.64485	0.95
1.10E+01	-1.09E+12	2.32635	0.99
1.20E+01	-8.25E+11	3.09025	0.999

Table C.9 Sensitivity and Probability levels for Rotor at 2000th iteration

R.V. name	X-value	Std. Dev. from Mean	Sensitivity factor
THERMAL	1.11E+01	-0.124536	-0.053217
MODULUS	2.34E+11	1.306276	0.558206
ALPHA	1.85E-05	-0.253262	-0.108226
POISSON	3.04E-01	0.128077	0.054731
PRESSURE	1.70E+05	0.005221	0.002231
TEMPERAT	1.07E+03	-0.000213	-0.000091
SPEED	1.07E+04	-1.904255	-0.813738
CHORD	7.51E-04	0.218164	0.093227

R.V. name	X-value	Std. Dev. from Mean	Sensitivity factor
THERMAL	1.11E+01	-0.128198	-0.058638
MODULUS	2.22E+11	0.71464	0.326878
ALPHA	1.85E-05	-0.260375	-0.119096
POISSON	3.04E-01	0.13201	0.060382
PRESSURE	1.70E+05	0.005365	0.002454
TEMPERAT	1.07E+03	-0.000219	-0.0001
SPEED	1.05E+04	-2.029014	-0.928076
CHORD	7.52E-04	0.224568	0.102718

R.V. name	X-value	Std. Dev. from Mean	Sensitivity factor
THERMAL	1.11E+01	-0.060874	-0.051692
MODULUS	2.16E+11	0.452207	0.383998
ALPHA	1.88E-05	-0.122965	-0.104417
POISSON	3.02E-01	0.063014	0.053509
PRESSURE	1.70E+05	0.002527	0.002145
TEMPERAT	1.07E+03	-0.000103	-0.000088
SPEED	1.18E+04	-1.071518	-0.909894
CHORD	7.43E-04	0.10661	0.09053

R.V. name	X-value	Std. Dev. from Mean	Sensitivity factor
THERMAL	1.12E+01	-0.035759	-0.048803
MODULUS	2.13E+11	0.306313	0.418046
ALPHA	1.89E-05	-0.072088	-0.098384
POISSON	3.01E-01	0.037089	0.050617
PRESSURE	1.70E+05	0.00148	0.002019
TEMPERAT	1.07E+03	-0.00006	-0.000082
SPEED	1.24E+04	-0.656722	-0.896274
CHORD	7.40E-04	0.062621	0.085463

R.V. name	X-value	Std. Dev. from Mean	Sensitivity factor
THERMAL	1.12E+01	-0.006861	-0.045124
MODULUS	2.08E+11	0.071413	0.469647
ALPHA	1.90E-05	-0.0138	-0.090758
POISSON	3.00E-01	0.007133	0.046907
PRESSURE	1.70E+05	0.000283	0.001861
TEMPERAT	1.07E+03	-0.000012	-0.000076
SPEED	1.31E+04	-0.132622	-0.872188
CHORD	7.36E-04	0.012015	0.079014

R.V. name	X-value	Std. Dev. from Mean	Sensitivity factor
THERMAL	1.12E+01	0.004506	-0.04352
MODULUS	2.06E+11	-0.051236	0.494874
ALPHA	1.90E-05	0.009054	-0.087452
POISSON	3.00E-01	-0.004688	0.04528
PRESSURE	1.70E+05	-0.000186	0.001792
TEMPERAT	1.07E+03	0.000008	-0.000073
SPEED	1.33E+04	0.088923	-0.858893
CHORD	7.35E-04	-0.007889	0.076202

R.V. name	X-value	Std. Dev. from Mean	Sensitivity factor
THERMAL	1.12E+01	0.015092	-0.041912
MODULUS	2.03E+11	-0.187806	0.521567
ALPHA	1.91E-05	0.0303	-0.084149
POISSON	3.00E-01	-0.015715	0.043643
PRESSURE	1.70E+05	-0.000621	0.001724
TEMPERAT	1.07E+03	0.000025	-0.00007
SPEED	1.36E+04	0.303802	-0.843705
CHORD	7.33E-04	-0.026424	0.073383

R.V. name	X-value	Std. Dev. from Mean	Sensitivity factor
THERMAL	1.12E+01	0.036761	-0.038137
MODULUS	1.95E+11	-0.56686	0.588077
ALPHA	1.91E-05	0.07368	-0.076438
POISSON	2.99E-01	-0.038344	0.039779
PRESSURE	1.70E+05	-0.001508	0.001564
TEMPERAT	1.07E+03	0.000062	-0.000064
SPEED	1.43E+04	0.771634	-0.800516
CHORD	7.31E-04	-0.06436	0.066769

R.V. name	X-value	Std. Dev. from Mean	Sensitivity factor
THERMAL	1.13E+01	0.049945	-0.035368
MODULUS	1.88E+11	-0.901552	0.638418
ALPHA	1.92E-05	0.100001	-0.070814
POISSON	2.98E-01	-0.05215	0.036929
PRESSURE	1.70E+05	-0.002046	0.001449
TEMPERAT	1.07E+03	0.000083	-0.000059
SPEED	1.47E+04	1.076361	-0.762206
CHORD	7.29E-04	-0.08744	0.061919

R.V. name	X-value	Std. Dev. from Mean	Sensitivity factor
THERMAL	1.13E+01	0.058823	-0.033219
MODULUS	1.82E+11	-1.198874	0.677042
ALPHA	1.92E-05	0.117692	-0.066464
POISSON	2.98E-01	-0.061462	0.03471
PRESSURE	1.70E+05	-0.002407	0.001359
TEMPERAT	1.07E+03	0.000098	-0.000055
SPEED	1.49E+04	1.290958	-0.729044
CHORD	7.28E-04	-0.102978	0.058155

R.V. name	X-value	Std. Dev. from Mean	Sensitivity factor
THERMAL	1.13E+01	0.071718	-0.029506
`ODULUS	1.70E+11	-1.801798	0.741286
ALPHA	1.93E-05	0.143347	-0.058975
POISSON	2.98E-01	-0.075012	0.030861
PRESSURE	1.70E+05	-0.00293	0.001205
TEMPERAT	1.07E+03	0.00012	-0.000049
SPEED	1.54E+04	1.616921	-0.665225
CHORD	7.26E-04	-0.125549	0.051653

R.V. name	X-value	Std. Dev. from Mean	Sensitivity factor
THERMAL	1.13E+01	0.081972	-0.025915
MODULUS	1.55E+11	-2.52474	0.79818
ALPHA	1.93E-05	0.163707	-0.051755
POISSON	2.97E-01	-0.085806	0.027127
PRESSURE	1.70E+05	-0.003345	0.001057
TEMPERAT	1.07E+03	0.000136	-0.000043
SPEED	1.57E+04	1.88932	-0.597296
CHORD	7.25E-04	-0.143493	0.045364

Table C.10

R.V. name	X-value	Std. Dev. from Mean	Sensitivity factor
THERMAL	1.11E+01	-0.12604	-0.054451
MODULUS	2.32E+11	1.212654	0.523883
ALPHA	1.85E-05	-0.256283	-0.110717
POISSON	3.04E-01	0.129645	0.056008
PRESSURE	1.70E+05	0.005283	0.002282
TEMPERAT	1.07E+03	-0.000262	-0.000113
SPEED	1.07E+04	-1.936689	-0.836676
CHORD	7.50E-04	0.1958	0.084588

R.V. name	X-value	Std. Dev. from Mean	Sensitivity factor
THERMAL	1.11E+01	-0.128339	-0.058712
MODULUS	2.22E+11	0.715937	0.327522
ALPHA	1.85E-05	-0.260666	-0.119248
POISSON	3.04E-01	0.132154	0.060457
PRESSURE	1.70E+05	0.005371	0.002457
TEMPERAT	1.07E+03	-0.000267	-0.000122
SPEED	1.05E+04	-2.030769	-0.929023
CHORD	7.50E-04	0.19935	0.091197

R.V. name	X-value	Std. Dev. from Mean	Sensitivity factor
THERMAL	1.11E+01	-0.060937	-0.051743
MODULUS	2.16E+11	0.452517	0.384245
ALPHA	1.88E-05	-0.123094	-0.104523
POISSON	3.02E-01	0.063079	0.053563
PRESSURE	1.70E+05	0.002529	0.002148

TEMPERAT	1.07E+03	-0.000126	-0.000107
SPEED	1.18E+04	-1.072545	-0.910728
CHORD	7.42E-04	0.094605	0.080332

R.V. name	X-value	Std. Dev. from Mean	Sensitivity factor
THERMAL	1.12E+01	-0.035789	-0.048844
MODULUS	2.13E+11	0.306505	0.418313
ALPHA	1.89E-05	-0.072149	-0.098468
POISSON	3.01E-01	0.03712	0.05066
PRESSURE	1.70E+05	0.001481	0.002021
TEMPERAT	1.07E+03	-0.000074	-0.0001
SPEED	1.24E+04	-0.65725	-0.897003
CHORD	7.39E-04	0.055552	0.075816

R.V. name	X-value	Std. Dev. from Mean	Sensitivity factor
THERMAL	1.12E+01	-0.006867	-0.045155
MODULUS	2.08E+11	0.071464	0.469937
ALPHA	1.90E-05	-0.013811	-0.090821
POISSON	3.00E-01	0.007138	0.04694
PRESSURE	1.70E+05	0.000283	0.001862
TEMPERAT	1.07E+03	-0.000014	-0.000092
SPEED	1.31E+04	-0.132725	-0.872785
CHORD	7.36E-04	0.010656	0.070075

R.V. name	X-value	Std. Dev. from Mean	Sensitivity factor
THERMAL	1.12E+01	0.004508	-0.043547
MODULUS	2.06E+11	-0.051261	0.495175
ALPHA	1.90E-05	0.009059	-0.087506
POISSON	3.00E-01	-0.00469	0.045308
PRESSURE	1.70E+05	-0.000186	0.001793
TEMPERAT	1.07E+03	0.000009	-0.000089
SPEED	1.33E+04	0.08897	-0.859434
CHORD	7.35E-04	-0.006995	0.067573

R.V. name	X-value	Std. Dev. from Mean	Sensitivity factor
THERMAL	1.12E+01	0.0151	-0.041935
MODULUS	2.03E+11	-0.187919	0.521878
ALPHA	1.91E-05	0.030318	-0.084196
POISSON	3.00E-01	-0.015724	0.043667
PRESSURE	1.70E+05	-0.000621	0.001725
TEMPERAT	1.07E+03	0.000031	-0.000086
SPEED	1.36E+04	0.303978	-0.844188
CHORD	7.34E-04	-0.023429	0.065067

R.V. name	X-value	Std. Dev. from Mean	Sensitivity factor
THERMAL	1.12E+01	0.036774	-0.038153
MODULUS	1.95E+11	-0.567138	0.588395

ALPHA	1.91E-05	0.073708	-0.07647
POISSON	2.99E-01	-0.038359	0.039796
PRESSURE	1.70E+05	-0.001509	0.001565
TEMPERAT	1.07E+03	0.000075	-0.000078
SPEED	1.43E+04	0.771941	-0.800874
CHORD	7.31E-04	-0.05705	0.059189

R.V. name	X-value	Std. Dev. from Mean	Sensitivity factor
THERMAL	1.13E+01	0.049962	-0.035379
MODULUS	1.88E+11	-0.902012	0.638738
ALPHA	1.92E-05	0.100034	-0.070837
POISSON	2.98E-01	-0.052168	0.036942
PRESSURE	1.70E+05	-0.002046	0.001449
TEMPERAT	1.07E+03	0.000102	-0.000072
SPEED	1.47E+04	1.076748	-0.762473
CHORD	7.30E-04	-0.077501	0.054881

R.V. name	X-value	Std. Dev. from Mean	Sensitivity factor
THERMAL	1.13E+01	0.058795	-0.033239
MODULUS	1.82E+11	-1.19779	0.677152
ALPHA	1.92E-05	0.117637	-0.066504
POISSON	2.98E-01	-0.061434	0.034731
PRESSURE	1.70E+05	-0.002406	0.00136
TEMPERAT	1.07E+03	0.000119	-0.000068
SPEED	1.49E+04	1.290268	-0.729433
CHORD	7.29E-04	-0.091197	0.051557

R.V. name	X-value	Std. Dev. from Mean	Sensitivity factor
THERMAL	1.13E+01	0.071729	-0.029512
MODULUS	1.70E+11	-1.802338	0.741546
ALPHA	1.93E-05	0.143369	-0.058987
POISSON	2.98E-01	-0.075024	0.030868
PRESSURE	1.70E+05	-0.00293	0.001206
TEMPERAT	1.07E+03	0.000146	-0.00006
SPEED	1.54E+04	1.617177	-0.665364
CHORD	7.27E-04	-0.111248	0.045771

R.V. name	X-value	Std. Dev. from Mean	Sensitivity factor
THERMAL	1.13E+01	0.081983	-0.025917
MODULUS	1.55E+11	-2.525605	0.798414
ALPHA	1.93E-05	0.16373	-0.05176
POISSON	2.97E-01	-0.085819	0.02713
PRESSURE	1.70E+05	-0.003345	0.001057
TEMPERAT	1.07E+03	0.000166	-0.000053
SPEED	1.57E+04	1.889596	-0.597354
CHORD	7.26E-04	-0.127142	0.040193

Table C.11

R.V. name	X-value	Std. Dev. from Mean	Sensitivity factor
THERMAL	1.11E+01	-0.128145	-0.056075
MODULUS	2.29E+11	1.07926	0.472272
ALPHA	1.85E-05	-0.260507	-0.113995
POISSON	3.04E-01	0.131837	0.05769
PRESSURE	1.70E+05	0.005369	0.00235
TEMPERAT	1.07E+03	-0.000286	-0.000125
SPEED	1.06E+04	-1.98181	-0.867218
CHORD	7.48E-04	0.168223	0.073612

R.V. name	X-value	Std. Dev. from Mean	Sensitivity factor
THERMAL	1.11E+01	-0.125725	-0.054266
MODULUS	2.32E+11	1.232266	0.531877
ALPHA	1.85E-05	-0.25565	-0.110345
POISSON	3.04E-01	0.129316	0.055816
PRESSURE	1.70E+05	0.00527	0.002275
TEMPERAT	1.07E+03	-0.000281	-0.000121
SPEED	1.07E+04	-1.929777	-0.832941
CHORD	7.47E-04	0.165053	0.071241

R.V. name	X-value	Std. Dev. from Mean	Sensitivity factor
THERMAL	1.11E+01	-0.06113	-0.051813
MODULUS	2.16E+11	0.453496	0.384375
ALPHA	1.88E-05	-0.123486	-0.104664
POISSON	3.02E-01	0.063278	0.053633
PRESSURE	1.70E+05	0.002537	0.00215
TEMPERAT	1.07E+03	-0.000135	-0.000115
SPEED	1.18E+04	-1.075598	-0.911658
CHORD	7.41E-04	0.08016	0.067942

R.V. name	X-value	Std. Dev. from Mean	Sensitivity factor
THERMAL	1.12E+01	-0.035825	-0.048889
MODULUS	2.13E+11	0.306744	0.418605
ALPHA	1.89E-05	-0.072221	-0.098558
POISSON	3.01E-01	0.037156	0.050706
PRESSURE	1.70E+05	0.001482	0.002023
TEMPERAT	1.07E+03	-0.000079	-0.000108
SPEED	1.24E+04	-0.657862	-0.897766
CHORD	7.39E-04	0.04696	0.064085

R.V. name	X-value	Std. Dev. from Mean	Sensitivity factor
THERMAL	1.12E+01	-0.006872	-0.045188
MODULUS	2.08E+11	0.071518	0.470262

ALPHA	1.90E-05	-0.013822	-0.090886
POISSON	3.00E-01	0.007144	0.046974
PRESSURE	1.70E+05	0.000283	0.001863
TEMPERAT	1.07E+03	-0.000015	-0.000099
SPEED	1.31E+04	-0.132828	-0.873405
CHORD	7.36E-04	0.009005	0.059209

R.V. name	X-value	Std. Dev. from Mean	Sensitivity factor
THERMAL	1.12E+01	0.00451	-0.043575
MODULUS	2.06E+11	-0.051291	0.495512
ALPHA	1.90E-05	0.009064	-0.087562
POISSON	3.00E-01	-0.004693	0.045337
PRESSURE	1.70E+05	-0.000186	0.001794
TEMPERAT	1.07E+03	0.00001	-0.000096
SPEED	1.33E+04	0.089019	-0.859991
CHORD	7.35E-04	-0.005909	0.057087

R.V. name	X-value	Std. Dev. from Mean	Sensitivity factor
THERMAL	1.12E+01	0.015109	-0.041959
MODULUS	2.03E+11	-0.188048	0.522228
ALPHA	1.91E-05	0.030335	-0.084244
POISSON	3.00E-01	-0.015733	0.043692
PRESSURE	1.70E+05	-0.000621	0.001725
TEMPERAT	1.07E+03	0.000033	-0.000092
SPEED	1.36E+04	0.304159	-0.844682
CHORD	7.34E-04	-0.019791	0.054961

R.V. name	X-value	Std. Dev. from Mean	Sensitivity factor
THERMAL	1.12E+01	0.036789	-0.038169
MODULUS	1.95E+11	-0.567466	0.588756
ALPHA	1.91E-05	0.073736	-0.076502
POISSON	2.99E-01	-0.038373	0.039813
PRESSURE	1.70E+05	-0.001509	0.001566
TEMPERAT	1.07E+03	0.00008	-0.000083
SPEED	1.43E+04	0.772257	-0.801231
CHORD	7.32E-04	-0.048174	0.049982

R.V. name	X-value	Std. Dev. from Mean	Sensitivity factor
THERMAL	1.13E+01	0.049978	-0.035391
MODULUS	1.88E+11	-0.90254	0.639102
ALPHA	1.92E-05	0.100067	-0.070859
POISSON	2.98E-01	-0.052185	0.036953
PRESSURE	1.70E+05	-0.002047	0.001449
TEMPERAT	1.07E+03	0.000109	-0.000077
SPEED	1.47E+04	1.077129	-0.762732
CHORD	7.31E-04	-0.065434	0.046335

R.V. name	X-value	Std. Dev. from Mean	Sensitivity factor
THERMAL	1.13E+01	0.05881	-0.033247

MODULUS	1.82E+11	-1.198409	0.677501
ALPHA	1.92E-05	0.117666	-0.066521
POISSON	2.98E-01	-0.061449	0.034739
PRESSURE	1.70E+05	-0.002406	0.00136
TEMPERAT	1.07E+03	0.000128	-0.000073
SPEED	1.49E+04	1.290616	-0.729629
CHORD	7.30E-04	-0.076987	0.043523

R.V. name	X-value	Std. Dev. from Mean	Sensitivity factor
THERMAL	1.13E+01	0.071713	-0.029525
MODULUS	1.70E+11	-1.801554	0.741714
ALPHA	1.93E-05	0.143336	-0.059013
POISSON	2.98E-01	-0.075007	0.030881
PRESSURE	1.70E+05	-0.002929	0.001206
TEMPERAT	1.07E+03	0.000156	-0.000064
SPEED	1.54E+04	1.616743	-0.665626
CHORD	7.28E-04	-0.093861	0.038643

R.V. name	X-value	Std. Dev. from Mean	Sensitivity factor
THERMAL	1.13E+01	0.081975	-0.025925
MODULUS	1.55E+11	-2.525165	0.798587
ALPHA	1.93E-05	0.163714	-0.051775
POISSON	2.97E-01	-0.08581	0.027137
PRESSURE	1.70E+05	-0.003344	0.001058
TEMPERAT	1.07E+03	0.000178	-0.000056
SPEED	1.57E+04	1.889352	-0.59751
CHORD	7.27E-04	-0.107277	0.033926

Table C.12